

# Tree structure and carbon cycling in a tropical rainforest under long-term drought

Sarah Ingrid Coughlin

A thesis presented to  
the Australian National University  
in fulfillment of the thesis requirement for the degree of  
Doctor of Philosophy  
in the Research School of Biology

Canberra, ACT, Australia, August 2022

© Sarah Ingrid Coughlin 2022

## **Author's Declaration**

I hereby declare that I composed this thesis and that this thesis has not been used for any other degrees internal and external to the Australian National University.

## Abstract

Tropical forests are highly productive and biodiverse, exchanging more carbon with the atmosphere than any other terrestrial ecosystem and representing the apex of taxonomic and structural diversity on land. However, their high productivity is sensitive to climate, which for many tropical regions, and especially the Amazon, is predicted to become more extreme this century, with stronger and more frequent drought events likely to occur. Extreme drought has been shown to alter net carbon gain in Amazon forests, causing a decline or sometimes a reversal in the natural carbon sink. The long-term effects of increasing drought exposure are poorly understood, but are thought likely to substantially weaken or reverse the future Amazon carbon sink, with impacts at the scale of the global carbon cycle. Our understanding of the response by any forest to drought is hampered by observational opportunity. One way to resolve this is to manipulate water availability experimentally at large scale.

This thesis uses one such 'ecosystem-scale' (1 ha) rainfall manipulation experiment in the Amazon rainforest, combining new structural, ecological and ecophysiological measurements on a forest that has experienced long-term experimental drought, over twenty years. The new structural measurements comprise terrestrial laser scanning (TLS) data that are analyzed to quantify detailed tree and forest structural metrics. The physiological measurements focus on using these novel structural datasets to estimate and scale woody tissue carbon dioxide effluxes from twig to forest. Finally, biomass and growth are analyzed over the twenty-year experimental drought period, using the new structural data to refine the quantification and understanding of change in biomass and growth during the period of experimentally-imposed drought.

Tree structural plasticity in response to drought may mitigate the sensitivity of tropical rainforests to climate change. Here, I find that tropical rainforest woody and leafy structural traits altered substantially under drought in a manner that may influence individual tree and whole forest hydraulic conductance, resource acquisition

efficiency and heat transfer. The tree structural plasticity found in droughted trees had implications for tree metabolic scaling, resulting in lower whole tree wood efflux for droughted trees in comparison to equivalent sized control trees. This alteration in metabolic scaling occurred on droughted trees despite minimal change in wood efflux rates per unit tree surface area. At the stand-scale, altered tree structure and high rates of tree mortality led to over 50% reduction in stand wood efflux.

Predicted drought scenarios in the tropics has led to substantial interest in climatic thresholds that can lead to ecosystem tipping points. The high mortality rate and accompanying loss of aboveground biomass during this drought experiment has provided the opportunity to test the potential for ecosystem collapse under extreme drought. By analyzing biomass dynamics, validated using TLS, and tree woody growth over 20 years of experimental drought, I find evidence that the ecosystem has reached a new stable state, with reduced rate of aboveground biomass loss due to mortality, and with stabilized growth rates.

There is large uncertainty about how climate change will influence carbon cycling in the tropics. I contribute to the understanding of the woody component of the carbon cycle in tropical rainforests under drought stress, using novel TLS techniques to link structure with function on a tree and forest-scale.

## Acknowledgements

To my dearest mother-in-law, Cris Curtarelli, thank you for taking care of little Cecilia while I finished this PhD. None of this would have been possible without you. To my father-in-law, Luiz Curtarelli, aka ‘Alvaro the best’ thank you for all of your ‘capricho’, and of course, your thesis programming magic. To all my family, thank you for the love and laughter throughout this PhD: Dylan, Oliver, Connor, Sophia, Grace, Rose, Leticia and Luciana. And a special thanks to Dylan for taking on the role as the family doctor, you’re incredible. To mom and dad, thanks for your support, I wouldn’t be here without you and the amazing advice you’ve given along the way.

To my advisor, Patrick Meir, it’s been a memorable and adventurous four years, and you are in a major way to blame for that. You’re an excellent and reliable advisor and teammate. Thank you for your input and vision during the development and completion of this thesis.

Marilyn Ball, it’s been a pleasure to be advised by such a determined and curious person. Your enthusiasm about this project has been very much welcomed, especially in these last months when baby-induced sleep deprivation made this project a bit more difficult. To Lucas Cernusak, thanks for your advice and your hospitality in Cairns.

To lab mate and unofficial co-advisor Oliver Binks – everyone knows that the post-doc of the lab ends up taking a lion’s share of the responsibility in the formation of a PhD student. Here, finally, you get the credit you deserve! It’s been truly enjoyable to work with you.

Tim, thanks for the Stato beers, the science, and the fights. The pro boxing fights, of course. To Callum, Rosie, Tommy, Hannah, Timmothe thanks for the insights, beers and laughs.

Lola, you’re a legend of the Brazilian Amazon. Thank you. To all the members of the various field teams over the last four years - it’s mind boggling thinking about all the work we’ve done. Thank you Raimundo de Souza Brasão Junior,

Moises Moraes Alves, Josenildo Costa Amaral, Juscelino Costa Amaral, Filomeno Martins do Amaral Filho, Cleidemar Araujo de Souza, João and Hildo and to anyone not mentioned that contributed to the field work. A very special thanks to Joca – you’re a constant inspiration. And a huge thank you to Carlos for your patience and organization. There would be no research without you and your monthly voyages.

To Cecilia. You did not contribute to thesis in any way but that’s not particularly surprising, since you’re currently only vocalizing words that sound like ‘goo’ and sticking your fist in your mouth. But an inspiration, you are. Thank you.

And lastly, and most importantly, to my husband Lucas Curtarelli. There’s so much I have to thank you for. It’s a joy to share this life with you.

## Dedication

To my gatão and gatinha, Lucas and Cecilia.

# Table of Contents

<b>Author's Declaration</b>	<b>ii</b>
<b>Abstract</b>	<b>iii</b>
<b>Acknowledgements</b>	<b>v</b>
<b>Dedication</b>	<b>vii</b>
<b>List of Figures</b>	<b>xiii</b>
<b>List of Tables</b>	<b>xvi</b>
<b>1 Introduction</b>	<b>1</b>
1.1 Overview . . . . .	1
1.2 The carbon balance of tropical rainforests and the influence of climate change . . . . .	2
1.3 Using lasers to measure tree shape and to test for new canopy scale ecological traits . . . . .	4
1.4 Woody tissue structure under drought conditions . . . . .	6
1.5 Woody tissue component of ecosystem respiration in tropical rainforests	7
1.6 Methodological constraints to measuring wood respiration . . . . .	10
1.7 Woody tissue CO <sub>2</sub> efflux under drought conditions . . . . .	12
1.8 The long term effects of drought on tropical rainforest: transition of a plant community to a new stable state . . . . .	12
1.9 Field Site . . . . .	13

1.10	Overview of thesis . . . . .	14
1.11	Layout of thesis . . . . .	17
1.11.1	Chapter 2: Tree structural plasticity under long-term experi- mental drought . . . . .	17
1.11.2	Chapter 3: Structural and process-based analysis of woody tissue respiration during long-term experimental drought . . .	18
1.11.3	Chapter 4: Forest dynamics over 20 years of experimental drought: tending to biomass collapse or a new stable state? .	19
<b>2</b>	<b>Tree structural plasticity under long-term experimental drought</b>	<b>21</b>
2.1	Introduction . . . . .	21
2.2	Materials and Methods . . . . .	24
2.2.1	Site . . . . .	24
2.2.2	Through-fall exclusion experiment (TFE) . . . . .	24
2.2.3	Sample selection . . . . .	24
2.2.4	Data collection . . . . .	25
2.2.5	TLS wood structural models . . . . .	26
2.2.6	TLS leaf structure . . . . .	28
2.2.7	Statistics . . . . .	30
2.3	Results . . . . .	30
2.3.1	Hydraulic conductance . . . . .	30
2.3.2	Resource acquisition efficiency . . . . .	33
2.3.3	Heat exchange . . . . .	33
2.3.4	Aggregate TFE structural properties . . . . .	33
2.4	Discussion . . . . .	37
2.4.1	Hydraulic Conductance . . . . .	39
2.4.2	Resource acquisition efficiency . . . . .	40
2.4.3	Optimizing heat transfer . . . . .	41
2.4.4	Aggregate structure . . . . .	42
2.5	Conclusion . . . . .	44

<b>3</b>	<b>Structural and process-based analysis of woody tissue respiration during long-term experimental drought</b>	<b>46</b>
3.1	Introduction . . . . .	46
3.2	Materials and Methods . . . . .	52
3.2.1	Site . . . . .	52
3.2.2	Terrestrial laser scanning (TLS) . . . . .	53
3.2.3	Wood CO <sub>2</sub> efflux . . . . .	55
3.2.4	Wood Respiration - ARQ . . . . .	57
3.2.5	Scalars of wood CO <sub>2</sub> efflux . . . . .	58
3.2.6	Wood CO <sub>2</sub> efflux model . . . . .	59
3.2.7	Wood temperature model . . . . .	59
3.2.8	Scaling wood CO <sub>2</sub> efflux . . . . .	60
3.2.9	Statistics . . . . .	60
3.3	Results . . . . .	61
3.3.1	TFE physical environment . . . . .	61
3.3.2	Tree and plot woody structure on TFE and Control . . . . .	62
3.3.3	Wood CO <sub>2</sub> efflux rates . . . . .	65
3.3.4	Scaling wood CO <sub>2</sub> efflux model to trees . . . . .	72
3.3.5	Scaling wood CO <sub>2</sub> efflux to stand . . . . .	72
3.3.6	ARQ: wood respiration . . . . .	74
3.4	Discussion . . . . .	77
3.4.1	Wood CO <sub>2</sub> efflux and wood respiration on the TFE relative to the Control . . . . .	79
3.4.2	Wood metabolic load on trees under drought . . . . .	81
3.4.3	R <sub>wood</sub> on the TFE in response to water deficit . . . . .	84
3.5	Conclusions . . . . .	86
<b>4</b>	<b>Forest dynamics over 20 years of experimental drought: tending to biomass collapse or a new stable state?</b>	<b>87</b>
4.1	Introduction . . . . .	87

4.2	Materials and Methods . . . . .	91
4.2.1	Site . . . . .	91
4.2.2	Through-fall exclusion experiment (TFE) . . . . .	91
4.2.3	Wood density . . . . .	91
4.2.4	Terrestrial Laser Scanning . . . . .	92
4.2.5	Allometric models of tree height and biomass . . . . .	93
4.2.6	Biomass monitoring: census and dendrometer data . . . . .	93
4.2.7	Spatial analysis . . . . .	95
4.2.8	Statistics . . . . .	96
4.3	Results . . . . .	96
4.3.1	Comparison between TLS and allometry . . . . .	96
4.3.2	Aboveground biomass dynamics . . . . .	98
4.3.3	Carbon gains due to growth and recruitment . . . . .	100
4.3.4	Carbon loss: tree mortality . . . . .	105
4.3.5	Tree spatial arrangement . . . . .	107
4.4	Discussion . . . . .	107
4.4.1	Comparison with Rowland et al. (2015) . . . . .	114
4.5	Conclusion . . . . .	114
<b>5</b>	<b>Discussion</b>	<b>115</b>
5.1	Thesis overview . . . . .	115
5.2	Chapter 2: Tree structural plasticity under long term experimental drought . . . . .	117
5.2.1	Chapter 2: Future research . . . . .	119
5.3	Chapter 3: Structural and process-based analysis of woody tissue respiration during long-term experimental drought . . . . .	120
5.3.1	Chapter 3: Future research . . . . .	122
5.4	Chapter 4: Forest dynamics over 20 years of experimental drought: tending to biomass collapse or a new stable state? . . . . .	123
5.4.1	Chapter 4: Future research . . . . .	126

5.5 Conclusion . . . . .	127
<b>Appendices</b>	<b>129</b>
<b>A Appendix for Chapter 2</b>	<b>130</b>
<b>B Appendix for Chapter 3</b>	<b>143</b>

# List of Figures

1.1	Map of Caxiuanã National Forest Reserve, Pará - Brazil . . . . .	13
1.2	Through fall exclusion (TFE) experiment . . . . .	15
1.3	TLS point cloud data . . . . .	16
1.4	Schematic overview of thesis data chapters . . . . .	17
2.1	Canopy leaf area distribution across cardinal and ordinal directions .	34
2.2	Vertical woody volume distribution on the TFE and Control . . . . .	35
2.3	Vertical canopy distribution of woody and leafy tissue across the TFE and Control . . . . .	36
2.4	Cumulative leaf area index and cumulative woody volume on the TFE and Control . . . . .	37
3.1	Seasonal variation in soil volumetric water content ( $\text{m}^3\text{m}^{-3}$ ) at 5 cm depth in the Control and TFE in 2019 . . . . .	61
3.2	Measurements of woody tissue surface temperature versus air tem- perature at 16 m height ( $^{\circ}\text{C}$ ) on the TFE and Control . . . . .	62
3.3	Diurnal measurements of woody surface temperature ( $^{\circ}\text{C}$ ) . . . . .	63
3.4	Modelled diurnal pattern in woody surface temperature . . . . .	63
3.5	Comparison of tree surface area from Chambers et al., 2004 with tree surface area using quantitative structural models derived from TLS .	64
3.6	The relationship between tree volume and tree surface area on the TFE and Control . . . . .	66
3.7	The cumulative sum of wood area index on TFE and Control . . . . .	66
3.8	Testing Levy-Jarvis scaling approaches . . . . .	67

3.9	Wood CO <sub>2</sub> efflux ( $\mu\text{mol CO}_2 \text{ m}^{-2}\text{s}^{-1}$ ) per month measured on the TFE and Control for stem, canopy and twig woody tissue . . . . .	68
3.10	Wood CO <sub>2</sub> efflux at 25°C in Control and TFE separated by genus and season for stem, canopy branches, and canopy twigs on TFE and Control . . . . .	70
3.11	Wood CO <sub>2</sub> efflux at 25°C in Control and TFE separated by species and season for stem measurements, canopy branches, and canopy twigs	71
3.12	The metabolic scaling of whole tree wood CO <sub>2</sub> efflux on TFE and Control . . . . .	74
3.13	ARQ measurements on 12 trees . . . . .	75
3.14	Sap flux rates during the hour that ARQ was measured in the canopy and the ground during the afternoon and at night . . . . .	75
3.15	ARQ measurements versus the sap flux at the time of ARQ measurement . . . . .	76
3.16	Whole tree wood CO <sub>2</sub> efflux ( $\text{Mg C tree}^{-1}\text{yr}^{-1}$ ) and whole tree wood respiration ( $\text{Mg C tree}^{-1}\text{yr}^{-1}$ ) versus tree volume ( $\text{m}^3$ ) . . . . .	77
4.1	The relationship between tree height measured using TLS versus tree height modelled from a published height allometric equation, calibrated for the region of this field site (Feldpausch et al., 2012) . . . . .	97
4.2	Density distribution of the percentage difference in tree allometric biomass estimates (Chave et al., 2014) when using tree height measured with TLS ( $\text{AGB}_{\text{tlsht}}$ ) versus height allometry calibrated for this region . . . . .	98
4.3	The density distribution of the percentage difference in tree above-ground biomass (AGB) when using TLS versus allometric methods of deriving AGB . . . . .	99
4.4	Aboveground biomass ( $\text{Mg C ha}^{-1}$ ) for Control and TFE from 2000 to 2022 . . . . .	100

4.5	Aboveground biomass and cumulative number of living recruits from 2002 to 2020 for Control and TFE . . . . .	101
4.6	Woody carbon production ( $NPP_{\text{wood}}$ ) of the stand on the TFE and the Control . . . . .	102
4.7	Woody carbon production ( $NPP_{\text{wood}}$ ) of the TFE and Control separated by size class for small, medium and large trees from 2005 to 2020 . . . . .	103
4.8	Mean growth increment (cm circumference/day) for TFE and Control grouped every 5 years for small, medium and large trees for four seasons per year . . . . .	105
4.9	Cumulative aboveground biomass loss due to mortality for Control and TFE from 2001 to 2022 . . . . .	106
4.10	Mortality rates of trees on the TFE and Control from 2002 to 2020 for small, medium, and large trees . . . . .	108
4.11	Number of hours air temperature at 28 m was above 33°C per year from 2000-2018 . . . . .	108
4.12	Nearest neighbor distance function testing for difference from complete spatial randomness in 2D arrangement of trees on the TFE and Control using Ripley's K test transformed to minimize variance ( $L_r$ ) .	109
A.1	Wind direction at Caxiuanã from 2017 to 2020 . . . . .	130
A.2	Examples of 2D and 3D convex hulls . . . . .	131
A.3	Methods for correcting tree woody tissue volume for each 3 meter height bin for trees on a 20 x 20 m . . . . .	132
A.4	Counterfactual plot for model of total leaf area ( $m^2$ ) of twigs . . . . .	142
B.1	Gap filling methods used for surface area of branches between 5 cm and 1 mm in basal diameter . . . . .	149

# List of Tables

2.1	Definitions of structural traits . . . . .	29
2.2	Coefficients for linear regression models describing tree structural traits using diameter at breast height (DBH) and TFE treatment. . .	31
2.3	Parameters estimates for linear model of mean path length for twigs .	32
2.4	Coefficients for linear models of twig leaf area, twig length, and twig volume . . . . .	32
3.1	The coefficients for linear regression models describing the relationship between canopy wood volume ( $\text{m}^3$ ) and tree woody volume ( $\text{m}^3$ ), and the effect of treatment. . . . .	65
3.2	The model coefficients of linear mixed effects model of wood $\text{CO}_2$ efflux at $25^\circ\text{C}$ ( $\text{WC}_{25}$ ) . . . . .	69
3.3	Model coefficients and standard error for nonlinear scaling equation of whole tree wood $\text{CO}_2$ efflux ( $\text{Mg C tree}^{-1}\text{yr}^{-1}$ ) versus tree woody volume ( $\text{m}^3$ ) . . . . .	73
3.4	Model coefficients of whole tree yearly wood $\text{CO}_2$ efflux ( $\text{Mg C tree}^{-1}\text{yr}^{-1}$ ) using tree surface area ( $\text{m}^2$ ) and tree canopy width (m), log transformed for linearity. . . . .	73
3.5	The yearly wood $\text{CO}_2$ efflux per hectare ( $\text{Mg C ha}^{-1} \text{yr}^{-1}$ ) for TFE and Control in 2019 at ambient temperature and at $25^\circ\text{C}$ . . . . .	74
A.1	Linear model coefficients of total canopy volume per tree, used to correct low resolution canopy volume models . . . . .	133

A.2	Linear model coefficients of canopy volume per height bin at high resolution used to correct low resolution canopy volume profiles . . .	134
A.3	Linear model coefficients of trunk volume per height bin, used to correct low resolution trunk volume profile . . . . .	135
A.4	Relationship between total number of leaf points of a tree (leaf.points), the tree canopy width (m), the tree DBH (cm), and the interaction between canopy width and tree DBH. . . . .	136
A.5	Genus-specific intercept for tree height mixed effect model . . . . .	137
A.6	Genus-specific intercept for canopy width mixed effect model . . . . .	140
B.1	Correction of surface area of low resolution QSMs to high resolution .	143
B.2	Correction of volume of low resolution QSMs to high resolution . . .	144
B.3	List of species sampled, and number of individuals on TFE and Control	145
B.4	Linear regression model coefficients that were used to predict cumulative surface area from 5 cm in diameter to 1 mm in diameter . . . .	150
B.5	Linear model coefficients for wood surface temperature for canopy wood and trunk wood . . . . .	151

# Chapter 1

## Introduction

### 1.1 Overview

This introductory chapter briefly summarizes (i) the carbon balance in the tropics under climate change, (ii) the new understanding that structural measurements derived from terrestrial laser scanning (TLS) can offer for interpreting and quantifying the structure and biomass of forest trees under drought, and (iii) the woody tissue component of the efflux of carbon dioxide from tropical forests, an understudied component of the forest carbon cycle globally, and particularly for tropical rainforests. My thesis builds on new analyses of tree and forest structure, which I then combine with measurements of the CO<sub>2</sub> efflux from wood to estimate tree and stand scale values for CO<sub>2</sub> emission following long-term experimentally-imposed drought. I complete the study by summarizing new data on the long-term changes in biomass resulting from experimental drought. I use a a multi-decadal and large-scale (1 ha) rainforest drought experiment in Amazonia as the focus of my studies.

## 1.2 The carbon balance of tropical rainforests and the influence of climate change

Total ecosystem respiration ( $R_{\text{eco}}$ ) and gross primary productivity (GPP) are similar in magnitude, and, in the absence of land use change or fire, the difference between the two accounts for whether a forest is a carbon source or carbon sink. The Amazon has consistently acted as a carbon sink (Brienen et al., 2015; Hubau et al., 2020), and has acted a globally significant brake on past and recent increases in atmospheric concentration of carbon dioxide (Phillips et al., 2009, IPCC, 2021). However, due to the combination of changing climate and land-use, the tropics are predicted to undergo a significant reduction in the rate of net carbon uptake (Huntingford et al., 2013; Cox et al., 2000). In the case of the Amazon, this could lead to parts of the region becoming a carbon source, with some recent publications suggesting that this has already occurred in areas where climate extremes and land-use have intersected (Baccini et al., 2017; Gatti et al., 2021).

One of the principal climatic drivers affecting the size of the net Amazon carbon sink is drought (Davidson et al., 2012; Phillips et al., 2009; Meir, Grace, 2002). Over the past quarter of a century the region has experienced several droughts previously considered to occur on a 100-year return timescale, and this increased frequency in extreme climate occurrence has been exacerbated by strong El Nino years, which, when they influence Amazonia, are associated with heating and drying (Davidson et al., 2012; Marengo et al., 2018). The impact of these drought events on the forests of the region has been substantive, with basin-wide plot network-based observational evidence first suggesting the potential for a temporary reversal of the regional sink (Phillips et al., 2009), followed by later studies suggesting a reduction in the long-term sink (Brienen et al., 2015).

A key response to extreme drought in forests globally is a reduction in productivity coupled with an increase in tree mortality, and Amazonia is no exception, but these effects are difficult to model (Allen et al., 2015). In order to improve our

predictions of the effects of drought on forests, the key underlying ecological mechanisms need to be better understood and included in land surface models (Meir et al., 2015), a process that is ongoing (e.g. Eller et al., 2020). These ecological mechanisms operate across multiple timescales (Meir et al., 2018), from seconds to months, years, decades and beyond; the decadal range of timescales is especially relevant in the context of likely continued and increasingly extreme drought impacts in the region this century (Duffy et al., 2015, IPCC, 2021).

A key long-standing uncertainty about the sensitivity of Amazonian rainforests to drought emerged with the publication of newly-coupled land surface and climate models (e.g. Cox et al., 2000; Huntingford et al., 2004), where some, though not all (Huntingford et al., 2013) indicated the potential for substantial biomass loss across Amazonia under 21st century climate change, including in some cases a transition to lower-biomass vegetation types such as dry forest or savanna (Nobre et al., 2016). The drivers of, and causal mechanisms for, such a vegetation transition might result from the combination of both climate change and increased regional deforestation rates. The idea of this transition in the South American tropics became known as the Amazon die-back hypothesis (Nobre et al., 2016). Whilst some model analyses have emphasised the potential for such a die-back, there is significant uncertainty as to how resistant and resilient rainforests might be to drought or at what climatic or deforestation thresholds significant risk of die-back could emerge (Sampaio et al., 2007; Davidson et al., 2012; Nobre et al., 2016; Staver et al., 2011; Zemp et al., 2017).

Both current land surface model analyses and the extrapolation into the future of plot network-based observational datasets have lacked sufficient process-based ecological understanding to adequately predict future responses by Amazonian rainforests to drought (Huntingford et al., 2017). Ecosystem scale drought experiments have been used as one tool to help fill this knowledge gap (Meir et al., 2015), with two implemented in Amazonia (Brando et al., 2008; Costa da et al., 2010), and one each in southeast Asia (Moser et al., 2014) and Australia (Pivovarov et al., 2021).

Here I make use of the only one of these large-scale field experiments in tropical forests that has been extended to decadal timescales: it is based in eastern Amazonia, at the Caxiuanã National Forest Reserve, in the State of Pará, Brazil. Forest biomass dynamics data published for this site up to 2015 (Rowland et al., 2015; Meir et al., 2018) demonstrated substantial biomass loss through rapidly increased drought-related tree mortality over the first 15 years of the drought experiment, suggesting the potential for further biomass collapse consistent with a die-back hypothesis. My measurements at this experiment now offer the potential to contribute to this discussion by analyzing a further six years of forest dynamics data. In addition to this, I focus on one key physiological process that has lagged, globally, in its study, woody tissue respiration. I start the thesis by analyzing new laser-based measurements of tree structure and then use these to inform my subsequent analyses of respiration and biomass change.

### **1.3 Using lasers to measure tree shape and to test for new canopy scale ecological traits**

Until recently, it was impossible to study the effects of detailed tree structure, still less the effects of climate change, on tree structure and its related functioning, at the scale of more than a few small trees (Bentley et al., 2013), let alone at the hectare scale or upwards. Detailed structural data is of particular importance in the tropics because the tropics have the largest carbon stores of all world forests (Pan et al., 2011), and are expected to be subject to increasingly severe and frequent droughts (Duffy et al., 2015; Fu et al., 2013; Good et al., 2013; Malhi et al., 2009b). Any systematic change in tree structure due to climate stress such as, for example, drought, could have a large impact on the carbon cycle in tropical forests. Recent advances in the measurement and modelling of tree architecture using high-precision spatial information obtained using terrestrial laser scanning (TLS, Disney et al., 2018; Malhi, 2018; Meir et al., 2017) have begun to make possible the quantification

of frequency and size distributions of woody limbs, from trunk to relatively small canopy tips of approximately 5 cm diameter, for hundreds-to-thousands of trees from a single measurement campaign. As a result of this new advance, there has been an increased focus on improving our understanding of carbon dynamics and, particularly, applying TLS to study tree woody structure to increase the accuracy and resolution of estimates of carbon stocks through time (Disney, 2019).

This new capability offers to enable the characterization of tree architecture such that the the study of tree form can move from description (e.g. Hallé et al., 1978) to quantification and statistically-driven structural examination at large scale, across hundreds or thousands of trees and species. This emerging ability transports forest science nearly to the resolution of agricultural science in facilitating analysis of the links between structure and function. My work here is an early attempt to contribute to this endeavour.

The quantification of canopy architecture at large scale has led to the suggestion that tree canopy form, widely recognized even by the untrained eye as distinct among many different species, can be described by structural metrics that are potentially consistent with different ecological characteristics (Verbeeck et al., 2019). Such canopy characteristics could be considered an extension of the list of plant traits considered suitable for study in ‘trait-based’ ecology (e.g. Kattge et al., 2011; Díaz et al., 2016). The treatment of canopy properties as ecological traits could only be strongly supported if these properties could be shown to change in response to the environment, thus demonstrating a plastic response that benefits a tree under stress in a way analogous to the known plasticity at the organ level of leaf, wood and root traits (Valladares et al., 2007; Binks et al., 2016; Lovelock et al., 2006). However, to demonstrate a plastic response in canopy-scale metrics to environmental stress, and thus to support the notion that these metrics may be considered as substantive ecological traits, requires study over a period of time long enough to account for differences in whole-tree growth responses to stress. Such a context is rare, but is provided by the drought experiment upon which my thesis is focused because of the

20 years of drought treatment that it spans. Here, I use this unique opportunity that the long-term TFE provides to study tree and canopy structural responses to drought. I then use this structural analysis to inform my analysis of woody tissue respiration and forest productivity at this site.

## 1.4 Woody tissue structure under drought conditions

Changes in tree structure in response to drought can affect whole tree woody CO<sub>2</sub> efflux by either altering the quantity of respiring tissue (e.g. by reducing canopy size through branch shedding) or by altering the position of the active woody tissue, and hence, microclimatic conditions (e.g. more sun-exposed branches vs. more shaded branches). These structural alterations under drought stress have the potential to mitigate hydraulic stress of a tree, although there has been limited research into linking tree architectural traits directly with tree hydraulic stress. For instance, if stand maximum tree height is restricted in part by annual rainfall (?), concurrent constraints on tree height could be manifested via tree die back (Rowland et al., 2015) or due to canopy plasticity by way of shedding of higher branches (Koçillari et al., 2021; Olson et al., 2021). During short-term droughts, there have been many recorded instances of canopy die-back (Li et al., 2018; Lloret et al., 2004; Mueller-Dombois, 1983; Nolan et al., 2021; Rood et al., 2000; Shen et al., 2022); yet, over long time periods, it remains wholly untested how tree architecture may alter in response to long-term drought and if changes occur, how the new architecture links with tree physiology.

One concern is that physiological process-level responses may differ between the larger trees dominating the upper canopy and smaller, understory trees (Bartholomew et al., 2020), making any potential benefit due to structural plasticity dependent on tree size. Since hydraulic vulnerability increases with tree height (Koçillari et al., 2021; Olson et al., 2018) there may be discrete limits to tree height under different

rainfall regimes (?) that may partially reflect the maximum possible hydraulic impact of architectural plasticity among species and forest stands. Thus, where trees below a certain height threshold might survive under long-term water deficit by means of architectural plasticity in combination with physiological plasticity, trees larger than a particular threshold might die under severe drought if maximum plastic response to drought is insufficient. In support of this concern, we have seen that during experimental tropical throughfall experiments (TFE), tree mortality rates have increased particularly for large trees (Costa da et al., 2010; Phillips et al., 2010; Rowland et al., 2015).

## 1.5 Woody tissue component of ecosystem respiration in tropical rainforests

There is substantial uncertainty about the current and future state of the carbon cycle in the Amazon (Baccini et al., 2017; Fatichi et al., 2019; Zscheischler et al., 2017), in part because of insufficient understanding of the components that make up total ecosystem respiration ( $R_{\text{eco}}$ ). The uncertainty around  $R_{\text{eco}}$  estimates for tropical rainforests range between 30-50% (Carnieli et al., 2016; Metcalfe et al., 2010a; Harris et al., 2021).  $R_{\text{eco}}$  consists of heterotrophic respiration ( $R_{\text{h}}$ ) pertaining to microbial decomposition and autotrophic respiration ( $R_{\text{a}}$ ), or plant respiration. In plants,  $R_{\text{a}}$  can be further subdivided into above-ground (trunk, branch, leaves) and below-ground (root) respiration. Each of these components reacts to changes in water availability and temperature in unique, usually non-linear, and sometimes opposite, manners (Bonal et al., 2008; Cleveland et al., 2010; Meir et al., 2008; Metcalfe et al., 2010b,a; Rowland et al., 2013; Zhou et al., 2019). Consequently, predictions of ecosystem level responses of respiration to climate change needs to model individual components.

The efflux of  $\text{CO}_2$  from woody tissue has large uncertainty, with recent scaling approaches showing differences of over 300% in stand-scale wood  $\text{CO}_2$  efflux esti-

mates (Rowland et al., 2018), suggesting a need for further research. Lower values of uncertainty have been reported elsewhere for stand wood CO<sub>2</sub> efflux in tropical rainforests (e.g. Malhi et al., 2009a; Costa da et al., 2014; Metcalfe et al., 2010b; Chambers et al., 2004), yet, critically, these reports consistently underestimate uncertainty because they omit the uncertainty associated with the method of scaling woody CO<sub>2</sub> fluxes, namely the measurement of scalars. The uncertainty of the woody component of R<sub>eco</sub> can be improved by (i) using TLS to improve the measurement of the scalars necessary (e.g. tree surface area, volume) to scale wood CO<sub>2</sub> efflux from a measurement chamber to a tree, and then to stand-scale; (ii) determining which scalar, woody tissue surface area or woody tissue volume, is the most appropriate for scaling organ-level woody tissue flux rates (Cavaleri et al., 2006; Levy et al., 1999; Meir, Grace, 2002; Rowland et al., 2018; Ryan, 1990; Yang et al., 2016); and (iii) improving the understanding of the drivers of CO<sub>2</sub> efflux rates, and the underlying processes.

Prior to the availability of structural analysis using TLS data, scalars of woody tissue CO<sub>2</sub> efflux were estimated using an allometric equation relating the scalar (e.g. tree surface area, tree volume) to tree diameter at breast height (DBH) and, sometimes, the height of the tree. Commonly, wood CO<sub>2</sub> efflux across all tropical rainforests is scaled using tree surface area derived from a single allometric equation, which was developed from a felled harvest in the Amazon (Chambers et al., 2004), despite recognition of regional differences in tree allometry (Feldpausch et al., 2012). Although useful tools, allometric models may be unsuitable for studies focusing on the long-term effects of climate change or other major perturbations because (i) the models do not take into account changes in tree allometry resulting from a perturbation and (ii) allometry errors themselves increase rapidly with tree size (Burt et al., 2020; Momo et al., 2020; Calders et al., 2015a), so large trees, which may be most sensitive to drought (Rowland et al., 2015), are the most poorly estimated. This is especially problematic for scaling to plot-level in the Amazonian rainforest or similar tropical forests where the biomass of the largest 2% of trees can account

for more than a quarter of stand aboveground biomass (Slik et al., 2013), and at times a single large tree can account for more than half of the estimated carbon stock in a stand (Longo et al., 2016).

To scale woody CO<sub>2</sub> efflux from a point measurement on a branch to an entire tree, or stand, it is necessary to determine how wood CO<sub>2</sub> efflux rates scale with tree structure. Tree surface area and volume scalars are readily available from quantitative structural models (QSMs) modelled from TLS data (Burt et al., 2021; Lau et al., 2019b; Tanago Gonzalez de et al., 2018); however, other commonly considered scalars like sapwood volume (Salomón et al., 2020; Ryan et al., 1994) or woody tissue mass (Mori et al., 2010) are not directly available in tropical rainforests without the use of previously available data, (as is sometimes available for temperate forests), or destructive methods. Some previous scaling approaches have focused on tree surface area as a scalar, based on the assumption that the highest rates of wood respiration occur in the thin cambium and phloem layer of woody tissue, as has been shown in some species (Spicer, Holbrook, 2007). Highly labour-intensive destructive harvest measurement programs have previously supported the idea of a surface area scalar (Yoda, 1983), and indeed these ideas were used in some earlier work in the Amazon (Chambers et al., 2004). However, scaling on a surface area basis ignores the axial and radial parenchyma fractions of woody tissue, which likely increase proportionally with branch diameter.

Scaling a chamber-based measurement of wood CO<sub>2</sub> efflux requires an understanding of the complex mixture of drivers influencing woody metabolism (?), which include branch diameter, season, time of day, meteorological conditions, location (canopy, trunk), temperature, ontogeny, and species (Cavaleri et al., 2006; Katayama et al., 2014; Rowland et al., 2018). Due to this complexity, a large sample size is required to successfully capture the effects of these variables in order to model woody tissue CO<sub>2</sub> efflux diurnally and seasonally across a forest. Current methods for scaling woody metabolism involve taking a measurement of wood CO<sub>2</sub> efflux at breast height, and multiplying by the tree surface area, with the tree surface area modelled

allometrically (e.g. Chambers et al., 2004; Girardin et al., 2014). Without modification, this method may underestimate whole-tree respiration, as wood in the canopy, irrespective of branch size, has been shown to have higher woody tissue CO<sub>2</sub> efflux rates than wood in the understorey, even after normalization for any differences in temperature (Asao et al., 2015; Cavaleri et al., 2006; Damesin et al., 2001; Katayama et al., 2014; Sprugel, 1990). An additional complication of scaling woody CO<sub>2</sub> efflux is that flux rates scale with branch diameter up to a certain size (Mori et al., 2010; Negisi, 1975; Yoda, 1983), with evidence that the interplay of volume and surface area components comprising the underlying respiration in live-tissue ultimately leads to saturation in the diameter-flux rate relationship (Meir, Grace, 2002). Thus, there is a fundamental need to have detailed structural data to estimate woody tissue respiratory fluxes, since two trees (or forests) of equal biomass, but different branch size distributions, may well have distinct distributions of wood CO<sub>2</sub> efflux rates.

## 1.6 Methodological constraints to measuring wood respiration

To further complicate the measurement of wood CO<sub>2</sub> efflux, current field methods do not, in fact, measure wood respiration *per se*, rather they measure efflux of CO<sub>2</sub> from the surface of woody tissue. The CO<sub>2</sub> derived from woody tissue respiration can move within woody tissue both radially, and axially via sap flow (Levy et al., 1999; McGuire, Teskey, 2002; Salomón et al., 2018; Teskey et al., 2017; Meir, Grace, 2002) or photosynthetic-driven CO<sub>2</sub> gradients (De Roo et al., 2019), leading to potential mismatches between the radial efflux rate of CO<sub>2</sub> and the rate of metabolism. In addition, CO<sub>2</sub> derived from respiratory processes in woody tissue can be re-assimilated by carboxylating enzymes like phosphoenolpyruvate carboxylase (PEPC) or ribulose-1,5-bisphosphate carboxylase oxygenase (RuBisCo, Dima et al., 2006; Gansert, Burgdorf, 2005; McGuire et al., 2009; Pfanz et al., 2002).

This complex arrangement of potential partial sinks of CO<sub>2</sub> means that the radial movement of CO<sub>2</sub> through wood will not directly translate to the respiration of live woody tissue that directly subtends a measurement chamber, without measurements of additional CO<sub>2</sub> sinks. To address this uncertainty, a number of difference approaches have been developed that require careful separation of the components of raw effluxes (Teskey et al., 2008); however, recently a compelling complement to CO<sub>2</sub>-derived measurements of wood respiration has been used: the measurement of the ratio of stem CO<sub>2</sub> efflux to O<sub>2</sub> efflux, known as the apparent respiratory quotient (ARQ, Angert et al., 2012; Hilman, Angert, 2016). This method provides a way of quantifying respiration without the confounding effects of carboxylation or of axial movement of CO<sub>2</sub>, since O<sub>2</sub> is much less soluble in sap than CO<sub>2</sub> (~28x less soluble).

Measurements of stem ARQ have consistently presented with values lower than the 1 CO<sub>2</sub> :1 O<sub>2</sub> expected (stoichiometry) if the main substrate for wood respiration is carbohydrate (Angert et al., 2012; Hilman, Angert, 2016; Hilman et al., 2019, 2022). Using this method, an average of approximately 41% of locally respired CO<sub>2</sub> appears to be withheld, but this can be as high as 61% (Angert et al., 2012; Hilman, Angert, 2016). Strikingly, stem ARQ values have not correlated with sap flow, and excised stem cores have presented with low ARQ values for up to two days, indicating that sap flow cannot account entirely for the ‘missing’ CO<sub>2</sub> sink (Angert et al., 2012; Hilman, Angert, 2016). This work has led to the hypothesis that carboxylating enzymes, like PEPC, may play a large role in the fixation of respiratory CO<sub>2</sub>, an idea bolstered by unexpectedly high concentrations of PEPC in stem, which can be 13 times higher than the concentration of PEPC in leaves (Berveiller, Damesin, 2008; Hibberd, Quick, 2002). Beyond informing our understanding of the underlying respiratory physiology in woody tissue, the quantification of ARQ could help with the interpretation of wood CO<sub>2</sub> efflux values in relation to wood respiration, improving the understanding of the overall wood-derived respiratory load on a tree, rather than only its total carbon budget.

## **1.7 Woody tissue CO<sub>2</sub> efflux under drought conditions**

Woody tissue metabolism is expected to decrease under water deficit because of turgor loss (Steppe et al., 2015) and the associated decrease in growth respiration; however, there has been little research into this topic, and of the studies published, there have been conflicting findings. Most studies have found wood CO<sub>2</sub> efflux declines under water stress (De Roo et al., 2020; Lauriks et al., 2022; Rodríguez-Calcerrada et al., 2014; Saveyn et al., 2007), although others show that it increases (Rowland et al., 2018), or is unaffected (D'Andrea et al., 2020). Of these few studies, only Rowland et al. (2018) was performed in the tropics, and over a multi-decadal experimental drought.

## **1.8 The long term effects of drought on tropical rainforest: transition of a plant community to a new stable state**

Over very long periods of drought, tropical rainforest can have major structural and floristic changes, and even transition to a new biome evidenced by the current distribution of rainforests (Dexter et al., 2018; Fauset et al., 2012; ?) and the historical isotope and pollen record (Mayle et al., 2004; Pessenda et al., 1998; ?). Current tropical rainforest occurrence appears to be determined by the length and severity of the dry season (Hirota et al., 2011; Murphy, Bowman, 2012), as well as the annual rainfall, which may have a critical threshold of approximately 1500 mm per year (?). Yet, these critical limits are surmised from the natural distribution of tropical rainforests; no experimental or natural drought has been active long enough to test these critical limits or to describe the complete transition from a tropical rainforest to a new stable state. The results I report on in my thesis go further than previous experimental studies by approximately 15 years (Brando et al.,

2008), and so provide new empirically-driven insight into the longer term ecological processes affecting forest function under extended climate stress (Meir et al., 2018). This wider question is of acute interest in the tropics because the trajectory leading up to a new stable state imposed by drought is likely to first occur through plastic changes within surviving trees at multiple trait scales, followed by possible high mortality and eventual alterations in species composition and vegetation structure.

## 1.9 Field Site



Figure 1.1: Map of Caxiuanã National Forest Reserve, Pará - Brazil

All field research was performed at Caxiuanã National Forest Reserve, State of Pará (  $1^{\circ}44'13.31''\text{S}$ ,  $51^{\circ}27'43.49''\text{W}$ , Figure 1.1) located in north-eastern Brazil, eastern Amazonia. The site is a *terra-firme* rain forest receiving approximately 2000-2500 mm of rain yearly (Fisher et al., 2007). The site has yellow oxisol soil (Ruivo, Cunha, 2003) and mean air temperature of c.  $25^{\circ}\text{C}$ . During six months, from July to December, there is a pronounced dry season regularly receiving less than 100 mm per month, and with median surface soil volumetric water content below  $0.15\text{ m}^3\text{m}^{-3}$  (Bittencourt et al., 2020). In 2002, an experimental drought treatment (through fall exclusion experiment, TFE) was imposed on one hectare of tropical rainforest, in

order for the forest to receive approximately half of the 2000 mm of rainfall per year (Figure 1.2). Plastic panels were installed at an angle at 1-2 m in height in order to divert approximately 50% of the canopy-penetrating rainfall into a system of gutters (Fisher et al., 2007; Costa da et al., 2010). A 1.5 -2 m deep trench was created around the TFE to restrict lateral flow of water into the plot and also to transport the water channeled from the panels and gutters away from the plot. Leaves were removed from above the plastic panels and placed underneath the panels on the forest floor every 2-3 days. A one-hectare Control plot was established approximately 50 meters from the TFE with a trench also established around the plot to avoid differences in root damage confounding differences between the plots during the early stages of the experiment. Inevitably, some edge effects can be expected, and so, while monitoring is maintained for all trees, those within the outer 10 m of the plots are excluded from the detailed growth and physiology studies. A recent summary of main findings preceding this study is provided by Meir et al. (2018), with recent ecophysiological Rowland et al. (2021b); Giles et al. (2022); Bartholomew et al. (2020); Bittencourt et al. (2020); Eller et al. (2020) and Eller et al. (2018).

I note that given the ‘ecosystem-scale’ size of the 1 ha treatment that was required to account for the presence of large trees and expansive lateral roots, treatment replication was restricted in this experiment by financial resources, but where possible pre-treatment calibration measurements were made in both plots to enable replication over time (Meir et al., 2001; Rowland et al., 2015; Meir et al., 2018; Davidson et al., 2012). I note further that this method follows the design of other un-replicated large-scale ecosystem manipulation experiments (e.g. Likens et al., 1970) whose strength is acknowledged, especially where large treatment effects are expected (Hurlbert, 2004).

## **1.10 Overview of thesis**

Despite the large potential impact of drought induced plasticity on tree productivity, water use and survival, it remains unknown how detailed tree structural traits



Figure 1.2: Through fall exclusion (TFE) experiment located in Caxiuanã National Forest Reserve. Inclined plastic paneling removes approximately 50% of the rainfall from 1-ha plot.

and emergent stand-scale canopy structural properties may respond to an altered rainfall regime in the tropics. The majority of preceding research on this topic was done at coarse resolution (Doughty et al., 2015; Leitold et al., 2018; Saatchi et al., 2013), and overwhelmingly conducted after short term droughts, which are not directly translatable to the long-term (Meir et al., 2018). Growth responses resulting in coherent large-scale changes can only emerge at multi-year timescales. These combined limitations mean that fundamental questions about if and how tree canopies respond to drought remain unanswered, and that the implications of tree structural acclimation to climate change have not been incorporated into predicted carbon emission scenarios.

Here, I tested the effect of long-term drought on i) tree and stand structure, ii) stand wood  $\text{CO}_2$  efflux and iii) the resulting effects on aboveground carbon stock and growth dynamics using a one-hectare through fall experiment (TFE) in an eastern Amazonian tropical rainforest that has been maintained since 2002 to receive approximately half of the annual 2000 mm of rainfall. All results were compared against a one-hectare Control plot where no drought treatment has been imposed,

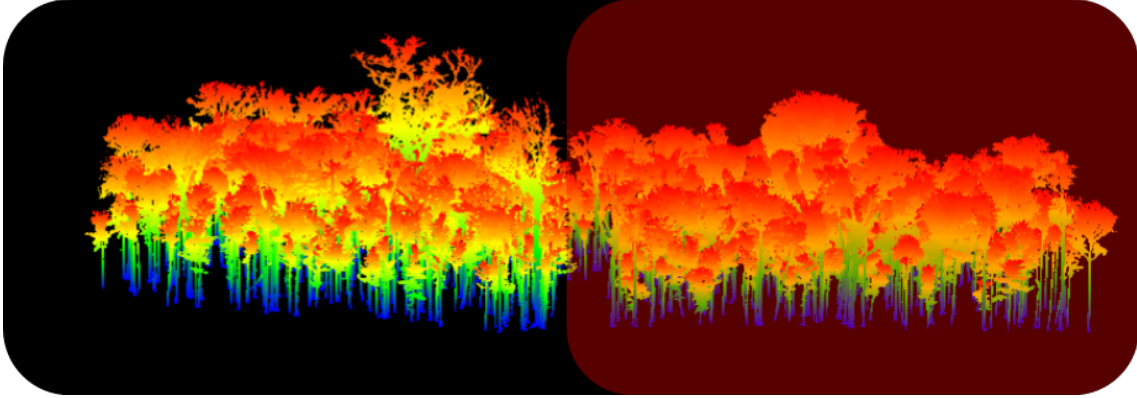


Figure 1.3: TLS point cloud data of Control (left) and TFE (red shading) in 2018 of all trees above 10 cm DBH, post-leaf extraction

but for which the same long-term datasets have been collected. TLS data were collected in 2018 for these two hectares of Amazonian rainforest (Figure 1.3) and quantitative structural models (QSMs) of over 500 individual trees were derived from the TLS data to determine tree structure and biomass. Very unusually, given the logistic difficulty of harvest-based studies, the QSMs were themselves also calibrated using destructive sampling of 4 trees in nearby forest, less than 10 km distant (Burt et al., 2021), enabling a level of precision in my structural analyses that is not usually available at any site, in remote or easily-accessible regions of the world.

In Figure 1.4, I show how this thesis progresses from assessing the effects of long-term drought on wood structure, wood tissue respiration, and forest growth dynamics, all of which aid in evaluating if trees experiencing long-term drought are likely to decline in function, or if, at stand-scale, there is evidence for their behaviour reaching a new stable state, perhaps in approximate steady state with the regime of water availability imposed by the experimental drought treatment. This thesis consists of an introduction, three data chapters, chapter 2 through chapter 4, and a final chapter discussing the thesis as a whole, describing the key findings in each chapter and the implications, and suggesting areas for future study.

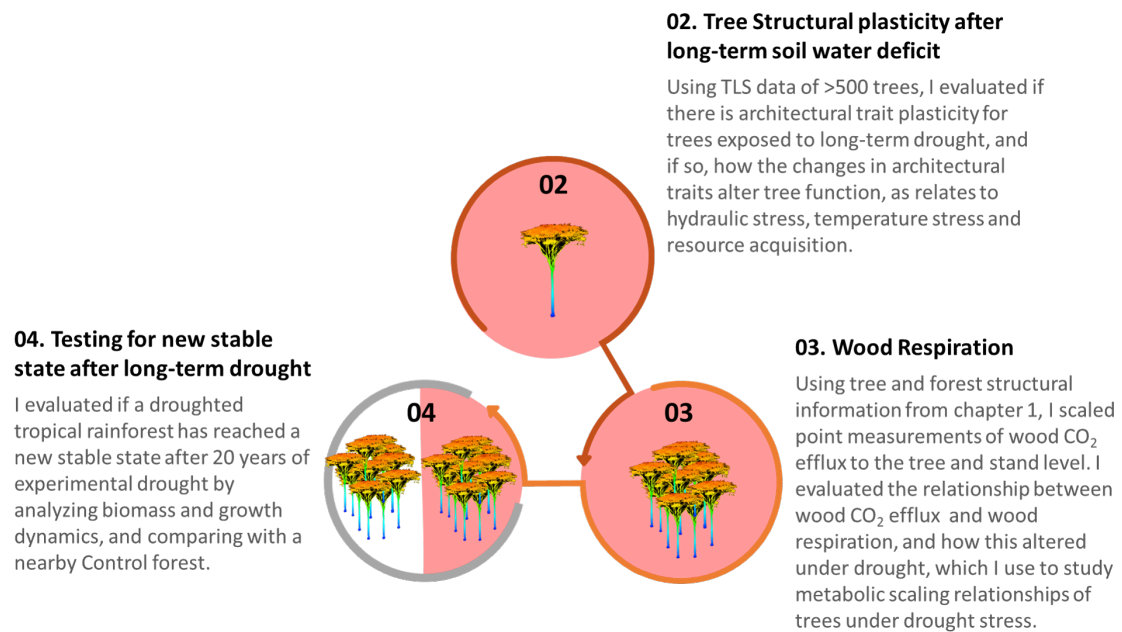


Figure 1.4: Schematic overview of thesis data chapters. Ch2: Tree structural plasticity under long-term experimental drought; Ch3: Structural and process-based analysis of woody tissue respiration during long-term experimental drought; Ch4: Forest dynamics over 20 years of experimental drought: tending to biomass collapse or a new stable state?

## 1.11 Layout of thesis

### 1.11.1 Chapter 2: Tree structural plasticity under long-term experimental drought

In Chapter 2, I tested for apparent plasticity in tree wood structural metrics, canopy-scale arrangement of leaves, and stand-scale structure of branches and twigs in response to drought stress to determine if changes occurred in the drought treatment, and if so, whether the changes were in line with *a priori* expectations of hydraulic stress mitigation. Using tree structural models derived from TLS data, I evaluated architectural changes that would indicate a change in whole tree hydraulic conductance, resource acquisition or thermal stress. Additionally, I determined whether hydraulic structural traits presented distinctly in small and large trees and if there was evidence of a maximum tree height-rainfall threshold resulting from the drought

manipulation experiment. The results will have application in helping to constrain fine and coarse scale land-surface models of vegetation function (Cleveland et al., 2015; Huntingford et al., 2017), and may ultimately enable connection of tree physiology with fundamental theories of plant structure and metabolism (Bentley et al., 2013; Enquist et al., 2007; Niklas, Enquist, 2001).

Key questions:

How do woody and leaf structural traits change in response to drought?

Do structural changes in trees have an interaction with tree size?

### **1.11.2 Chapter 3: Structural and process-based analysis of woody tissue respiration during long-term experimental drought**

In the Chapter 3, I scaled measurements of wood CO<sub>2</sub> efflux from organ to tree to stand on the TFE and adjacent Control plot using tree structural data derived from terrestrial laser scanning (TLS) in conjunction with extensive measurements of wood CO<sub>2</sub> efflux rates in the canopy and the stems of trees. Measurements of ARQ were used to translate woody tissue CO<sub>2</sub> efflux to woody tissue respiration, which was used to model whole tree woody respiratory load. Metabolic scaling approaches were compared using whole tree woody respiratory load versus whole tree wood CO<sub>2</sub> efflux. This approach offered to advance understanding of the respiration load experienced by large trees under drought (Mori et al., 2010; Reich et al., 2006) and to provide the first detailed data-based estimates of stand-scale efflux of woody CO<sub>2</sub>.

Key questions:

Have respiration rates altered due to TFE for woody tissue?

Has metabolic scaling of trees altered under drought due to tree structure or changes in metabolic rates?

Has stand wood CO<sub>2</sub> efflux decreased in response to water deficit?

### **1.11.3 Chapter 4: Forest dynamics over 20 years of experimental drought: tending to biomass collapse or a new stable state?**

In Chapter 4, I described the effect of drought on aboveground biomass (AGB) and growth dynamics using a one-hectare through fall experiment (TFE) in a tropical rainforest that has been maintained for 20 years to receive half of the yearly 2000 mm of rainfall at the site. I evaluated yearly AGB on the TFE and Control for 20 years, and studied the underlying components of AGB: tree woody growth ( $NPP_{\text{wood}}$ ), tree recruitment (trees that have reached 10 cm in DBH) and tree mortality. Prior to this study, the carbon dynamics of the TFE were studied 4, 7, 10 and 13 years after the experiment commenced (Metcalf et al., 2010a; Costa da et al., 2010, 2014; Rowland et al., 2015). The most recent assessment, in 2015, indicated that (i) the AGB of the TFE was declining rapidly due to biomass loss from large trees, resulting in 40% loss of the AGB in comparison to pre-experiment, and (ii) small and medium-sized trees were growing at accelerated rates, potentially indicating a plastic responses that resulted in improved tree function for this subset of trees. Here, I evaluated (i) the rate of AGB loss due to mortality, (ii) the rate of recruitment, (iii) and  $NPP_{\text{wood}}$  both as a stand, and for different size classes, to determine if the TFE reached a new stable state or continued to decline in function.

Key questions:

Does the TFE present with lower but stable biomass?

Are growth rates for small and large trees on the TFE reflecting altered competition for water and light following drought-related mortality?

Has rate of biomass loss due to tree mortality decreased on the TFE, following a steep decline in 2015?

# Chapter 2

## Tree structural plasticity under long-term experimental drought

### 2.1 Introduction

Environmental stress influences growth and reproductive success in all plants. The effects of stress can be predicted prior to the stress event by linking specific plant traits, and their plasticity, with success or failure. Predicting plant performance using traits is an idea that has attracted considerable attention in recent years (Wright et al., 2004; Kattge et al., 2011; Díaz et al., 2016); however, almost all of these trait-based approaches have considered structure or physiology at the scale of the organ, rather than at whole-tree or canopy scales, despite the recognition that canopies can reduce leaf area or shed whole branches in response to stress (Verbeeck et al., 2019; Nolan et al., 2021). New technology has led to discussion surrounding the quantification of whole-tree or canopy structure from a trait based perspective in order to better understand and quantify tree responses to environmental drivers (Meir et al., 2017; Malhi, 2018; Verbeeck et al., 2019; Calders et al., 2020). This also has application in trait theory and metabolic scaling theory (Enquist et al., 2009), as well as in practice, such as in silviculture (Calders et al., 2020).

While canopy architecture in relation to resource capture has long been studied

(Horn, 1971), and distinct canopy-scale traits exist across species and species groups (Verbeeck et al., 2019; Terryn et al., 2020), there are, to our knowledge, no tests to date of whether such canopy traits show consistent responses to manipulations in environmental conditions. Tree-scale properties change relatively slowly because growth is slow and trees are large organisms. In order to test whether plants are able to respond to environmental changes at the scale of the organism as well as the organ, and indeed a key test of whether there are other larger aggregate-scale effects that extend to the community, requires long-term monitoring in the context of a specific environmental change.

We present an ecosystem-scale test of these ideas using structural data for > 500 trees ranging from 10 to 173 cm in diameter at breast height, half of which have been exposed to a long-term (17-yr) reduction in soil water in a tropical rainforest. If growth patterns of rainforest trees can respond to water limitation within one generation, it is possible that the tree structures emerging after 17 years of water limitation would tend towards configurations that are hydraulically more robust to droughted conditions than in a non-droughted forest. Different trade-offs are possible. Alteration in display of leaves can enable optimization of carbon gain relative to light capture, with minimal water loss and heat damage; woody tissue may maximize growth, water supply, stability and spatial advantage for light capture, while minimizing hydraulic limitations such as overall hydraulic resistance in xylem (Valladares et al., 2007; Ishii, Asano, 2010; Kawamura, 2010; Niinemets, 2010; Kunz et al., 2019).

Plasticity in external tree structure during extended drought could impact tree survival by altering tree hydraulic conductance, resource acquisition efficiency and heat exchange. Architectural plasticity can be achieved by altering the absolute quantity and/or spatial distribution of individual organs over the whole tree. For example, hydraulic conductance could be increased by structural change that decreases friction- or gravity-related resistances in the hydraulic pathway, e.g. by reducing the mean path length (the mean distance from the base of the tree to the

tip of all branches), by reducing path length fraction (mean path length divided by maximum path length) or by re-distributing the majority of functional organs closer to the ground.

The potential role of any structural response to drought in ameliorating hydraulic performance could also be influenced by overall tree size. Since hydraulic vulnerability may increase with tree height (Olson et al., 2018; Koçillari et al., 2021), there may be discrete limits to tree height under different rainfall regimes (?) that partially reflect the maximum possible hydraulic impact of architectural plasticity among species and forest stands. Thus, where trees below a certain height threshold might survive under long-term water deficit by means of architectural plasticity in combination with physiological plasticity, trees larger than a particular threshold might die under severe drought if their maximum plastic response to drought is insufficient.

Here, we defined a set of tree structural traits, and tested whether these traits respond to drought stress in a manner that would favour hydraulic stress mitigation, specifically to improve the following: (i) tree hydraulic conductance by decreasing tree path length and reducing the overall height of tree organs; (ii) resource acquisition efficiency by minimizing carbon use while maximizing light interception; and (iii) thermal stress amelioration by biasing the location of canopy leaf area towards reduced afternoon sun exposure or increased exposure to sectors in the canopy space with higher average wind speeds and related turbulence. Overall we examine properties of architectural traits by testing for (i) apparent plasticity in tree structural metrics; (ii) whether hydraulic structural traits differ in small and large trees; and (iii) if there is evidence of a maximum tree height-rainfall threshold resulting from the drought manipulation experiment.

## 2.2 Materials and Methods

### 2.2.1 Site

Measurements were taken at Caxiuanã National Forest, Pará State in north-eastern Brazil (1°43'S, 51°27'W). This site is a *terra-firme* seasonal rainforest that receives approximately 2000 mm of rainfall a year, with six months of the year receiving less than 100 mm. The site has yellow oxisol soil (Ruivo, Cunha, 2003) and mean air temperature of c. 25 °C. The volumetric water content at 5 cm depth varies seasonally from approximately 0.05 in the dry to 0.30 m<sup>3</sup>m<sup>-3</sup> in the wet season (Bittencourt et al., 2020). Prevailing winds come from the north-east throughout the year (Appendix A.1).

### 2.2.2 Through-fall exclusion experiment (TFE)

In 2002, a through-fall exclusion experiment (TFE) was constructed on one hectare of tropical rainforest at Caxiuanã National Forest and paired with an adjacent one-hectare Control plot (Meir et al., 2018). Transparent panels were installed in the TFE plot at 1-2 meters above the ground to redirect approximately 50% of the rainfall to a system of gutters. A trench was dug around the TFE to prevent sub-soil water movement towards the droughted trees, and the Control plot was also trenched to facilitate comparison. The experiment requires daily maintenance and the leaf litter was removed from above the panels every 2-3 days and placed below the panels. See Fisher et al. (2007); Costa da et al. (2010); Rowland et al. (2015); Meir et al. (2018) for more details of the experimental design.

### 2.2.3 Sample selection

All individual trees in the 1 ha Control and 1 ha TFE were included in the analysis except for (1) trees  $\leq 10$  cm diameter at breast height (DBH), (2) trees within 10 meters of the edge of the treatment, which were not included to avoid possible edge effects caused by trenching (Rowland et al., 2015) and (3) lianas and palms. Census

data from October 2019 were used for measurements of DBH. All trees that had died throughout the experiment prior to 2020 were removed from the analysis, which in total resulted in 602 individuals, 298 individuals on the TFE, 304 individuals on the Control.

#### **2.2.4 Data collection**

Terrestrial laser scanning (TLS) measurements were made in October 2018, the dry season, with a RIEGL VZ-400 terrestrial laser scanner (RIEGL Laser Measurement Systems GmbH). Scans were conducted on a 10 m x 10 m grid for the Control and a 20 m x 20 m grid for the TFE treatment. Sampling strategy differed between treatments because of unexpected weather-related time restrictions. The RIEGL VZ-400 operates at a wavelength of 1500 nm, has a beam divergence of 0.35 mrad, and an exit diameter of 7 mm.

Terminal twigs ( $< 2.5$  cm basal diameter,  $N = 116$ ) were cut from trees in the Control and TFE by climbing and using pole pruners and were scanned individually using a Riegl VZ-400 indoors. Branches this small are not able to be adequately modelled using TLS data collected in the forest at this site, and therefore these close-range scans allowed for improved understanding of tree twig architecture. Tip diameters were measured manually for 3-5 different tips, and the basal diameter was measured twice. Retro-reflective tape was placed at 3-5 locations on the twigs, and the branch diameter was manually measured below the tape. This tape is visible on the TLS scans, and allows for comparison between the QSM models and the manual measurement of twig diameter.

All leaves were removed from the 116 twigs prior to scanning, and fresh and dry leaf mass were measured. Three sample leaves per twig were used to measure leaf mass to area (LMA), which was then applied to convert the mass of all leaves to an estimate of total leaf area of the branch. Previously, in September 2016, we also collected 128 measurements of twig diameter (basal diameter  $< 0.7$  cm) leaf area and LMA, which we have included in this study.

### 2.2.5 TLS wood structural models

The in-plot terrestrial laser scans were co-registered into a common coordinate system using RiSCAN PRO (v2.7.0) and the point clouds of trees above 10 cm DBH were partially automatically extracted using treeseg (?) and partially extracted manually. After extraction, leaf material returns were separated from wood using TLSeparation v1.0 (Vicari, Wilkes, 2018). Each tree was visually inspected to determine adequate leaf-wood separation using CloudCompare (CloudCompare, 2021), and some trees were manually edited to improve the final separation when necessary. Tree point clouds were matched to individual tree tags by manual identification in the field.

Prior to leaf separation, tree point clouds were used to measure: (i) tree height, which is the height of the tallest leaf; (ii) fork height, the height of first major branch; (iii) canopy depth, the difference between tree height and fork height; (iv) canopy projected area, which is the ground area of the canopy from a bird’s eye view; (v) canopy width, defined as the projected area multiplied by four, divided by the perimeter of the projected area; (vi) canopy convex hull volume, which is the minimum required volume to enclose the entire canopy; and (vii) canopy convex hull surface area, which is the surface area of the canopy hull volume. Three dimensional convex hulls were quantified using RLiDAR package (Silva et al., 2017); see Appendix A.2 for visual description of canopy hull and canopy projected area.

Whole tree quantitative structural models (QSMs) were constructed from woody tissue point clouds on the TFE and the Control, with point clouds extracted on a 20 x 20 m grid, using TreeQSM (v2.3.2) and the input parameters were automatically generated using optqsm v0.1.0 (Raumonen et al., 2013; Burt et al., 2021). Trees with buttresses were visually identified, and processed using TreeQSM with a triangulation for buttresses. Trees were also separately modelled using treegraph (Wilkes et al., 2021), after applying a branch path retrace during leaf-wood separation (Vicari et al., 2019) which detects the main pathways of all branches. Models from TreeQSM were used for all volume metrics, including canopy volume, tree vol-

ume, and height at 50% canopy volume, which is the height at which the cumulative sum of the canopy volume, starting from the base of the canopy, reaches 50% total canopy volume. QSMs from treegraph were used to quantify length metrics, including: (i) leaf-weighted mean path length ( $p_{mw}$ ), which is the length along the tree from the base of the tree to the tips of all the branches, with the mean of all path lengths weighted by the proportion of total tree leaf point cloud closest to a given branch tip; (ii) leaf-weighted path length fraction ( $p_{fw}$ ), which is  $p_{mw}$  divided by the maximum path length; and (iii) total tree length, which is the summed length of all the branches.

Aggregated profiles of woody volume were compared using Control trees extracted on a 10 x 10 m grid and modelled using optqsm v0.1.0, and TFE trees extracted and modelled on a 20 x 20 m grid. Since aggregate profiles on a subset of Control trees differed when extracted on a 10 x 10 m grid versus a 20 x 20 m grid, TFE tree profiles were corrected using a modelled relationship between volume per height on a 10 x 10 m versus 20 x 20 m grid of 146 trees. Profiles for tree canopy and tree stem were corrected separately; see Appendix A.1, A.3, for further information. The error for each QSM was estimated by using mean tree error from a nearby destructive harvest study of several trees (Burt et al., 2021) and the error was distributed equally per height bin. It was not possible to aggregate triangulated buttress volumes into height bins, so all buttresses were identified and were fitted using a cylinder that was the length of the buttress and the diameter of DBH. This correction was only necessary for aggregated profiles, and all individual tree comparisons were made with the triangulated volume of buttresses.

All structural parameters for twigs were cleaned and modelled using treegraph (Wilkes et al., 2021), which has been optimized for determining tree length metrics and for small twig structural modeling. The modeling of twig radius below 2 mm was not possible with current models, and therefore the model was corrected using a relationship between manual measurements and model values at 2-5 locations per branch.

### 2.2.6 TLS leaf structure

Leaf point clouds were separated from wood point clouds using TLSeparation v1.0 (Vicari, Wilkes, 2018) and were visually checked for adequate separation using CloudCompare (CloudCompare, 2021). All leaf points below the tree fork height were excluded, and separation was manually improved after extraction when necessary. Leaf point clouds were downsampled by finding the mean of the four nearest neighbor distance per 2 meter bins, and the maximum mean nearest neighbor distance was used to downsample the remaining leaf point cloud. The fraction of tree leaf area per 2 m bin within an individual tree was taken as the total number of points in a given 2 m bin, divided by all points in the tree. The same process was performed across the plot, however, when points were aggregated by plot the down-sampling was performed using the maximum nearest neighbor distance of all trees in a given plot to obtain the plot level distribution of leaves.

The division between cardinal sides of the tree was defined as the tallest point of the canopy, due to the shading effects of the canopy on either side of the point of maximum tree height. Leaf distributions are presented as the mean percent of leaves of all sampled trees in a treatment at a particular compass direction. The total number of leaf points on the Control plot trees was modelled using an allometric relationship of total points in a tree leaf point cloud, with dependent variables of canopy width and DBH ( $R^2 = 0.88$ , Appendix A.4 ,  $N = 310$ ), where all leaf point clouds were downsampled by plot maximum nearest neighbor of the leaf point clouds; this relationship was applied to all remaining trees in the Control plot. Using previously measured mean leaf area index (LAI) of  $5.6 \pm 0.3$  (Malhi et al., 2009b) in the Control, the percentage of leaf points per tree with respect to total leaf points of the plot was converted to leaf area. The same allometric relationship relating total tree leaf points to tree structure (Appendix A.4) was applied to the TFE plot trees. Definitions and further details for all tree structural properties measured can be found in Table 2.1.

Table 2.1: Definitions of structural traits referenced in text and which TLS dataset used for the structural trait.

\*See Appendix A.2 for visual description of structural characteristics.

Variable	Units	Definition	Dataset
Tree height	m	Maximum height of leaf minus minimum height of tree	Point clouds
Canopy depth	m	Tree height minus height of first branch, where first branch is considered first major branching fork	Point clouds
Height at 50% $V_{\text{canopy}}$	m	Height at which cumulative sum of canopy volume, starting from the base of the canopy, reaches 50% total canopy volume	Volume-optimized QSM
Canopy width*	m	4* area of 2D projected convex hull of canopy in the xy plane, divided by perimeter of the convex hull polygon	Point clouds
Mean leaf-weighted tree path length ( $P_{\text{mw}}$ )	m	Path length is the minimum distance along a tree from the base of the tree to the tip of a branch. All branches consisting of a single cylinder were excluded from the analysis. The mean of the path length is weighted by the proportion of leaves closest to a given branch tip	Length-optimized QSM
Mean twig path length ( $P_{\text{mtwig}}$ )	m	Mean path length from the base of a twig to the tip of a twig	Close-range indoor scanning, length-optimized QSM
Leaf-weighted path length fraction of tree ( $P_{\text{fw}}$ )	m/m	Mean leaf-weighted tree path length divided by maximum path length	Length-optimized QSM
Total tree length ( $L_{\text{tree}}$ )	m	Length of all individual cylinders excluding cylinders below 5 cm in diameter	Length-optimized QSM
Twig length ( $L_{\text{twig}}$ )	m	Length of all cylinders within a twig	Close-range indoor scanning, length-optimized QSM
Total tree woody tissue volume ( $V_{\text{tree}}$ )	$\text{m}^3$	Volume of entire tree woody tissue, excluding branches <5 cm in diameter	Volume-optimized QSM
Total canopy volume ( $V_{\text{canopy}}$ )	$\text{m}^3$	Volume of tree woody tissue above and including height of first major branch, excluding branches <5 cm diameter.	Volume-optimized QSM
Canopy surface area: volume ratio ( $cs/cv$ )*	$\text{m}^{-1}$	The surface area of the 3D convex hull of the canopy divided by the volume of the 3D convex hull of the canopy, where canopy includes both leaf and wood point cloud	Point clouds
Canopy leaf distribution by compass direction	%	Number of points in leaf point clouds every 30 degree divided by all the points in the leaf point cloud	Leaf point clouds

## 2.2.7 Statistics

All statistical analyses were performed in R (v4.0.3, R Core Team, 2020). We fit linear mixed effects models to test for treatment effects on structural traits, with genus as a random effect. Genus-specific coefficients are listed in Appendix A.6. Marginal  $R^2$  ( $R^2_m$ ) and conditional  $R^2$  ( $R^2_c$ ) for linear mixed models are presented. When the random effect was not significant, we used linear models. Excluding random effects did not change any of the conclusions presented here. Where noted, we log-transformed variables for linearity prior to fitting. Akaike Information Criteria (AIC) was used to compare models after stepwise removal of the fixed effects. When comparing aggregate tree structure characteristics, trees were classified according to size class, where size class was separated into small trees (10-20 cm DBH), medium trees (20-40 cm DBH) and large trees ( $> 40$  cm DBH).

## 2.3 Results

The results are presented in terms of structural traits as they relate to tree: (i) hydraulic conductance, (ii) resource acquisition and (iii) heat exchange, with a final section describing the effects of structural changes at the aggregate (forest stand) scale.

### 2.3.1 Hydraulic conductance

TFE tree height was lower by  $1.2 \pm 0.3$  m than in the Control plot when adjusted for fixed effects of DBH ( $R^2_c = 0.81$ ,  $R^2_m = 0.76$ ,  $N = 560$ , Table 2.2). Additionally, the height at which the cumulative canopy volume of trees reaches 50% of the total volume, when measured starting from the lowest canopy branches, is lower on the TFE by  $2.8 \pm 0.3$  m, when adjusted by DBH ( $R^2 = 0.74$ ,  $N = 314$ , Table 2.2).

We found differences in length metrics for trees on the TFE in comparison to the Control for (i) total tree length, which is the sum of lengths of all branches in the tree ( $L_{\text{tree}}$ ); (ii) leaf weighted mean path length ( $p_{\text{mw}}$ ), which is the mean path

Table 2.2: Tree architectural traits. Parameter estimates for linear regression models describing tree structural traits using diameter at breast height (DBH) and TFE treatment. No interaction term between TFE and DBH was present for any trait. Tree structural traits modelled include: tree height (m), canopy depth (m), height at 50% canopy volume ( $H_{t_{50\%V_c}}$ , m), canopy width (width, m), leaf weighted path fraction ( $p_{fw}$ ), leaf-weighted path length mean ( $p_{mw}$ , m), tree length ( $L_{tree}$ , m), the ratio of leaf canopy surface area to leaf canopy volume, as measured using convex hulls ( $cs/cv$ ,  $m^{-1}$ ), tree woody tissue volume ( $V_{tree}$ ,  $m^3$ ), tree canopy woody tissue volume ( $V_{canopy}$ ,  $m^3$ ). For more detail on how dependent variables are calculated or definition thereof, refer to Table 2.1. Dash indicates that variable dropped out of final model. Where noted, variables are log transformed for linearity. Standard error of coefficients reported in parentheses. \*,\*\*,\*\*\* indicates significance at 90%, 95% and 99% level, respectively. Genus was tested as a random effect for each model, and if significant, the conditional  $R^2$  ( $R^2_c$ ) and marginal  $R^2$  ( $R^2_m$ ) are presented.

	intercept	log(DBH)	TFE	N	$R^2$	$R^2_c$	$R^2_m$
Tree height	-12.87 (0.95) ***	11.93 (0.30) ***	-1.23 (0.30) ***	560		0.81	0.76
$H_{t_{50\%V_c}}$	-10.36 (0.96) ***	8.43 (0.31) ***	-2.83 (0.32) ***	314	0.74		
log(width)	0.14 (0.07) *	0.58 (0.02) ***	-0.07 (0.02) ***	530		0.65	0.61
$p_{fw}$	0.78 (0.01) ***	-	-0.06 (0.01) ***	264	0.14		
$p_{mw}$	-14.64 (1.1) ***	12.1 (0.38) ***	-1.40 (0.37) ***	265	0.81		
log( $L_{tree}$ )	2.49 (0.22) ***	0.81 (0.07) ***	-0.45 (0.07) ***	249	0.41		
log( $cs/cv$ )	1.50 (0.06) ***	-0.53 (0.02) ***	0.07 (0.02) ***	574	0.59		
log( $V_{tree}$ )	-6.81 (0.13) ***	2.08 (0.04) ***	-0.35 (0.04) ***	318	0.89		
log( $V_{canopy}$ )	-9.03 (0.33) ***	2.49 (0.11) ***	-0.60 (0.11) ***	272	0.69		

length between the base of the tree and the tips, with the mean weighted by the proportion of total tree leaves located near the branch tip; and (iii) leaf-weighted path fraction ( $p_{fw}$ ), which is the  $p_{mw}$  divided by the maximum length from the base of the tree to the tip (see Table 2.1 for details on each variable).  $L_{tree}$  was modelled by DBH and treatment, and was found to be  $37 \pm 4\%$  smaller on TFE trees in comparison to Control ( $R^2 = 0.41$ ,  $N = 249$ , Table 2.2). The  $p_{mw}$ , modelled by DBH and treatment, was  $1.4 \pm 0.4$  m smaller on the TFE than Control trees ( $R^2 = 0.81$ ,  $N = 265$ , Table 2.2), and  $p_{fw}$  was  $0.06 \pm 0.01$  smaller for TFE trees than the Control, with DBH dropping out of the final model ( $R^2 = 0.14$ ,  $N = 264$ , Table 2.2).

For excised twigs (basal diameter  $< 2$  cm,  $N = 99$ ), mean path length ( $p_{mtwig}$ ), measured as the mean length between the base and tip of the twig tips, was smaller

Table 2.3: Twig mean path length. Parameters estimates for linear model of mean path length for twigs ( $p_{\text{mtwig}}$ , m) for twigs between 0.5 and 1.5 cm basal diameter with fixed effects of total twig length ( $L_{\text{twig}}$ , m) and TFE treatment. Variables are log transformed for linearity where noted. Standard error of coefficients reported in parentheses. \*, \*\*, \*\*\* indicates significance at 90%, 95% and 99% level, respectively.

	intercept	TFE	$\log(L_{\text{twig}})$	N	$R^2$	rse
$\log(P_{\text{mtwig}})$	-0.48 (0.09) ***	-0.13 (0.05) *	0.18 (0.04) ***	99.00	0.32	0.24

by approximately  $12.5 \pm 4.4\%$  on TFE branches in comparison to the Control when modelled with fixed effects of total twig length and treatment (Table 2.3,  $R^2 = 0.32$ ). Additionally, the allometry for twig length ( $L_{\text{twig}}$ ) was distinct on the TFE, with  $L_{\text{twig}}$  on the TFE approximately  $37 \pm 8\%$  shorter when length is modelled as a function of twig basal diameter (Table 2.4,  $R^2 = 0.26$ ,  $N = 110$ ).

Twig leaf area modelled by twig basal diameter, treatment, and interaction between DBH and treatment ( $R^2 = 0.75$ ,  $N = 351$ , Table 2.4), indicated that the TFE had a slightly larger leaf area by approximately 11% on small diameter trees (10 cm DBH), but that there was a negative relationship between DBH and TFE, such that trees larger than approximately 20 cm DBH on the TFE plot had relatively less leaf area per twig basal diameter than in the Control plot trees; a counterfactual plot for the model of leaf area is attached in Appendix A.4 for visualization.

Table 2.4: Twig allometric models. Linear models of twig (0.5 - 1.5 cm basal diameter) leaf area (LA,  $\text{m}^2$ ), twig volume ( $V_{\text{twig}}$ ,  $\text{m}^3$ ), and twig length ( $L_{\text{twig}}$ , m) using basal diameter (diameter, cm), tree diameter at breast height (DBH, cm) and TFE treatment. Dash indicates that variable was not included in the model. Standard errors reported in parentheses. \*, \*\*, \*\*\* indicates significance at 90%, 95% and 99% level, respectively.

	intercept	TFE	$\log(\text{diameter})$	$\log(\text{dbh}):TFE$	N	$R^2$	rse
$\log(LA)$	-0.58 (0.10) ***	0.57 (0.17) ***	1.61 (0.06) ***	-0.21 (0.05) ***	351	0.75	0.51
$\log(V_{\text{twig}})$	-14.9 (0.8) ***	-0.38 (0.16) *	2.0 (0.33) ***	-	110	0.39	0.73
$\log(L_{\text{twig}})$	0.18 (0.69)	-0.47 (0.27) ***	0.80 (0.27) **	-	110	0.26	0.61

### 2.3.2 Resource acquisition efficiency

The ratio between leaf canopy surface area and volume, as measured with 3D convex hulls (for clarification on 3D hulls, see Appendix A.2), was larger on the TFE than the Control plot by  $7.2 \pm 2.1\%$ , when modelled as a function of DBH ( $R^2 = 0.59$ ,  $N = 574$ , Table 2.2). The mean canopy width, modelled by tree DBH, was  $6.7 \pm 1.9\%$  smaller on the TFE ( $R^2_c = 0.65, R^2_m = 0.61$ ,  $N = 530$ , Table 2.2). The allometry of tree woody tissue volume ( $V_{\text{tree}}$ ) and woody canopy volume ( $V_{\text{canopy}}$ ) also showed differences, with smaller  $V_{\text{tree}}$  and  $V_{\text{canopy}}$  on the TFE than the Control when modelled using  $\log(\text{DBH})$  by approximately  $30.6 \pm 2.6\%$  ( $R^2 = 0.89$ ,  $N = 318$ , Table 2.2) and  $44.5 \pm 5.8\%$  ( $R^2 = 0.69$ ,  $N = 272$ , Table 2.2), respectively. At the twig-scale, the allometry of twig woody tissue, modelled using twig basal diameter, showed a smaller twig volume in the TFE than in the Control, by approximately  $32 \pm 11\%$  ( $R^2 = 0.39$ ,  $N = 110$ , Table 2.4).

### 2.3.3 Heat exchange

The distribution of leaf area by compass direction differed between TFE and Control trees, with relatively more leaf area within a tree between  $330^\circ$  to  $60^\circ$ , that is north to north-east, on TFE trees. By contrast, Control plot trees had a mean leaf distribution similar to a perfect circle (Figure 2.1, Control  $N = 109$ , TFE  $N = 116$ ). Fewer leaves on average were distributed between  $180^\circ$  and  $240^\circ$ , south to south west, on the TFE than on the Control (Figure 2.1). There was no effect of tree height on the distribution of leaves to the north-east.

### 2.3.4 Aggregate TFE structural properties

The aggregated woody biomass in the TFE plot showed a vertical profile that was distinct from the Control, with (i) a higher percentage of woody biomass distributed below 12 m; a lower percentage of woody biomass distributed between 12 and 30 m; and a higher percentage between 30 and 39 m (Figure 2.2). Aggregate canopy structure on the TFE was also different from the Control, with the peak density of

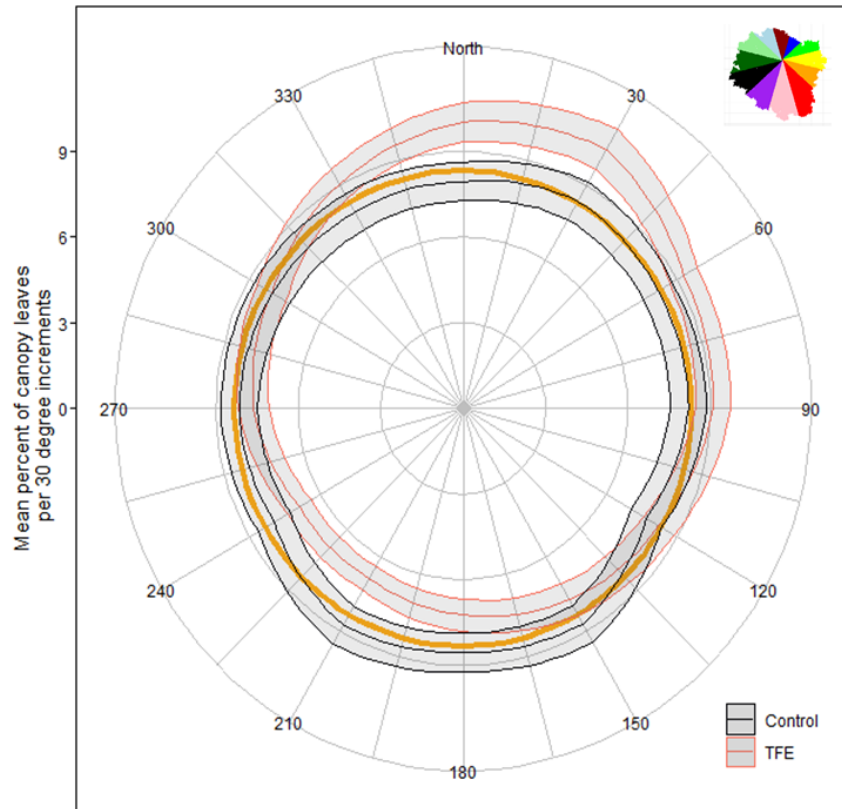


Figure 2.1: Canopy leaf area distribution. Graph of mean leaf distribution across cardinal and ordinal directions (every 30°) with lines indicating the mean percent of leaves per 30° interval across leaf canopies in the Control (black, N = 108) and TFE (red, N = 116), and a perfect circular canopy (bold orange), ie the black line at 180° is 8.5%, meaning that on average 8.5% of Control canopy leaves are located on the south side of the canopy (165° to 195°). The centre of the canopy is the highest point of the canopy. Shading represents standard error. Coloured inset demonstrates the partitioning of leaves for a sample canopy, as seen from bird's eye view, with the centre point the highest point of the tree, and a pie slice every 30°.

leaf area between 12 and 15 m above the ground on the TFE in comparison to the peak on the Control higher up, between 18 and 24 m (Figure 2.3A). The canopy woody volume profile is only moderately different on the TFE with respect to the Control, with more woody tissue below 15 m on the TFE, and no woody tissue above 39 m on the TFE. When comparing aggregate structure across different size classes, small trees (10-20 cm DBH), medium trees (20-40 cm DBH) and large trees (>40 cm DBH), the peak of the distribution of canopy woody and leaf tissue is lower on the TFE than in the Control (Figure 2.3B), with the shift in tissue height most apparent in small trees.

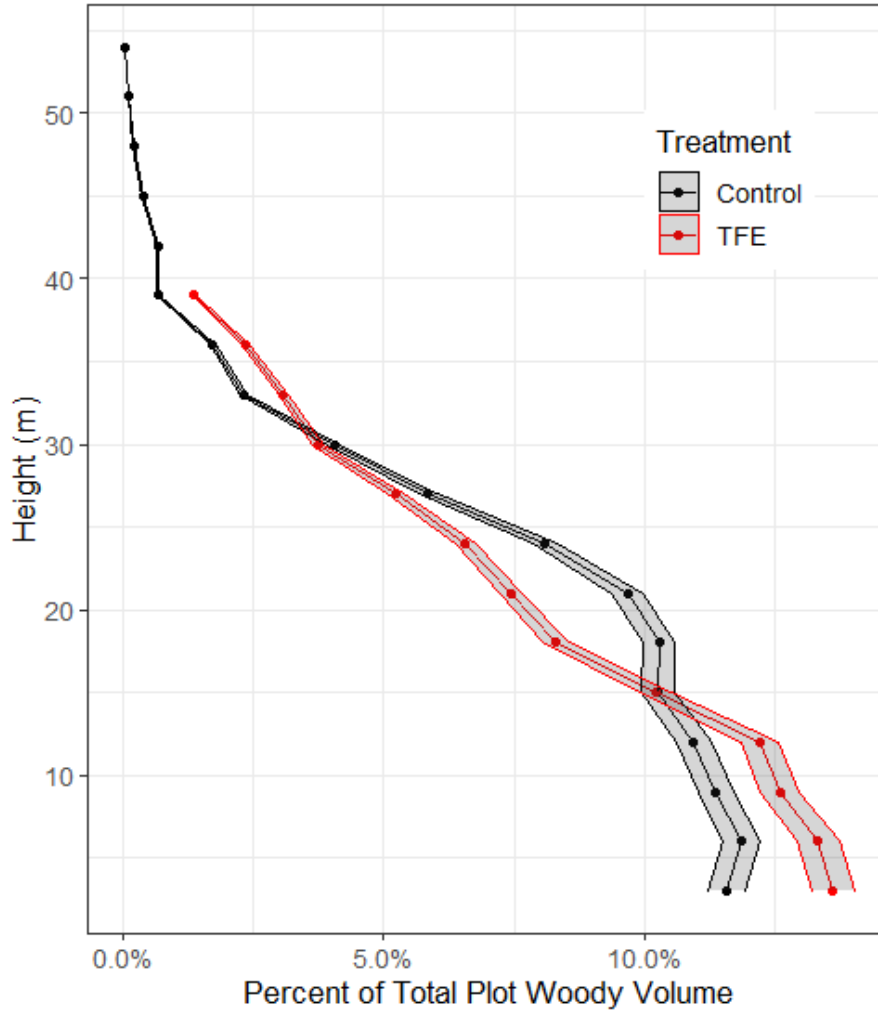


Figure 2.2: Woody volume distribution of trees above 10 cm DBH plotted against the height of the plot, where volume is binned every 3 meters for Control (black,  $N = 269$ ) and TFE (red,  $N = 170$ ). Not all trees in each treatment were included in this graph, since many trees were not successfully modelled using QSMS. Error (shaded) is estimated from nearby felled tree TLS- comparison (Burt et al., 2021).

Leaf area index (LAI) on the TFE was  $29 \pm 6\%$  lower than the Control (Figure 2.4A), and total woody tissue volume on the TFE was  $55.6\% \pm 3.0\%$  lower than the Control (Figure 2.4B), resulting in the ratio of plot-level leaf area to woody tissue volume in the TFE to be approximately  $22 \pm 9\%$  larger than the Control. When LAI and woody tissue are cumulatively summed starting from the shortest tree, a decrease in LAI after 25 m height and woody tissue after 22 m height occurs in the TFE compared to the Control (Figure 2.4).

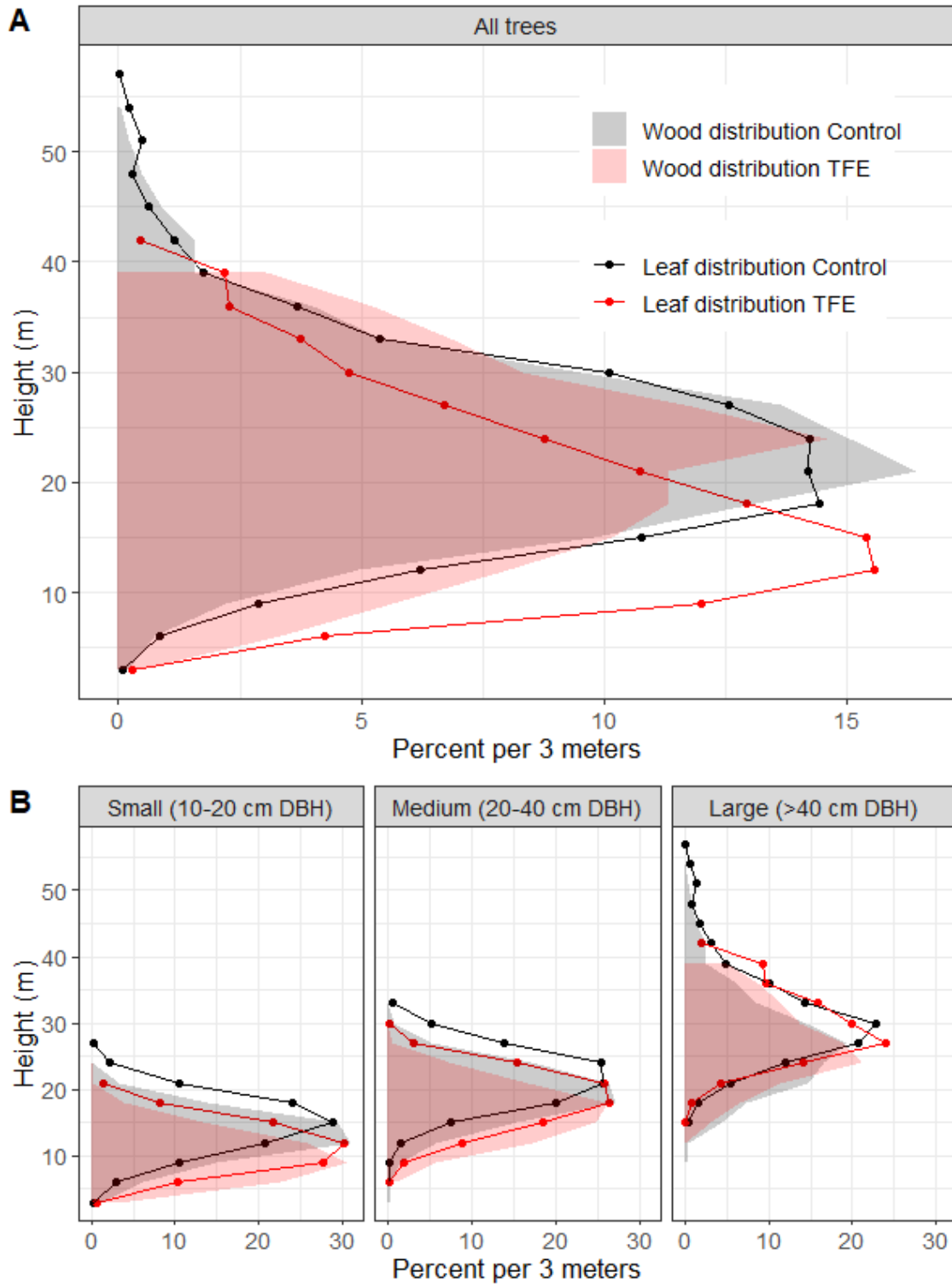


Figure 2.3: Canopy distribution of woody tissue volume (shaded) and percentage of total leaf area (points) every 3 meters (A) for all trees above 10 cm DBH, aggregated across the entire plot and (B) aggregated by tree size: small trees (10-20 cm DBH), medium trees (20-40 cm DBH) and large trees (>40 cm DBH) for Control (black) and TFE treatment (red). The amount of leaf and wood are binned every 3 meters, and the distributions are presented as a percent of total leaf area or woody tissue volume in given size class and treatment.

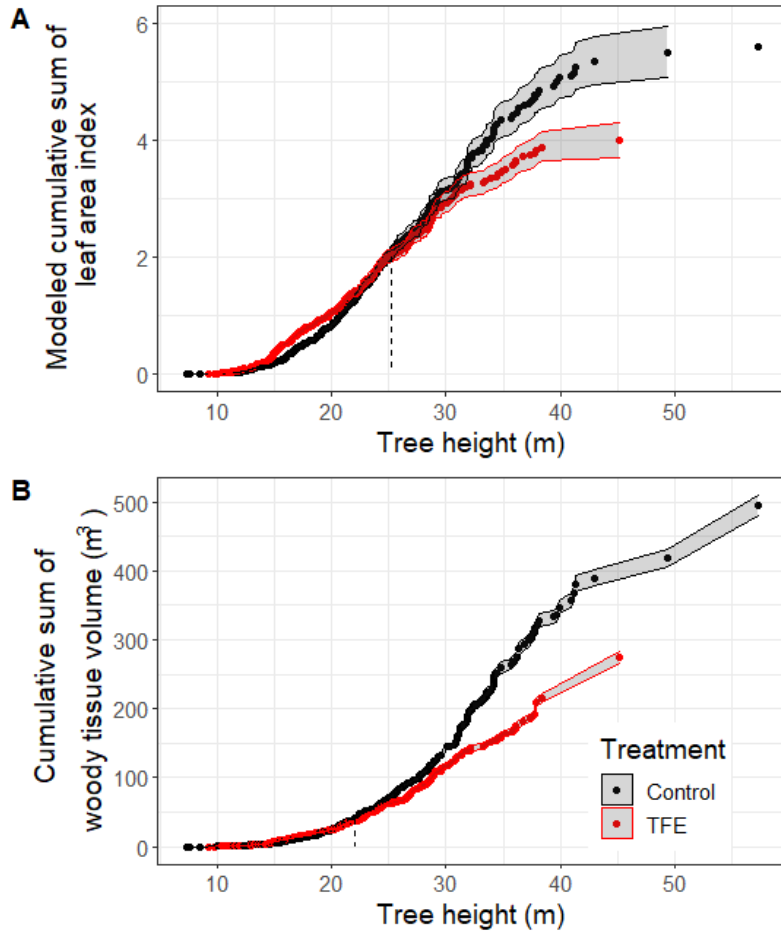


Figure 2.4: Cumulative sum of (A) leaf area index (LAI,  $\text{m}^2\text{m}^{-2}$ ) and (B) wood volume ( $\text{m}^3$ ), where wood volume is presented as the sum of all tree wood volume in the inner 80 x 80 m sampling plot on TFE (red) and Control (black) starting from shortest tree in each treatment. Each point represents an individual on the treatment. Shaded region on the leaf area graph is the 95% confidence interval, in addition to the error of the measured LAI. Shaded region on the wood volume graph is an estimate of error based on nearby felled experiment (Burt et al., 2021). Dashed lined indicates the first height at which TFE cumulative sum is lower than Control.

## 2.4 Discussion

Our analysis focused on testing for differences between adjacent 1 ha plots of tropical rainforest, one of which had been subjected to a soil water deficit for 17 years that generated increased long-term plant moisture stress (Costa da et al., 2018; Bittencourt et al., 2020). We found substantial differences between the droughted (TFE) and non-droughted (Control) treatments for several structural metrics of whole-tree woody and leaf tissue arrangement within the canopies of hundreds of individual trees. Our analysis also demonstrated that these individual tree differ-

ences were expressed in aggregate, highlighting the differences at scale of the forest canopy between droughted and non-droughted forests. To our knowledge, this analysis provides the first holistic picture of the response by adult trees to long-term manipulation of drought in terms of architectural metrics, from twig to tree canopy, to forest canopy. The individual-level responses to the long-term drought imposed by the TFE treatment suggests that these metrics can be considered as plant traits, such that plasticity in them is consistent with the avoidance of drought stress, at the scales of individual trees and the forest stand, by improving hydraulic conductance, resource acquisition efficiency, and/or optimizing heat transfer. Only some of these differences in trait values can be attributed definitively to changes in the growth response to drought, as whole-tree structural traits can also be a function of branch mortality, increased post-mortality light levels (Rowland et al., 2015, 2021a), canopy-canopy collision of falling trees due to elevated tree mortality, or water deficit-related slowing in growth. Many of these whole-tree structural traits are also reflected in structural traits of twigs, which are themselves small enough to have grown fully during the TFE treatment, and whose interpretation is not confounded by branch mortality or canopy-canopy collisions.

The recent emergence of TLS measurement and analysis methods (Calders et al., 2015a; Vicari et al., 2019; Disney, 2019; Verbeeck et al., 2019) means that a similar structural analysis from the start of the experiment 17 years previous to the measurements reported here is not possible. For this reason, while we argue that our analysis provides very strong evidence for the existence of plasticity in trait response at multiple architectural scales, we acknowledge that we cannot definitively ascribe the differences between the plots to individual tree responses over time, although we note that twin-plot analyses demonstrated extremely close structural and functional similarity prior to the TFE treatment, followed by progressive alterations in biomass and function in the droughted forest trees, as the TFE treatment extended into the longer term (Fisher et al., 2007; Costa da et al., 2010; Metcalfe et al., 2010b; Rowland et al., 2015; Meir et al., 2018).

### 2.4.1 Hydraulic Conductance

The differences observed in the droughted trees on the TFE versus Control indicate alterations that would improve leaf water access by reducing leaf-specific hydraulic resistance of woody tissue while, for large trees, decreasing leaf area, resulting in increased water transport efficiency. Leaf-weighted mean path length ( $p_{mw}$ ), leaf-weighted path fraction and total tree length were smaller on the TFE trees across all tree sizes, which may reduce friction-related hydraulic resistance (Smith, Sperry, 2014). If conduit tapering were negligible, hydraulic resistance would be linearly and negatively related to length of conduit, and the decrease of total tree length TFE by  $37 \pm 4\%$  (Table 2.2) would translate to a 1.6-fold increase in hydraulic conductance. However, the magnitude of the effect of tree length on total tree resistance is not clear as conduit tapering has not been measured, and tapering can mitigate the effect of length on total tree resistance (Becker et al., 2000; Mencuccini et al., 2007). Since water potential decreases 0.0098 MPa per meter of increased height, gravity-related resistance in trees would also be marginally smaller on the TFE since tree height was shorter for a constant DBH by  $1.2 \pm 0.3$  m, and the height at 50% canopy volume was lower by  $2.8 \pm 0.3$  m (Table 2.2).

The mechanism for alterations in  $p_{mw}$ , tree length and tree height may result from a mismatch between minimum vessel diameter and abiotic conditions in the experiment (Koçillari et al., 2021; Olson et al., 2021). Theory and field measurements (Olson, Rosell, 2013; Olson et al., 2018; Koçillari et al., 2021) indicate that the minimum twig conduit diameter is linked to abiotic conditions, and when abiotic conditions become drier, the minimum twig conduit diameter decreases, to lower the risk of embolism occurrence. Branch mortality at tree extremities during or following drought has been documented (McDowell et al., 2008; Anderegg et al., 2016; Li et al., 2018; Nolan et al., 2021), and may occur because of minimum twig conduit diameter limitations, contributing to the smaller  $p_{mw}$ , tree height and total tree length recorded for the TFE.

Reductions in leaf area decrease maximum canopy transpiration rates and in-

crease sapwood to leaf area ratio, improving efficiency of water transport to the remaining leaves. Interestingly, leaf area measured on twigs (basal diameter < 2.5 cm) was affected by a size interaction with TFE: trees below 20 cm DBH had more leaf area and trees above 20 cm DBH had less leaf area relative to Control plot trees (Table 2.2, Appendix A.4). This could indicate that large trees are more affected by the soil moisture deficit in the TFE, and respond by reducing leaf area, while small trees may benefit from reduced competition and increased light levels due to previous tree mortality (Rowland et al., 2021a), and maintain their leaf area. This outcome would be consistent with the higher observed tree mortality in larger trees (Rowland et al., 2015) and previously measured organ-scale traits, such as reduced metabolic rates (Rowland et al., 2021a) and leaf water potential (Bittencourt et al., 2020) and reduced hydraulic conductance (Giles et al., 2022) relative to smaller trees.

## 2.4.2 Resource acquisition efficiency

Our canopy structural analysis showed that, relative to non-droughted Control trees, droughted TFE trees had an altered outer leafy canopy structure and inner network of branches such that carbon use (estimated by branch tissue volume) was reduced, and light capture was increased, potentially increasing their net acquisition efficiency for light and carbon. The leafy canopy of TFE trees had a higher surface area to volume ratio (cs:cv) by  $7.2 \pm 2.1\%$ , when compared to Control, likely a by-product of TFE tree canopies being smaller with a  $44.5 \pm 5.8\%$  reduction of canopy woody tissue volume on the TFE for a given tree size, as smaller canopies have higher cs:cv ratios. The reduced leaf-weighted tree path fraction ( $p_{fw}$ ) in the TFE versus Control trees may also enable a higher carbon-use efficiency, as a shorter path length requires shorter tissue length and smaller tissue volume for a given tree size (Smith, Sperry, 2014). This was reflected in the  $37 \pm 4\%$  smaller total tree length and the  $30.6 \pm 2.6\%$  smaller tree woody tissue volume by DBH for trees exposed to TFE in comparison to Control trees (Table 2.2). Importantly, the structural metrics

for twigs ( $< 2.5$  cm diameter, Table 2.3, 2.4), which, unlike whole-tree metrics, are not potentially confounded by the effects of branch mortality or canopy-canopy collisions, were consistent with the whole-tree patterns of lower  $p_{mw}$ , smaller volume, and shorter length. The TFE vs Control differences for twigs thus provide a clear link connecting observed structural trait differences with a growth-response strategy that influenced measurable structural traits, in this case, minimizing path length, improving transport efficiency and decreasing carbon cost under drought stress.

### 2.4.3 Optimizing heat transfer

At the time of measurement, the trees on the TFE plot would have experienced a long term (17-year) reduction in soil water availability, and in addition, many would have been exposed to higher daily radiation than in the Control plot, as a result of canopy gaps created from elevated large-tree mortality on the TFE since 2001. This suggests that heat stress is likely to have been higher in the TFE trees, consistent with differences in leaf-scale gas exchange capacity and temperature response data for the TFE vs Control plots (Rowland et al., 2021a, Doherty et al., in review)

While changes in leaf orientation have been observed in multiple contexts to reduce leaf-scale interception of radiation in high temperature environment (Medina et al., 1978; He et al., 1996), the extent to which trees can mitigate temperature stress through structural plasticity is largely unstudied at the scale of the full canopy. Here, we consider two possible strategies for mitigating temperature stress: (i) reducing solar exposure of leafy tissue during the afternoon when solar radiation is high and soil moisture availability is at a minimum (Pons, Welschen, 2003; Brodrigg, Holbrook, 2004; Kamakura et al., 2011) and (ii) increasing leaf tissue area in the part of the canopy where wind speed and related turbulence is routinely high, thereby potentially increasing water use efficiency (Schymanski, Or, 2016).

Our analysis shows that more leaf tissue was allocated to the east and north sides of the TFE tree canopies, in the direction of the morning (eastern) sun and the prevailing winds (Figure 2.1, Appendix A.1). Westerly afternoon sun reaches

the leaves when pre-dawn soil xylem and leaf water reserves have been maximally depleted, air and leaf temperatures are highest, and stomatal conductance tends to be strongly reduced. We suggest that greater leaf growth on the eastern side of TFE tree canopies would have contributed to more favourable leaf and canopy temperature regimes, thereby enhancing gas exchange under reduced soil water supply.

We note a further possible explanation for the bias in leaf area to the north. High wind speed maximizes turbulent heat exchange from leaf to air for leaves with stomatal conductance below  $0.4 \text{ mol m}^{-2}\text{s}^{-1}$  (Schymanski, Or, 2016). Mean maximum stomatal conductance on the TFE trees is four-fold smaller than for the Control trees, at  $0.09 \pm 0.05 \text{ mol m}^{-2}\text{s}^{-1}$  (Rowland et al., 2021a) suggesting that increased turbulence would have a considerable ameliorating effect on WUE for leaves on the side of the canopy that faces prevailing wind. The leaf area on drought-stressed TFE trees may thus have built up a long-term bias towards the prevailing northerly wind direction, in contrast to the non-droughted Control plot trees, where no cardinal bias in leaf area was detected (Figure 2.1). We note, however, that the increase in leaf area on the northern side of the TFE tree canopies did not have any relationship with tree size: large trees are most exposed to prevailing winds, but dominant eddy size in the prevailing winds may be sufficient to penetrate all major canopy layers. We are not aware of prior evidence of trees increasing leafy tissue on the side of the morning sun or prevailing winds under an independent environmental cue, such as drought, and further research is needed to examine cause and effect behind changes in leaf distribution in tree canopies, and their effects on local temperature environments and net gas exchange.

#### **2.4.4 Aggregate structure**

Aggregate forest structure on the TFE altered considerably, with the forest distribution of leaf and woody tissue closer to the ground (Figure 2.2),  $55.6 \pm 3.0\%$  less woody volume, and  $29 \pm 6\%$  lower leaf area index (Figure 2.4), resulting in an increased leaf area index to woody volume ratio of  $22 \pm 9\%$ . These aggregate struc-

tural differences are due to large tree mortality (Rowland et al., 2015), increased number of small trees filling in gaps created by tree mortality, increases in leaf area of small trees, decreases in leaf area of large trees (Table 2.4, Appendix A.4), and the summed changes in woody tissue architecture on the TFE as described in previous sections. Specifically, the overall decrease in woody tissue volume and leaf area on the TFE appears to be occurring due to changes in the woody volume and leaf area of trees above 22 to 25 m height (Figure 2.4): trees below  $\sim 25$  m height have similar or higher wood volume and LAI in aggregate, and trees above  $\sim 25$  m height have lower aggregated volume and LAI. The decrease in aggregate wood and leaf tissue for trees above 25 m could be due to heightened hydraulic stress expected in tall trees (Rowland et al., 2015; Olson et al., 2018; Liu et al., 2019), however we found that no architectural woody traits had a negative interaction between tree size and treatment, such that treatment affected large trees more than small trees, which might be expected if there was a height-rainfall threshold. Canopy plasticity for trees above a certain height may be functionally useless, especially if the canopy fork height is above a certain threshold, as increased energy spent redistributing woody tissue within a hydraulic danger zone would provide no benefit. If so, then hydraulic conductance of large trees would be preferentially manipulated by reducing leaf area of the tree, which we do in fact see in large trees on the TFE (Table 2.4, Appendix A.4). However, loss of leaf area would also reduce carbon gain, potentially increasing large risk of carbon deficiencies for large trees, which could lead to additional vulnerability of large trees to further reduction in soil water.

In evaluating the drought tolerance of the aggregate forest after 17 years of TFE, we note that many of the same characteristics that increase individual tree hydraulic conductance or resource acquisition efficiency were present when comparing whole forest structure of the TFE and Control. The water status of forest canopies would improve on the TFE due to decreased frictional losses and reduced effect of the gravitational component of water potential, as more woody tissue is located lower to the ground, specifically below 15 meters (Figure 2.2), and leaf distribution was

approximately 3 meters lower to the ground (Figure 2.3A) Interestingly, on the TFE the woody tissue of forest canopies of large trees has not shifted lower (Figure 2.3B), likely due to limited ability to shed and regrow first order branches, which may increase large tree vulnerability to soil water availability. In contrast, small and medium sized trees had woody tissue volume at lower heights than the Control.

Resource acquisition of the TFE as an aggregate would also increase, due to increased leaf area to woody tissue volume ratio by  $22 \pm 9\%$ , driven by increased leaf area on small trees, decrease in leaf area on large trees, and mortality-related decreases in woody volume of the large trees on the TFE (Rowland et al., 2015). This has implications for carbon use efficiency, since a smaller amount of woody tissue requires relatively more leaves in the TFE. This could also indicate that, at the plot-level, there would be increases in transpiration per unit biomass. Earlier analysis of transpiration at the plot level of TFE (Costa da et al., 2018) did not show an overall reduction in yearly transpiration on the TFE in comparison to the Control. This discrepancy may be explained by differences in stomatal conductance, not measured in this study, which could be altering under droughted conditions leading to a null change in transpiration.

## 2.5 Conclusion

We used terrestrial laser scanning to evaluate the effects of drought on structural metrics that describe the architecture of Amazonian rainforest trees. We compared adjacent forest plots, one of which was subject to long-term experimental drought whereby 50% of incoming rainfall was removed continuously over 17 years. Our data indicate that our key structural metrics altered plastically in response to the drought treatment so as to ameliorate long-term hydraulic stress, in a manner analogous to the known plasticity in organ-scale plant traits. Our selected architectural plant traits altered consistently in a manner favoring hydraulic stress mitigation at multiple scales, from twig to tree to stand. Additionally, we found that the variation in these architectural traits can be described well with simple ground-based

measurements, making it straightforward to tease apart environmental effects, and critically, to predict these traits. Our findings have wide application in understanding and advancing trait-based plant ecology, and in predicting the response of trees to environmental stressors across multiple environments.

# Chapter 3

## Structural and process-based analysis of woody tissue respiration during long-term experimental drought

### 3.1 Introduction

The tropics have the highest carbon uptake and largest aboveground carbon stores of all the world's forests (Pan et al., 2011). There is a fine balance between tropical forest carbon uptake (gross primary productivity, GPP) and carbon release (ecosystem respiration,  $R_{eco}$ ), which ultimately determines if the forest is a net carbon source or carbon sink; currently most years, intact tropical rainforests are an important carbon sink (Cox et al., 2013; Huntingford et al., 2013). Ecosystem stress caused, in part, by increased temperature and decreases in soil moisture have potentially led to a decline in the magnitude of the carbon sink of tropical rainforests, particularly the largest rainforest, the Amazon (Brienen et al., 2015; Gatti et al., 2021; Hubau et al., 2020). This has important implications for the global carbon cycle.

In recent years, ecosystem stress may have resulted in the Amazon turning into a

carbon source (Gatti et al., 2021). Recent analyses, however, show high uncertainty around estimates of the tropical rainforest carbon balance, which result in a tropical carbon balance that could be a large carbon sink, removing  $9.7 \text{ GtCO}_2\text{eyr}^{-1}$  or the largest terrestrial forest carbon source, at  $6.3 \text{ GtCO}_2\text{eyr}^{-1}$  (Harris et al., 2021). Uncertainty around  $R_{\text{eco}}$  estimates alone may be as high as 50% in the tropics (Campioli et al., 2016; Harris et al., 2021; Metcalfe et al., 2010b), and the uncertainties become even larger when predicting the sensitivity of  $R_{\text{eco}}$  to temperature and drought stress (Cleveland et al., 2015).

$R_{\text{eco}}$  is made up of three main source components: soil, wood and leaf. Generally, soil accounts for the largest source of  $\text{CO}_2$ , leaves are the second largest source, and wood is the smallest source (Campioli et al., 2016). Of the three principal components of  $R_{\text{eco}}$ , the smallest component – the wood – may have the highest uncertainty in tropical rainforests, with recent scaling attempts resulting in a range  $>300\%$  of estimates of stand wood  $\text{CO}_2$  efflux in a single tropical rainforest (Rowland et al., 2018). Even though wood may be the smallest source of  $\text{CO}_2$ , it can still account for up to one third of  $R_{\text{eco}}$  (Campioli et al., 2016; Cavaleri et al., 2006; Chambers et al., 2004; Malhi et al., 2009b), therefore this high uncertainty in stand wood  $\text{CO}_2$  efflux can have a large effect on the uncertainty of  $R_{\text{eco}}$  estimates.

The key issues involved in scaling wood  $\text{CO}_2$  efflux are measuring the scalar (e.g. surface area, volume, sapwood volume), and determining which scalar to use. New ground lidar technology applied to forestry (Calders et al., 2020; Lau et al., 2019b; Terryn et al., 2020; Verbeeck et al., 2019) may resolve this methodological problem by providing detailed models of woody structure which can be used to extract measurements of tree and forest scalars. This structural data can be used to test different methods of scaling wood  $\text{CO}_2$  efflux. Wood  $\text{CO}_2$  efflux rates scale with branch size (Mori et al., 2010; Rowland et al., 2018; Yoda, 1983), and this new technology can provide the structural information necessary to model wood  $\text{CO}_2$  efflux rates per individual branch radius within a tree, vastly improving estimates of wood  $\text{CO}_2$  efflux at stand scale.

Uncertainty exists as to whether CO<sub>2</sub> efflux scales with surface area, volume, sapwood volume or mass of the woody tissue section under study (Levy et al., 1999; Meir, Grace, 2002; Rowland et al., 2018; Ryan, 1990; Yang et al., 2016), with most efforts focusing on area-based estimates. Surface area based scaling relies on assumptions that the majority of wood respiration comes from the thin cambium and phloem layer, which has been shown to be the case for select species (Spicer, Holbrook, 2007). Volume, sapwood volume or mass based scaling assumes axial and radial parenchyma tissue are substantial contributors to wood respiration. Sapwood volume scaling approaches have drawbacks, as measuring living tissue or sapwood volume is currently not possible without destructive harvesting. Mass or volume scalars are easier to estimate than sapwood volume, however the contribution of dead heartwood tissue confounds the functional link between woody volume or mass and woody living tissue. A method to test whether woody tissue respiration scales on a surface area or volume basis has been developed (?), which, when applied to diverse tropical rainforest wood, has shown mixed and sometimes branch size-dependent results (Cavaleri et al., 2006; Rowland et al., 2018).

Estimating current and future ecosystem respiration relies heavily on understanding how wood responds to climate (Anderegg et al., 2015; Brando et al., 2019; Meir et al., 2018). The collective effect of drought responses on wood is generally a reduction in quantity of forest woody tissue and reduced respiration rates (De Roo et al., 2020; Lauriks et al., 2022; Rodríguez-Calcerrada et al., 2014; Saveyn et al., 2007), which results in reduced forest wood CO<sub>2</sub> efflux. Reduced quantity of woody tissue under drought can occur due to increased tree mortality rates (Nepstad et al., 2015; Phillips et al., 2009; Rowland et al., 2015) and increased frequency of canopy branch shedding in comparison to non-droughted periods (Li et al., 2018; Lloret et al., 2004; Mueller-Dombois, 1983; Nolan et al., 2021; Rood et al., 2000; Shen et al., 2022). Temperature can often increase in conjunction with water deficit, and can have a large impact on wood CO<sub>2</sub> efflux, as autotrophic respiration is expected to respond exponentially to increases in temperature. Over longer time periods,

plant respiration can acclimate to temperature (Atkin et al., 2015; Slot, Kitajima, 2015; Smith et al., 2019; Vanderwel et al., 2015), although the length of time required for acclimation and the magnitude of acclimation is not well characterized (Reich et al., 2021).

When trees are drought stressed, the collective changes in organ structure (e.g. branch shedding) and metabolic rates may alter the whole tree woody metabolism, that is, the total amount of carbon that is consumed by woody tissue for maintenance and growth processes. There are large scale patterns relating organism size with metabolic rate (Kleiber, 1932), which are described by the equation:

$$Y = y_0 V^\alpha \tag{3.1}$$

where  $Y$  is metabolic rate,  $y_0$  is a normalization constant,  $V$  is organism volume (or organism mass), and  $\alpha$  is a scaling exponent that determines how metabolic load tapers with size. Although universal scaling exponents have been suggested for trees (Enquist et al., 2009; Mori et al., 2010; Reich et al., 2006; West et al., 1999), changes within a tree affecting its structural allometry could alter the relationship between whole tree metabolic rate and tree volume (Muller-Landau et al., 2006; Pretzsch, 2021). For example, replacing large diameter branches with an equivalent volume of small diameter branches might result in lower wood  $\text{CO}_2$  efflux per unit tree volume, since respiration (on a surface area basis) increases with branch size (Chambers et al., 2004; Mori et al., 2010; Yoda, 1983). Shedding branches, and regrowing woody and leafy tissue in places with lower temperature or lower light could reduce metabolic load, as metabolic rates increase in high temperature and high light environments; decreasing the canopy:trunk woody tissue volume ratio could reduce tree metabolic load, since canopy branches respire at higher rates than the tree stem irrespective of temperature and branch size (Asao et al., 2015; Cavaleri et al., 2006). Each of these examples could result in lower tree woody metabolic rate, which may be beneficial in the event of drought-induced limitations to carbon supply (e.g. reduced leaf or bark photosynthesis, Cernusak, Cheesman, 2015). Importantly, structural modifications

that reduce tree metabolic load can have detrimental impacts. For example, branch shedding could lead to less spatial advantage to capture incoming light or lead to less carbon supply due to leaf shedding. Therefore woody structural modifications need to be taken within a wider context as they can have both positive and negative consequences for the tree carbon balance and the tree's performance.

Scaling of organ metabolism to tree and stand requires the drivers and variance of wood CO<sub>2</sub> efflux rates to be well characterized. There are particular difficulties in measuring and interpreting wood metabolism, as respiratory-derived wood CO<sub>2</sub> efflux can diffuse radially, axially (Levy et al., 1999; McGuire, Teskey, 2002; Salomón et al., 2018; Teskey et al., 2017), or be removed by carboxylating enzymes in woody tissues (Dima et al., 2006; Gansert, Burgdorf, 2005; McGuire et al., 2009; Pfanz et al., 2002), meaning the commonly measured wood radial CO<sub>2</sub> efflux is not directly translatable to the respiration rate of underlying live woody tissue. Hence, the term 'wood CO<sub>2</sub> efflux', commonly considered to be the radial CO<sub>2</sub> efflux, is distinguished from wood respiration, which is all CO<sub>2</sub> derived from respiration in woody tissue. Currently, most measurements of woody tissue metabolism in the field are based on measurements of wood CO<sub>2</sub> efflux. Measuring respiratory oxygen uptake has been suggested as an improved alternative to measuring wood respiration (Angert, Sherer, 2011; Hilman, Angert, 2016), as oxygen is not consumed in carboxylating processes, and has 28x lower solubility in water at 20°C than CO<sub>2</sub>, resulting in relatively less axial diffusion of O<sub>2</sub>. The ratio of CO<sub>2</sub> efflux to respiratory O<sub>2</sub> consumption in the stem, known as the apparent respiratory quotient (ARQ), is 1 when cells are metabolizing carbohydrates (stoichiometry), the principal substrate for respiration in wood (Hilman, Angert, 2016). Therefore, the CO<sub>2</sub> sink of woody tissue (e.g. axial movement or carboxylation) can be measured as the difference of ARQ from unity, and can inform methods to translate CO<sub>2</sub> efflux rates to wood respiration.

An important advance in modelling tree architecture, using high-precision spatial information obtained using terrestrial laser scanning (TLS, Disney et al., 2018; Malhi, 2018; Meir et al., 2017), can provide the structural data needed to evaluate

metabolic rates of entire trees. This is a step-change from previous studies, which were limited to comparing point-measurements of woody metabolic rates. This new technology can be applied to improve understanding of individual tree metabolic changes, and forest carbon efflux estimates (Calders et al., 2020; Lau et al., 2019b; Meir et al., 2017; Brugnara Porcia e et al., 2019; Verbeeck et al., 2019). Prior to TLS, scalars of woody tissue CO<sub>2</sub> efflux were modelled using an allometric equation relating the scalar (e.g. surface area, volume) and tree diameter at breast height (DBH) and, sometimes, the height of the tree. Although useful tools, allometric models are particularly unsuitable for drought/climate change studies because (i) the models do not take into account drought-induced changes in tree allometry and (ii) allometry errors increase with tree size (Burt et al., 2020; Momo et al., 2020), so large trees, which may be most sensitive to drought (Rowland et al., 2015), are the most poorly estimated.

The basis of this study is a 18-year through-fall exclusion experiment (TFE) with 50% of throughfall removed from one-hectare of tropical rainforest in eastern Amazonia; all results from the TFE are compared against a nearby one-hectare Control plot, where no drought-treatment has been imposed. The TFE has changed since the beginning of the experiment in July 2002, with approximately 40% of tree biomass lost due to high mortality rates in large trees (Rowland et al., 2015). The death of large trees reduced the uppermost canopy coverage of the forest, allowing greater light penetration on the TFE than Control (Rowland et al., 2021a). Wood CO<sub>2</sub> efflux was previously measured between 2014-2017 on 215 trees (Rowland et al., 2018), and was found to be seasonally higher on the TFE than the Control in the wet season. Small trees have adjusted to the changes in water availability (Bartholomew et al., 2020; Giles et al., 2022); however, trees above 10 cm diameter at breast height (DBH) have shown no hydraulic adjustment, resulting in significant hydraulic stress (Bittencourt et al., 2020).

Here, we evaluated wood CO<sub>2</sub> efflux, and wood respiration on the TFE at the organ, tree and stand level, using methods relying on terrestrial laser scanning (TLS)

to model woody tissue structure. We measured CO<sub>2</sub> efflux in the canopy (N = 789) and the stem (N = 962) and additionally measured ARQ (N= 48), which we used to translate wood CO<sub>2</sub> efflux to wood respiration. We scaled measurements of wood CO<sub>2</sub> efflux to the tree-level (N = 329): we use a model of wood CO<sub>2</sub> efflux developed from canopy and stem measurements, which is applied to tree structural models to determine CO<sub>2</sub> efflux rate per tree branch, the sum of which is tree wood CO<sub>2</sub> efflux. This allowed us to test how alterations in wood CO<sub>2</sub> efflux rates and tree structure under water deficit jointly affect metabolic load of whole trees. Finally, we scaled wood CO<sub>2</sub> efflux to the stand, by applying an allometric relationship of tree woody CO<sub>2</sub> efflux to all trees on the treatments. To account for potential differences in temperature environments between treatments due to higher light environment on the TFE than Control (Rowland et al., 2021b), we model hourly wood surface temperature in 2019. Specifically, we address the following hypotheses:

- Wood CO<sub>2</sub> efflux and wood respiration have increased on the TFE.
- Wood metabolic load on trees has reduced under drought due to structural changes in trees on TFE.
- Total stand wood CO<sub>2</sub> efflux ( $R_{\text{wood}}$ ) has decreased due to decreases in above-ground biomass on the TFE in response to long term water deficit.
- Ambient  $R_{\text{wood}}$  will increase in the TFE in response to environmental warming due to greater penetration of high irradiance following drought-induced death of large trees.

## 3.2 Materials and Methods

### 3.2.1 Site

All measurements were taken at an old-growth *terra-firme* tropical rainforest site in eastern Amazonia, Caxiuanã National Forest Reserve (1°43'S, 51°27'W), where the annual precipitation is 2000-2500 mm, with yellow oxisol soil (Ruivo, Cunha, 2003).

The site is seasonal, with rainfall below 100 mm for 6 months of the year. Seasons are classified as Dry (September-November), Dry-Wet transition (December-February), Wet (March-May), and Wet-Dry transition (June-August) based on monthly median surface soil volumetric water content on the Control plot (VWC,  $\text{m}^3 \text{ m}^{-3}$ , CS616, Campbell Scientific Inc.). A through-fall drought experiment (TFE) was installed in January of 2002 on one hectare of tropical rainforest and had been continuously maintained for 18 years prior to the reported year of study. Alongside the TFE, a Control experiment was established, enabling a comparison of the long term effects of water deficit on tree hydraulics and carbon cycling in tropical rainforest.

The TFE excluded approximately 50% of the throughfall using inclined transparent panels at 1-2 meters in height and a system of gutters. Litter was removed from above the panels and placed below the panels on the forest floor every 2-3 days. A 1-2 m trench was dug around the perimeter of the TFE to prevent lateral soil water flow, which was replicated on the Control (see Costa da et al., 2010; Fisher et al., 2007; Meir et al., 2009, 2018, for further information on experimental set-up). All trees within the outer 10 meters of the experiment are excluded, due to potential edge effects. For an overview of principal findings, see Meir et al. (2018).

The TFE experiment is located in a remote eastern Amazonian rainforest, and was resource intensive to establish and maintain, restricting replication of the treatment design. Although replication would have been possible had the experiment sample plots been smaller, this would have precluded an ecosystem-scale study of water-deficit, which was the objective of this experiment. This large-scale experiment design has been used elsewhere (Likens et al., 1970).

### **3.2.2 Terrestrial laser scanning (TLS)**

#### **TLS methods**

Terrestrial laser scanning data (TLS) were collected using a Riegl VZ-400 (RIEGL Laser Measurement Systems GmbH) in October 2018, the dry season. The RIEGL VZ-400 operates at a wavelength of 1500 nm, has a beam divergence of 0.35 mrad,

and an exit diameter of 7 mm. Lidar scans were co-registered into a common coordinate system using RiSCAN PRO (v2.7.0) and the point clouds of trees above 10 cm DBH in the two hectares were partially automatically extracted using treeSeg (?) and partially extracted manually. All point clouds were extracted on a 20 m x 20 m grid sampling. After extraction, leaf material returns were separated from wood using TLSeparation v1.0 (Vicari, Wilkes, 2018). Each tree was visually inspected to determine adequate leaf-wood separation using CloudCompare, and the tree was manually edited to improve the final separation when necessary (CloudCompare, 2021).

### **TLS tree structure**

Tree volume and tree surface area information was extracted from quantitative structural models (QSMs) constructed using TreeQSM (v 2.3.2, Raunonen et al., 2013, 2015) from wood point clouds of 329 trees, where input parameters were automatically selected using optQSM v 0.1.0 (Burt et al., 2021). Error for each QSM volume was estimated by using mean tree error from a nearby destructive harvest TLS-calibration experiment in a tropical rainforest 8 km distant from the drought experiment site (Burt et al., 2021). This destructive harvest – TLS calibration study (Burt et al., 2021) provides rare high-quality validation in tropical rainforests for the structural metrics derived for this study using TLS.

The 20 m x 20 m sampling grid of TLS data provided low resolution point clouds for modelling tree QSMs from point clouds of a dense tropical rainforest. TLS data on the Control were available in a 10 m x 10 m grid sampling, therefore a subset of 146 trees, extracted in both the 10 m x 10 m and 20 m x 20 m sampling grid, were compared, and the relationship was used to correct surface area and volume of all trees on the Control and TFE extracted in a 20 m x 20 m sampling grid (Appendix B.1, B.2 N = 146; surface area,  $R^2=0.94$ ; volume,  $R^2=0.97$ ).

The height at which the first major branching fork in the canopy occurred was measured manually using woody tissue point clouds, and subtracted for the min-

imum height at the base of the tree. All branches above and including this fork height were considered to be the canopy of that tree. Tree canopy width was measured using leaf point clouds: a 2D convex hull was fit to the leaf point clouds from a bird’s eye orientation and then the perimeter of the convex hull (P) and the area (A) of the convex hull were used to attain a mean width of the canopy:

$$4\frac{A}{P} \tag{3.2}$$

### 3.2.3 Wood CO<sub>2</sub> efflux

#### Sample selection

Wood CO<sub>2</sub> efflux, which is the radial efflux of CO<sub>2</sub> from woody tissue, was measured monthly at breast height between October-2018 and December-2019 on 51 trees in the Control, and 52 trees in the TFE, alongside measurements of surface wood temperature. Measurements could not be taken in December-2018 and February-2019 for logistical reasons. Additionally, two campaigns were performed in October-2018 (peak dry season) and March-2019 (peak wet season) in which canopy wood CO<sub>2</sub> efflux was measured *in situ* as well as on excised branches using rope access techniques. In total, we measured wood CO<sub>2</sub> efflux on 192 individuals, 103 trees on the Control and 89 trees on the TFE, which ranged from 10.3 cm to 103.7 cm DBH. The diameters of measured branches and stems ranged from 0.1 cm to 103.7 cm.

In these two hectares, there were 100 genera present, however some genera were more common than others. We sampled 41 genera at this site, which represents 41% of all genera, and 80% of all trees on the two hectares. Three or more individuals were measured to provide replication for the following genera on each treatment: *Aspidosperma*, *Eschweilera*, *Inga*, *Licania*, *Manilkara*, *Micropholis*, *Minquartia*, *Pouteria*, *Protium*, *Swartzia* and *Vouacapoua*. Within this group there were 8 species that had at least three individuals per treatment: *Eschweilera coriacea*, *Licania octandra*, *Manilkara bidentata*, *Minquartia guianensis*, *Pouteria anomala*, *Protium tenuifolium*, *Swartzia racemosa*, and *Vouacapoua americana*. See Appendix B.3 for

the full list of species measured, and the number of individuals. During the 2018-2019 measurement period, 467 wood CO<sub>2</sub> efflux measurements were taken at breast height on the Control, and 495 on the TFE. In addition, 432 measurements were taken of canopy branches in the Control, and 357 in the TFE during two campaigns, one in peak dry season, October-2018, and one in peak wet season, March-2019.

### Wood CO<sub>2</sub> efflux measurement methods

Wood CO<sub>2</sub> efflux was measured using an infra-red gas analyser (EGM-5 PP Systems, Hitchin, UK) in a closed system for a minimum of 3 minutes per measurement. Chambers were tested for leaks, and if a leak was detected, the measurement was aborted. The slope of the linear regression of CO<sub>2</sub> over the last 30 seconds of sampling was used to calculate the rate of CO<sub>2</sub> efflux using the following equation:

$$R = \frac{\Delta C}{\Delta t} \frac{PV}{8.314A(T + 273.15)} \quad (3.3)$$

where  $\Delta C / \Delta t$  is the change in CO<sub>2</sub> concentration over the last thirty seconds of the measurement ( $\mu\text{mol s}^{-1}$ ), P is pressure (Pa), T is temperature of air within the chamber ( $^{\circ}\text{C}$ ), A is surface area of the ground or tissue covered by the chamber ( $\text{m}^2$ ), V is chamber volume ( $\text{m}^3$ ) and R is wood CO<sub>2</sub> efflux ( $\mu\text{mol m}^{-2} \text{s}^{-1}$ ). If the R<sup>2</sup> of the linear regression was below 0.9, the linear regression was visually checked to determine whether the data should be discarded or whether inclusion was appropriate (on a subset of measurements, R<sup>2</sup> was lower than 0.9 due to slow efflux of CO<sub>2</sub> from the woody tissue). If necessary (<1% of data), the linear regression was performed on the last 1 minute of sampling, and the value was included in subsequent analyses.

Wood CO<sub>2</sub> efflux values were temperature corrected, using a standard exponential equation:

$$r_1 = r_{25} Q^{10^{((T_1 - T_{25})/10)}} \quad (3.4)$$

where  $r_1$  is CO<sub>2</sub> efflux rate at ambient temperature ( $\mu\text{mol CO}_2 \text{ m}^{-2} \text{ s}^{-1}$ ),  $r_{25}$  is CO<sub>2</sub> efflux rate at 25°C ( $\mu\text{mol CO}_2 \text{ m}^{-2} \text{ s}^{-1}$ ),  $T_1$  is ambient temperature (°C). We note that Q10 is expected to alter under drought scenarios, ontogenetically, due to growth rate and seasonality. The Q10 for woody tissue was not measured for these sites, therefore no adjustment was possible to account for potential differences in tissue temperature response between the TFE and Control. Additionally, the measured surface temperature of the woody tissue is likely to be higher than that of underlying tissue. Here we used a Q10 of 2.0, which has been used for our site and other tropical rainforest sites (Cavaleri et al., 2006; Rowland et al., 2018), based on Q10 measurements of tropical rainforest trees elsewhere (Meir, Grace, 2002; Ryan et al., 1994).

For *in situ* measurements of wood CO<sub>2</sub> efflux, measurement chambers were fixed to the stem using ratchet straps and closed-cell foam, and a small perforated tube was connected to the air inlet inside the chamber to promote passive mixing whilst avoiding vortex effects on efflux rates potentially caused by an internal fan (Rayment et al., 2002). Chambers were similar in size and design to previous methods used in tropical rainforests (Rowland et al., 2018). Surface wood temperature was measured using a type T thermocouple near the measurement chamber, and the diameter of each branch was measured directly below the measurement chamber. Measurements were taken throughout the day (8:00-17:00 h). For measurements of excised twigs, the ends of twigs were sealed with parafilm, and the twig was placed within a chamber where wood CO<sub>2</sub> efflux was measured. The dimensions of the twig were used to measure the volume and surface area of the twig. Wood CO<sub>2</sub> efflux was temperature corrected to 25°C, using equation 3.4.

### 3.2.4 Wood Respiration - ARQ

The ratio of CO<sub>2</sub> efflux to O<sub>2</sub> influx (Hilman, Angert (apparent respiratory quotient, or ARQ, 2016)) was measured in March 2019 and was used to estimate woody tissue respiration from wood CO<sub>2</sub> efflux rates by dividing wood CO<sub>2</sub> efflux by ARQ. The

ARQ measurements were taken at peak sap flow (12:00-14:00 hrs) and at low sap flow (21:00-24:00 hrs) in the canopy and at breast height (1.3 meters) on 12 trees of two species, *Pouteria anomola*, *Eschweilera coriacea*, ranging in DBH from 16.3 cm to 42.75 cm. We used branches no smaller than 10 cm in diameter, and in total a maximum of 48 ARQ measurements were possible. Measurement of ARQ followed protocols developed by Angert et al. (2012); Hilman, Angert (2016); Hilman et al. (2019, 2022). CO<sub>2</sub> efflux rates were measured prior to installing glass flasks (3.7 mL) on an air-tight chamber flush with the stem. After a period of equilibration of 2-3 hours, the flasks were removed, stored, and transported to a laboratory where ARQ was measured.

To determine if an axial sink of CO<sub>2</sub> accounted for differences in ARQ, sap flow was measured adjacent to each ARQ chamber for 2-9 days, logging every 15 minutes. The sap flow sensor was logging during the period of ARQ measurements. Sap flow was measured using the heat ratio method (Burgess et al., 2001) using two sap flow sensors per tree (ICT, SFM1, ICT International, Australia); one was located in the canopy, one at breast height. Sap flow was baselined using a constant value for minimum sap flow per tree, which was the mean nightly sap flow between 4:00-6:00 h throughout the entire measurement period. This method of baselining has limitations as it does not take into account reverse sap flow or nighttime transpiration (Forster 2014) in trees by excluding values from nights with high evaporative demand (Hoelscher et al., 2018), although it has been widely used (Dugas 1994, Lindroth 1995, Langensiepen et al., 2014).

### **3.2.5 Scalars of wood CO<sub>2</sub> efflux**

We tested scaling wood CO<sub>2</sub> efflux by tree surface area and by volume only, since we did not have any measurements of sapwood volume or direct measurements of wood density for trees at the site, which would have allowed us to additionally test scaling of wood CO<sub>2</sub> efflux by sapwood volume or mass. The scalar for wood CO<sub>2</sub> efflux was tested using an approach developed by (?): if CO<sub>2</sub> efflux scales on a surface area

basis, CO<sub>2</sub> efflux on a volume basis is positively linearly related to the reciprocal of stem diameter; if a volume scalar should be used, there will be a positive linear relationship between CO<sub>2</sub> efflux on an area basis with diameter (?).

### **3.2.6 Wood CO<sub>2</sub> efflux model**

Wood CO<sub>2</sub> efflux, temperature corrected to 25°C (WC<sub>25</sub>), was modelled on a surface area basis, where nonsignificant variables were excluded using a stepwise mixed multiple linear regression analysis (Zuur et al., 2009). Only WC<sub>25</sub> data for stems and branches larger than 5 cm in diameter were included in the final model of WC<sub>25</sub>. The initial model of WC<sub>25</sub> for branches greater than 5 cm in diameter included treatment, month, branch diameter, location of the wood (canopy or stem), time of day, morning (8:00-11:00 h), midday (11:00-14:00 h), and afternoon (after 14:00 h), total yearly growth rate (cm circumference yr<sup>-1</sup>), and an interaction between treatment and each fixed effect. A random effect of tree individual and genus was also tested.

### **3.2.7 Wood temperature model**

Wood surface temperature was measured during October-2018 and March-2019 and was applied to model hourly wood surface temperature for trees in the Control and TFE, in order to scale WC<sub>25</sub> to ambient temperature conditions. The final model of local wood temperature includes air temperature at 16 m, total global radiation (W/m<sup>2</sup>), the light score of the tree (1-5, 1 low light, 5 high light), the season (Wet, Wet-Dry transition, Dry, Dry-Wet transition), the experiment (TFE, Control), and the location of the temperature measurement (canopy, trunk). Half hourly meteorological data were gap filled using the weekly, monthly, or seasonal mean for the given hourly increment, resulting in gap filling for 4.7% of air temperature values, and 2.5% of total global radiation in 2019.

### 3.2.8 Scaling wood CO<sub>2</sub> efflux

To scale wood CO<sub>2</sub> efflux to stand ( $R_{\text{wood}}$ , Mg C ha<sup>-1</sup>yr<sup>-1</sup>), all trees above 10 cm DBH were included in the analysis except for lianas and palms. The method for scaling wood CO<sub>2</sub> efflux to stand wood CO<sub>2</sub> efflux used QSMs, which provide structural information for each tree, including tree branch sizes and quantities per tree. We applied a model of wood CO<sub>2</sub> efflux, which relies on branch diameter and tree location (canopy, stem) to each QSM, to calculate a distribution of modelled wood CO<sub>2</sub> efflux values associated with individual branches on each QSM. The modelled wood CO<sub>2</sub> efflux was multiplied by the surface area of the respective branch, and the sum of this was taken per tree, resulting in whole tree wood CO<sub>2</sub> efflux rate. TLS methods do not have adequate resolution to model small diameter branches, therefore the branches below 5 cm were modelled separately (Appendix B.1). Whole tree wood CO<sub>2</sub> efflux per month was modelled by tree surface area, and applied to all remaining trees on the plots. The wood temperature model was applied to correct wood CO<sub>2</sub> efflux values to ambient temperatures in each plot, and scaled to determine yearly efflux of CO<sub>2</sub>. Error is estimated as the sum of TLS error from the harvest comparison using felled tree biomass (3%, Burt et al., 2021), and the standard error of the wood CO<sub>2</sub> efflux rates divided by the mean of the wood CO<sub>2</sub> efflux rates.

### 3.2.9 Statistics

All analyses were performed in R (4.0.3 R Core Team, 2021). All errors presented are standard errors of the mean, unless otherwise noted. The 95% confidence intervals of parameter estimates were computed using a parametric bootstrap, applying function `bootMer` from the `lme4` package (Bates et al., 2015). The 95% confidence intervals were calculated for nonlinear models using the `predictNLS` function from the `propagate` package (Spiess, 2018). Mixed effects models were performed using the `lme4` package. Marginal and conditional  $R^2$  are reported ( $R^2_{\text{m}}$ ,  $R^2_{\text{c}}$ , respectively) for mixed effects models. For all models, fixed effects were iteratively tested for in-

clusion, and genus and tree individual were tested as random effects, using methods outlined in Zuur et al. (2009). One-way ANOVA was used to compare the effect of the interaction of species/genus, treatment, season, and measurement type, where measurement type was considered twigs (<2 cm diameter), canopy branches (> 2 cm diameter) and stem measurements taken at 1.3 m height on wood CO<sub>2</sub> efflux. All ANOVA were followed with a Tukey’s post-hoc test.

### 3.3 Results

#### 3.3.1 TFE physical environment

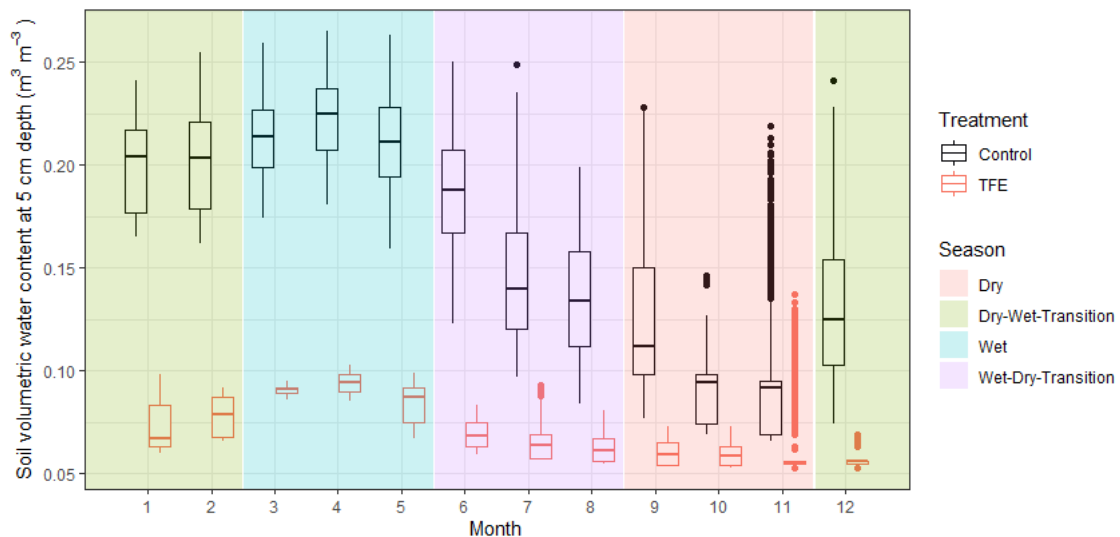


Figure 3.1: Seasonal variation in soil volumetric water content (VWC, m<sup>3</sup> m<sup>-3</sup>) at 5 cm depth in the Control (black) and TFE (red) in 2019, where VWC was measured hourly. Colored background represents seasonal classification as Dry, Dry-Wet Transition, Wet and Wet-Dry Transition.

The TFE treatment resulted in a median soil VWC in 2019 between 38-67% lower than the Control, dependent on the month (Figure 3.1). Woody surface temperature in the wet and dry season were higher than the Control (N = 601, Figure 3.2, 3.3), hence all values presented for scaled respiration are presented at 25°C and at ambient temperature. The temperature environment for trees on the TFE was modelled as a function of hourly total global radiation (W/m<sup>2</sup>), hourly air temperature at 16

meters ( $^{\circ}\text{C}$ ), season (Wet, Dry), location of wood (Canopy, Trunk), tree light score (1-5, high-low) and experiment (TFE, Control), resulting in higher hourly woody temperature during the day on the TFE than Control by up to  $2.3^{\circ}\text{C}$  (Figure 3.4A, 3.4B). The temperature model described 83.5% of the variance in measured wood temperature (Appendix B.5), and was applied to predict local wood temperature for each hour of each day of 2019 for canopy and trunk wood. Although modelled hourly woody temperature in the TFE was higher than in the Control diurnally (Figure 3.4A, 3.4B), the median yearly difference between TFE and Control in hourly temperature was  $0.01^{\circ}\text{C}$ , as a result of modelled temperatures having no treatment effect between approximately 18:00- 8:00 h. Additionally, differences in modelled temperature between treatments were less than  $1^{\circ}\text{C}$  for 76% of the year.

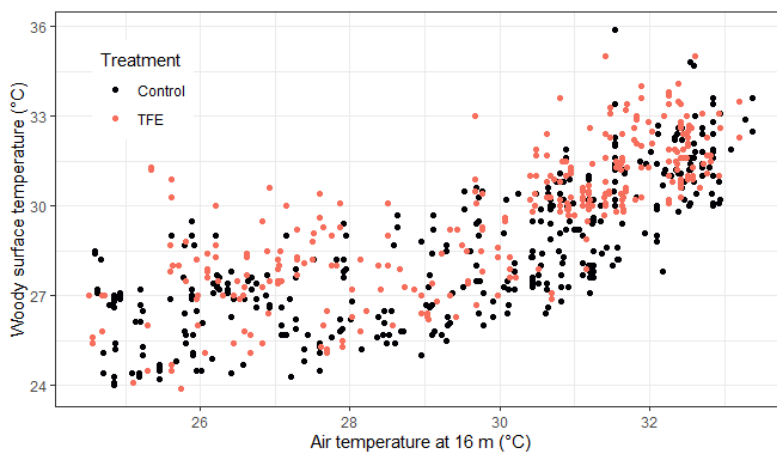


Figure 3.2: Point measurements of woody tissue surface temperature ( $^{\circ}\text{C}$ ) on Control (black) and TFE (red) versus air temperature measured at 16 m height ( $^{\circ}\text{C}$ ).

### 3.3.2 Tree and plot woody structure on TFE and Control

The surface area values of trees modelled using TLS were lower than the previously published tropical tree allometric model relating surface area to DBH (Figure 5A, Chambers et al., 2004). The widely used surface area model from Chambers et al. (2004) indicates that the slope of the surface area of trees vs. DBH decreases above approximately 80 cm DBH (Figure 3.5B), and that there is a negative relationship between DBH and surface area for trees above 250 cm DBH. In contrast, TLS

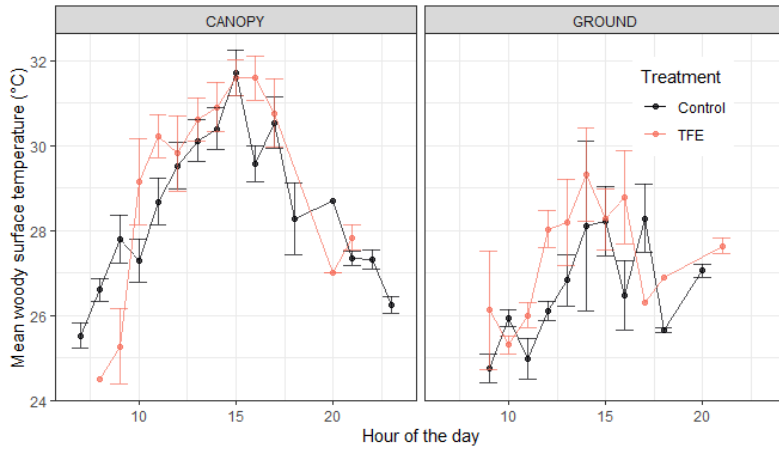


Figure 3.3: Measurements of woody surface temperature (°C) per hour of the day in Control (black) and TFE (red) on woody tissue located in the canopy (left panel), and at 1.3 m height (right panel).

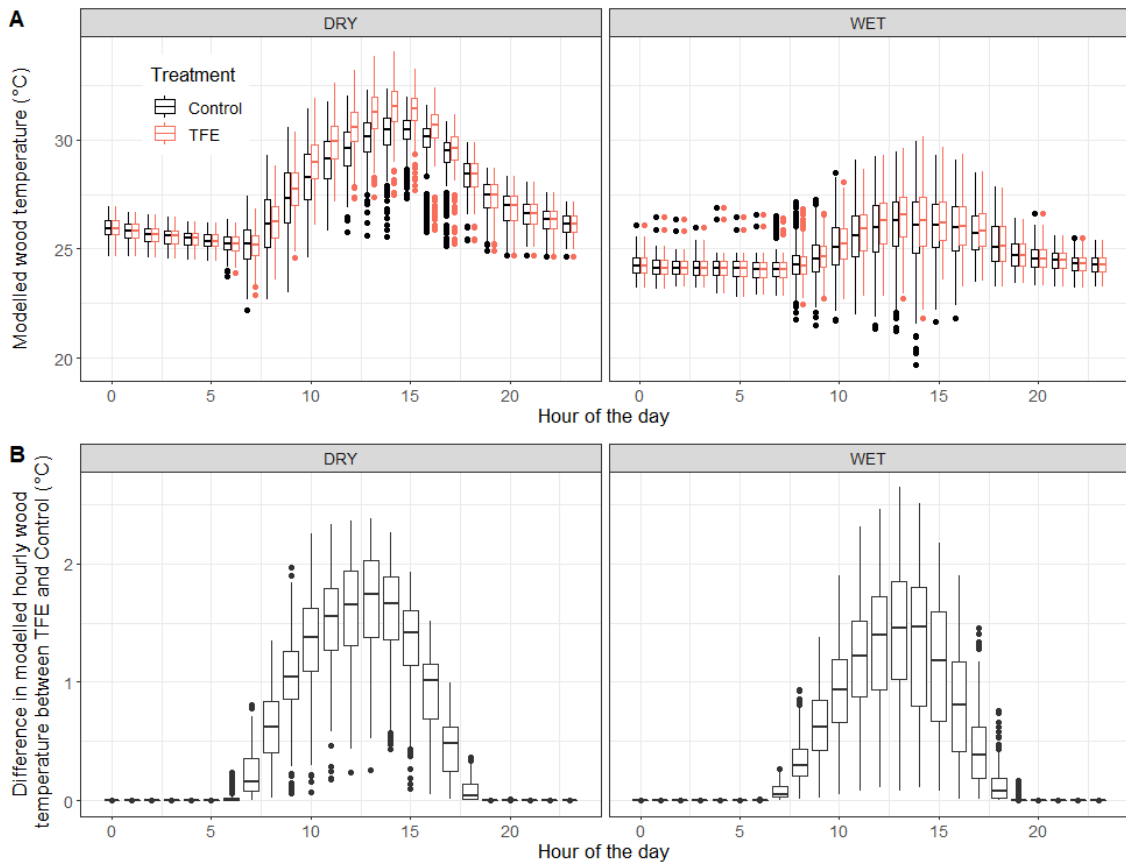


Figure 3.4: A. Modelled diurnal pattern in wood surface temperature on the Control (black) and TFE (red) using a wood surface temperature model that relates measured wood surface temperature with half hourly measurements of air temperature (16 m), total global radiation, season, location of wood (canopy, stem), experiment (TFE, Control), and tree light score (1-5, low-high light), and an interaction between the air temperature and tree light score, and an interaction between air temperature, total global radiation and tree light score ( $R^2 = 0.84$ , Appendix B.5). B. The difference in hourly modelled wood surface temperature between TFE and Control.

indicates that the surface area continues to increase, potentially exponentially with tree DBH, although we do not have sufficient data for large trees to test whether the increase is exponential (Figure 3.5B).

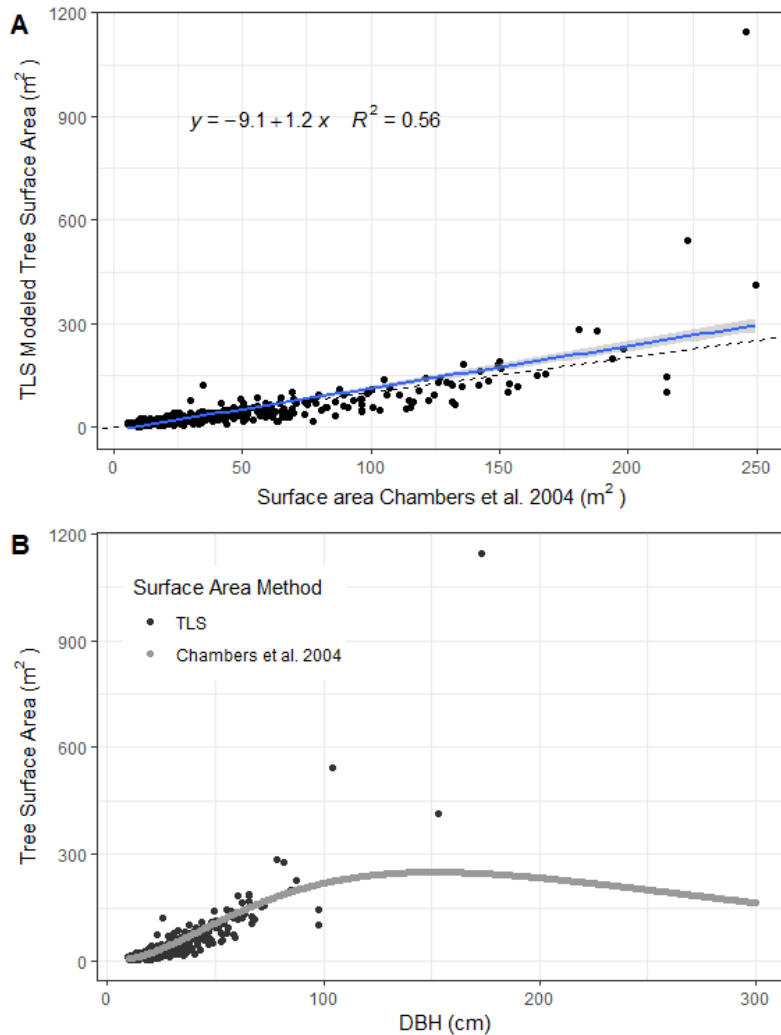


Figure 3.5: A) A comparison of tree surface area from Chambers et al., 2004 with tree surface area using quantitative structural models derived from TLS. The  $R^2$  and linear regression equation are shown at top left of graph. The dashed line has slope of 1, intercept of 0. B) The surface area of trees using TLS methods (black) and Chamber et al., 2014 (grey) versus tree DBH.

Treatment had an effect on tree structure. Trees on the TFE had a lower tree surface area for an equivalent-sized tree volume on the TFE in comparison to the Control (Figure 3.6A). Specifically, canopy woody volume was lower on TFE than Control trees of the same size (Table 3.1), resulting in a higher tree mean branch radius, where mean is weighted by branch volume (Figure 3.6B). This resulted in lower surface area to volume ratios on the TFE than the Control (Figure 3.6A),

since the surface area to volume ratio decreases with increasing branch radius.

Table 3.1: The coefficients for linear regression models describing the relationship between canopy wood volume (m<sup>3</sup>) and tree woody volume (m<sup>3</sup>), and the effect of treatment.

	<i>Dependent variable:</i>
	log(Canopy volume)
log(Tree volume)	1.015*** (0.043)
plotTFE	-0.428*** (0.104)
Constant	-1.336*** (0.075)
Observations	318
R <sup>2</sup>	0.682
Adjusted R <sup>2</sup>	0.680
Residual Std. Error	0.896 (df = 315)
F Statistic	337.593*** (df = 2; 315)
<i>Note:</i>	*p<0.1; **p<0.05; ***p<0.01

When evaluating the total forest surface area on a per tree basis, the cumulative woody surface area, starting from trees of 10 cm DBH, was lower on the TFE than the Control for all trees greater than 12.5 cm DBH (Figure 3.7). The total wood area index (WAI, m<sup>2</sup>m<sup>-2</sup>), which is projected wood surface area per m<sup>2</sup> ground area, on the Control was 0.59 ± 0.02 m<sup>2</sup>/m<sup>2</sup>, and on the TFE 0.34 ± 0.01 m<sup>2</sup>/m<sup>2</sup> (Figure 3.7).

### 3.3.3 Wood CO<sub>2</sub> efflux rates

#### Levy-Jarvis method to test for the best scalar for Wood CO<sub>2</sub> efflux

The analysis of the raw data using Levy-Jarvis method (?) indicated that wood CO<sub>2</sub> efflux scaled on a surface area basis for all tissue branch sizes. The Levy-Jarvis method demonstrates that if wood CO<sub>2</sub> efflux rate is related to surface area, then

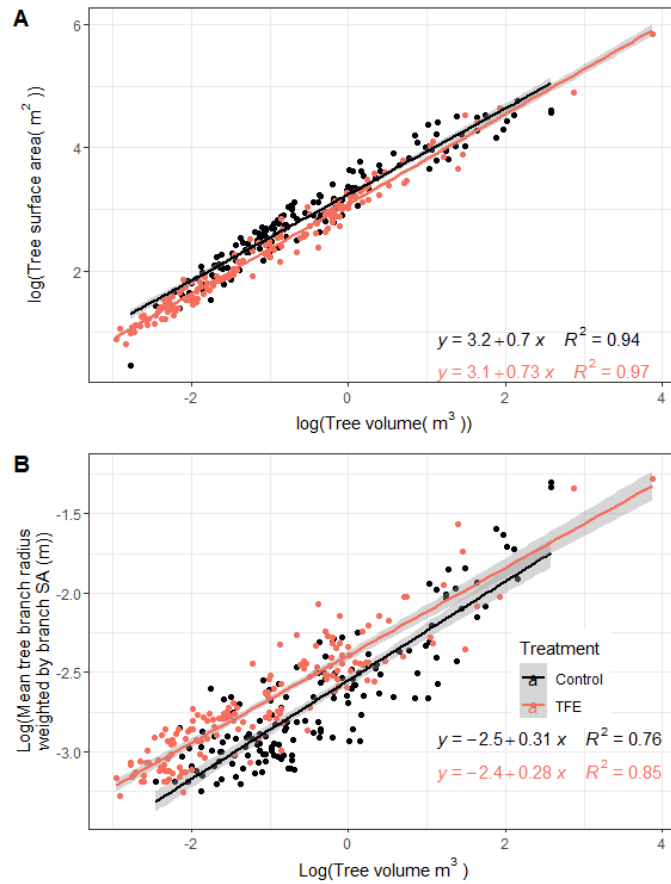


Figure 3.6: A) The relationship between tree volume (m<sup>3</sup>) and tree surface area (m<sup>2</sup>). B) The relationship between tree mean radius, where mean radius is weighted by branch volume, and tree woody volume (m<sup>3</sup>) for Control (black) and TFE (red). The linear regression equation is shown at the bottom right.

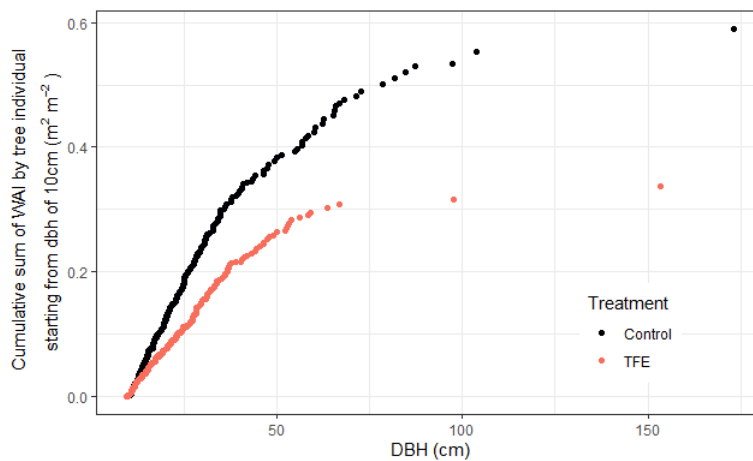


Figure 3.7: The cumulative sum of wood area index (WAI) on TFE (red) and Control (black), where the cumulative sum starts from trees with a DBH of 10 cm, and ends with the largest tree in each treatment.

dividing both the wood CO<sub>2</sub> efflux rate and the wood surface area by woody tissue volume would result in wood CO<sub>2</sub> efflux rates on a volume basis proportional to the reciprocal of the branch radius, relying on the fact that the ratio of surface area to volume for a cylinder of equal length and equal radius is 2 divided by the radius (for further explanation see ?). For data presented here, wood CO<sub>2</sub> efflux on a volume basis is linearly related with the reciprocal of the branch diameter, suggesting surface area scaling (Figure 3.8, R<sup>2</sup> =0.37). Therefore, throughout the results, all models and values of wood CO<sub>2</sub> efflux are presented on a surface area basis, and wood CO<sub>2</sub> efflux is scaled using surface area as a scalar.

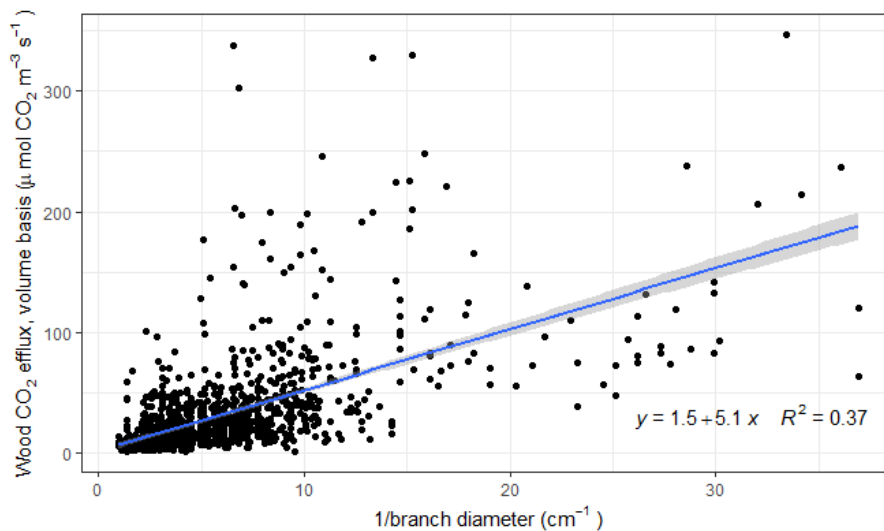


Figure 3.8: Wood CO<sub>2</sub> efflux on a volume basis ( $\mu\text{mol CO}_2 \text{ m}^{-3}\text{s}^{-1}$ ), versus the reciprocal of branch diameter ( $\text{cm}^{-1}$ ). The linear regression equation is shown at the bottom right.

### Wood CO<sub>2</sub> efflux

Mean wood CO<sub>2</sub> efflux at 25 °C (WC<sub>25</sub>) in 2018-2019 was  $1.1 \pm 0.02 \mu\text{mol CO}_2 \text{ m}^{-2} \text{ s}^{-1}$  (N = 1625, range 0.05-3.9  $\mu\text{mol CO}_2 \text{ m}^{-2} \text{ s}^{-1}$ ), where branch and stem diameters ranged from 0.1 to 103.7 cm. For twigs smaller than 2 cm in diameter (hereafter, ‘twigs’), mean WC<sub>25</sub> was  $0.90 \pm 0.04 \mu\text{mol CO}_2 \text{ m}^{-2} \text{ s}^{-1}$  (N= 378); for canopy branches larger than 2cm (hereafter, ‘canopy branches’), WC<sub>25</sub> was  $1.3 \pm 0.04 \mu\text{mol CO}_2 \text{ m}^{-2} \text{ s}^{-1}$  (N = 319); and for tree stems, measured at 1.3 m, WC<sub>25</sub> was  $1.1 \pm 0.02 \mu\text{mol CO}_2 \text{ m}^{-2} \text{ s}^{-1}$  (N=928). There was no treatment effect on WC<sub>25</sub> for stems or

canopy branches, although  $WC_{25}$  of twigs on the TFE was higher than the Control in March (wet season) by  $0.52 \pm 0.16 \mu\text{mol CO}_2 \text{ m}^{-2} \text{ s}^{-1}$  (Figure 3.9). Month had an effect on  $WC_{25}$  for twig, canopy branches, and stem measurements: twig  $WC_{25}$  was  $1.46 \pm 0.13 \mu\text{mol CO}_2 \text{ m}^{-2} \text{ s}^{-1}$  higher in March (peak wet season) than October (peak dry season); canopy  $WC_{25}$  was  $0.33 \pm 0.2 \mu\text{mol CO}_2 \text{ m}^{-2} \text{ s}^{-1}$  higher in March (peak wet season) than October (peak dry season); and monthly stem  $WC_{25}$  was different each month, with the maximum difference between mean monthly stem measurements being  $1.1 \pm 0.2 \mu\text{mol CO}_2 \text{ m}^{-2} \text{ s}^{-1}$  (Figure 3.9).

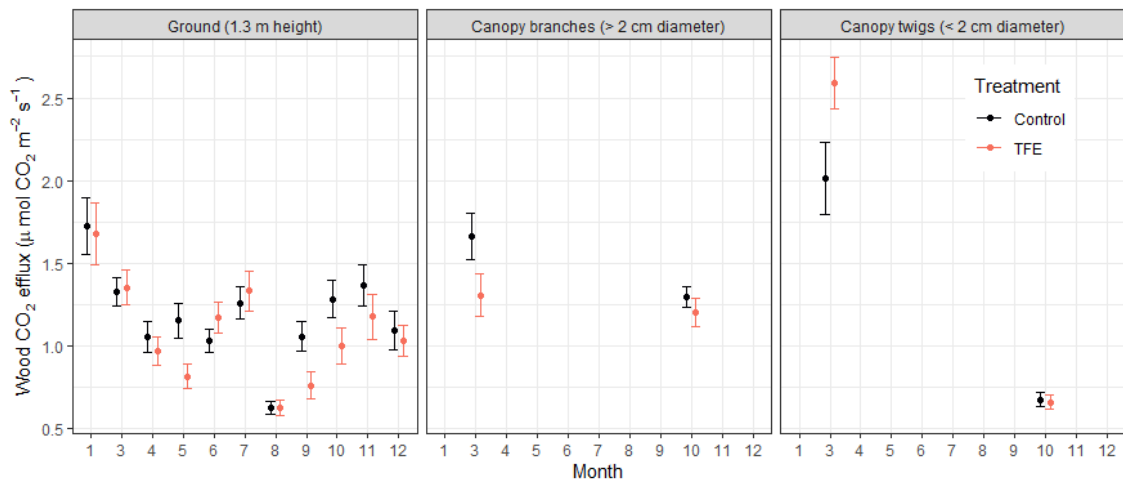


Figure 3.9: Wood CO<sub>2</sub> efflux ( $\mu\text{mol CO}_2 \text{ m}^{-2}\text{s}^{-1}$  per month measured on the TFE (red) and Control (black) for stem woody tissue (1.3 m height,  $N = 928$ ), and canopy branches, where the canopy measurements are separated into categories of branches larger 2 cm in diameter ( $N = 319$ ), and twigs, which are considered branches smaller than 2 cm in diameter ( $N = 378$ ). Stem wood CO<sub>2</sub> efflux was measured for all months in 2019, except February. Stem wood CO<sub>2</sub> efflux was measured on the same 103 trees (Control, 51; TFE, 52) each month. No treatment effect was present for wood CO<sub>2</sub> efflux within a given month for stem or canopy branch measurements, although canopy twig wood CO<sub>2</sub> efflux was higher on the TFE in March than Control twigs. The final model of wood CO<sub>2</sub> efflux included the variables month, branch diameter, tree growth rate, time of day, location of the wood (canopy, ground), and a random effect of tree individual (Table 3.1).

The final model of  $WC_{25}$ , using  $WC_{25}$  of branches only above 5 cm in diameter, included month of the year, branch diameter, location of the wood (canopy, ground), time of day (morning, midday, afternoon), and total yearly growth rate of the tree (cm circumference  $\text{yeartree}^{-1}$ ), with a random effect of tree individual ( $R^2_c = 0.34$ ,  $R^2_m = 0.16$ , Table 3.2); genus as a random effect was not significant.  $WC_{25}$  was

highest after 15:00 hrs in comparison to morning (7:00-11:00) or midday (11:00-15:00), and was higher in the canopy than the trunk by  $0.24 \pm 0.07 \mu\text{mol CO}_2 \text{ m}^{-2} \text{ s}^{-1}$ .  $\text{WC}_{25}$  increased with branch diameter and total yearly growth rate.

Table 3.2: The model coefficients of linear mixed effects model of wood  $\text{CO}_2$  efflux at  $25^\circ\text{C}$  ( $\text{WC}_{25}$ ) for woody tissue with a diameter above 5 cm. The final fixed effects were month, growth (circumference growth  $\text{cm day}^{-1}$ ), time of day (morning, 7:00-11:00h, midday 11:00-14:00h; afternoon > 14:00 h), tree location (canopy measurements or ground measurements at 1.3 m height), and branch diameter (m), with tree individual as a random effect (uniqueid).

Predictors	Estimates	std. Error	p
(Intercept)	1.73	0.12	<0.001
month [3]	-0.36	0.10	0.001
month [4]	-0.72	0.12	<0.001
month [5]	-0.71	0.12	<0.001
month [6]	-0.64	0.11	<0.001
month [7]	-0.40	0.12	<0.001
month [8]	-1.08	0.11	<0.001
month [9]	-0.82	0.11	<0.001
month [10]	-0.59	0.11	<0.001
month [11]	-0.41	0.11	<0.001
month [12]	-0.64	0.12	<0.001
growth	0.02	0.01	0.002
tod [Midday]	-0.09	0.04	0.038
tod [Morning]	-0.18	0.07	0.010
Tree.location [Ground]	-0.24	0.07	0.001
branch.diameter	0.66	0.21	0.001
Random Effects			
$\sigma^2$	0.38		
$\tau$ uniqueid	0.11		
ICC	0.22		
N uniqueid	143		
Observations	1163		
Marginal $R^2$ / Conditional $R^2$	0.150 / 0.338		

When evaluating  $\text{WC}_{25}$  data of 3 or more individuals per genus, per experiment (Figure 3.10), genus had an effect on  $\text{WC}_{25}$  for *Minquartia*, *Eschweilera*, and *Vouacapoua*.  $\text{WC}_{25}$  increased in the wet season in comparison to dry for *Eschweilera* by  $0.42 \mu\text{mol CO}_2 \text{ m}^{-2} \text{ s}^{-1}$  (95% CI 0.003-0.84,  $p = 0.05$ ), *Licania* by  $0.53 \mu\text{mol CO}_2$

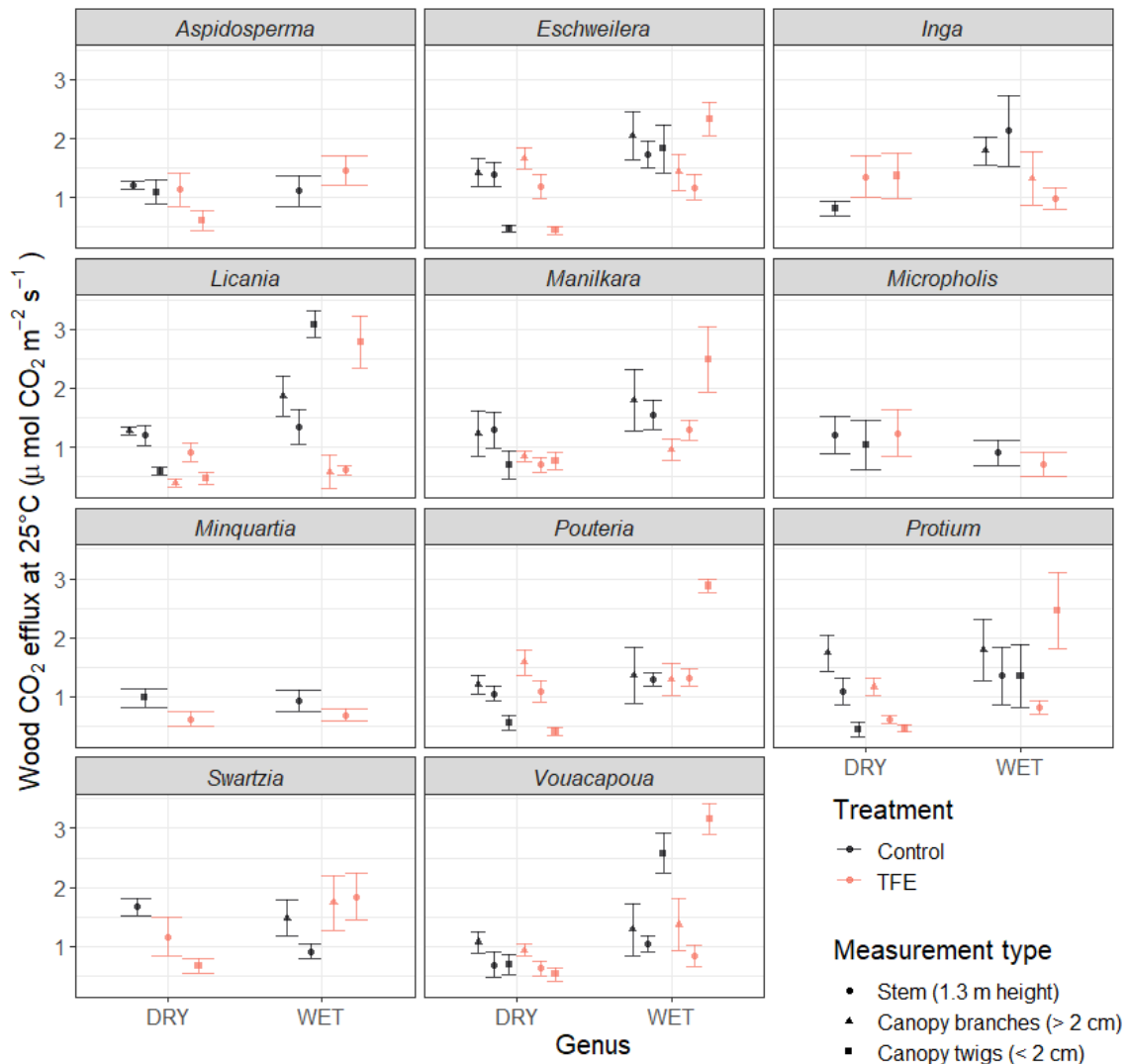


Figure 3.10: Wood CO<sub>2</sub> efflux at 25°C (WC<sub>25</sub>,  $\mu\text{mol CO}_2 \text{ m}^{-2} \text{ s}^{-1}$  in Control (black) and TFE (red) separated by genus and season for stem measurements (measured at 1.3m, circles), and canopy measurements, where canopy measurements are separated by branch diameter into two categories: canopy branches greater than 2 cm in diameter (triangles), and canopy twigs less than 2 cm in diameter (square). TFE treatment had an effect on *Licania*, resulting in lower WC<sub>25</sub> by  $0.49 \mu\text{mol CO}_2 \text{ m}^{-2} \text{ s}^{-1}$  (95% CI 0.127-1.11,  $p = 0.001$ ) on the TFE than the Control, however no other treatment effect was found. Genus had an effect on WC<sub>25</sub> for *Minquartia*, *Eschweilera*, and *Vouacapoua*. WC<sub>25</sub> increased in the wet season in comparison to dry for *Eschweilera* by  $0.42 \mu\text{mol CO}_2 \text{ m}^{-2} \text{ s}^{-1}$  (95% CI 0.003-0.84,  $p = 0.05$ ), *Licania* by  $0.53 \mu\text{mol CO}_2 \text{ m}^{-2} \text{ s}^{-1}$  (95% CI 0.023-1.03,  $p = 0.02$ ), *Pouteria* by  $0.52 \mu\text{mol CO}_2 \text{ m}^{-2} \text{ s}^{-1}$  (95% CI 0.16-0.88,  $p = 10^{-5}$ ) and *Vouacapoua* by  $0.65 \mu\text{mol CO}_2 \text{ m}^{-2} \text{ s}^{-1}$  (95% CI 0.13-1.18,  $p = 0.002$ ).

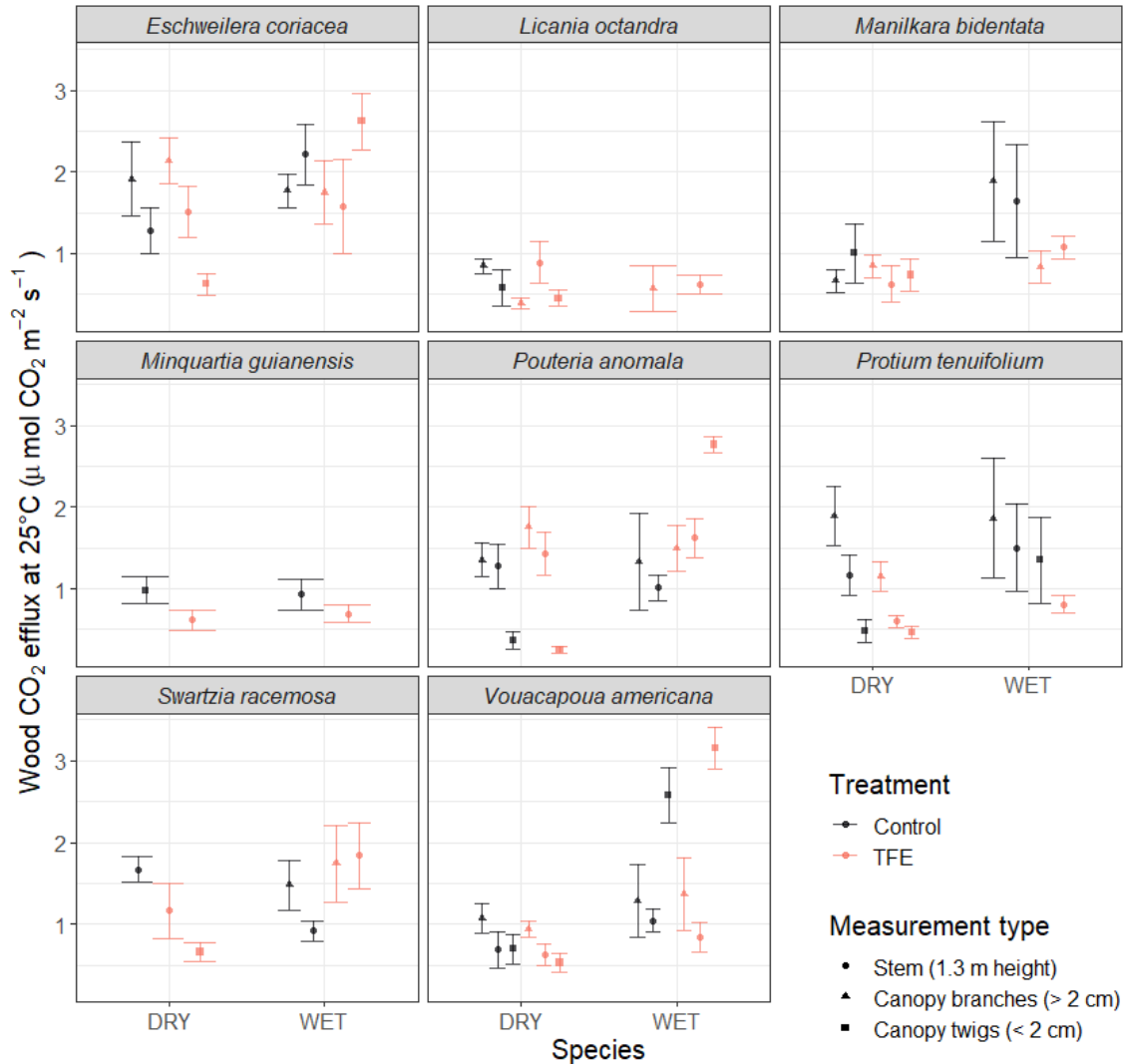


Figure 3.11: Wood CO<sub>2</sub> efflux in Control (black) and TFE (red) measured on tree stems (measured at 1.3m, circles), canopy branches greater than 2 cm in diameter (triangle), and canopy twigs less than 2 cm in diameter (square) for 8 species in the dry season and wet season. There was no TFE treatment effect on any species, however there was a species effect on WC<sub>25</sub> for *Licania octandra*, *Manilkara bidentata*, *Pouteria anomala*, *Vouacapoua americana*, and *Eschweilera coriacea*. The WC<sub>25</sub> of *Vouacapoua americana* was different seasonally, with the wet season higher than the dry season by  $0.67 \mu\text{mol CO}_2 \text{ m}^{-2} \text{ s}^{-1}$  ( $p = 0.001$ , 95% CI 0.15-1.17).

$\text{m}^{-2} \text{s}^{-1}$  (95% CI 0.023-1.03,  $p = 0.02$ ), *Pouteria* by  $0.52 \mu\text{mol CO}_2 \text{ m}^{-2} \text{ s}^{-1}$  (95% CI 0.16-0.88,  $p = 10^{-5}$ ) and *Vouacapoua* by  $0.65 \mu\text{mol CO}_2 \text{ m}^{-2} \text{ s}^{-1}$  (95% CI 0.13-1.18,  $p = 0.002$ ). Only one genus, *Licania*, was affected by the TFE drought treatment, resulting in an overall lower  $\text{WC}_{25}$  by  $0.49 \mu\text{mol CO}_2 \text{ m}^{-2} \text{ s}^{-1}$  (95% CI 0.127-1.11,  $p = 0.001$ ) on the TFE in comparison to Control. When evaluating  $\text{WC}_{25}$  of data with 3 or more individuals per species per experiment (Figure 3.11), there was no treatment effect on species, although there was a species effect on  $\text{WC}_{25}$  for *Licania octandra*, *Manilkara bidentata*, *Pouteria anomala*, *Vouacapoua americana*, and *Eschweilera coriacea*. Only *Vouacapoua americana* had seasonal differences, with an increase in the wet season by  $0.67 \mu\text{mol CO}_2 \text{ m}^{-2} \text{ s}^{-1}$  ( $p = 0.001$ , 95% CI 0.15-1.17).

### 3.3.4 Scaling wood $\text{CO}_2$ efflux model to trees

The model of  $\text{WC}_{25}$  was applied per branch cylinder for the QSMs of 321 trees, resulting in a modelled  $\text{WC}_{25}$  value per cylinder on each tree. The  $\text{WC}_{25}$  was multiplied by the surface area of each cylinder, the sum of which was the whole tree woody  $\text{CO}_2$  efflux. The relationship between whole tree woody  $\text{CO}_2$  efflux and tree volume was fit with a nonlinear scaling equation (equation 3.1). Both the normalization constant ( $y_0$ ) and the scaling exponent ( $\alpha$ ) were different between treatments, with the exponent on the TFE higher than the Control, at  $0.83 \pm 0.02$  versus  $0.69 \pm 0.01$ , respectively (Figure 3.12, Table 3.3) and  $y_0$  on the TFE lower than the Control,  $0.0091 \pm 0.003$ ,  $0.011 \pm 0.0002$ , respectively.

### 3.3.5 Scaling wood $\text{CO}_2$ efflux to stand

We applied a model of whole tree  $\text{WC}_{25}$  using tree surface area (Table 3.4,  $R^2 = 0.88$ ) to all trees on the TFE and the Control, the sum of which was used to estimate plot-level wood  $\text{CO}_2$  efflux. When tree wood  $\text{CO}_2$  efflux was scaled to plot (1 ha),  $R_{\text{wood}}$  at ambient temperature was  $3.9 \pm 0.9 \text{ Mg C ha}^{-1} \text{ yr}^{-1}$  for the TFE ( $3.4 \pm 0.7 \text{ Mg C ha}^{-1} \text{ yr}^{-1}$  at  $25^\circ\text{C}$ ),  $6.8 \pm 1.6 \text{ Mg C ha}^{-1} \text{ yr}^{-1}$  for the Control ( $6.5 \pm 1.4 \text{ Mg C ha}^{-1} \text{ yr}^{-1}$  at  $25^\circ\text{C}$ ), which is a difference in  $R_{\text{wood}}$  at ambient temperature between TFE and

Table 3.3: Model coefficients and standard error for nonlinear scaling equation of whole tree wood CO<sub>2</sub> efflux (Mg C tree<sup>-1</sup>yr<sup>-1</sup>) versus tree woody volume (m<sup>3</sup>), using equation 3.1 where  $y_0$  is a normalization constant,  $V$  is tree volume (m<sup>3</sup>) and  $\alpha$  is a scaling exponent.

Whole tree wood CO <sub>2</sub> efflux			
Predictors	Estimates	std. Error	p
$\alpha$ [Control]	0.6869	0.0145	<0.001
$\alpha$ [TFE]	0.8288	0.0235	<0.001
$y_0$ [Control]	0.0111	0.0002	<0.001
$y_0$ [TFE]	0.0091	0.0003	<0.001
Observations	321		

Control of 57.8% (Table 3.5). The lower  $R_{\text{wood}}$  on the TFE is accounted for by  $57.4 \pm 1.7\%$  less total woody surface area on the TFE than the Control (Figure 3.7), following substantially higher mortality among TFE trees (Rowland et al., 2015) as well as tree structural changes on TFE trees (Figure 3.6A, Figure 3.6B, Table 3.1).

Table 3.4: Model coefficients of whole tree yearly wood CO<sub>2</sub> efflux (Mg C tree<sup>-1</sup>yr<sup>-1</sup>) using tree surface area (m<sup>2</sup>) and tree canopy width (m), log transformed for linearity.

log(Whole tree wood CO <sub>2</sub> efflux)			
Predictors	Estimates	std. Error	p
(Intercept)	-8.17	0.12	<0.001
Tree surface area [log]	0.85	0.04	<0.001
Tree canopy width [log]	0.32	0.10	0.002
Observations	324		
$R^2$ / $R^2$ adjusted	0.880 / 0.880		

The effect of higher temperature on the TFE only marginally influenced the difference between  $R_{\text{wood}}$  on the TFE versus the Control, resulting in a  $3.2 \pm 0.5\%$  increase in  $R_{\text{wood}}$  on the TFE in comparison to the Control due to temperature.

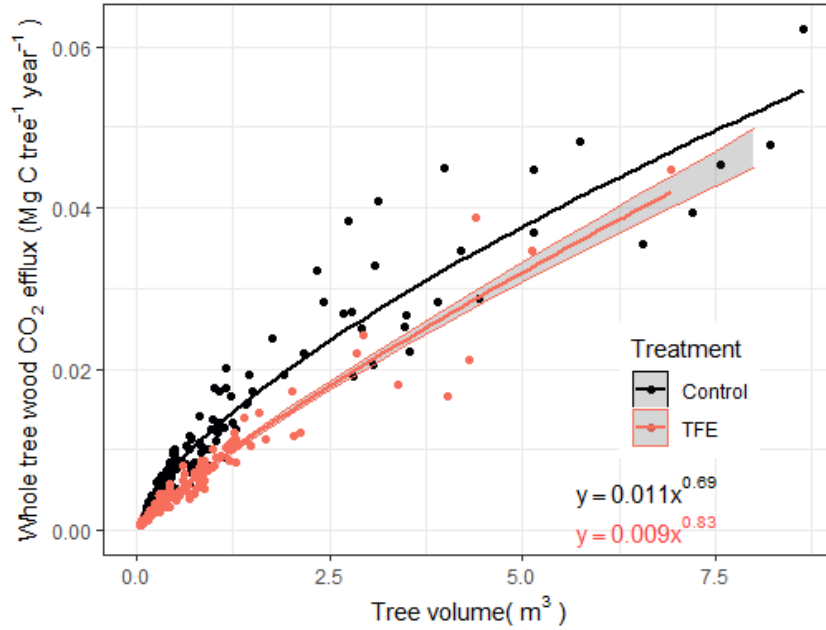


Figure 3.12: The metabolic scaling of whole tree wood CO<sub>2</sub> efflux (Mg C tree<sup>-1</sup>yr<sup>-1</sup>) versus tree volume (m<sup>3</sup>) for Control (black) and TFE (red), which was fit with nonlinear scaling equation (equation 3.1). The shaded region is 95% confidence interval of model. See Table 3.3 for coefficient details.

Table 3.5: The yearly wood CO<sub>2</sub> efflux per hectare (Mg C ha<sup>-1</sup> yr<sup>-1</sup>) for TFE and Control in 2019 at ambient temperature and at 25°C.

	R <sub>ambient</sub>	R <sub>25</sub>
Control	6.8±1.6	6.5±1.4
TFE	3.9±0.9	3.4±0.7

### 3.3.6 ARQ: wood respiration

Apparent respiratory quotient (ARQ) ranged from 0.28 to 0.84, with a mean value of  $0.60 \pm 0.12$  (Figure 3.13). ARQ was not related to tree DBH ( $p = 0.6$ ), but was influenced by time of day, treatment and species: ARQ was 0.08 ( $p = 0.006$ , 95% CI 0.02-0.13) higher at night in comparison to daytime; ARQ was 0.1 ( $p = 0.0006$ , 95% CI 0.04-0.15) higher on the TFE relative to Control, and ARQ was 0.1 ( $p = 0.0002$ , 95% CI 0.05-0.16) higher for species *Pouteria anomala* than *Eschweilera coriacea* (Figure 3.13). There was no difference in ARQ between canopy and stem measurement locations, even though sap flux was higher at ground level (1.3 m) than in the canopy in the afternoon by 0.07 kg/h ( $p = 0.05$ , 0.002-0.13, Figure 3.14). There was no treatment or species effect on afternoon sap flux, nor was there

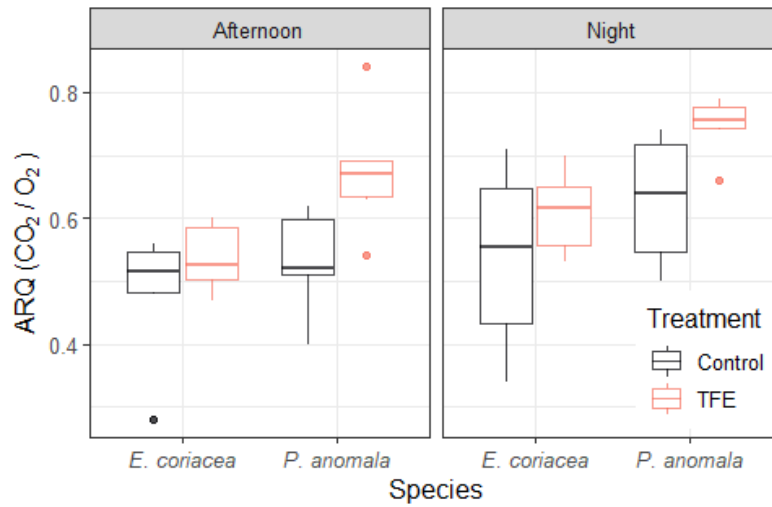


Figure 3.13: ARQ measurements on 12 trees on the TFE (N= 6), and Control (N=6) for two species, *Pouteria anomala* and *Eschweilera coriacea*. The final model excluded location of measurement in the tree (canopy or stem). ARQ was influenced by time of day, treatment and species, with ARQ 0.08 ( $p = 0.006$ , 95% CI 0.02-0.13) higher at night than during the day, an ARQ 0.1 ( $p = 0.0006$ , 95% CI 0.04-0.15) higher on the TFE relative to Control, and an ARQ 0.1 ( $p = 0.0002$ , 95% CI 0.05-0.16) higher in *Pouteria anomala* than *Eschweilera coriacea*.

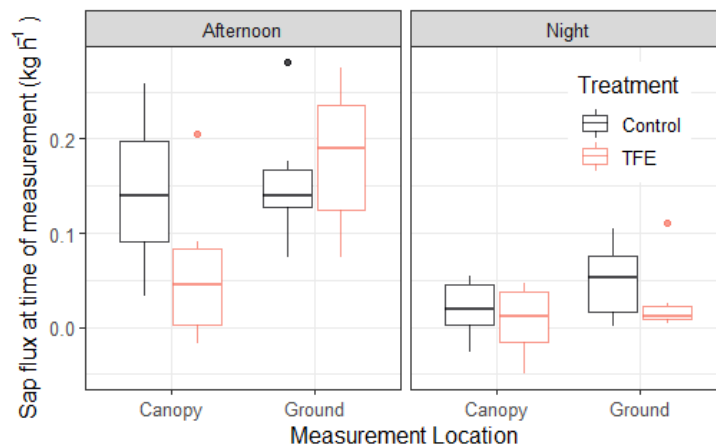


Figure 3.14: Sap flux rates during the hour that ARQ was measured in the canopy and the ground during the afternoon and at night. There was no treatment effect on sap flux. During the afternoon sap flux was higher at ground level (1.3 m) than in the canopy by 0.07 kg/h ( $p = 0.05$ , 0.002-0.13, Figure 14). The apparent difference in afternoon flux rates in the canopy between TFE and Control were not significant ( $p = 0.3$ ).

a relationship between sap flux and ARQ during the afternoon (Figure 3.15). Using the mean value of ARQ for TFE and Control we estimated that wood respiration rates were  $1.6 \pm 0.08$  and  $1.8 \pm 0.11$  times higher than what is measured using radial wood CO<sub>2</sub> efflux for TFE and Control, respectively.

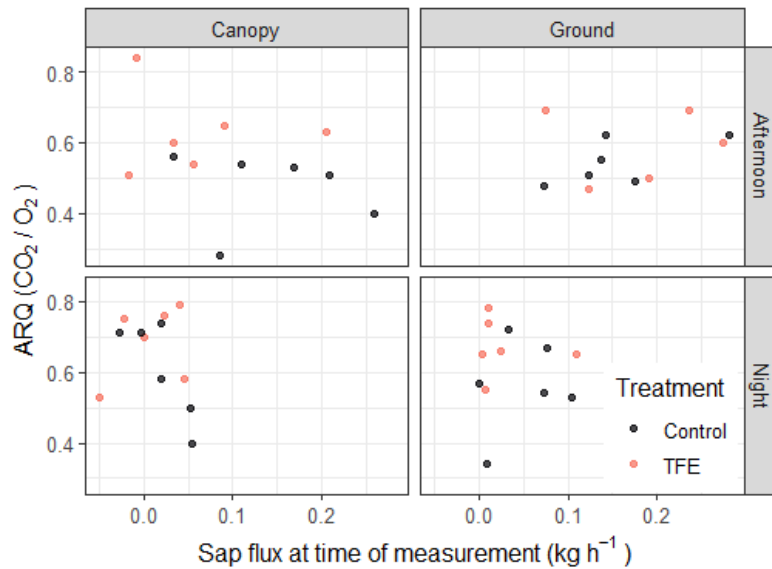


Figure 3.15: ARQ (CO<sub>2</sub>/O<sub>2</sub>) versus the sap flux (kg h<sup>-1</sup>) at time of ARQ measurement for Control (black) and TFE (red) in the stem (measured at 1.3 m) and canopy during the afternoon and at night.

For the 12 trees with ARQ measurements, wood respiration was scaled to tree using tree surface area derived from each of the 12 tree QSMs. The relationship between whole tree wood respiration and tree volume was modelled using nonlinear metabolic scaling (equation 3.1). The resulting scaling exponent for whole tree wood respiration was  $0.84 \pm 0.2$ , and had too large of an error to evaluate if the exponent was different from 1 (Figure 3.16). The scaling exponent of whole tree wood CO<sub>2</sub> efflux was identical to scaling exponent of whole tree wood respiration, at  $0.84 \pm 0.2$ . No treatment effect on whole tree wood respiration or whole tree wood CO<sub>2</sub> efflux was found. Overall, whole tree wood respiration was a mean of  $91.0 \pm 14.1\%$  higher than whole tree wood CO<sub>2</sub> efflux (range 35.8-203.6%, Figure 3.16).

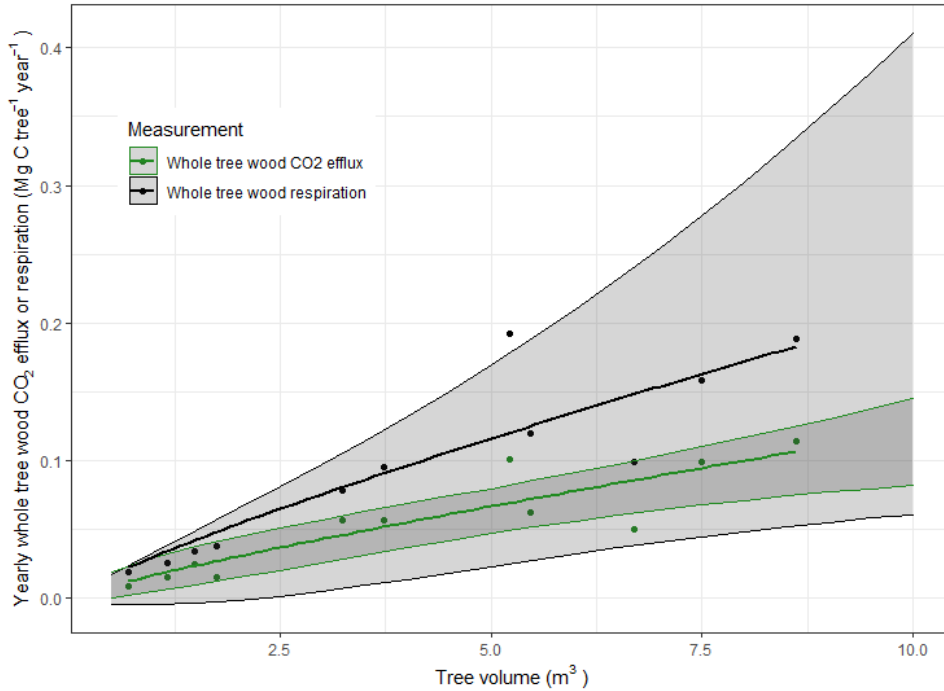


Figure 3.16: The whole tree wood CO<sub>2</sub> efflux (black, Mg C tree<sup>-1</sup>yr<sup>-1</sup>) and whole tree wood respiration (green, Mg C tree<sup>-1</sup>yr<sup>-1</sup>) versus tree volume (m<sup>3</sup>) fit with nonlinear scaling equation (equation 3.1). The shaded region is 95% confidence interval of model.

### 3.4 Discussion

Following 18-years of an ecosystem-scale (1 ha) drought treatment in an eastern Amazonian rainforest, our results show substantial changes in the physical environment and the vegetation. Earlier reports demonstrated large impacts on the droughted forest (TFE plot) relative to the undroughted (Control plot) forest, including reduced soil moisture content (Bittencourt et al., 2020; Sotta et al., 2007), increased mortality leading to 40% loss of aboveground biomass (Rowland et al., 2015), and increased light exposure to parts of the remaining canopy following magnified incidence of mortality (Rowland et al., 2021b). Here, we expand these findings, reporting a 38-67% reduction in surface soil volumetric water content, dependent on season (Figure 3.1) and higher daytime woody surface temperatures (Figure 3.2, 3.3, 3.4A, 3.4B). We also report changes in the physical environment by using terrestrial laser scanning (TLS) to describe detailed 3D tree woody structure, demonstrating that trees on the TFE have a lower woody surface area to woody volume ratio be-

cause TFE trees have proportionally less canopy woody volume per unit tree volume (Figure 3.6A, 3.6B, Table 3.1), resulting in a larger mean tree branch radius (Figure 3.6B) and consequently, a lower surface area.

Coupled with extensive sampling of wood CO<sub>2</sub> efflux from branches in the canopy and on the stem of 192 trees, we demonstrate that the altered environment on the TFE has resulted in lower whole-tree wood CO<sub>2</sub> efflux relative to the Control for trees of equivalent tree volume (Figure 3.12, Table 3.3), despite minimal difference in wood CO<sub>2</sub> efflux rates at 25°C (WC<sub>25</sub>) on a woody surface area basis (Table 3.2, Figure 3.9). The reduction in whole tree wood CO<sub>2</sub> efflux occurred entirely due to structural changes in TFE trees. This suggests that structural acclimation on TFE trees has resulted in lower carbon use by the woody component of the whole tree, and that this occurred without loss of function associated with reduced WC<sub>25</sub> rates during drought (Rodríguez-Calcerrada et al., 2021).

When wood CO<sub>2</sub> efflux was scaled to the plot, R<sub>wood</sub> was 57.8% lower on the TFE in comparison to the Control (Table 3.5), due to an equivalent decrease in forest woody surface area on the TFE (Figure 3.7) following earlier drought-related mortality (Rowland et al., 2015) and tree structural changes on the TFE (Figure 3.6A, 3.6B, Table 3.1). The difference in R<sub>wood</sub> between treatments is more than two times larger than previously reported difference (22% versus 57%) between treatments (Rowland et al., 2018, ,Table 3.5), although notably the total aboveground biomass has not decreased since the previous study (Chapter 3). The discrepancy between previous reports of stand wood CO<sub>2</sub> and current reports are due to (i) lack of treatment effect on WC<sub>25</sub> reported here, in contrast to higher WC<sub>25</sub> reported in trees on the TFE during wet season previously (Rowland et al., 2018) and (ii) structural changes on TFE trees that resulted in a lower surface area to volume ratio (Table 3.1, Figure 3.6A, 3.6B).

### 3.4.1 Wood CO<sub>2</sub> efflux and wood respiration on the TFE relative to the Control

The WC<sub>25</sub> values presented here,  $1.1 \pm 0.02 \mu\text{mol m}^{-2} \text{ s}^{-1}$ , were not significantly different from previous measurements reported at the site (Rowland et al., 2018) and were within the range reported elsewhere in tropical rainforests (Cavaleri et al., 2006; Katayama et al., 2014, 2019; Jardine et al., 2022). Previous data from this site indicated that WC<sub>25</sub> for woody tissue in the TFE was higher than for Control forest trees during the wet season (Rowland et al., 2018). Here, twigs had higher WC<sub>25</sub> during the wet season on the TFE than on the Control; however, there was no treatment effect on WC<sub>25</sub> in any month for woody tissue larger than 2 cm in diameter. We found large differences in monthly stem, canopy and twig WC<sub>25</sub> (Figure 3.9), indicating an important effect of seasonality on wood CO<sub>2</sub> efflux.

Consistent with other studies of canopy WC<sub>25</sub> (Asao et al., 2015; Cavaleri et al., 2006), canopy branches had higher rates of wood CO<sub>2</sub> efflux than stem by  $0.24 \pm 0.07 \mu\text{mol CO}_2 \text{ m}^{-2} \text{ s}^{-1}$  (Figure 3.9, Table 3.2), possibly because of higher rates of growth related metabolism in canopy branches (Asao et al., 2015; Cavaleri et al., 2006). Twigs had low WC<sub>25</sub> in October (dry season) in comparison to stem and canopy branch measurements (Figure 3.9). The reduction in WC<sub>25</sub> in twigs during the dry season could be due to twigs existing in exposed environment, with higher evaporative demands, which result in higher temperature and water stress limiting twig growth. In the wet season, twigs had highest WC<sub>25</sub> of all three measurement locations (Figure 3.9), potentially due to high growth rates.

In line with Rowland et al. (2018), we found rates of WC<sub>25</sub> increased with branch diameter and tree growth rate (Table 3.2). Additionally we found that WC<sub>25</sub> changes diurnally, with highest rates after 15:00 h in comparison to measurements between 7:00 h – 15:00 h. A daytime decrease in WC<sub>25</sub> has been widely reported (Rodríguez-Calcerrada et al., 2014; Salomón et al., 2016, 2018) and is thought to occur due to low turgor pressure and the transport of locally produced respiratory CO<sub>2</sub> through the xylem. We tested separately for an effect of sap flow on wood CO<sub>2</sub> efflux on

12 trees by examining the relationship between ARQ and sap flux at the time of measurement, but no relationship was observed (Figure 3.15), suggesting that sap flow may not have an effect on WC<sub>25</sub> at this site. As we measured wood surface temperature, it is possible that our temperature correction of woody CO<sub>2</sub> efflux did not accurately represent the temperature of the underlying actively respiring woody tissue. This could have created systematic biases in temperature correction of wood CO<sub>2</sub> efflux if the difference between surface temperature and underlying woody tissue temperature follows a diurnal pattern.

In contrast with previous work showing limited taxonomic differences in WC<sub>25</sub> (Rowland et al., 2018), genus and species analysis of WC<sub>25</sub>, reported here, in the dry and wet season showed a taxonomic effect on WC<sub>25</sub> for 3 of 11 genera, 5 out of 8 species, and a strong seasonal component for 4 of 11 genera and 1 of 8 species, indicating that differences in WC<sub>25</sub> are potentially conserved taxonomically (Figure 3.10, 3.11). This may be an indication of differences in underlying woody tissue structure, as fraction of living parenchyma varies widely among tropical rainforest tree species, with one study finding a range of 12-66% (Ziemińska et al., 2015) across species.

The genus *Licania*, which has been shown to be resistant to treatment effect (Rowland et al., 2015) had lower WC<sub>25</sub> on the TFE than the Control, although when the same genus was evaluated on a species-level, *Licania octandra*, there was no difference between treatments (Figure 3.10, 3.11). This could indicate the importance of studying species-specific differences in physiology rather than classifying physiological differences according to genus; however, we also note that measurement replicates in the species-level comparison were only present in the dry season, during which time rates of all species are reduced in comparison to wet season. Therefore, the difference in species could have been an artefact of insufficient sampling seasonally.

Mean ARQ was  $0.60 \pm 0.12$ , which converges on the same mean value of ARQ from a previous study of 85 trees (Hilman et al., 2019). ARQ was higher on the

Control than the TFE, ie more respiratory-derived CO<sub>2</sub> is lost to alternate pathways in the Control than the TFE (Figure 3.13). The higher ARQ values obtained on the TFE plot trees suggests lower woody tissue respiration rates per unit surface area on the TFE relative to the Control plot trees, despite minimal difference in measured radial wood CO<sub>2</sub> efflux rates due to treatment (Table 3.2, Figure 3.9). This is consistent with expectations that drought stress generally leads to reduction in woody tissue respiration (De Roo et al., 2020; Rodríguez-Calcerrada et al., 2014). The preliminary ARQ analysis on two species suggests significant species differences in ARQ may occur (Figure 3.13). Additional sampling is necessary to use ARQ to interpret woody tissue respiration on a stand-scale, though on the basis of this initial analysis stand wood respiration would be  $1.6 \pm 0.08$  times higher than stand wood CO<sub>2</sub> efflux on the TFE and  $1.8 \pm 0.11$  times higher than wood CO<sub>2</sub> efflux on the Control. This would result in stand wood respiration values of approximately 11 Mg C ha<sup>-1</sup>yr<sup>-1</sup> on the Control and 6 Mg C ha<sup>-1</sup>yr<sup>-1</sup> on the TFE. This estimated stand wood respiration value on the Control would be higher or comparable with yearly respiration rates for soil and leaf for this experiment and in other tropical rainforests (Metcalf et al., 2010b; Malhi et al., 2009b; Costa da et al., 2010).

There was no difference in sap flow between treatments (Figure 3.14), nor any relationship between sap flow and ARQ (Figure 3.15), which could have driven changes in axial transport of respiratory-derived CO<sub>2</sub> resulting in differences in ARQ between treatments. Activity of carboxylating enzymes, for instance, phosphoenolpyruvate carboxylase, could have accounted for differences in ARQ between treatments (Berveiller et al., 2007; Berveiller, Damesin, 2008; Hilman et al., 2019), but this was not measured.

### **3.4.2 Wood metabolic load on trees under drought**

Whole tree wood CO<sub>2</sub> efflux for an equivalent-sized tree woody volume was lower on the TFE than the Control (Figure 3.12, Table 3.3), despite no treatment effect on WC<sub>25</sub> (Table 3.2). The lower whole tree wood CO<sub>2</sub> efflux on the TFE occurred due

to changes in tree structure that result in lower surface area for an equivalent-sized tree volume on the TFE in comparison to the Control (Table 3.1, Figure 3.6A, 3.6B). Specifically, we found that for an equivalent-sized tree, trees on the TFE have less tree canopy volume (Table 3.1), which resulted in larger mean branch radius per tree (Figure 3.6B), and consequently less surface area per unit volume in comparison to the Control (Figure 3.6A).

There is a large range of metabolic scaling exponents that have been suggested for trees (Cheng et al., 2010; Coomes, Allen, 2009; Lau et al., 2019b; Pretzsch, 2021; Sperry et al., 2012; West, 1997) with many studies suggesting a universal  $\frac{3}{4}$  power scaling or isometric scaling or both. Empirical evidence often conflicts with the idea of a universal metabolic scaling exponent for trees, as there have been differences in scaling exponents attributed to species (Bentley et al., 2013; Price et al., 2009), ontogenetic changes in trees (Mori et al., 2010) or tree allometry (Muller-Landau et al., 2006; Pretzsch, 2021). Here we test metabolic scaling in the context of abiotic stress, using direct measurements of tree structure, and we found a treatment effect on the metabolic scaling exponent (TFE =  $0.83 \pm 0.02$ ; Control =  $0.69 \pm 0.01$ ) and normalization constant (TFE =  $0.09 \pm 0.003$ , Control =  $0.01 \pm 0.002$ , Table 3.3, Figure 3.12), as a result of differences in tree structural allometry between treatments (Figure 3.6A, 3.6B, Table 3.1). Functionally, the change in exponent and normalization constant on the TFE reflected lower whole tree wood CO<sub>2</sub> efflux for trees smaller than 4 m<sup>3</sup> (Figure 3.12). Tree woody CO<sub>2</sub> efflux for trees above approximately 4 m<sup>3</sup> was indistinguishable from equivalent-sized trees on the Control, although we had limited sampling above 4 m<sup>3</sup>, resulting in large confidence intervals (Figure 3.12). This suggests that changing branch size distribution on trees can alter whole tree woody CO<sub>2</sub> efflux per unit tree volume, particularly if a tree growth strategy results in decreases in the proportion of small branches, and increases in the proportion of large branches. This may seem contradictory, since wood CO<sub>2</sub> efflux rates scale with branch diameter on a surface area basis (Mori et al., 2010; Negisi, 1975; Yoda, 1983, Table 3.1), therefore, larger branches would be expected to

lead to higher whole tree wood CO<sub>2</sub> efflux. However, there are numerous variables driving wood CO<sub>2</sub> efflux (Table 3.2, ?) which need to be evaluated to determine the ultimate outcome of changes in tree architecture on whole tree wood CO<sub>2</sub> efflux. In this particular case, reducing the scalar, that is, the surface area of the tree, had a larger impact on the whole tree wood CO<sub>2</sub> efflux than the relative increase in WC<sub>25</sub> due to proportionally more large diameter branches in trees on the TFE. This has important implications for branch shedding.

Any reduction in woody tissue CO<sub>2</sub> efflux per unit tree volume due to structural change needs to be evaluated within a larger frame of reference to determine if the result is a net positive effect. In the case of small trees on the TFE, the trees are growing faster (Rowland et al., 2015), have significant plasticity in hydraulic and metabolic responses (Bartholomew et al., 2020; Giles et al., 2022), and have maintained similar or higher sap flow than Control counterparts (Costa da et al., 2017), which may indicate that the alteration in surface area to volume of small woody trees on the TFE has had a net positive effect.

Importantly, our analysis of whole tree wood CO<sub>2</sub> efflux does not take into account any differences in treatment for structure and quantity of branches smaller than 5 cm in diameter. There was not sufficient resolution in TLS of branches below 5 cm in diameter to produce reliable models in dense tropical canopies. The methods for including surface area and wood CO<sub>2</sub> efflux for twigs below 5 cm does not account for treatment differences (Appendix B.1), therefore the differences encountered here in tree surface area, and tree mean branch radius are a reflection of differences in branch architecture larger than 5 cm only; results may change if branches smaller than 5 cm diameter are measured.

Additionally, we note that our analysis of whole tree wood respiration (in contrast to whole tree wood CO<sub>2</sub> efflux) using the ratio of woody tissue efflux of CO<sub>2</sub> to woody tissue influx of O<sub>2</sub> (apparent respiratory quotient, or ARQ, Figure 3.16), showed that whole tree wood respiration was  $91.0 \pm 14.1\%$  higher than whole tree wood CO<sub>2</sub> efflux (range 35.8-203.6%, N = 12), indicating that woody CO<sub>2</sub> efflux is

a considerable underestimate of tree woody metabolic load. This also implies that the relationship between tree wood respiration and tree volume (Figure 3.12) may have a different metabolic scaling coefficient and exponent. Although, there was no relationship between tree size and ARQ which would indicate systematic size-related changes in the relationship between wood CO<sub>2</sub> efflux and wood respiration. The sample size of whole tree wood respiration was not large enough to test for a change in scaling exponent and coefficient directly between whole tree wood respiration and whole tree wood CO<sub>2</sub> efflux (Figure 3.16).

### 3.4.3 $R_{\text{wood}}$ on the TFE in response to water deficit

$R_{\text{wood}}$  values reported here for the Control (Table 3.5) were similar to the most recent estimates for surface area scaled  $R_{\text{wood}}$  (Rowland et al., 2018) and similar to other reported values in the tropics (Malhi et al., 2009b). We anticipated a higher rate of  $R_{\text{wood}}$  on the Control than previously estimated, because we accounted for canopy wood CO<sub>2</sub> efflux, which is known to be higher than ground efflux measurements (Asao et al., 2015; Cavaleri et al., 2006). However, the values for  $R_{\text{wood}}$  were not higher than previously reported values (Rowland et al., 2018), despite the higher wood CO<sub>2</sub> efflux rates in the canopy branches than stem (Table 3.2, Figure 3.9), because the TLS-modelled surface area of the trees (Figure 3.5A, 3.5B), was smaller than previous allometric models of tree surface area for the majority of tree sizes, for example those used in Rowland et al. (2018). Variations in allometric models may be expected regionally if tree height is not included in the allometric model (Feldpausch et al., 2012), as is the case for the allometric surface area equation applied in the tropics (Chambers et al., 2004). Importantly, we note that tree surface area values of allometric equation from Chambers et al. (2004) have the largest error for the largest trees (Figure 3.5A, 3.5B), and in fact models a negative relationship with increasing DBH for trees above 250 cm DBH.

Total woody surface area on the TFE and Control, modelled using TLS, and presented as wood area index (WAI, Figure 3.7) was  $0.59 \pm 0.02 \text{ m}^2/\text{m}^2$  on the

Control and  $0.34 \pm 0.01 \text{ m}^2/\text{m}^2$  on the TFE. The value of WAI on the Control is within a normal range of WAI as seen from destructive harvest studies in a tropical rainforest (Clark et al., 2008; Olivas et al., 2013) and indirect measurements of WAI in tropical rainforests (Kalácska et al., 2005; Kalacska et al., 2005), noting that the WAI of from Olivas et al. (2013) is erroneously presented as woody surface area per  $\text{m}^2$  ground area divided by 2 instead of divided by  $\pi$ .

$R_{\text{wood}}$  was 57% lower on the TFE in comparison to the Control, which is largely driven by previous large-tree mortality on the TFE resulting in 40% loss of above-ground biomass (Rowland et al., 2015). The difference in  $R_{\text{wood}}$  between the Control and TFE reported here was considerably larger than what was previously reported (Costa da et al., 2014; Metcalfe et al., 2010b; Rowland et al., 2018), which showed a maximum change of 22% (Rowland et al., 2018). This difference is accounted for by (i) TLS tree surface area models demonstrating lower surface area on trees on the TFE than the Control for an equivalent tree volume (Figure 6A) and (ii) large discrepancies between large tree surface area modelled using TLS and surface area allometric equation previously applied to the site (Chambers et al., 2004, Figure 5A, B) and finally (iii) a lack of treatment effect on  $WC_{25}$  in branches and stems above 2 cm in diameter between treatments, whereas previous measurements of  $WC_{25}$  were reported to be higher on the TFE than the Control (Rowland et al., 2018, Table 3.2, Figure 3.9).

Woody surface temperature on the TFE was higher than the Control, resulting in a relative increase in ambient  $R_{\text{wood}}$  of  $3.2 \pm 0.5\%$  (Table 3.5) on the TFE versus the Control due to the hotter temperature experienced by trees on the TFE. We anticipated a larger effect of temperature on  $R_{\text{wood}}$ ; however, median temperature differences were minimal at  $0.01^\circ\text{C}$ , despite modelled differences of up to  $2.3^\circ\text{C}$  during the daytime (Figure 3.4A, 3.4B).

### 3.5 Conclusions

We present new methods to model stand wood CO<sub>2</sub> efflux, using TLS data in a unique long-term tropical drought experiment. After 18-years of TFE, TFE tree structure may have acclimated to the new water-limited environment by altering in a manner that reduced whole tree wood CO<sub>2</sub> efflux. This alteration in tree structure, along with heightened mortality on the TFE, has resulted in a 57% lower  $R_{\text{wood}}$  on the TFE than Control. Importantly, we show that actual wood respiration rates may be almost double what is measured with radial wood CO<sub>2</sub> efflux. Although the difference between radial wood CO<sub>2</sub> efflux and wood respiration may be irrelevant for understanding whether an ecosystem is a net carbon source or sink, this missing respiratory-derived CO<sub>2</sub> may be part of important and unstudied physiological processes. As a whole, these results demonstrate the importance of using detailed structural information to understand how ecosystems respond to climate change, as tree structural acclimation has substantial impact on tree metabolic processes, and are currently invisible when using commonly adopted field monitoring practices.

# Chapter 4

## Forest dynamics over 20 years of experimental drought: tending to biomass collapse or a new stable state?

### 4.1 Introduction

The tropics have the largest above ground carbon stores of all world forests (Pan et al., 2011) and tropical forests strongly affect interannual variations in CO<sub>2</sub> flux (Liu et al., 2017). The carbon cycle in the tropics is predicted to be compromised by drought stress this century (Anderegg et al., 2015; Cox et al., 2013; Fu et al., 2013; Wang et al., 2014). The effects of long-term drought on tropical ecosystems are not well understood (Meir et al., 2018). Long-term observational studies indicate that water deficit, among other factors, may be causing a decline in the carbon sink of tropical rainforests (Brienen et al., 2015; Hubau et al., 2020). This has led to the largest tropical rainforests, the Amazon, turning from carbon sink to carbon source in recent years (Gatti et al., 2021).

In addition to observational studies, there have been attempts to probe drought

responses of tropical rainforests by large-scale manipulation, which has led to the creation of tropical rainforest through-fall exclusion experiments (TFE) in the Amazon (Brando et al., 2008; Costa da et al., 2010; Fisher et al., 2007; Meir et al., 2015; Nepstad et al., 2015), southeast Asia (Moser et al., 2014) and Australia (Tng et al., 2018). Evidence from these TFE experiments and from observational network-based studies of drought all indicate the potential for drought to cause substantial biomass loss and a decline in forest productivity (Bauman et al., 2022; Brando et al., 2008; Costa da et al., 2010; Phillips et al., 2010; Rifai et al., 2018; Rowland et al., 2015).

One key remaining uncertainty is whether drought in tropical rainforests, extended to the long term, results in further loss of biomass or a new stable state. The current relationship between forest type and rainfall reflects structural and floristic changes due to long-term climate variations (Dexter et al., 2018; Fauset et al., 2012; ?), and provide insights into how changing climate will affect the carbon balance of tropical rainforests in the future. However, the observational studies showing meteorological limits to vegetation type do not describe the manner in which ecosystems transition between states in response to long-term changes in precipitation regimes. This transition is of acute interest in the tropics, because it begins to reveal the nature of a new stable state imposed by drought: will the ecosystem gradually lose biomass due to increased tree mortality, until reaching a stable state that is substantially reduced in biomass, or will it reach a tipping point, leading to an ecosystem collapse, with eventual regrowth leading to a new forest system/vegetation type (Cox et al., 2000; Davidson et al., 2012; Huntingford et al., 2013; Malhi et al., 2009b); naturally, either outcome is dependent on the extremity of drought.

In addition to biomass dynamics, assessing tree size class and spatial distributions after a disturbance can provide information about the stability of an ecosystem (Casalini, Bisigato, 2018; Ledo, Schnitzer, 2014; Pillet et al., 2018; Zang et al., 2021). Stable state conditions in tropical rainforests often demonstrate both aggregated and uniform distributions between trees at varying distances, due to a mixture of processes, including competition for resources, dispersal limitations, and microclimate

(Condit et al., 2000; Lan et al., 2009; Law et al., 2009; Pillet et al., 2018; Zhang et al., 2017). In the case of a long-term drought, spatial distribution of trees may alter due to mortality and recruitment dynamics, governed by competition for water. These growth and mortality dynamics could result in a range of outcomes including: tree spatial aggregation due to heterogeneous water availability, potentially from hydraulic redistribution by plant roots (Hafner et al., 2020; Oliveira et al., 2005) or due to canopy gaps from tree mortality resulting in clustered growth of recruits (Salas et al., 2006); uniformity due to competition for water; or a random distribution potentially indicating competitive release (O'Brien et al., 2014) caused by many years of high mortality rates (Rowland et al., 2015).

The basis of the research presented here is a 20-year TFE (2002-2022) in a tropical rainforest located in eastern Amazonia. After 4, 7, 10 and 13 years of the TFE, aboveground biomass dynamics were evaluated by measuring loss of biomass due to mortality as well as any gains in biomass due to recruitment and aboveground woody production ( $NPP_{\text{wood}}$ , Costa da et al., 2014, 2010; Metcalfe et al., 2010b; Rowland et al., 2015). Stem recruitment rates were evaluated for the first three years of the experiment, and there was no difference between treatments (Costa da et al., 2010). After the commencement of the TFE,  $NPP_{\text{wood}}$  was 30-40% lower on the TFE than the Control (Costa da et al., 2010; Metcalfe et al., 2010b).  $NPP_{\text{wood}}$  recovered to levels comparable to the Control after 8 years of TFE (Costa da et al., 2014); the  $NPP_{\text{wood}}$  has not been evaluated since. After seven years of TFE, growth rates were higher for small and medium sized trees on the TFE in comparison to the Control counterparts (Costa da et al., 2014; Rowland et al., 2015), and these high rates have been maintained until the most recently reported year, 13 years after the start of the TFE. This increase in growth may be related to competitive release, after elevated mortality of large trees potentially increased light, water and nutrient availability for remaining trees (Bartholomew et al., 2020; Costa da et al., 2014; Rowland et al., 2015, 2021b).

Over the first 13 years of the TFE, there were substantial losses of carbon due

to high mortality rates, particularly of large trees (Costa da et al., 2014, 2010; Rowland et al., 2015). The high mortality rates resulted in approximately 40% loss of AGB after 13 years of the TFE (Rowland et al., 2015). Biomass loss accelerated substantially in the last reported year (after 13 years of TFE) potentially boding ecosystem collapse (Rowland et al., 2015).

Here, I further developed the analysis of aboveground biomass on the TFE using new field-calibrated quantification of aboveground biomass using terrestrial laser scanning (TLS, Burt et al., 2021). I use the TLS data to revise previous analyses of aboveground biomass and extend them until 2022, 20 years after the commencement of the TFE experiment. I used the data to evaluate long-term trends in  $NPP_{\text{wood}}$ , recruitment, and tree mortality in the TFE, to determine if the ecosystem has reached a new stable state, or if elevated mortality rates continued after 13 years of TFE (Rowland et al., 2015). I evaluated the spatial distribution of trees on the TFE to assess if trees are distributed in a manner indicating competition, aggregation or alternatively, competitive release. All results were compared against a one-hectare Control plot where no drought treatment had been imposed, but for which the same long-term datasets have been collected. Specifically we tested the hypotheses that extended drought stress over 20 years, led to:

- i) substantially lower but stable overall aboveground biomass value, following earlier substantial drought-related mortality
- ii) slowing growth rates in small trees after a period of increased growth rates
- iii) increasing number and biomass of new recruits  $>10$  cm DBH
- iv) a plateau of aboveground biomass loss due to mortality after 20 years of heightened mortality on TFE
- v) a final spatial distribution of trees indicating competitive release on the TFE after earlier increases in mortality and recruitment

## 4.2 Materials and Methods

### 4.2.1 Site

Measurements were taken at Caxiuanã National Forest Reserve, Pará State in north-eastern Brazil (1°43'S, 51°27'W) . This site is a *terra-firme* seasonal rainforest and receives 2000-2500 mm of rainfall a year, with six consecutive months of the year receiving less than 100 mm from July to December. The site has yellow oxisol soil (Ruivo, Cunha, 2003) and mean air temperature of c. 25°C. The surface volumetric water content varies seasonally from approximately 0.05 in the dry to 0.30 m<sup>3</sup>m<sup>-3</sup> in the wet season.

### 4.2.2 Through-fall exclusion experiment (TFE)

In January 2002, a through-fall exclusion experiment (TFE) was constructed on one hectare of tropical rainforest at Caxiuanã National Forest. Transparent panels were installed 1-2 meters above the ground to redirect approximately 50% of the rainfall to a system of gutters. A trench was dug around the TFE to transport the water away from the experiment. The experiment requires daily maintenance and the leaf litter is removed from above the panels every 2-3 days and placed below the panels. See Costa da et al. (2010); Fisher et al. (2007); Meir et al. (2018); Rowland et al. (2021b) for more details of experimental design. In 2019, the soil volumetric water content was lower on the TFE in comparison to the Control by 38-67%, dependent on the month (Chapter 2).

### 4.2.3 Wood density

Wood density values were taken from literature (Kattge et al., 2020; Patiño et al., 2008). In total 108 trees had no species-level wood density values. Of these 108 trees, 84 trees were only identified to the genus-level, 1 tree had genus identified but no wood density recorded in the literature, 23 trees had no taxonomic identification. For the 84 trees with genus-only identification, the wood density value was gap

filled with a mean genus wood density value. For the 23 trees with no taxonomic identification and for the single tree with no wood density record in literature, the wood density was gap filled with the mean wood density representing the control and TFE plots.

#### 4.2.4 Terrestrial Laser Scanning

Terrestrial laser scanning (TLS) measurements were made in October 2018, the dry season, with a RIEGL VZ-400 terrestrial laser scanner (RIEGL Laser Measurement Systems GmbH). The laser pulse has a wavelength of 1500 nm, beam divergence of 0.35 mrad, and the diameter of footprint at emission is 7 mm. Lidar scans were first co-registered onto a common coordinate system using RiSCAN PRO (v2.7.0) and the point clouds of all individual trees above 10 cm DBH in the two hectares were extracted manually from the larger area point clouds and were matched to individual tree tags. After extraction, leaf material returns were separated from wood using TLSeparation v1.0 (Vicari, Wilkes, 2018). Each tree was visually inspected to determine adequate leaf-wood separation using CloudCompare, and the tree was manually edited to improve the final separation when necessary (CloudCompare, 2021). Quantitative structural models (QSMs) were constructed from the wood point clouds using TreeQSM (v2.3.2) and the input parameters were automatically generated using optqsm v0.1.0 (Raumonen et al., 2013). Trees with buttresses were visually identified, and processed using TreeQSM with a triangulation for buttresses.

A destructive harvest experiment of four trees, ranging from 0.6 to 1.2 m DBH, occurred in 2018, 8 km distant from the Control and TFE plots (Burt et al., 2021). The destructive harvest compared tree biomass estimates from TLS with allometric methods. Mean tree-scale biomass error was 3% for TLS, in comparison to 15% for allometric methods (Burt et al., 2021).

## 4.2.5 Allometric models of tree height and biomass

An allometric equation relating tree height to DBH was used to estimate the height of all trees since year 2000. The data for this allometry were taken from the height extracted from tree point clouds in the Control and TFE treatment, and the measured DBH from a census in 2019. The height allometric model was fitted using a Weibull function (Bailey, Dell, 1973):

$$H = a(1 - \exp(-bD^c)) \quad (4.1)$$

where  $H$  is height (m), and  $D$  is DBH (cm). Previously, regional tree height allometry for the Brazilian Shield was used to estimate tree height at this site (Feldpausch et al., 2012), where fitted model coefficients of the Weibull function were: 227.35, 0.139 and 0.5550 for  $a$ ,  $b$ , and  $c$ , respectively (Feldpausch et al., 2012). An allometric equation relating tree aboveground biomass (AGB, kg) to tree DBH (cm), tree height (m), and wood density ( $\text{g cm}^{-3}$ ) was used to estimate stand aboveground biomass from 2000 to 2022. The data for this allometry were taken from QSMs of the TFE and the Control, the tree DBH measured in 2019, tree height extracted from TLS point clouds, and wood density taken from literature. The AGB allometric model took the form:

$$AGB_{TLS} = a((\rho HD)^2)^b \quad (4.2)$$

where  $\rho$  is wood density ( $\text{g cm}^{-3}$ ),  $H$  is height (m), and  $D$  is DBH (Chave et al., 2014, cm). The global tropical allometric model of AGB used for comparison purposes in this study is equation 4.2, with model coefficients of 0.673 and 0.976 for  $a$  and  $b$ , respectively (Chave et al., 2014).

## 4.2.6 Biomass monitoring: census and dendrometer data

In 2000, all trees above 10 cm DBH were tagged and identified. Since 2000, there have been censuses performed in years: 2001, 2002, 2003, 2004, 2005, 2006, 2007, 2009, 2013, 2014, 2015, 2017, 2019 and 2022. During a census, the DBH of all trees

is measured at 1.3 meters above the base of the tree and trees are assessed to be alive or dead. For trees with buttresses, DBH is measured above the buttress using a ladder, at a permanently-marked location. Death was recorded if the tree had no leaves along with a zero or negative stem increment, or had fallen over.

Dendrometer bands were installed on all trees in the experimental plots and quarterly stem circumference increment measurements were taken at 1.3 meters, except on trees with buttresses, where the dendrometer band was installed above the buttress. These methods are widely used to study incremental change in tree growth (Meir, Grace, 2002; Malhi et al., 2009b). Measurements were taken at the start of January, April, July and October. The difference in stem circumference increment between January and April was considered wet season, April to July was wet to dry transition, July to October was dry season, and October to January was dry to wet transition based on monthly volumetric water content data.

As found elsewhere, over long time periods, dendrometer data can occasionally contain errors and standardized error checking was performed across all datasets (Rowland et al., 2015). Each tree's historical growth record was manually assessed to determine if any growth measurement was greater than 3 standard deviations from the mean. If the measurement was removed based on this statistical test, the value was gap filled with the mean value of the given epoch (2005-2010, 2010-2015, 2015-2020) in that season. In the event that no data were available to gap fill, the yearly change in DBH for any one tree was gap filled using linearly interpolated values of DBH of that tree from the 14 census measurements. Patterns of swelling and shrinkage can occur due to water dynamics, and not growth; however, over time the impacts of these changes are small relative to growth. It is possible to separate these components using (high-cost) linear variable displacement transducers (Mencuccini et al., 2017), but these are not yet implemented at census-scale over long time periods, so shrinkage and expansion factors were not applied to the data. Growth increment (GI) was defined as cm of circumference growth increment per day. GI was analyzed by size-class, which was separated into small (10-20 cm DBH), medium

(20-40 cm DBH), and large (>40 cm DBH) trees. GI was evaluated seasonally, in wet, dry, wet-dry transition and dry-wet transition. A mean GI per size class and per season was taken for a 5 year period, from 2005-2010, 2010-2015 and 2015-2020.

The dendrometer data were used to estimate  $NPP_{\text{wood}}$ , the amount of carbon accumulated in woody tissue, yearly. The  $NPP_{\text{wood}}$  was estimated using the yearly difference in dendrometer growth in the month of January. Data were gap-filled using the change in diameter of a tree from the census data. The biomass and height allometry described above was used to estimate biomass from the manual measurements of DBH.  $NPP_{\text{wood}}$  was analyzed across the stand, that is, all trees on the Control and the TFE, and it was additionally analyzed across three size classes: small (10-20 cm DBH), medium (20-40 cm DBH) and large (>40 cm DBH). Additionally,  $NPP_{\text{wood}}$  was divided by the total woody biomass of the stand or  $NPP_{\text{wood}}$  in a given size class was divided by the total woody biomass of the the size class ( $NPP_{\text{standard}}$ ) to determine the amount of woody carbon accumulated per unit woody biomass.

#### 4.2.7 Spatial analysis

Using xy coordinates for all living trees, we also calculate a nearest neighbour distribution function to determine the degree of clustering or aggregation of trees by detecting deviance from a Poisson process of the cumulative distribution of distances between each tree and all other trees on the plot using spatstat library (Baddeley, Turner, 2005). We used the Ripley's K test transformed to minimize variance ( $L_r$ ) to characterize the 2D spatial distribution of trees in TFE and Control, and the 95% confidence envelope was modelled from 99 simulations using the envelope function from spatstat library. An isotropic correction was performed for border effects. The Poisson distribution represents complete spatial randomness (CSR): positive deviation from the confidence limits indicates significant aggregation between trees; negative deviation indicates potential competition due to a more uniform spacing than expected between trees, potentially caused by competitive interactions or al-

lelopathy among trees (for further information see Condit et al., 2000; Moeur, 1993; Szmyt, 2014).

## 4.2.8 Statistics

All trees were included in the analysis except for: (1) trees under 10 cm diameter at breast height (DBH), (2) trees within the outer 10x10 meter grid, which were removed due to the edge effects caused by trenching and (3) lianas and palms. The census AGB data were analyzed for the entirety of the 20 years of the TFE, from 2002 to 2022. Error bars on the stand AGB reflect the summed standard error of wood density for all trees and the 3% biomass error from nearby destructive harvest. The growth data were analyzed only over 15 years, from 2005 to 2020, because COVID resulted in limited transportation to the site after 2020, causing quarterly growth measurements to be discontinued for a period of time. All statistical analyses were carried out in R v 4.0.3 (R Core Team, 2021) and all errors reported are as standard error of the mean.

## 4.3 Results

### 4.3.1 Comparison between TLS and allometry

The allometry of both tree height and tree AGB were affected by treatment, with tree height lower on the TFE than the Control for an equivalent-sized tree DBH, and tree AGB lower on the TFE than the Control for a tree with an equivalent sized DBH and height (Chapter 2). Since these allometric relationships were affected by treatment, the use of published regional allometric models of tree height (Feldpausch et al., 2012), or pantropical allometric models of tree AGB (Chave et al., 2014) resulted in treatment-specific biases. A regional allometric model of tree height ( $ht_{\text{allo}}$ , Feldpausch et al., 2012), previously applied to this site for purposes of estimating aboveground biomass (AGB, Rowland et al., 2015), consistently underestimated tree height when compared with height measurements from TLS

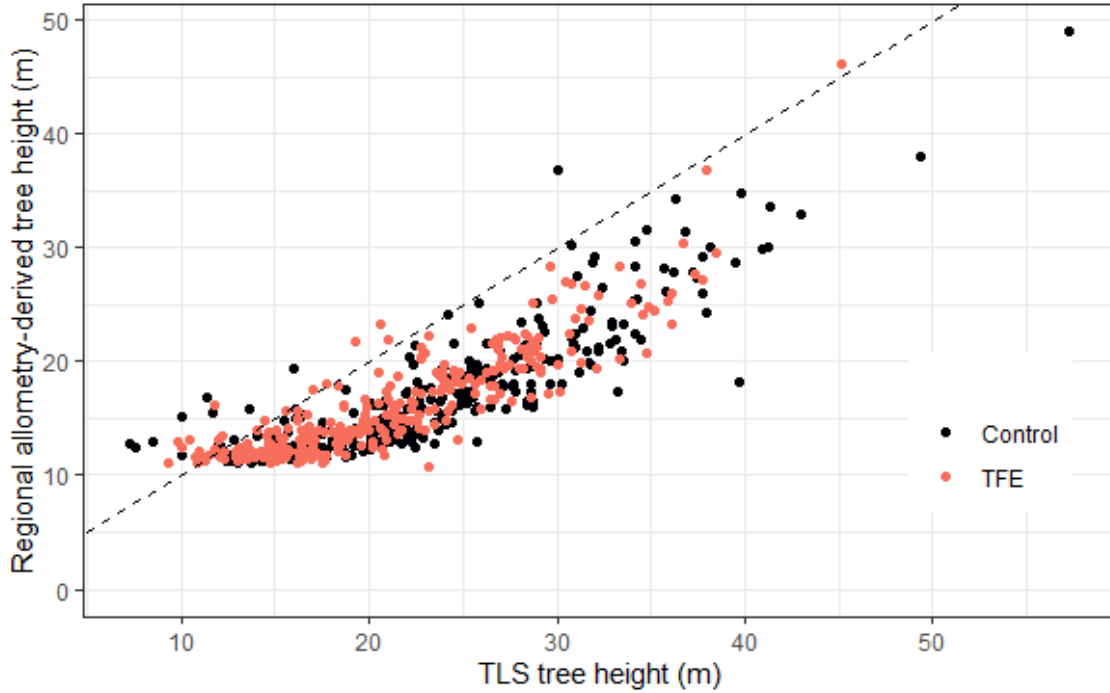


Figure 4.1: The relationship between tree height measured using TLS versus tree height modelled from a published height allometric equation, calibrated for the region of this field site (Feldpausch et al., 2012)

( $ht_{\text{TLS}}$ ). The error between  $ht_{\text{allo}}$  and  $ht_{\text{TLS}}$  was nonlinear resulting in the largest error in the tallest trees (Figure 4.1). The use of  $ht_{\text{allo}}$  instead of  $ht_{\text{TLS}}$  resulted in considerable underestimates of tree AGB (Figure 4.2), when tree AGB was modelled using a global pantropical allometric equation ( $\text{AGB}_{\text{Chaves}}$ , Chave et al., 2014), with  $\text{AGB}_{\text{Chaves}}$  underestimated by  $23.0 \pm 0.95\%$  on the Control and  $20.6 \pm 0.76\%$  on the TFE (Figure 4.2). When the  $\text{AGB}_{\text{Chaves}}$  of all trees was summed, the cumulative effect of using  $ht_{\text{allo}}$  instead of  $ht_{\text{TLS}}$  was an underestimate of stand AGB by 17.9% on the Control and 17.1% on the TFE.

When  $\text{AGB}_{\text{Chaves}}$ , calculating using  $ht_{\text{TLS}}$ , was compared with AGB derived from TLS-methods ( $\text{AGB}_{\text{TLS}}$ ),  $\text{AGB}_{\text{Chaves}}$  overestimated tree AGB on the droughted plot by  $13.2 \pm 2.4\%$ , and underestimated tree AGB on the Control, in comparison to  $\text{AGB}_{\text{TLS}}$  by  $8.5 \pm 2.8\%$  (Figure 4.3). When the AGB was summed for both treatments, the cumulative effect of these differences was that the allometric methods overestimated stand AGB by 12.2% on the TFE and underestimated stand AGB on the Control by 7.4% in comparison to the TLS-methods.

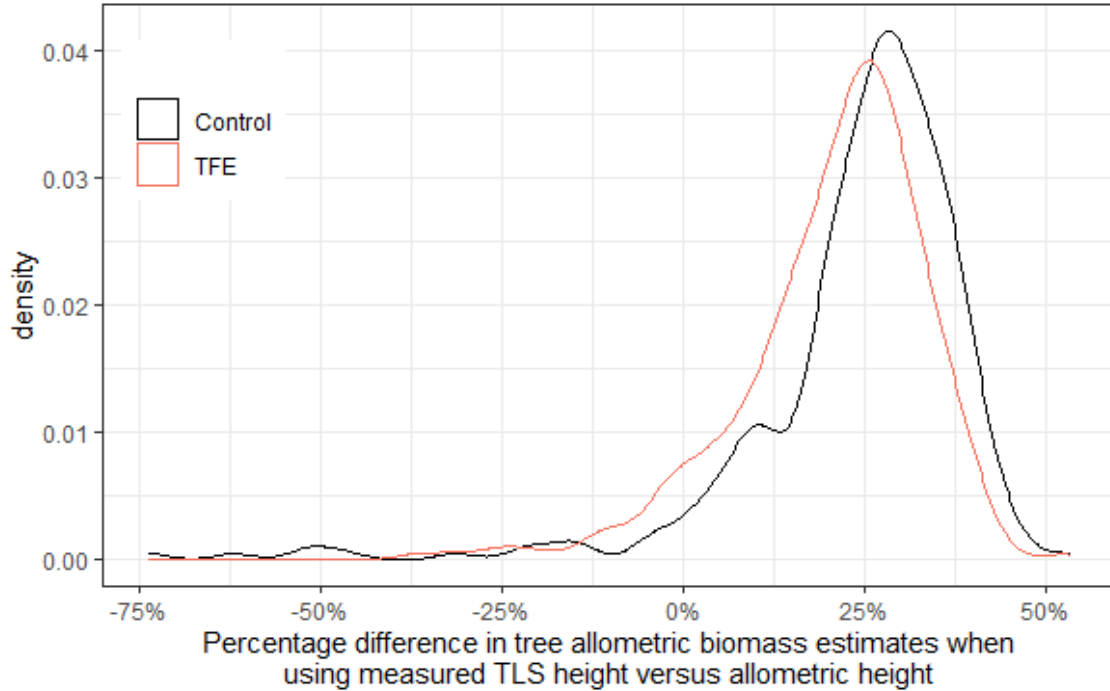


Figure 4.2: The percentage difference in tree allometric biomass estimates (Chave et al., 2014) when using tree height measured with TLS ( $AGB_{\text{tlsht}}$ ) versus published regional height allometry to estimate tree height ( $AGB_{\text{regionalht}}$ , Feldpausch et al., 2012).  $(AGB_{\text{tlsht}} - AGB_{\text{regionalht}}) / AGB_{\text{tlsht}}$  is shown as a density distribution, where Control is black and TFE is red. The mean difference in the Control is  $23.9 \pm 0.95\%$ , mean for TFE is  $20.6 \pm 0.76\%$ .

### 4.3.2 Aboveground biomass dynamics

Based on my standardized analysis of the full census datasets, and using the site-calibrated biomass-allometry relationships made possible by the additional analysis of TLS and destructive harvest data, the change in AGB across the full period to date of the TFE is shown in Figure 4.4, using two methods: (i) AGB on the TFE estimated based on the Control AGB allometry, which is assumed to reflect the TFE allometry pre-treatment and (ii) AGB estimated based on the TFE allometry in 2018. The allometry on the TFE in 2018 is assumed to represent the allometry for all years subsequent, for the purposes of the calculations below. At the start of the reporting period, before the experimental treatment began, AGB on both plots was statistically similar (Control  $303.2 \pm 12.6 \text{ Mg C ha}^{-1}$ , TFE  $279.4 \pm 9.2 \text{ Mg C ha}^{-1}$ ), and also similar to surrounding long-term inventory plots (Costa da et al., 2010). By the end of the reporting period, in 2022, AGB on the TFE had declined

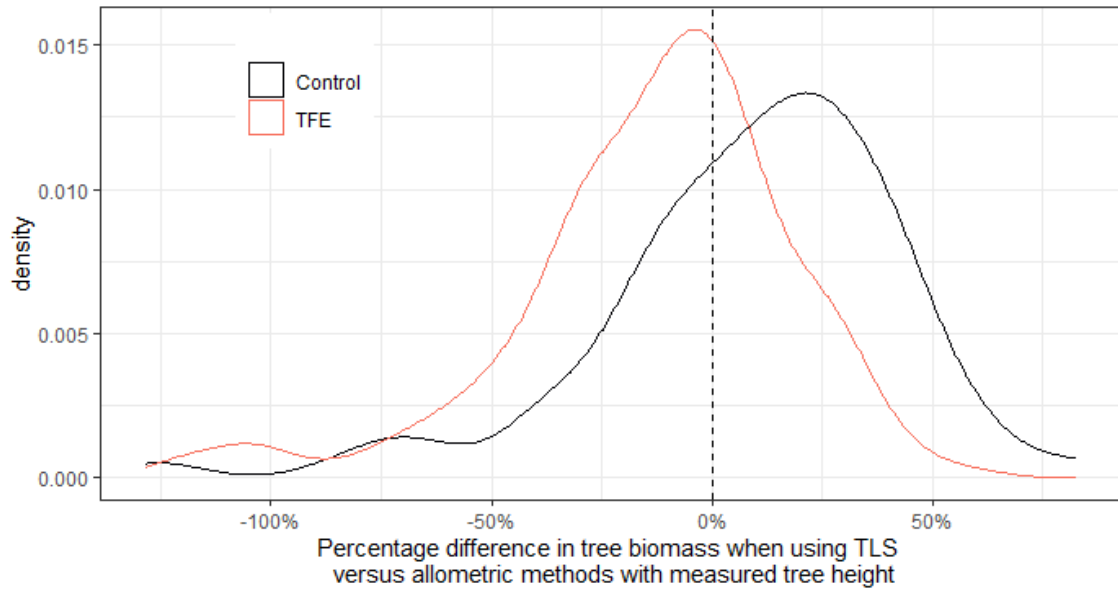


Figure 4.3: The percentage difference in tree aboveground biomass (AGB) when using TLS versus allometric methods of deriving AGB (Chave et al., 2014). Allometric method of deriving AGB used here were calculated using tree height measured from TLS. The percentage difference in tree aboveground biomass (AGB) is shown as a density distribution for trees on the TFE (red) and the Control (black).

to  $156.9 \pm 4.3 \text{ Mg C ha}^{-1}$ , while on the Control it was  $295.4 \pm 10.3 \text{ Mg C ha}^{-1}$ . Control forest AGB varied by approximately  $26 \text{ Mg C ha}^{-1}$  over the reporting period, but did not change significantly overall; the mortality rate on the Control was  $1.4 \pm 0.2\%$ , very similar to surrounding inventory plots, and consistent with the earlier analysis of Costa da et al. (2010).

The AGB on the TFE decreased by  $43.9 \pm 5.7\%$  (Figure 4.4) over the course of the reporting period, with a net loss of  $122.6 \text{ Mg C ha}^{-1}$ . Had the TFE trees continued to present with AGB allometry equivalent to the Control, AGB on the TFE would have decreased by  $33.5 \pm 6.4\%$ . There were pulses of decline in biomass on the TFE from 2000-2013, followed by a larger pulse in 2014-2015; these pulses raised the mortality rate from a value similar to the surrounding forest at the start of the experiment ( $1.5 \pm 0.4\% \text{ yr}^{-1}$ ) to an average of  $2.0 \pm 0.3\% \text{ yr}^{-1}$ , with a maximum of  $6.0\% \text{ yr}^{-1}$ . After 2015, AGB appeared to stabilize on the TFE from 2016-2022, with no significant change over this six year period, and a mortality rate of  $1.5 \pm 0.4\% \text{ yr}^{-1}$ .

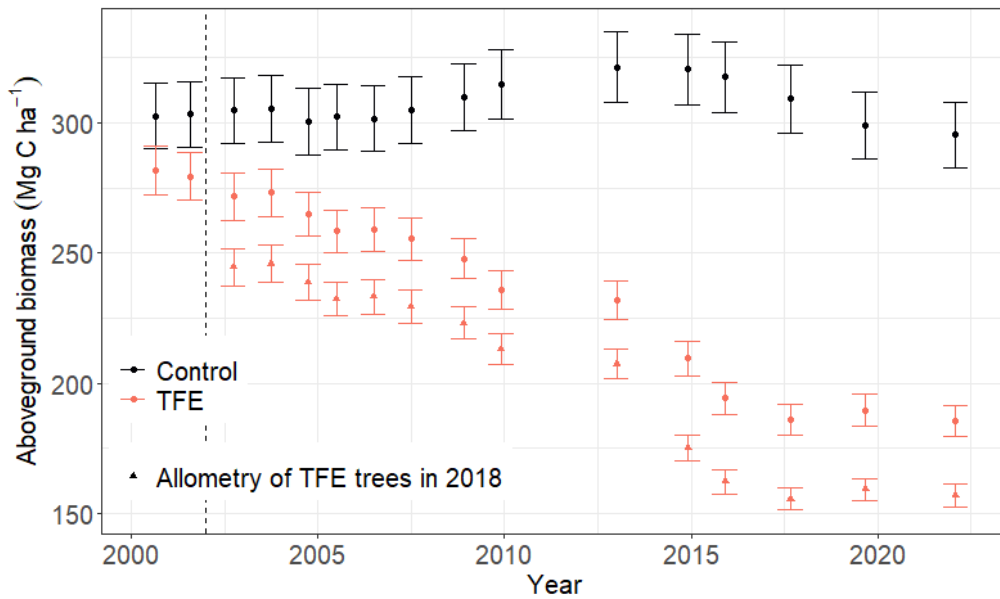


Figure 4.4: Aboveground biomass ( $\text{Mg C ha}^{-1}$ ) for Control (black) and through-fall exclusion experiment (TFE, red) from 2000 to 2022, with TFE commencing in January of 2002, indicated by dashed black line. Aboveground biomass was modelled using TLS-derived allometric equation for Control (circles), and TLS-derived allometric equation for TFE (triangles), based on allometry derived TLS data in 2018.

### 4.3.3 Carbon gains due to growth and recruitment

#### Recruitment

Recruits on the TFE, that is trees that grew to above 10 cm DBH after the experiment commenced, accounted for  $8.4 \pm 0.4 \text{ Mg C ha}^{-1}$ , in comparison to  $2.9 \pm 0.1 \text{ Mg C ha}^{-1}$  on the Control in 2022 (Figure 4.5A); this reflects an active response in the smaller tree-size classes to the drought treatment and higher mortality in the TFE, as also reported in Giles et al. (2022); Bartholomew et al. (2020). The number of recruits to the  $> 10 \text{ cm}$  cohort in the TFE was much larger than in the Control, with 143 recruits per hectare in the TFE, and 58 recruits per hectare in the Control (Figure 4.5B).

#### Growth: net primary productivity ( $\text{NPP}_{\text{wood}}$ )

Based on growth measurements from dendrometer data,  $\text{NPP}_{\text{wood}}$ , that is aboveground woody production, was  $1.06 \pm 0.02$  times higher on the TFE than the Control from 2009-2015 (Figure 4.6A, B). However,  $\text{NPP}_{\text{wood}}$  was lower on the TFE than the

Control for all other years, except 2017 (Figure 4.6A,B). Mean  $\text{NPP}_{\text{wood}}$  between 2005 and 2020 was  $1.9 \pm 0.02 \text{ Mg C ha}^{-1}\text{yr}^{-1}$  on the Control (range:  $1.4\text{-}2.7 \text{ Mg C ha}^{-1} \text{ yr}^{-1}$ ) and  $1.7 \pm 0.03 \text{ Mg C ha}^{-1}$  on the TFE (range:  $1.08\text{-}2.42 \text{ Mg C ha}^{-1} \text{ yr}^{-1}$ , Figure 4.6B).  $\text{NPP}_{\text{wood}}$  divided by woody biomass ( $\text{NPP}_{\text{standard}}$ , Figure 4.6C), was lower on the TFE than Control prior to 2008, after which it was a mean of  $1.5 \pm 0.02$  times higher on the TFE than the Control.

When  $\text{NPP}_{\text{wood}}$  was separated by size class into small (10-20 cm DBH), medium (20-40 cm DBH) and large ( $>40$  cm DBH) trees, distinct temporal patterns emerged for different size classes (Figure 4.7A, B).  $\text{NPP}_{\text{wood}}$  for small trees on the TFE initially had rates similar to the Control, before increasing steadily until 2011 to rates 2.6 times higher than the Control, after which  $\text{NPP}_{\text{wood}}$  on the TFE decreased

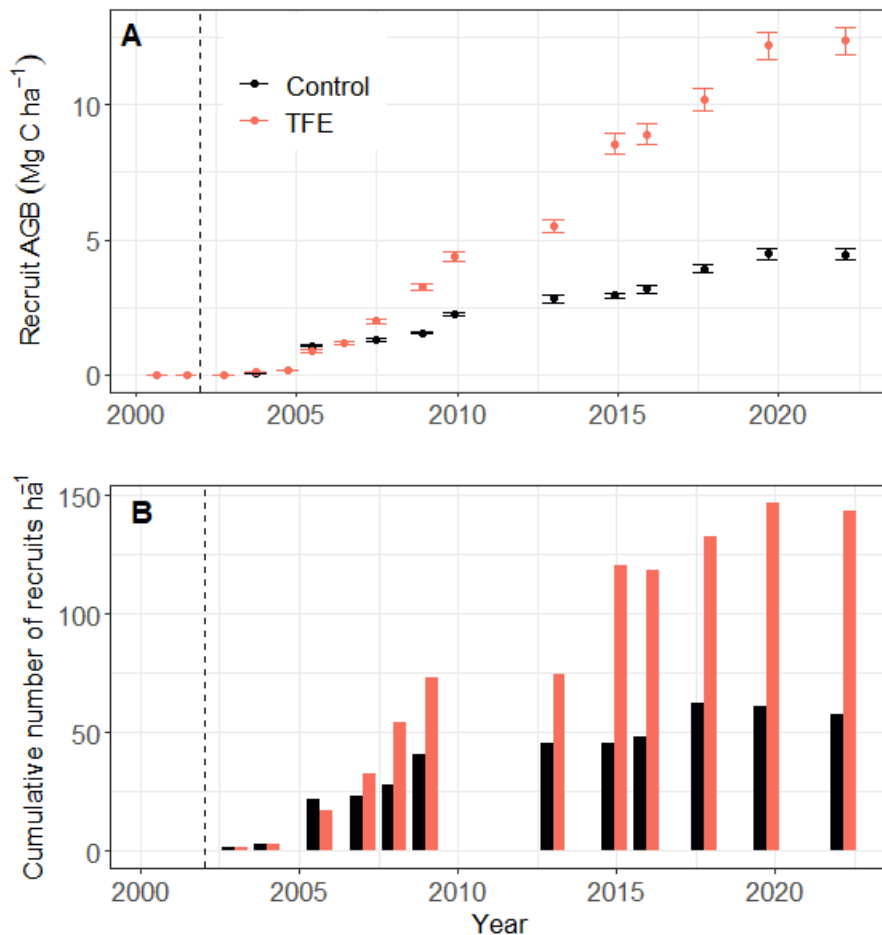


Figure 4.5: A) Aboveground biomass of living recruits (AGB,  $\text{Mg C ha}^{-1}$ ), which are trees that have grown above 10 cm in diameter since the start of the experiment, for Control (black) and TFE (red). Dashed black line indicates start of TFE. B) Cumulative number of living recruit trees per hectare since start of TFE.

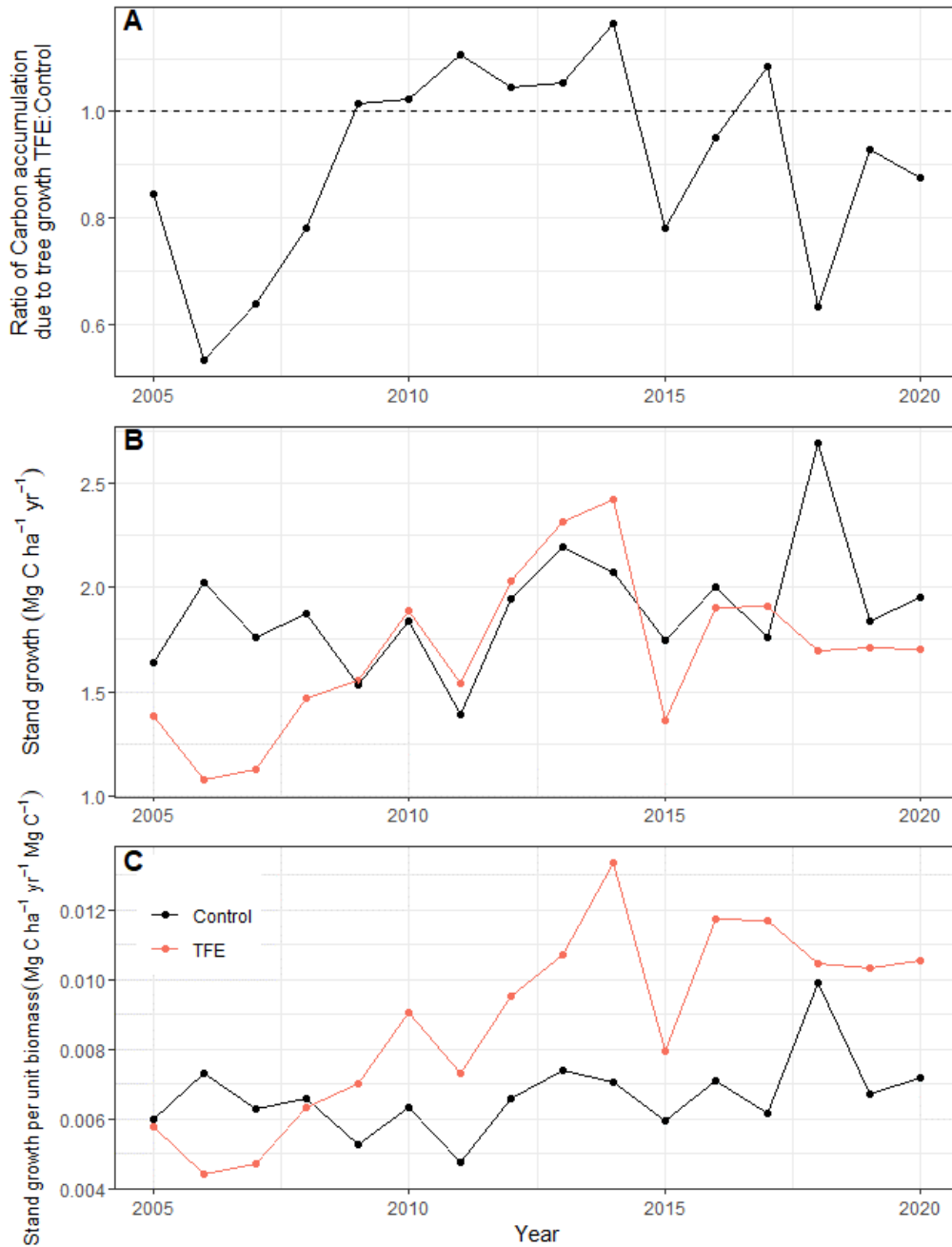


Figure 4.6: A) Ratio of woody carbon production ( $NPP_{\text{wood, TFE/Control}}$ ) from 2005 to 2020. Dashed horizontal line marks a ratio of 1, where  $NPP_{\text{wood}}$  on the TFE is equal to the Control. B)  $NPP_{\text{wood}}$  ( $\text{Mg C ha}^{-1}\text{yr}^{-1}$ ) on TFE (red) and Control (black) from 2005 to 2020 and C)  $NPP_{\text{wood}}$  per unit biomass on TFE and Control

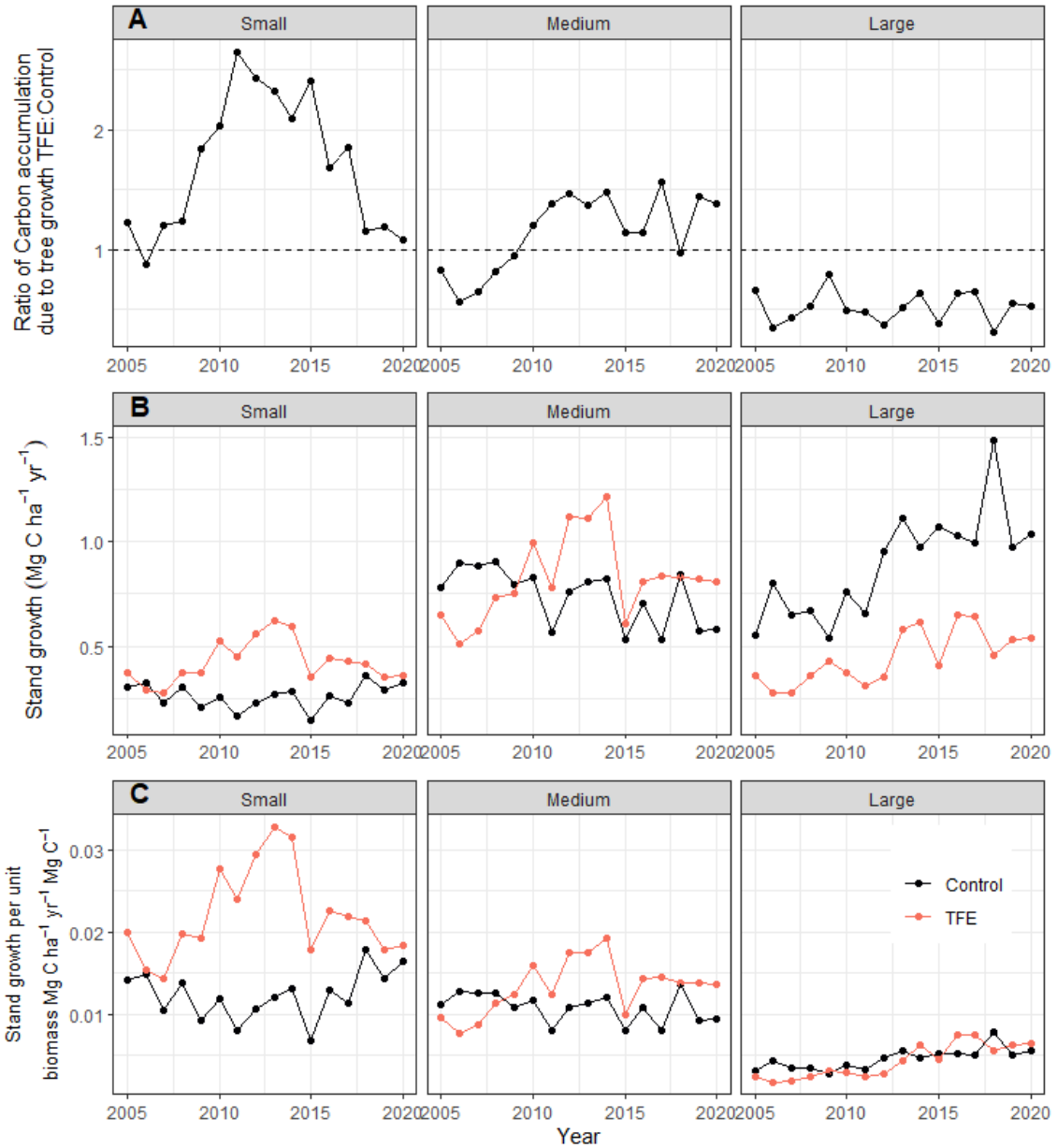


Figure 4.7: Separated by size class, small (10-20 cm DBH), medium (20-40 cm DBH) and large (>40 cm DBH) the A) ratio of  $NPP_{wood}$  (TFE/Control) from 2005 to 2020, where dashed horizontal line marks a ratio of 1, where  $NPP_{wood}$  on TFE is equal to the Control. B)  $NPP_{wood}$  (Mg C ha<sup>-1</sup>) on TFE (red) and Control (black) from 2005 to 2020 and C)  $NPP_{wood}$  per unit biomass on TFE and Control.

to similar rates as the Control (Figure 4.7A, B). Mean rates of  $NPP_{\text{wood}}$  in small trees were  $1.7 \pm 0.01$  times higher on the TFE than the Control.  $NPP_{\text{wood}}$  per unit biomass (Figure 4.7C) was consistently higher for small trees on the TFE after 2007, with a mean of  $1.9 \pm 0.2$  times higher on the TFE than the Control, ranging from 1.02 to 3.0 times higher throughout the 15 year period from 2005 to 2020.

$NPP_{\text{wood}}$  for medium sized trees on the TFE was higher than the Control from 2010 to 2020 by a mean of  $1.3 \pm 0.05$  times (Figure 4.7A,B). Prior to 2010, medium-sized trees on the TFE had lower rates of  $NPP_{\text{wood}}$  than the Control.  $NPP_{\text{standard}}$  was higher on the TFE than the Control for medium-sized trees from 2009 onwards, with a mean rate after 2009 of  $1.4 \pm 0.06$  times higher than the Control (Figure 4.7C).  $NPP_{\text{standard}}$  for medium-sized trees stabilized from 2016-2020.

During the period 2005 to 2020, large trees on the TFE had lower rates of  $NPP_{\text{wood}}$  than the Control, with a mean  $0.52 \pm 0.03$  times lower than the Control (Figure 4.7A, B). Large trees had a lower  $NPP_{\text{standard}}$  on the TFE from 2005 to 2015, except for the year 2014, with  $NPP_{\text{standard}}$   $0.77 \pm 0.08$  times lower on the TFE than the Control prior to 2015 (Figure 4.7C). From 2015-2020,  $NPP_{\text{standard}}$  for large trees was higher on the TFE than the Control for 4 of the 5 years, with the TFE  $1.15 \pm 0.13$  times higher than the Control during this time period.

### **Growth: Growth increment (GI)**

Seasonal growth increment (GI, cm circumference/day, Figure 4.8) was highest in the wet season, and lowest in the dry season for all size classes. Small trees on the TFE plot grew faster than Control counterparts in all seasons except for the dry season, with the strongest dry season effect found early and late on in the reporting period (2005-2010 and 2015-2020). Medium-sized trees on the TFE initially had lower growth in 2005-2010 than the Control, which recovered from 2010-2020, with GI higher than the Control in all seasons in the TFE except for the dry season.

Initially, during 2005-2010, large trees experienced a lower GI than Control trees in both the dry and wet seasons. During 2010-2015, large tree growth varied with

season in relation to their Control counterparts, with evidence of strong dry season impacts on the TFE (Figure 4.8). In the most recent period (2015-2020), large trees on the TFE had a consistently lower GI throughout the year, with some evidence that growth was most restricted in the TFE during the dry-wet transition (Figure 4.8).

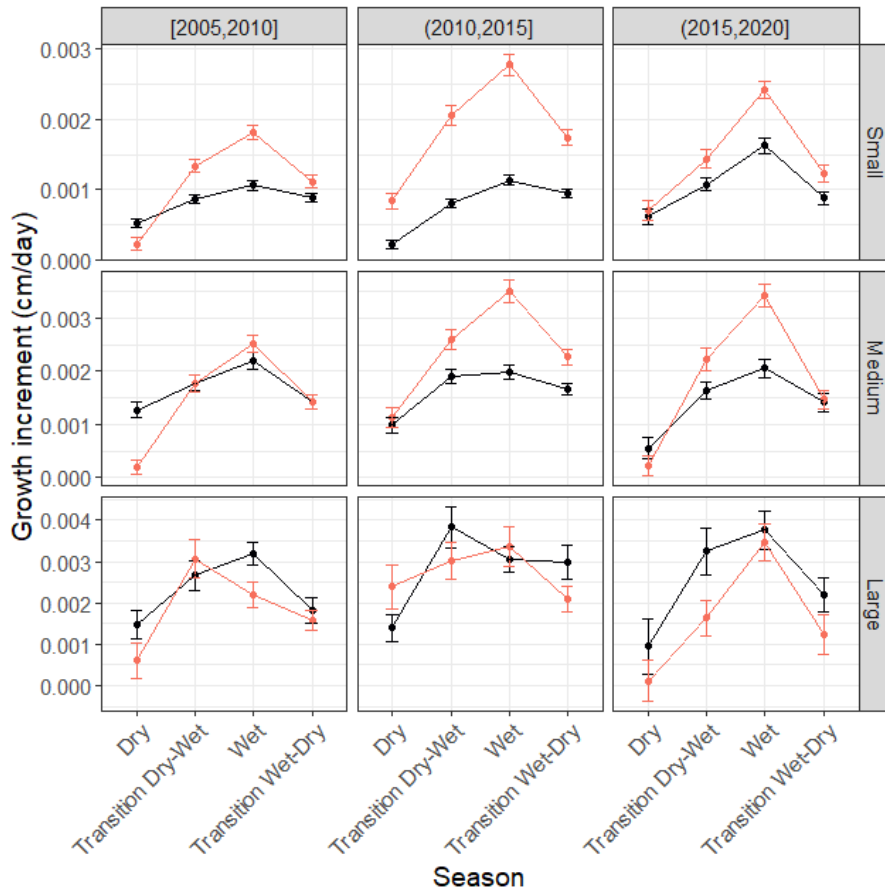


Figure 4.8: Growth increment (cm circumference/day) for TFE (red) and Control (black) grouped every 5 years from [2005-2010], (2010-2015] and (2015-2020], grouped by tree size Small (10-20 cm), Medium (20-40 cm), and Large (> 40 cm), and grouped by season: Dry, Transition from Dry to Wet season, Wet season and Transition from Wet to Dry season. Brackets “[” indicate inclusive, parentheses “(“ indicate exclusive.

### 4.3.4 Carbon loss: tree mortality

#### Tree mortality

In total, 202 trees ha<sup>-1</sup> died in TFE and 150 trees ha<sup>-1</sup> on the Control, accounting for losses of 153.0 ± 5.8 Mg C ha<sup>-1</sup> on the TFE and 63.8 ± 2.7 Mg C ha<sup>-1</sup> on the

Control (Figure 4.9). The rate of AGB loss due to tree mortality on the TFE was high prior to 2017, with a rate of  $9.1 \pm 0.3 \text{ Mg C ha}^{-1} \text{ yr}^{-1}$ . From 2017 to the most current measurement in 2022, AGB loss due to tree mortality decreased, and was at a rate of  $2.1 \pm 0.4 \text{ Mg C ha}^{-1} \text{ yr}^{-1}$ . In comparison, the Control initially had a low rate of AGB loss due to tree mortality between 2002 and 2015 at  $1.7 \pm 0.2 \text{ Mg C ha}^{-1} \text{ yr}^{-1}$ , which increased from 2015 to 2022 to a mean rate of  $4.2 \pm 0.9 \text{ Mg C ha}^{-1} \text{ yr}^{-1}$ .

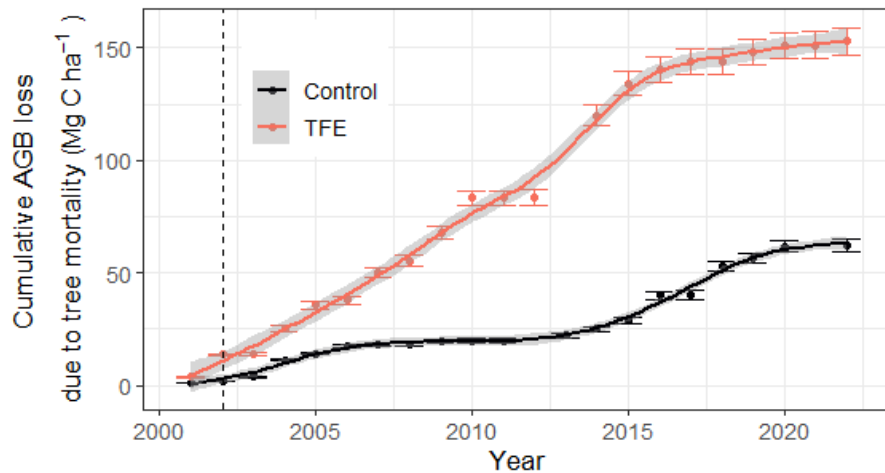


Figure 4.9: Cumulative aboveground biomass (AGB) loss ( $\text{Mg C ha}^{-1}$ ) due to mortality for Control (black) and TFE (red) from 2001 to 2022, with dashed line indicated commencement of experiment in January 2002.

Mortality rates were slightly higher for small trees on the TFE for the reporting period, with rates on the TFE at  $1.75 \pm 0.3\% \text{ yr}^{-1}$  and for the Control,  $1.4 \pm 0.3\% \text{ yr}^{-1}$ . There were brief periods of higher mortality rates for small trees on the TFE between 2005-2008, and in 2013, 2015 and 2021 in comparison to the Control (Figure 4.10). Medium-sized tree mortality rates were higher for the first 7 years of the TFE (2002-2009), as well as in 2015, 2016, 2017 and 2019 in comparison to the Control (Figure 4.10), resulting in mortality rates for the medium-sized trees on the TFE for the reporting period of  $1.89 \pm 0.4\% \text{ yr}^{-1}$  and for the Control  $1.3 \pm 0.3\% \text{ yr}^{-1}$ . Large tree mortality rates were the highest of all three size classes on the TFE, with mortality rates for the reporting period at  $3.89 \pm 0.9\% \text{ yr}^{-1}$  on the TFE and  $1.3 \pm 0.5\% \text{ yr}^{-1}$  on the Control. Mortality rates for large trees on the TFE had multiple peaks, which occurred in 2003, 2007, 2009 and 2015, the largest of which

was a mortality rate of 16.7% yr<sup>-1</sup>. Most peaks in mortality rates did not occur in the same year across size classes, however there was a peak in mortality in 2015, which occurred in all size classes on the TFE, with mortality rates of 5.6% yr<sup>-1</sup>, 5.3% yr<sup>-1</sup>, and 10.7% yr<sup>-1</sup> for small, medium and large trees, respectively (Figure 4.10). Interesting, mean mortality rates in each size class and overall from 2011 to 2022 on the TFE were equivalent, or lower than the Control, when the mortality rate of 2015 was excluded, with overall rate of mortality on the TFE  $1.2 \pm 0.3\%$  yr<sup>-1</sup> and on the Control  $1.5 \pm 0.4\%$  yr<sup>-1</sup>. The peak in mortality in 2015 coincided with the year that the canopy air temperature at 28 m spent the most time above 32°C (Figure 4.11), with air temperature above 32°C for 436 hours in 2015, 6.4 times longer than any other year from 2000 to 2018 (Figure 4.11). The air temperature in 2015 was above 33°C for 31 times longer than a typical year, at 94 hours (note that air temperature at this height in the canopy did not reach this temperature most years, Figure 4.11).

### 4.3.5 Tree spatial arrangement

Spatial competition, as determined by a nearest neighbour distribution function to determine clustering or aggregation of trees by detecting deviance from Poisson prediction of the cumulative distribution of distances ( $L_{est}$ ), was absent on the TFE plot, which demonstrates no spatial aggregation or competition between TFE trees. On the Control, positive deviation from complete spatial randomness (CSR) occurred at 0.1 m, indicating that trees are aggregated at short distances. Additionally, negative deviation from CSR occurred at 1 to 2.5 m, which indicates spatial competition through that range of distances (Figure 4.12).

## 4.4 Discussion

Widespread observations across tropical forests have suggested that, while nutrient availability moderates vegetation response, when rainfall declines below approximately 1500 mm/yr, or when the dry season extends for >6 months, then signif-

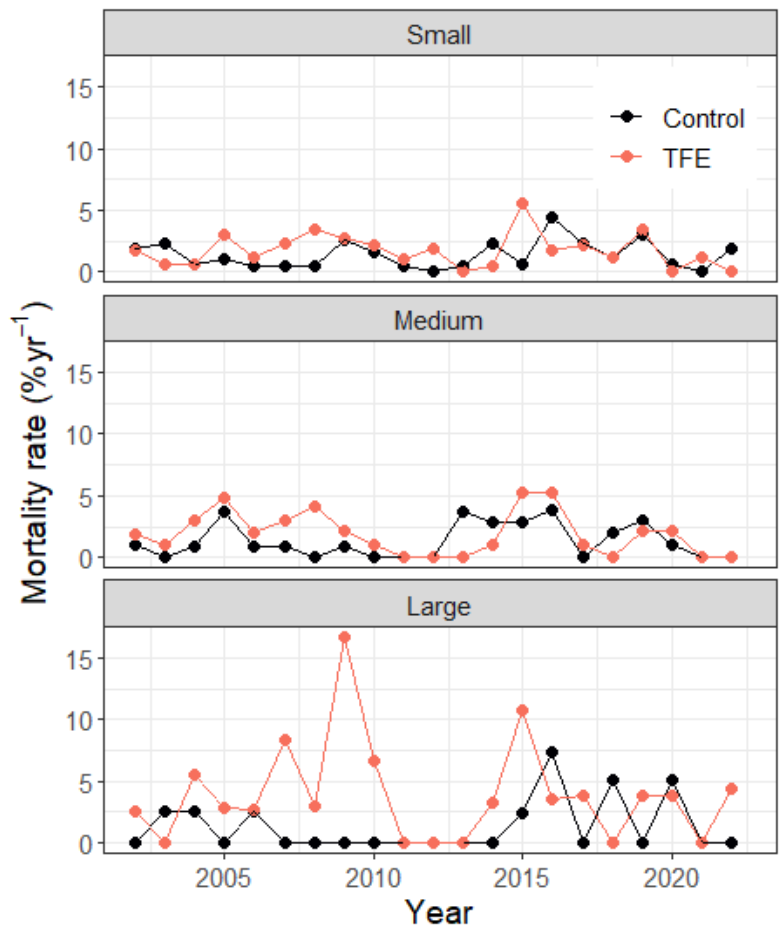


Figure 4.10: Mortality rates ( $\% \text{ yr}^{-1}$ ) of trees on the TFE (red) and Control (black) for the reporting period from 2002, which was the year the TFE was established, to 2022 for small (10-20 cm DBH), medium (20-40 cm DBH), and large ( $>40$  cm DBH) trees.

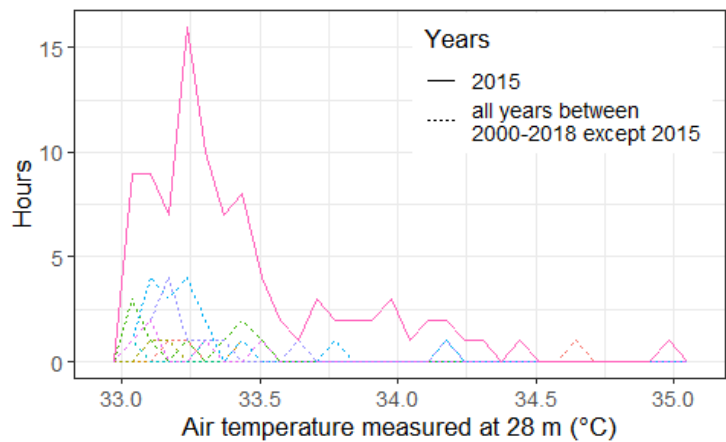


Figure 4.11: Number of hours air temperature at 28 m was above  $33^{\circ}\text{C}$  per year from 2000-2018, with year 2015 in solid line, and all other years in dashed line.

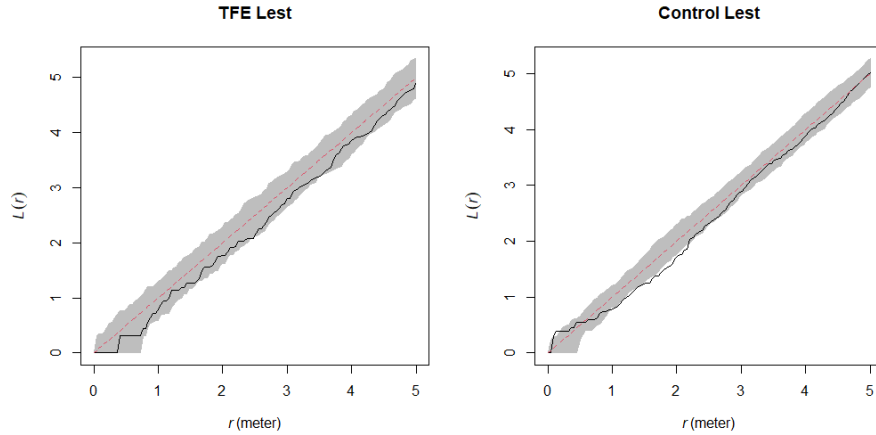


Figure 4.12: Using xy coordinates for all living trees, a nearest neighbour distribution function was calculated to determine clustering or aggregation of trees by detecting deviance from a Poisson process of the cumulative distribution of distances between each tree and all other trees on the plot on the TFE (left panel), and Control (right panel). We used the Ripley’s K test transformed to minimize variance ( $L_r$ ), and the shaded region is the 95% confidence envelope. The dashed red line indicates complete spatial randomness. A positive deviation from confidence envelope indicate aggregation; negative deviation indicates competition. Deviation from the dashed red line that is not outside of the confidence interval is not significant. The x axis,  $r$ , is distance (m).

icantly reduced biomass can be supported (e.g. Malhi et al., 2009a; Furley, 1994; Xu et al., 2016; Hirota et al., 2011; Staver et al., 2011), with evidence of bistability between low-biomass savanna ecosystems and high-biomass tropical rainforest ecosystems. For Amazonia, in addition to natural gradients in rainfall and vegetation, there has been a long-standing debate about the risk under a drying climate of a transition from rainforest to lower-biomass vegetation forms, including savanna (Sampaio et al., 2007), with attendant losses of carbon from biomass to the atmosphere. Nobre et al. (2016) examined the prospect of such a ‘dieback’, indicating a rough, but untested, threshold related to climatic drying, warming and deforestation. Recently, Gatti et al. (2021) used atmospheric data to demonstrate that these interactive effects can combine to alter significantly the carbon balance of parts of Amazonia. However, our understanding of a key part of the underlying processes, the long-term effects of drying and warming on tropical rainforest stability, remain poorly informed because of a lack of data.

The results from this analysis contribute to our understanding of the effects

of drought on Amazonian rainforest stability, and in particular, provide a multi-decadal scale timeframe of reference. Earlier studies at this hectare-scale throughfall exclusion experiment demonstrated that for an approximately 50% reduction in rainfall, although GPP declined quickly (Fisher et al., 2007), the forest was resilient to the imposed drought for 2-3 years (Costa da et al., 2010). However, large pulses in mortality were observed in subsequent years, with an overall loss in AGB of 40% occurring between 2005-2015 (Costa da et al., 2010; Rowland et al., 2015; Meir et al., 2018). Total water use was maintained by the forest such that nearly all of the water available to the trees was recycled through transpiration, even after the high mortality pulses, potentially leaving the forest vulnerable to future warming, more extreme drought, or even fire (Costa da et al., 2018; Bittencourt et al., 2020).

The analysis presented here extends our understanding by analyzing an additional 5-7 years of growth, recruitment and mortality data. The combination of these metrics describes basic forest dynamics and enables us to test for evidence of resilience, or loss of stability under climate stress. The data up to 2015 (Rowland et al., 2015) suggested that extended drought imposed very significant risk to biomass maintenance in eastern Amazonian rainforest, with evidence that a rapid collapse in biomass was possible under extended drought, perhaps supporting the forest transition arguments (Sampaio et al., 2007; Nobre et al., 2016). This new analysis enables a test of the potential for further biomass losses beyond the 40% reported in 2015 (Rowland et al., 2015), and an examination of whether the forest is likely to reach a new equilibrium under an extension of the imposed 50% rainfall reduction, or to substantially alter in biomass (upwards or downwards).

After 20 years of the TFE, we found evidence for a new stable state with (1)  $43.9 \pm 5.7\%$  lower but stable AGB for 5 years from 2017-2022 as tree growth and recruitment rate balanced tree mortality (Figure 4.4), (2) small and medium tree stand growth stabilized in the TFE since 2017 and the stand growth has stabilized as a whole from 2018 on the TFE at  $1.75 \pm 0.2 \text{ Mg C ha}^{-1}\text{yr}^{-1}$  (Figures 4.6, 4.7), (3) growth increment (GI) slowed in trees under 40 cm DBH, after five years (2010-

2015) of heightened GI on the TFE relative to the Control (Figure 4.8), (4) biomass loss due to tree mortality from 2016 to 2022 decreased to approximately  $\frac{1}{4}$  of the rate of biomass loss pre-2016 (Figure 4.9) and (5) mortality rates on the TFE since 2016 are equivalent to mean mortality rates on the Control for the reported period (Figure 4.10). This may be a temporary hiatus in tree mortality, and the TFE may continue to cause heightened mortality rates in the future; however, the remaining trees under 40 cm on the TFE have higher growth rates than the Control (Figure 4.8), indicating that they may be thriving under droughted conditions. Although large trees have lower GI on the TFE than the Control, since 2015 the aboveground woody production per unit biomass ( $NPP_{\text{standard}}$ ) of large trees on the TFE has increased to  $1.15 \pm 0.13$  times the Control, after 10 years of  $0.77 \pm 0.08$  times lower  $NPP_{\text{standard}}$  than the Control (Figure 4.7). This may indicate that large trees have recovered partially from the TFE, and may be taking advantage of decreased spatial competition (Figure 4.12) on the TFE. Stand growth of large trees on the TFE continues to be nearly half of the Control, although this is caused mainly by less large tree biomass on the TFE due to earlier large tree mortality (Rowland et al., 2015).

Since the trees on the TFE are distributed in a manner indicating that competition has been relieved for resources in comparison to the Control (Figure 4.12), this may suggest that there is space for additional expansion of recruitment in the future. In support of this, the recruitment rate on the TFE is high and there is no indication that the recruitment rate is slowing, yet (Figure 4.5). However, the rate of carbon accumulation of small trees on the TFE appears to have returned to levels similar to the Control, after 10 years of heightened carbon accumulation, which could indicate that rate of recruitment will stabilize as well (Figure 4.7A).

Despite the reduction of  $43.9 \pm 5.7\%$  in AGB on the TFE (Figure 4.4), the  $NPP_{\text{wood}}$  on the TFE was slightly higher than the Control for 9 years of the experiment (2009-2014, 2017, Figure 4.6). The  $NPP_{\text{wood}}$  on the TFE was higher than the Control due to small and medium trees on the TFE, which have higher  $NPP_{\text{wood}}$ ,

with  $NPP_{\text{wood}}$  rates of small trees peaking at 3.1 times higher than the Control rates (Figure 4.7). The higher rates of GI and  $NPP_{\text{wood}}$  in small and medium trees is in line with previous research showing that small trees (although in their case trees below 10 cm DBH) are responding well to TFE (Bartholomew et al., 2020; Giles et al., 2022). Small and medium trees may be thriving because of less spatial competition (Figure 4.12) and increased light availability on the TFE due to large tree mortality (Rowland et al., 2015). This is in contrast to expectations that small trees are more susceptible to drought damage, as small tree roots are expected to be located in shallower, drier, soil layers than large trees (Brun et al., 2020; Giardina et al., 2018). It is possible that the reduction in plot biomass on the TFE has reduced competition for water, and additionally, that small and medium trees may have plasticity that makes them more resistant to limited water availability.

The GI of large trees was slower on the TFE than the Control since 2005 in 1-2 of 4 seasons (Figure 4.8). Slower GI may be an indication that large trees are struggling under the TFE, but could also be an artefact of different size distributions of trees within each treatment, since GI scales with tree size.  $NPP_{\text{wood}}$  of large trees on the TFE has been stable from 2005-2015. Previously, there has been limited plasticity shown in large TFE trees, and large trees have indications of hydraulic stress, with lower leaf water potentials and higher dry season percentage loss of hydraulic conductivity than Control trees (Bittencourt et al., 2020). Additionally, large trees are inherently more vulnerable to hydraulic stress (Bennett et al., 2015; Olson et al., 2021), have longer path lengths, which increases the distance that water needs to travel to reach leaves, have larger xylem vessels that are more prone to cavitation (Koçillari et al., 2021; Olson et al., 2021; Olson, Rosell, 2013), and experience more extreme abiotic environment due to more canopy exposure, and therefore higher temperature and higher vapour pressure deficit (Meakem et al., 2017; Muller-Landau et al., 2020). This makes the stability in stand growth of large trees (Figure 4.7B) interesting, as it would be expected that large trees may have a declining trend in stand growth. Additionally, the  $NPP_{\text{standard}}$  (Figure 4.7C) was

higher on the TFE than the Control in large trees since 2015, which could indicate that large trees responded well to potentially lower competition for resources, after earlier tree mortality (Rowland et al., 2015).

Although  $NPP_{\text{wood}}$  has been apparently stable on the TFE since 2018 (Figure 4.6), measurements of  $NPP_{\text{wood}}$  rely on allometry to determine the relationship between changes in tree DBH and changes in tree biomass. Change in tree DBH does not directly relate to canopy growth; this is relevant on the TFE, as trees on the TFE had smaller canopies than equivalent-sized trees on the Control (Chapter 2). This difference in allometry was not taken into account when estimating  $NPP_{\text{wood}}$  (Figures 4.6, 4.7). Consequently, the magnitude of  $NPP_{\text{wood}}$  may be lower on the TFE than what is presented here, although the relative temporal pattern is likely the same.

Overall mortality rates, as well as mortality rates per tree size, were lower on the TFE between 2016-2022, in comparison to rates of mortality on the TFE between 2002-2016 and in comparison to mean mortality rates on the Control (Figure 4.10). This multi-decadal trend in mortality rate could indicate that the remaining trees on the TFE were not stressed after 2016. Interestingly, mean mortality rates from 2011 to 2022 on the TFE were equivalent, or lower than the Control per size class and overall, when the mortality rate of 2015 was excluded. In 2015, air temperatures were anomalously higher for a longer period of time than the rest of the reporting period (Figure 4.11). It is possible that the higher-than-normal temperatures interacted with the existing stress of the TFE, resulting in higher mortality rates across all size classes (Figure 4.10). This is consistent with evidence that the trees on the TFE are transpiring nearly all water available, making the forest potentially more vulnerable to temperature or rainfall anomalies (Costa da et al., 2018). We note, though, that tree mortality can occur over a long period after a stressor, and that this relationship between high mortality rates and air temperature within a single year suggests a more immediate mortality response.

#### 4.4.1 Comparison with Rowland et al. (2015)

The most recent work on the TFE reported a steep decline in 2015 in AGB, potentially boding a system collapse (Rowland et al., 2015). Data from 2015-2022 indicated that biomass has since stabilized (Figure 4.4). Of note, is that the stand AGB values presented in this paper are higher than Rowland et al. (2015), because of the new biomass and height allometry applied in this chapter, based on site calibrated data (Figure 4.1, 4.2, 4.3). Prior tree biomass estimates were between 18.1-24.0% lower than the current estimates, because height was underestimated when using height allometry from the Brazilian Shield (Figure 4.1, 4.2 Feldpausch et al., 2012), highlighting the importance of locally calibrated height allometric equations. Notably, the AGB on the TFE between 2002 and 2022 reduced by an additional 10% when accounting for changes in TFE tree allometry due to drought.

### 4.5 Conclusion

We found that reducing throughfall by half from 2000 mm yr<sup>-1</sup> to approximately 1000 mm yr<sup>-1</sup> reduced biomass by  $43.9 \pm 5.7\%$ , and it took 15 years for the ecosystem to stabilize. Large trees immediately and severely reduced woody growth rates and woody carbon accumulation from the start of the experiment, and suffered high rates of mortality for the first 15 years of the experiment. Throughout much of the experiment, trees below 40 cm DBH thrived, and likely have trait plasticity that allowed them to maximize growth under soil water deficit. Our results indicate that tropical rainforests may house less carbon by the end of the 21st century, if climate change in Amazonia follows the current projections. Any die-back may be expected to occur over the course of multiple decades, with low chance of a catastrophic die-back event leading to ecosystem collapse.

# Chapter 5

## Discussion

### 5.1 Thesis overview

Tropical rainforests play a central role in the global carbon cycle, comprising high standing biomass (Pan et al., 2011), generating the highest rates of gross primary productivity of any major terrestrial ecosystem (Beer et al., 2010) and housing a well-known peak in terrestrial biodiversity. If we are to understand the future Earth system, sound knowledge of how climate change will impact tropical rainforest carbon dynamics is essential. In this thesis, better understanding of a set of fundamental metrics and processes is sought, including (i) the allometry of tropical forests trees, (ii) the relationships under long-term drought stress among tree size, growth, metabolism, and (iii) new metrics of canopy structure.

The basis of this thesis was a continuously maintained 20-year tropical drought experiment (through-fall exclusion experiment, TFE). The drought treatment was delivered through partial restriction of incoming rainfall via a system of panels and gutters; a summary of preceding results can be found in Meir et al. (2018). In this study, terrestrial laser scanning (TLS) was combined with multiple new measurements and long-term ecophysiological datasets to deliver a new analysis connecting structure with function in the TFE and adjacent Control forest.

In Chapter 2, I found that plasticity in tree woody canopy architecture due to drought may be related to tree hydraulic stress mitigation strategies. Because of the

capacity the experiment afforded to test for differences in canopy structural metrics, my analysis provides some of the first evidence that not only organ-scale entities, such as leaves, but also canopy- and branch-scale architectural features can be considered as plant traits that may respond plastically to long-term perturbations, in this case, drought stress.

In Chapter 3, I used the detailed canopy structural analysis possible with the TLS data to develop a novel approach to studying wood respiration in droughted and non-droughted trees. I made standard and novel measurements of CO<sub>2</sub> efflux from woody tissue, and combined them with measurements of canopy structure derived from TLS data to demonstrate that the metabolic load represented by woody tissue respiration at the whole-tree level was substantially reduced under long term drought, and that this was driven by changes in vegetation structure, rather than by changes in the efflux rate from woody tissue.

In Chapter 4, I extended the use of TLS to improve estimates of aboveground biomass, based on site-calibrated high-resolution structural information, rather than relying on regionally generalized allometric relationships of tree size. I re-analyzed the 20 year data set of growth, recruitment and mortality at the experiment to estimate biomass changes over time. This enabled new insight into long-standing questions regarding the risk of a tropical rainforest transitioning to a lower biomass vegetation under extreme drought in Amazonia, with the associated risk of large emissions of CO<sub>2</sub> to the atmosphere. Earlier data had shown that nearly 40% of standing biomass was lost in the first 13 years of the experiment (Rowland et al., 2018), with evidence of rapid pulses of mortality or biomass collapse (Rowland et al., 2015; Meir et al., 2015). A key issue under consideration, therefore, was whether it was possible to determine if the long-term droughted forest would be vulnerable to further biomass collapse or whether it was likely to tend towards a new stable state. My analysis of the growth, recruitment and mortality dynamics of the droughted forest indicated a stabilization in biomass during the 6 years of new data presented here for the first time, and following a 15 year period of heightened

mortality. Whether this stabilization persists or is followed by further biomass loss is unclear. This thesis thus provides new insights into structural, functional and carbon-use related metabolic dynamics that may develop in tropical rainforests under predicted tropical drought scenarios this century. In this chapter I review and summarize the main findings of this thesis, discuss implications of each chapter and include suggestions of future research directions.

## **5.2 Chapter 2: Tree structural plasticity under long term experimental drought**

In Chapter 2, I examined the response to long-term water stress in trees on the TFE by testing for changes in the vertical and horizontal distribution of woody and foliar tissue, together with branch pathlength. There were substantial differences between TFE treatment and Control for multiple structural metrics of whole-tree woody and leaf tissue arrangements, as well as in twig structure. Together, my analyses indicated that trees avoid drought stress via mechanisms that improve hydraulic conductance in woody tissue, resource acquisition efficiency as determined by canopy metrics, and heat transfer, as inferred from canopy shape and position. I found that:

1. Hydraulic conductance may have increased for trees on the TFE because, in comparison to a Control tree of equivalent diameter at breast height (DBH), tree height was lower by  $1.2 \pm 0.3$  m, total tree length of all branches and stem decreased by 37%, mean path length, that is, the continuous length from the base of the tree to each canopy tip, was lower by  $1.4 \pm 0.4$ m, and path fraction, which is the mean path length divided by the maximum path length, was lower by  $0.06 \pm 0.01$ m. For twigs of equivalent basal diameters on the TFE, in comparison to the Control, the length of the twig was shorter on the TFE by  $12.5 \pm 4.4\%$ .
2. Resource acquisition efficiency may have increased on the TFE in response to long-term drought, in comparison to a tree of equivalent DBH on the Control.

On the TFE the leaf canopy surface area to volume ratio was larger by  $7.2 \pm 2.1\%$ , mean canopy width was  $6.7 \pm 1.9\%$  smaller, whole-tree woody tissue volume was smaller by  $30.6 \pm 2.6\%$ , and whole tree woody canopy volume was smaller by  $44.5 \pm 5.8\%$ . For twigs, woody tissue volume was smaller by  $32 \pm 11\%$  on the TFE in comparison to an equivalent twig basal diameter on the Control.

3. The distribution of leaf area by compass direction differed between TFE and Control trees, with relatively more leaf area within a tree found between  $330^\circ$  to  $60^\circ$ , that is north to north-east, on TFE droughted trees. By contrast, Control plot trees had a mean leaf distribution similar to a perfect circle. A key consequence of this difference in azimuthal leaf distribution is that, relative to the un-droughted forest trees, the droughted trees tended to have a smaller proportion of their canopies exposed to the hotter and lower-humidity conditions experienced in the afternoons, thus presenting a canopy-scale response to long-term drought that is analogous to trait plasticity and is of ecological significance to the growth and survival of each tree.
4. The plot-wide structural analysis showed a larger leaf area index to woody volume ratio by  $22 \pm 9\%$  on the TFE in comparison to Control. This was interpreted to have been driven by size dependent changes in tree structure over the course of long-term drought, specifically: trees below  $\sim 25$  m in height that had experienced long-term drought stress, relative to undroughted trees, had similar or higher wood volume and LAI as an aggregate; and trees above 25 m in height had lower aggregated volume and LAI than in the undroughted forest. This relationship was consistent with results found on twigs, with twig leaf area modelled by twig basal diameter, treatment, and interaction between DBH and treatment showing that small TFE trees ( $\sim 10$ - $20$  cm DBH) had a slightly larger leaf area by approximately 11% in comparison to Control trees, but that leaf area declined for larger trees on the TFE, such that trees larger than approximately 20 cm DBH on the TFE plot had relatively less leaf area per twig basal diameter than in the Control plot trees.

To my knowledge, no previous high-resolution analysis of trait plasticity in such aggregate canopy- and stand-scale properties has been made. Although TLS-based analyses of tree structural properties are emerging in the literature (Shenkin et al., 2020; Terryn et al., 2020), the long-term nature of growth responses means that the unusual context of this long-term ecosystem-scale drought experiment provided an empirical context to enable an examination, not only of novel traits at new scales of the tree and stand, but also of otherwise theoretical trait-based responses to the altered environment. I found existence of structural plasticity at different aggregated scales (tree canopy, stand), interpretable as trait-based responses to drought. This is potentially important for extending how we understand trait-based ecology of all forests, and is of specific interest at the Amazonian rainforest drought experiment site in this study in the context of preceding data showing variable and sometimes limited plasticity in more classical organ-scale physiological traits in response to long-term experimental drought in the larger trees that dominate the current canopy (e.g. hydraulic vulnerability Bittencourt et al. (2020); and leaf physiological capacity, Rowland et al. (2021a)). The architectural plasticity reported in this study may act to mitigate the sensitivity of tropical rainforests to drought, as tree architecture altered in a manner that was consistent with improved function under water deficit.

### **5.2.1 Chapter 2: Future research**

1. The links presented here between tree structure and tree function are inferred based on expectations of hydraulic mitigation strategies, rather than directly tested through a detailed network of extended physiological measurements. Measuring and linking the effects of alterations in architectural trait patterns directly with key physiological and growth performance metrics would clarify and quantify the extent to which changes in architecture can alter tree function.
2. Leaf point cloud data analysis using TLS is in its infancy, and validation studies are exceedingly rare. Validation studies relating leaf area to TLS-driven

allometrically-derived leaf area estimates are necessary to improve methods of processing leaf point cloud data. This can lead to improvements in leaf area estimates, as current field techniques used to measure LAI are known to often saturate in high leaf area environments like tropical rainforests. Integrating detailed TLS-derived leaf area estimates with TLS-derived light profiles and 3D leaf distribution, could vastly advance the resolution and our consequent understanding of tree leaf carbon dynamics. If combined with detailed canopy monitoring of meteorological data, new patterns may be identified that link tree growth patterns with environment.

### **5.3 Chapter 3: Structural and process-based analysis of woody tissue respiration during long-term experimental drought**

In this chapter, I evaluated wood CO<sub>2</sub> efflux, and wood respiration at the organ, tree and stand level, using methods relying on TLS to model woody tissue structure and woody tissue CO<sub>2</sub> efflux rate per tree branch diameter. Most measurements of CO<sub>2</sub> effluxes are performed on tree stems, from the ground (e.g. Meir, Grace, 2002). Here, I measured wood CO<sub>2</sub> efflux in both the canopy and on the stems. I also measured the apparent respiratory quotient (ARQ) for a subset of trees using the method developed by Angert et al. (2012), which I used to interpret the difference between measured radial wood CO<sub>2</sub> efflux and respiration: CO<sub>2</sub> derived from wood respiration can diffuse axially, radially or be removed by carboxylation, confounding direct measurements of wood respiration using measurements only of radial wood CO<sub>2</sub> efflux (Angert et al., 2012; Teskey, McGuire, 2002; Salomón et al., 2018). The key findings for this chapter were:

1. Wood CO<sub>2</sub> efflux was not altered as a result of the drought (TFE) treatment (N = 1751), except for twigs, which showed a higher wood CO<sub>2</sub> efflux rate (on a

surface area basis) on the TFE than Control in the wet season, when growth rates were high on the TFE (Rowland et al., 2018). Using novel ARQ measurements on a subset of trees (12 individuals, 2 species) to derive respiration rates in wood from the raw CO<sub>2</sub> efflux data, I demonstrated lower wood respiration rates (on a surface area basis) on the droughted TFE trees than the undroughted Control trees.

2. Whole tree wood CO<sub>2</sub> efflux was lower under drought treatment due to lower surface area to volume ratios for long-term droughted TFE trees relative to equivalent-sized trees on the undroughted Control plot.
3. Total stand wood CO<sub>2</sub> efflux ( $R_{\text{wood}}$ ) was lower on the TFE in comparison to the Control by approximately 58%, directly related to an equivalent reduction in stand vegetation surface area as determined using the new structural analysis data from TLS. This difference in stand wood CO<sub>2</sub> efflux was over 2x larger than what had previously been estimated for this site (Rowland et al., 2018), in part due to drought-related changes in surface area allometry and due to the previous study applying a surface area allometry that was not calibrated for the site.
4. Tree surface area measured using TLS was consistently lower than surface area derived from the commonly and globally applied tropical tree surface area allometry equation (Chambers et al., 2004), except for large trees, which were considerably underestimated when using the allometry equation from Chambers et al., 2004.

Overall, I examine the primary scalars describing wood CO<sub>2</sub> efflux in a tropical rainforest, its expression at tree and stand scales, and how respiration in woody tissue differs from raw CO<sub>2</sub> efflux under drought stress. The observed difference in tree structure under drought stressed conditions has led to reduction in metabolic load of trees, as a consequence of tree structural plasticity. This could be a manner of acclimation, and suggests that tropical rainforest trees could have higher levels of resistance to water deficit than previously anticipated, when plasticity was examined

using organ-scale measurements of metabolism and hydraulics (Rowland et al., 2015; Bittencourt et al., 2020).

Importantly, woody tissue respiration, as derived from ARQ measurements, was lower under long-term drought in the TFE than in the Control despite no significant difference in radial wood CO<sub>2</sub> efflux rates that might otherwise be expected under drought stress (Salomón et al., 2018). Since trees on the TFE are maintaining growth rates that are higher or equivalent to rates on the Control (Chapter 4 Rowland et al., 2015), it is unlikely that the decreased wood respiration resulted in turgor-restricted growth, as is normally seen under short-term droughts (De Roo et al., 2020; Lauriks et al., 2022; Rodríguez-Calcerrada et al., 2014; Saveyn et al., 2007). This may be yet another example of how drought responses on the short term do not predict long-term tree response to drought (Meir et al., 2018).

Of particular importance in this study is the issue of applying allometric relationships that are not locally calibrated. Most studies rely on regional or pantropical allometry to estimate biomass and height of forests (Chave et al., 2014; Feldpausch et al., 2012). I show that there was considerable error when using uncalibrated regional or global allometry to estimate biomass and tree height. Additionally, the error was distinct for trees on the Control and the TFE treatment. This suggests that there are systematic biases in studies to date of the effect of climate change on forest carbon cycles due to the use of uncalibrated allometric relationships, and that these biases may conceal effects of climate change on trees.

### **5.3.1 Chapter 3: Future research**

1. I found that approximately 40% of respiratory CO<sub>2</sub> from wood does not diffuse radially, consistent with measurements made in multiple woody ecosystems (Hilman, Angert, 2016). Since ARQ did not correlate with sap flow, and showed no relationship with location in tree (canopy, stem), there may be evidence that the missing sink is related to local enzymatic re-fixation processes that capture respiratory-derived CO<sub>2</sub> in woody tissue. To test for a relationship between

enzyme activity and ARQ, additional extensive ARQ measurements would be necessary, along with tissue enzyme assays, and a much wider species sampling, as my pilot data showed that ARQ varied between the two species suggesting that internal movement of CO<sub>2</sub> or rate of re-fixation processes may conceivably be constrained phylogenetically.

2. Stand wood CO<sub>2</sub> efflux needs to be discussed within a wider context of R<sub>eco</sub> and GPP to determine how stand wood CO<sub>2</sub> efflux influences the ecosystem carbon balance. The results from Chapter 2 showed an increase in the leaf area to tree biomass ratio on the TFE in comparison to the Control. Recent data using extensive species sampling have shown that leaf photosynthetic capacity were, at most, only marginally reduced under TFE and that leaf respiration rates were not significantly altered under long-term TFE (Rowland et al., 2015, 2021b), therefore the increase in leaf area:biomass ratio reported here could result in an enhanced carbon sink on the TFE. The overall carbon balance of this rainforest following long-term drought also depends on variation the remaining components of R<sub>eco</sub>, principally, soil respiration and estimates of GPP, which may be modelled using leaf area data from Chapter 2.

## **5.4 Chapter 4: Forest dynamics over 20 years of experimental drought: tending to biomass collapse or a new stable state?**

In this chapter, I used the experiment to inform the long-running discussion on the risk of biomass collapse via transition from rainforest to a lower-biomass vegetation form, in response to the level of drought-stress for Amazonia this century that is predicted in some climate-change scenarios (Duffy et al., 2015): the possibility of so-called Amazon die-back (Huntingford et al., 2008; Galbraith et al., 2010; Marengo et al., 2018). I describe the effect of severe drought on aboveground biomass (AGB)

in the TFE over the course of 20 years, testing and validating estimates using TLS, itself pre-calibrated using destructive sampling of nearby trees. I calculated any gains in AGB resulting from recruitment, tree growth or loss through mortality. All results were compared against a one-hectare Control plot where no drought treatment had been imposed, but for which the same long-term datasets have been collected. In addition to a re-analysis of existing data up to 2015 (Rowland et al., 2015; Costa da et al., 2010, 2014; Metcalfe et al., 2010b), I added six years of new biomass dynamics data to enable me to address the understanding of the long-term stability of the biomass in this forest, following earlier biomass loss driven by drought-induced high rates of tree mortality. Under the long-term TFE water exclusion regime, I found:

1. AGB on the TFE had decreased by  $43.9 \pm 5.7\%$ , after 20 years of exposure to substantial water deficit (50% rainfall removal). Most of this biomass loss occurred during mortality pulses in the first 13 years of the experiment as reported previously (Rowland et al., 2015), whereas during the most recent years, from 2016-2022, the new data showed AGB on the TFE to be approximately constant, suggesting that the forest may be approaching an equilibrium with current water supply.
2. Stand  $\text{NPP}_{\text{wood}}$  on the TFE was constant from 2018 to the most recently measured year, 2020. In comparison to the undroughted Control plot, the TFE plot had higher rates of  $\text{NPP}_{\text{wood}}$  per unit biomass from 2009 to present, and, in fact, had higher or very similar absolute values of stand  $\text{NPP}_{\text{wood}}$ , despite significant biomass loss on the TFE, for 10 of the 20 years in the reporting period. This trend has been driven by high growth rates in small and medium sized trees ( $\text{DBH} < 40 \text{ cm}$ ) on the TFE.
3. Following high rates of AGB loss from 2002-2015, the slope of cumulative AGB loss on the TFE has reached a horizontal asymptote between 2016 and 2022. Mortality rates on the TFE for the period between 2016-2022 are similar to pre-

treatment and Control mortality rates. Of note, is that the high temperatures recorded in 2015 coincided with high mortality rates on the TFE across all size classes, as well as a reduction in  $NPP_{\text{wood}}$  for small medium and large trees on both the TFE and the Control.

Dramatic improvements to quantifying biomass have occurred with the introduction of TLS (Calders et al., 2015a,b; Burt et al., 2021; Lau et al., 2019a). Here, I apply TLS to validate AGB estimates on two hectares of tropical rainforest. Estimates of AGB on the TFE indicate that the capacity of an ecosystem to support AGB is directly linked with precipitation regime, with  $\sim 45\%$  loss of AGB due to a 50% decrease in rainfall. The majority of the AGB loss occurred over the first 13 years of the TFE, with the growth and mortality dynamics of the most recently reported years indicating that the ecosystem has likely reached a new stable state. This suggests that tropical ecosystems may respond relatively quickly, on the scale of decades, to changes in water regimes, and that the risk of catastrophic die-back resulting in sparse savanna landscape is low, in the absence of other drought-related stressors such as fire. The manner in which the TFE responded to the additional stressor of the high temperatures in 2015 could be an indication that the ecosystem is not as resilient to climate anomalies as the Control. This is relevant for predicting future carbon scenarios, as this may indicate that the interaction between climate change and anomalous climate events, like El Nino years, could result in substantial mortality.

Although woody growth is only one metric of forest health, the high  $NPP_{\text{wood}}$  on the TFE, across all size classes, indicates potential acclimation and drought resistance of surviving trees on the TFE. It is particularly surprising that the large tree  $NPP_{\text{wood}}$ , standardized per unit biomass of large trees, was higher on the TFE than the Control in the final years of the reporting period, as this may indicate that large trees, which may be the most sensitive to drought (Rowland et al., 2015; Bittencourt et al., 2020; Nepstad et al., 2015) have acclimated to the TFE, despite recent hydraulic measurements in 2016 indicating that these trees are hydraulically

stressed (Bittencourt et al., 2020).

Importantly, at the basis of these  $\text{NPP}_{\text{wood}}$  values presented in this chapter are allometric assumptions relating an incremental change in DBH with an increase in total plant carbon. Since drought altered tree allometry on the TFE, any assumption relating growth at breast height with tree biomass, may be worth revisiting. This drought-induced change in allometry undermines comparison of growth dynamics at this site, during any experimental manipulation, or virtually any interpretation of forest growth dynamics under climate change using currently adopted measurements relying on DBH. Direct measurement of forest structure and growth via TLS, therefore, is pivotal to properly measure ecosystem carbon cycling, and evaluate the effect of climate change on forests.

#### **5.4.1 Chapter 4: Future research**

1. The analysis of growth data in this chapter is limited to describing change in tree growth over time, and does not include analysis of growth dynamics directly related to variations in soil water content. The reanalysis of growth dynamics, particularly during anomalously low rainfall years, would provide further information regarding how an already stressed, albeit, structurally acclimated, rainforest responds to further stress and how, in comparison, a non-stressed but potentially structurally sub-optimal rainforest responds to temporary water stress. Such a study would further advance our understanding of the resilience of trees to water deficit.
2. Large trees may be most susceptible to drought stress (Rowland et al., 2015; Bittencourt et al., 2020; Nepstad et al., 2015); however, it appears that the remaining large trees on the TFE are managing to cope with drought, and, as an aggregate, may have improved function compared to the Control, considering the rate of  $\text{NPP}_{\text{wood}}$  per unit biomass was higher on the TFE than the Control for large trees in most recently reported years. This leads to intriguing questions about what aspects of tree architectural trait plasticity have allowed for these

large trees to survive, acclimate, and potentially begin to thrive under extreme drought. This question might be considered difficult to answer due to small sample sizes of large trees in a single hectare; however, this analysis of structural traits suggests an advantage, in that the allometry in tree structure appears to have low variance, and may be well conserved within a given environment, making it possible to tease apart effects of treatment on the degree of plasticity in tree structural traits using relatively small sample sizes.

## 5.5 Conclusion

This work introduces new measurements of structure and function, focusing on the use of terrestrial laser scanning to quantify tree structure and biomass, and combining the structural measurements with basic and advanced measurements of metabolism via the quantification of CO<sub>2</sub> effluxes from woody tissue. Using these high resolution measurements of tree structure with TLS, I demonstrate considerable plasticity in several woody architectural metrics that I argue can be considered as new ecological traits (Díaz et al., 2016) based on the evidence uniquely provided by the long-term experiment that, not only can these architectural metrics be defined, but they also change under water stress on multi-year and decadal timescales in ways that promote growth and/or survival of individual trees. Further, my analysis uses this quantification of structure to show that respiratory metabolism at tree and stand scales declines substantially as a result of the distinct effects of long-term drought on vegetation structure.

Finally, I analyze the full 20 year forest dynamics dataset from this experiment. Here I use my TLS analysis to calibrate the previously assumed (Costa da et al., 2010; Rowland et al., 2015) allometric relationship at this site between DBH and height. A form of this relationship is used globally to determine tropical tree and forest biomass (Chave et al., 2014) but is known to vary biogeographically (Feldpausch et al., 2012). I further calibrate biomass estimates at this site using a local tree harvest-based TLS calibration. The updated 20-year forest dynamics dataset is

then used to extend earlier analyses showing rapid biomass loss in the first 13 years of the drought treatment during which 40% of the pre-existing biomass was lost to elevated mortality. New data for another five years are presented to test whether forest biomass would collapse further or tend towards a new stable state under the drought treatment, informing wider debates about possible Amazon forest die-back under extended severe drought (Sampaio et al., 2007; Davidson et al., 2012; Nobre et al., 2016). The results suggest that the forest may have reached a new stable state that supports a lower biomass (Slik et al., 2010). The evidence indicates that these forests are likely to lose considerable biomass, with consequent emissions of CO<sub>2</sub> to the atmosphere, but ultimately show long-term resilience as lower-biomass forest, rather than a scant savanna environment.

In summary, this thesis substantiates a novel extension of trait based ecological thinking, provides key new data to advance estimates of whole tree and forest stand metabolism, and, using an extension of a prior 13 year forest dynamics field-experiment dataset, provides evidence for decadal-scale reductions in biomass under drought followed by subsequent stability. These insights offer new advances in, and constraints to, our understanding and prediction of the likely responses by Amazonia tropical rainforest to climate change this century.

# Appendices

# Appendix A

## Appendix for Chapter 2

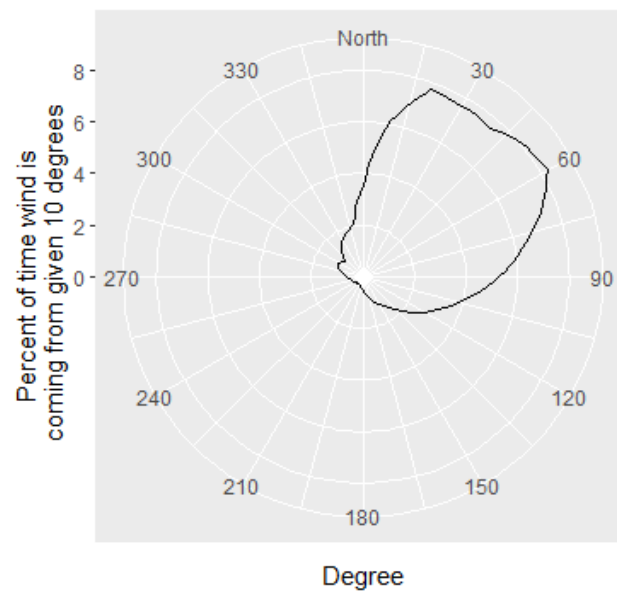


Figure A.1: Wind direction at Caxiuanã from 2017 to 2020, where wind direction is defined as the direction the wind is coming from. Data are presented as percent of total time that wind is coming from a given 10 degrees for the reported period (2017-2020)

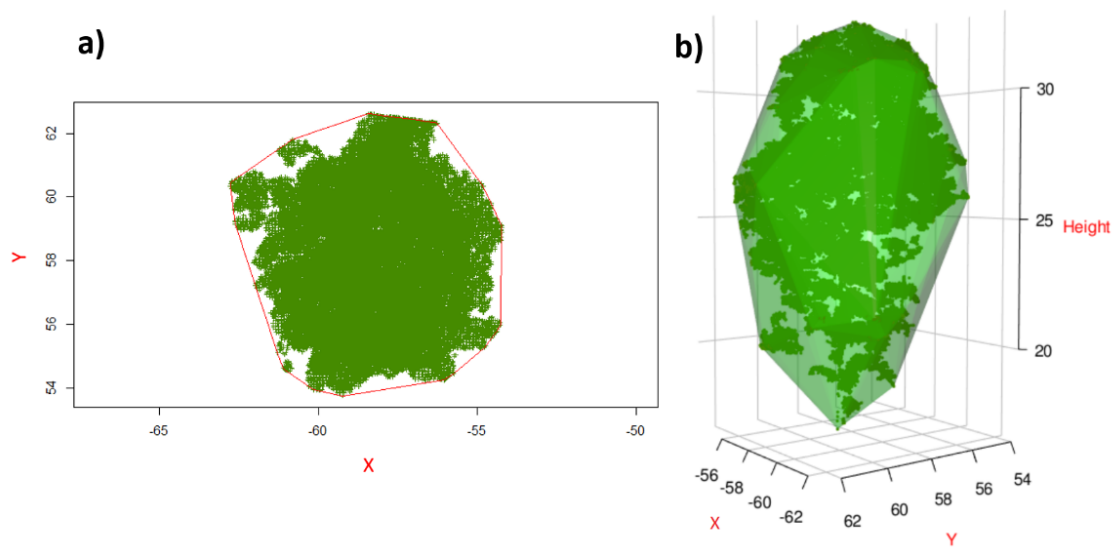


Figure A.2: Examples of a) 2D convex hull which was used to calculate mean width of canopy as  $4 \times \text{area of the 2D convex hull projected in the x-y direction} / \text{perimeter of the convex hull polygon}$  and b) 3D convex hull which was used to calculate the surface area to volume ratio of the leafy-canopy.

Methods for correcting volume per 3 meter height bin for trees on a 20 x 20 m (low-resolution) to 10 x 10 m grid (high-resolution). Firstly, total canopy volume was corrected to per tree with a model of using dependent variables, total canopy volume extracted at 20 x 20 m ( $m^3$ ), DBH (cm), 3D convex hull volume (crownvolume,  $m^3$ ), and the interaction between canopy volume and DBH ( $R^2 = 0.96$ ,  $N = 139$ , A.1). The difference between 10 x 10 and 20 x 20 canopy volume is added to each 3 meter height bin of the canopy equally. Next, the canopy volume distribution is corrected for the previously assumed equal distribution of the added canopy volume, with a model relating canopy volume per height bin at 10 x 10 (canopy.vol.10.perz,  $m^3$ ) to the interaction between corrected canopy volume per height bin at 20 x 20 (canopy.vol.20.perz,  $m^3$ ) and the height bin (m, A.2). Trunk volume per height bin is corrected using the interaction between trunk volume extracted at 20 x 20 m ( $m^3$ ) and the height bin (m) of the volume (A.3). Graph of the application of correction models of trunk and canopy for an aggregate profile of 146 trees, with fine scale 10 x 10 m aggregate profile in red, corrected profile in blue, and uncorrected profile in green A.3.

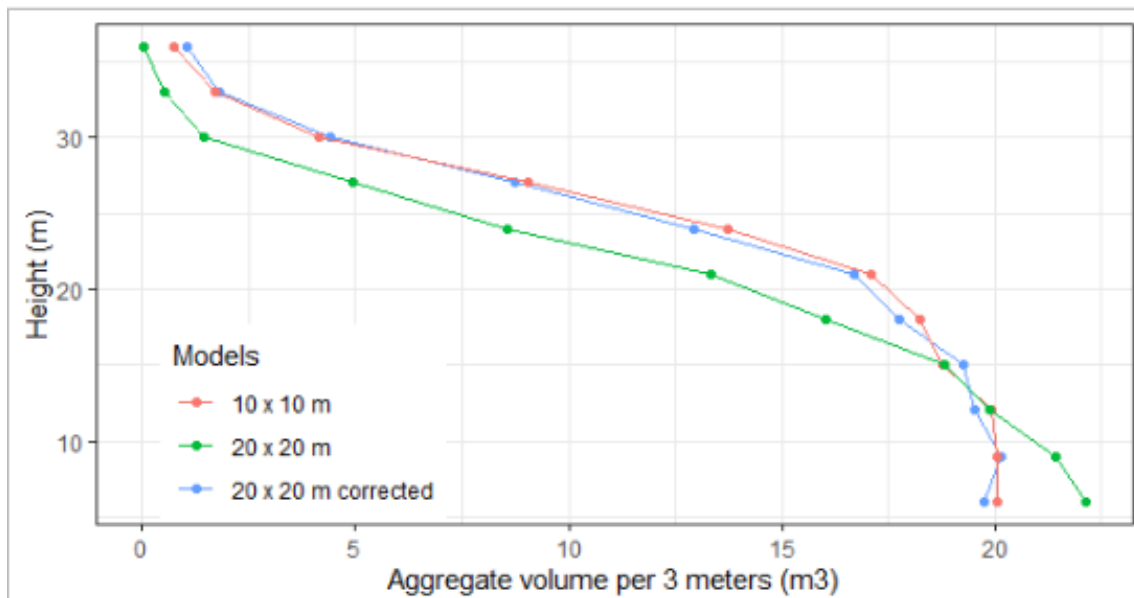


Figure A.3: Methods for correcting tree woody tissue volume for each 3 meter height bin for trees on a 20 x 20 m

Table A.1: Linear model coefficients of total canopy volume per tree, using total canopy volume extracted at 20 x 20 m (m<sup>3</sup>), DBH (cm), 3D convex hull volume (crownvolume, m<sup>3</sup>), and the interaction between canopy volume and DBH (R<sup>2</sup> = 0.96, N = 139)

Dependent variable: canopy.volume.10x10	
canopy.vol.20	0.278*** (0.077)
DBH	0.006*** (0.002)
crownvolume	0.001*** (0.0001)
canopy.vol.20.total:DBH	0.006*** (0.001)
Constant	-0.150*** (0.038)
<hr/>	
Observations	139
R <sup>2</sup>	0.961
Adjusted R <sup>2</sup>	0.960
Residual Std. Error	0.170 (df = 134)
F Statistic	822.556*** (df = 4; 134)
<hr/>	
Note:	*p<0.1; **p<0.05; ***p<0.01

Table A.2: Second step to correcting low resolution canopy volume profiles by relating canopy volume per height bin at 10 x 10 (canopy.vol.10.perz, m<sup>3</sup>) to the interaction between corrected canopy volume per height bin at 20 x20 (canopy.vol.20.perz, m<sup>3</sup>) and the height bin

Dependent variable: canopy.vol.per.z	
canopy.vol.20.perz.corr	0.496*** (0.056)
height.bin	-0.002*** (0.001)
canopy.vol.20.perz.corr:height.bin	0.024*** (0.003)
Constant	0.045*** (0.012)
Observations	468
R <sup>2</sup>	0.907
Adjusted R <sup>2</sup>	0.906
Residual Std. Error	0.065 (df = 464)
F Statistic	1,508.284*** (df = 3; 464)
Note:	*p<0.1; **p<0.05; ***p<0.01

Table A.3: Linear model coefficients of trunk volume per height bin, used to correct low resolution trunk volume profile

Dependent variable:trunk.vol.10.perz	
trunk.vol.20.perz	0.694*** (0.011)
trunk.vol.20.perz:height.bin	0.023*** (0.002)
Constant	0.010** (0.005)
Observations	641
R <sup>2</sup>	0.893
Adjusted R <sup>2</sup>	0.892
Residual Std. Error	0.106 (df = 638)
F Statistic	2,655.339*** (df = 2; 638)
Note:	*p<0.1; **p<0.05; ***p<0.01

Table A.4: Relationship between total number of leaf points of a tree (leaf.points), the tree canopy width (m), the tree DBH (cm), and the interaction between canopy width and tree DBH. Variables are log transformed as noted for linearity. Coefficients are presented with standard error of coefficients in parentheses.

---

Dependent variable: log(leaf.points)	
log(width)	2.342 (0.072)***
DBH	0.013 (0.006) **
log(width):DBH	-0.006 (0.002)***
Constant	5.735 (0.131)***
Observations	310
R <sup>2</sup>	0.876
Adjusted R <sup>2</sup>	0.874
Residual Std. Error	0.332 (df = 306)
F Statistic	717.945*** (df = 3; 306)
Note:	*p<0.1; **p<0.05; ***p<0.01

Table A.5: Genus-specific intercept for tree height mixed effect model

<b>Genus</b>	<b>Random effect intercept</b>
Abarema	-0.831625734
Adenocalymma	0.951755262
Amaioua	-0.066473891
Ambelania	-0.330091453
Anacardium	0.005482656
Aptandra	0.32420176
Aspidosperma	1.09765822
Astronium	-0.191858121
Bignonia	0.998672261
Bocageopsis	-0.229973366
Bowdichia	-0.175729725
Brosimum	0.254707702
Buchenavia	0.305400289
Chrysophyllum	0.472238558
Couepia	0.28104185
Couma	-0.435460354
Couratari	0.543350472
Cupania	0.20596177
Dendrobangia	-0.055821708
Dialium	0.262267246
Dinizia	0.646079877
Diptropis	0.254189509
Dipteryx	0.002053814
Duguetia	-0.405744414
Duroia	-0.254699504
Ecclinusa	-0.11854316
Endlicheria	0.149928096
Endopleura	-0.058743181
Ephedranthus	-0.190354649
Erisma	-0.179737506
Eschweilera	-1.341879483
Eugenia	0.080246835
Ferdinandusa	-0.112078157
Geissospermum	-1.058144078
Goupia	-0.709641264
Guapira	-0.24572866
Guatteria	0.000234722
Hirtella	-0.142521593
Hymenaea	0.595464163
Hymenolobium	0.293206166
Ilex	-0.090071357
Inga	-0.194704976
Iryanthera	0.361664101
Lacunaria	-0.675510631

Continued on next page

**Table A.5 – continued from previous page**

<b>Genus</b>	<b>Random effect intercept</b>
Lecythis	-0.288569627
Licania	0.139625488
Licaria	-0.230270163
Manilkara	0.13717478
Maquira	-0.167002467
Martiodendron	-0.412238305
Matayba	-0.004434512
Maytenus	-0.066614864
Mezilaurus	-0.090937793
Micropholis	0.365653421
Minquartia	-0.928929636
Mouriri	-0.834804337
Myrciaria	-0.059333997
Naucleopsis	0.336028412
Ocotea	-0.505868592
Oenocarpus	-0.227723433
Ouratea	0.501247708
Parkia	0.058436911
Paypayrola	-0.464721269
Peltogyne	0.354608766
Pourouma	0.216716101
Pouteria	0.520176158
Protium	0.560371093
Pseudopiptadenia	0.808665412
Pterocarpus	0.022873782
Qualea	0.941077075
Quararibea	-0.020827859
Quiina	0.055585971
Rhodostemonodaphne	-0.404969992
Rinorea	-1.091471182
Sclerolobium	0.478465763
Stachyarrhena	0.086742001
Sterculia	0.043094964
Stryphnodendron	-0.279663423
Swartzia	-0.455709242
Tachigali	0.661812219
Talisia	-0.146031053
Tetragastris	-0.355906063
Theobroma	-0.00208366
Tovomita	-0.177281338
Trattinickia	-0.298621171
Vantanea	0.066715991
Vatairea	0.289741748
Virola	-0.110345512
Vouacapoua	0.460966783
Continued on next page	

**Table A.5 – continued from previous page**

<b>Genus</b>	<b>Random effect intercept</b>
Xylopia	0.004092776
Zygia	0.390131336

Table A.6: Genus-specific intercept for canopy width mixed effect model

<b>Genus</b>	<b>Random effect intercept</b>
Abarema	-3.12E-02
Adenocalymma	1.44E-02
Amaioua	-1.73E-02
Ambelania	3.80E-02
Anacardium	1.31E-02
Aptandra	-2.20E-02
Aspidosperma	-5.79E-02
Astronium	-2.69E-02
Bignonia	4.98E-03
Bocageopsis	3.85E-02
Bowdichia	1.57E-02
Brosimum	-2.55E-02
Buchenavia	-3.50E-03
Chrysophyllum	-4.80E-02
Couepia	-1.34E-02
Couma	5.14E-03
Couratari	-5.32E-02
Cupania	6.84E-03
Dendrobangia	-1.84E-02
Dialium	3.21E-02
Dinizia	-3.93E-03
Diptropis	2.87E-03
Dipteryx	3.50E-03
Duguetia	1.71E-02
Duroia	-2.89E-02
Ecclinusa	-4.62E-03
Endlicheria	-2.60E-02
Endopleura	2.57E-02
Ephedranthus	2.05E-02
Erisma	2.93E-02
Eschweilera	3.94E-02
Eugenia	2.30E-02
Ferdinandusa	1.08E-03
Geissospermum	3.71E-02
Goupia	2.04E-02
Guapira	1.42E-02
Guatteria	-1.45E-03
Hirtella	-9.95E-03
Hymenaea	8.79E-03
Hymenolobium	-1.66E-02
Ilex	-2.81E-02
Inga	5.05E-02
Iryanthera	-4.28E-03
Lacunaria	6.66E-03

Continued on next page

**Table A.6 – continued from previous page**

<b>Genus</b>	<b>Random effect intercept</b>
Lecythis	1.08E-01
Licania	3.96E-02
Licaria	3.10E-03
Manilkara	-1.28E-02
Maquira	-3.56E-03
Martiodendron	-5.42E-04
Matayba	-3.45E-03
Maytenus	1.89E-02
Mezilaurus	3.81E-03
Micropholis	1.40E-02
Minquartia	-6.01E-02
Mouriri	-2.52E-02
Myrciaria	-8.52E-03
Naucleopsis	-2.05E-02
Ocotea	2.89E-02
Oenocarpus	4.65E-03
Ouratea	3.13E-03
Parkia	4.88E-05
Paypayrola	-9.16E-03
Peltogyne	8.08E-03
Pourouma	-7.08E-03
Pouteria	-1.87E-02
Protium	1.61E-02
Pseudopiptadenia	1.87E-03
Pterocarpus	-5.96E-03
Qualea	-2.06E-02
Quararibea	-3.18E-02
Quiina	9.10E-03
Rhodostemonodaphne	4.15E-03
Rinorea	1.32E-02
Sclerolobium	2.04E-02
Stachyarrhena	-6.45E-02
Sterculia	-3.37E-02
Stryphnodendron	-4.55E-04
Swartzia	3.91E-02
Tachigali	-2.21E-03
Talisia	3.26E-03
Tetragastris	2.51E-02
Theobroma	-2.87E-02
Trattinickia	2.92E-02
Vantanea	1.58E-02
Vatairea	-1.65E-02
Virola	-7.93E-03
Vouacapoua	-2.45E-02
Xylopia	-7.55E-03
Continued on next page	

Table A.6 – continued from previous page

Genus	Random effect intercept
Zygia	-2.46E-02

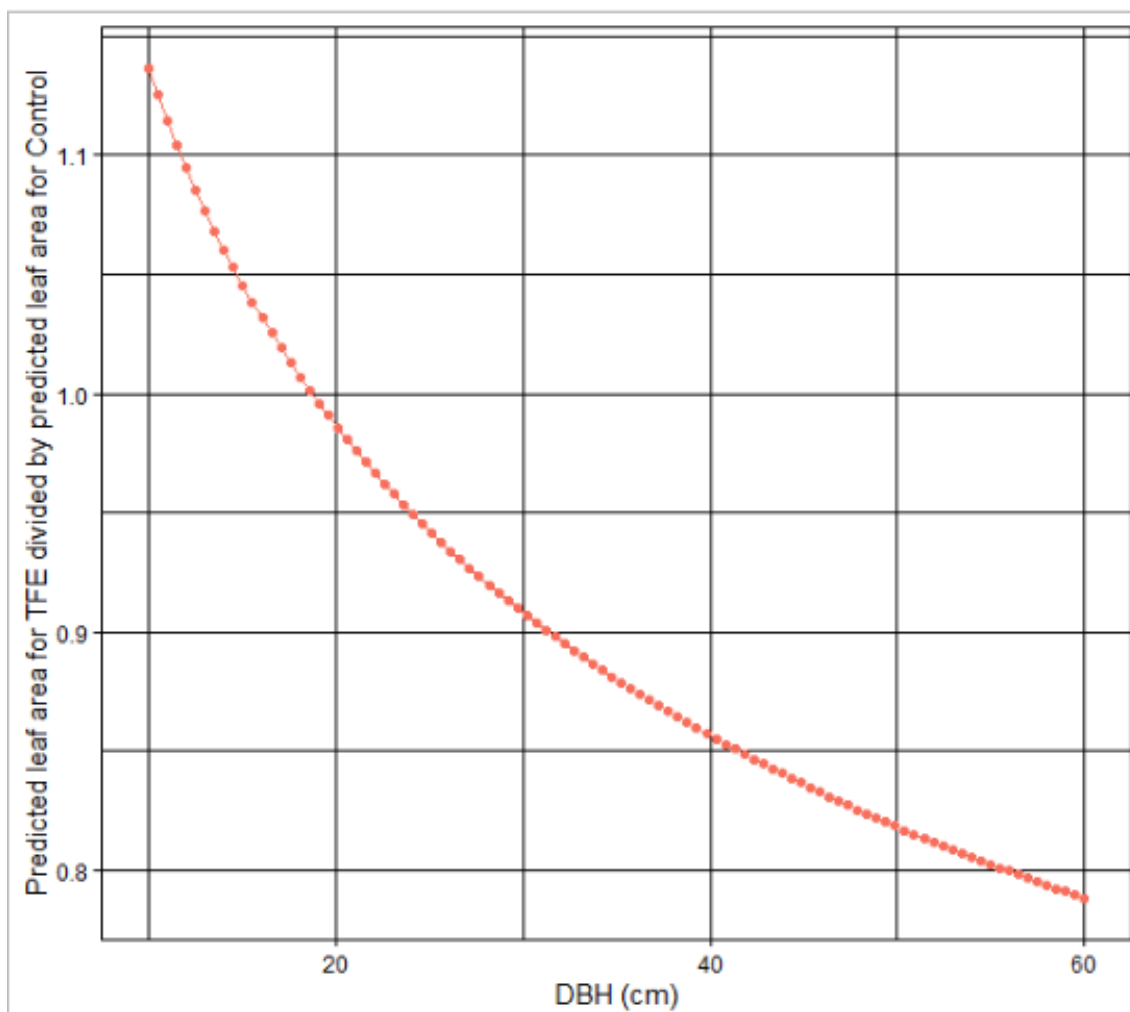


Figure A.4: Counterfactual plot for model of total leaf area ( $\text{m}^2$ ) of twigs. Plot has predicted leaf area of TFE twigs divided by predicted leaf area for Control for a constant twig basal diameter plotted against the diameter of the tree (DBH, cm).

# Appendix B

## Appendix for Chapter 3

Table B.1: Correction of surface area of low resolution models (20 x 20 m sampling grid, SA.20x20) to high resolution (10 x 10 m sampling grid) using 146 trees on the Control. SA.20x20, transformed tree height (height), and the interaction between the two were used to model tree surface area at 10 x 10 m resolution (SA.10x10)

SA.10x10 Predictors	Estimates	CI	p
(Intercept)	-1.50	-4.05 – 1.06	0.248
SA.20x20	0.75	0.63 – 0.87	<0.001
height <sup>3</sup>	0.00	0.00 – 0.00	<0.001
SA.20x20 * height <sup>3</sup>	0.00	0.00 – 0.00	<0.001
Observations	146		
R <sup>2</sup> / R <sup>2</sup> adjusted	0.944	0.943	

Table B.2: Correction of volume of low resolution models (20 x 20 m sampling grid) to high resolution (10 x 10 m sampling grid) using 146 trees on the Control. Tree volume at 20x20 and the interaction between tree volume at 20 x 20 resolution with tree height was used to model tree volume at 10 x 10.

Predictors	Vol.10x10		
	Estimates	CI	p
(Intercept)	0.05	-0.04 – 0.15	0.243
Vol.20x20	0.44	0.24 – 0.64	<0.001
Vol.20x20 * height	0.02	0.01 – 0.02	<0.001
Observations	146		
R <sup>2</sup> / R <sup>2</sup> adjusted	0.970 / 0.970		

Table B.3: List of the species sampled, and number of individuals on TFE and Control. Where noted, only genus-level identification was known, or species and genus level identification unknown.

<b>Binomial</b>	<b>Experiment</b>	<b>N. Individuals</b>
<i>Anacardium tenuifolium</i>	TFE	1
<i>Aptandra</i>	TFE	2
<i>Aspidosperma araracanga</i>	TFE	3
<i>Aspidosperma desmanthum</i>	Control	3
<i>Aspidosperma desmanthum</i>	TFE	1
<i>Aspidosperma nitidum</i>	Control	2
<i>Aspidosperma nitidum</i>	TFE	1
<i>Bocageopsis multiflora</i>	Control	2
<i>Bowdichia nitida</i>	TFE	1
<i>Brosimum guianense</i>	Control	1
<i>Buchenavia grandis</i>	Control	1
<i>Couepia guianensis</i>	Control	1
<i>Couepia guianensis</i>	TFE	2
<i>Couma guianensis</i>	Control	1
<i>Couratari multiflora</i>	Control	1
<i>Dendrobangia boliviana</i>	TFE	1
<i>Duguetia echinophora</i>	Control	1
<i>Ecclinusa guianensis</i>	Control	1
<i>Erisma uncinatum</i>	TFE	3
<i>Eschweilera</i>	Control	1
<i>Eschweilera coriacea</i>	Control	4
<i>Eschweilera coriacea</i>	TFE	4
<i>Eschweilera decolorans</i>	Control	1
<i>Eschweilera decolorans</i>	TFE	2
<i>Eschweilera grandiflora</i>	Control	2
<i>Eschweilera grandiflora</i>	TFE	1
<i>Eschweilera pedicellata</i>	Control	1
<i>Ferdinandusa elliptica</i>	TFE	1
<i>Goupia glabra</i>	Control	1
<i>Hirtella bicornis</i>	Control	1
<i>Ilex inundata</i>	Control	1
<i>Inga</i>	Control	1
<i>Inga alba</i>	Control	2
<i>Inga alba</i>	TFE	1
<i>Inga capitata</i>	Control	1
<i>Inga gracilifolia</i>	Control	1
<i>Inga gracilifolia</i>	TFE	4
<i>Lecythis idatimon</i>	TFE	1
<i>Licania glabriflora</i>	TFE	1
<i>Licania membranacea</i>	Control	3
<i>Licania membranacea</i>	TFE	2
<i>Licania octandra</i>	Control	3
Continued on next page		

**Table B.3 – continued from previous page**

<b>Binomial</b>	<b>Experiment</b>	<b>N. Individuals</b>
<i>Licania octandra</i>	TFE	4
<i>Manilkara bidentata</i>	Control	4
<i>Manilkara bidentata</i>	TFE	7
<i>Manilkara huberi</i>	Control	3
<i>Manilkara huberi</i>	TFE	1
<i>Manilkara paraensis</i>	Control	2
<i>Mezilaurus mahuba</i>	Control	1
<i>Micropholis egensis</i>	TFE	1
<i>Micropholis venulosa</i>	Control	4
<i>Micropholis venulosa</i>	TFE	2
<i>Minquartia guianensis</i>	Control	4
<i>Minquartia guianensis</i>	TFE	5
<i>Mouriri duckeana</i>	TFE	1
<i>Ocotea tabacifolia</i>	Control	1
<i>Pouteria anomala</i>	Control	5
<i>Pouteria anomala</i>	TFE	4
<i>Pouteria cladantha</i>	Control	1
<i>Pouteria cladantha</i>	TFE	1
<i>Pouteria decorticans</i>	Control	3
<i>Pouteria decorticans</i>	TFE	1
<i>Pouteria erythrochrysa</i>	Control	1
<i>Pouteria guianensis</i>	Control	1
<i>Pouteria jariensis</i>	TFE	1
<i>Pouteria oppositifolia</i>	Control	1
<i>Pouteria oppositifolia</i>	TFE	2
<i>Pouteria ramiflora</i>	Control	1
<i>Pouteria ramiflora</i>	TFE	1
<i>Pouteria trilocularis</i>	Control	1
<i>Pouteria venosa</i>	TFE	2
<i>Protium pilosimum</i>	Control	1
<i>Protium pilosimum</i>	TFE	1
<i>Protium tenuifolium</i>	Control	4
<i>Protium tenuifolium</i>	TFE	5
<i>Pseudopiptadenia psilostachya</i>	TFE	1
<i>Qualea</i>	Control	1
<i>Qualea paraensis</i>	Control	2
<i>Rinorea guianensis</i>	Control	8
<i>Stryphnodendron</i>	Control	2
<i>Swartzia racemosa</i>	Control	5
<i>Swartzia racemosa</i>	TFE	5
<i>Symphonia globulifera</i>	TFE	1
<i>Tetragastris panamensis</i>	Control	1
<i>Tetragastris panamensis</i>	TFE	1
<i>Tovomita choisyana</i>	Control	1
<i>Virola michelii</i>	Control	1

Continued on next page

**Table B.3 – continued from previous page**

<b>Binomial</b>	<b>Experiment</b>	<b>N. Individuals</b>
<i>Virola michelii</i>	TFE	2
<i>Vouacapoua americana</i>	Control	6
<i>Vouacapoua americana</i>	TFE	6
<i>Zygia racemosa</i>	Control	1
<i>Unknown</i>	TFE	2

Gap filling methods used for surface area of branches between 5 cm and 1 mm in basal diameter:

1. Plotted branch radius versus cumulative sum of branch surface area or cumulative sum of branch volume, from largest branch radius to smallest branch radius (see Appendix B.1).
2. A linear regression performed, using branch radius below 3 cm in diameter (see Appendix B.1).
3. Linear regression model was used to predict cumulative surface area at 5 cm in diameter and 1 mm in diameter and the difference between 5 cm and 1 mm predicted cumulative surface area was considered the gap filled surface area of branch under 5 cm in diameter.
4. A model of surface area/volume of branches below 5 cm was created using fixed effects of total tree surface area (tot.sa, m<sup>2</sup>) and dbh (cm,  $R^2 = 0.77$ ,  $N = 325$ , see coefficients in A.2,below)

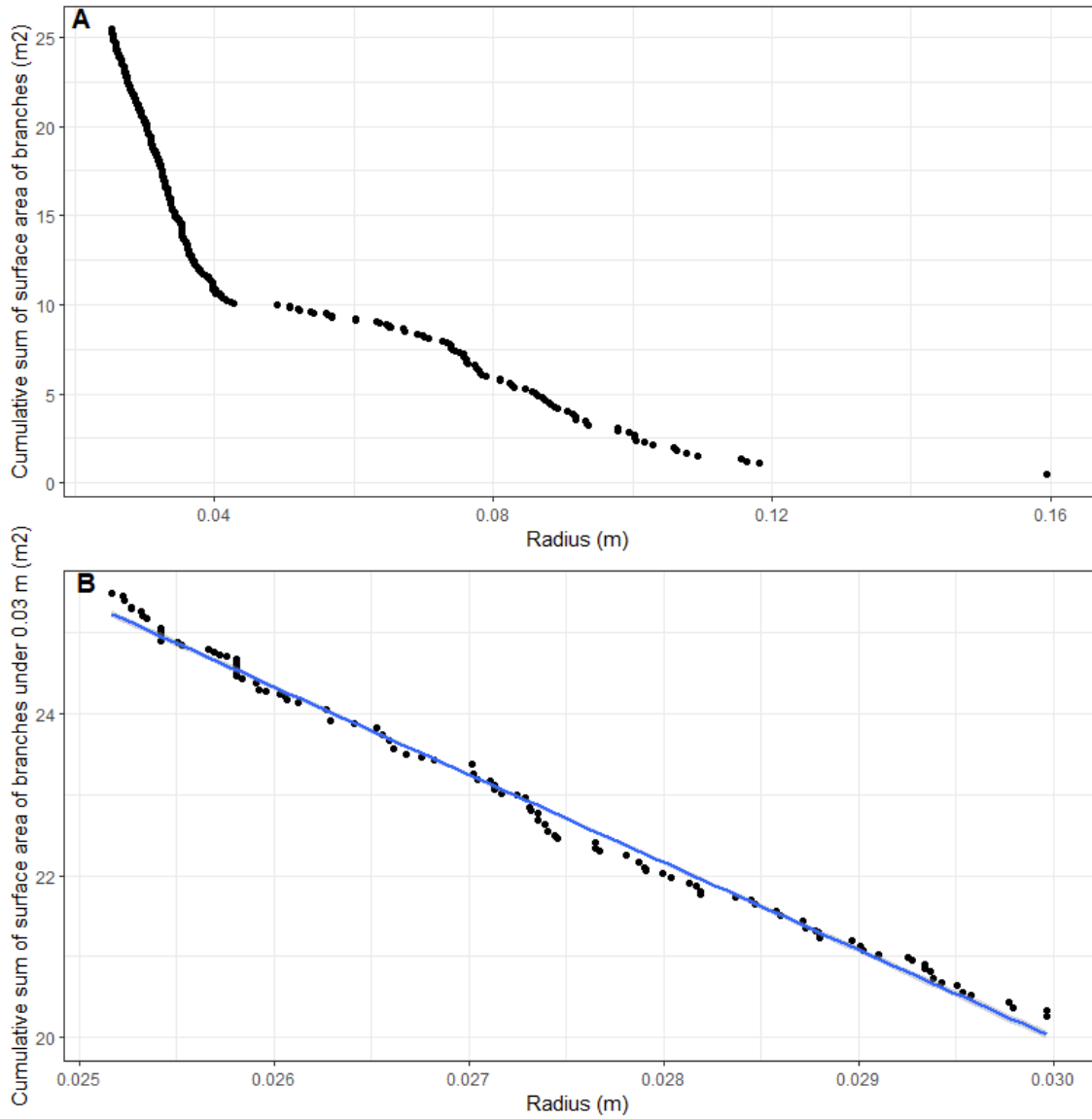


Figure B.1: Plotted branch radius versus cumulative sum of branch surface area or cumulative sum of branch volume, from largest branch radius to smallest branch radius

Table B.4: Linear regression model coefficients that were used to predict cumulative surface area from 5 cm diameter to 1 mm in diameter and the difference between 5 cm and 1 mm predicted cumulative surface area was considered the gap filled surface area of branch under 5 cm in diameter.

Predictors	log(SA under 5 cm diameter)		
	Estimates	CI	p
(Intercept)	1.74	1.53 – 1.95	<0.001
tot.sa [log]	0.89	0.83 – 0.96	<0.001
dbh [log]	-0.95	-1.06 – -0.83	<0.001
Observations	325		
$R^2$ / $R^2$ adjusted	0.766 / 0.765		

Table B.5: Linear model coefficients of wood surface temperature for canopy wood and trunk wood. The final model described 83% of the variance in wood temperature by using total global radiation ( $\text{W}/\text{m}^2$ ), air temperature at 16 meters ( $^{\circ}\text{C}$ ), season (Wet, Dry), location (Canopy, Trunk), Tree light score (1-5, high-low) and experiment (TFE, Control). Air temperature was measured at 16 meter height (Air.T.16m) from a meteorological tower at the same time as wood temperature measurement. Total global radiation was measured above the canopy, at the same time as the wood temperature measurement. Tree light score is a metric for light received by a tree ranging from 1 to 5, where 1 is low light and 5 is high light. Wood temperature was measured in October 2018 and March 2019, for a total of 601 point measurements taken between 5:00 and 21:00.

Twood			
Predictors	Estimates	CI	p
(Intercept)	10.98	9.27 – 12.68	<0.001
Air.T.16m	0.61	0.54 – 0.67	<0.001
TGR	-18.71	-24.36 – -13.07	<0.001
Season [WET]	-1.64	-1.91 – -1.37	<0.001
location [canopy]	-0.56	-0.83 – -0.29	<0.001
experiment [TFE]	1.19	1.00 – 1.38	<0.001
Air.T.16m * TGR	0.59	0.41 – 0.77	<0.001
TGR * Tree.Light.Score	4.94	2.62 – 7.25	<0.001
Air.T.16m* TGR*Tree.Light.Score	-0.15	-0.22 – -0.07	<0.001
Observations	601		
$R^2$ / $R^2$ adjusted	0.838 / 0.835		

# Bibliography

- Allen Craig D., Breshears David D., McDowell Nate G.* On underestimation of global vulnerability to tree mortality and forest die-off from hotter drought in the Anthropocene // *Ecosphere*. 8 2015. 6, 8. art129.
- Anderegg William R. L., Flint Alan, Huang Cho-ying, Flint Lorraine, Berry Joseph a., Davis Frank W., Sperry John S., Field Christopher B.* Tree mortality predicted from drought-induced vascular damage // *Nature Geoscience*. 2015. 8, 5. 367–371.
- Anderegg William R.L., Klein Tamir, Bartlett Megan, Sack Lawren, Pellegrini Adam F.A., Choat Brendan, Jansen Steven.* Meta-analysis reveals that hydraulic traits explain cross-species patterns of drought-induced tree mortality across the globe // *Proceedings of the National Academy of Sciences of the United States of America*. 2016. 113, 18. 5024–5029.
- Angert A., Muhr J., Negron Juarez R., Alegria Muñoz W., Kraemer G., Ramirez Santillan J., Barkan E., Maze S., Chambers J. Q., Trumbore S. E.* Internal respiration of Amazon tree stems greatly exceeds external CO<sub>2</sub> efflux // *Biogeosciences*. 2012. 9, 12. 4979–4991.
- Angert Alon, Sherer Yossi.* Determining the relationship between tree-stem respiration and CO<sub>2</sub> efflux by O<sub>2</sub>/Ar measurements // *Rapid Communications in Mass Spectrometry*. 2011. 25, 12. 1752–1756.
- Asao Shinichi, Bedoya-Arrieta Ricardo, Ryan Michael G.* Variation in foliar respiration and wood CO<sub>2</sub> efflux rates among species and canopy layers in a wet tropical forest // *Tree Physiology*. 2015. 35, 2. 148–159.
- Atkin Owen K., Bloomfield Keith J., Reich Peter B., Tjoelker Mark G., Asner Gregory P., Bonal Damien, Bönisch Gerhard, Bradford Matt G., Cernusak Lucas A., Cosio Eric G., Creek Danielle, Crous Kristine Y., Domingues Tomas F., Dukes Jeffrey S., Egerton John J G, Evans John R., Farquhar Graham D., Fyllas Nikolaos M., Gauthier Paul P G, Gloor Emanuel, Gimeno Teresa E., Griffin Kevin L., Guerrieri Rossella, Heskell Mary A., Huntingford Chris, Ishida Françoise Yoko, Kattge Jens, Lambers Hans, Liddell Michael J., Lloyd Jon, Lusk Christopher H., Martin Roberta E., Maksimov Ayal P., Maximov Trofim C., Malhi Yadvinder, Medlyn Belinda E., Meir Patrick, Mercado Lina M., Mirotnick Nicholas, Ng Desmond, Niinemets Ülo, O’Sullivan Odhran S., Phillips Oliver L., Poorter Lourens, Poot Pieter, Prentice I. Colin, Salinas Norma, Rowland Lucy M., Ryan Michael G., Sitch Stephen, Slot Martijn, Smith Nicholas G., Turnbull Matthew H.,*

- Vanderwel Mark C., Valladares Fernando, Veneklaas Erik J., Weerasinghe Lanthana K., Wirth Christian, Wright Ian J., Wythers Kirk R., Xiang Jen, Xiang Shuang, Zaragoza-Castells Joana.* Global variability in leaf respiration in relation to climate, plant functional types and leaf traits // *New Phytologist*. 2015. 206, 2. 614–636.
- Baccini A., Walker W., Carvalho L., Farina M., Sulla-Menashe D., Houghton R. A.* Tropical forests are a net carbon source based on aboveground measurements of gain and loss // *Science*. 10 2017. 358, 6360. 230–234.
- Baddeley Adrian, Turner Rolf.* spatstat: An R Package for Analyzing Spatial Point Patterns // *Journal of Statistical Software*. 2005. 12, 6.
- Bailey Robert L., Dell T.R.* Quantifying Diameter Distributions with the Weibull Function // *Forest Science*. 1973. 19, 2. 97–104.
- Bartholomew David C., Bittencourt Paulo R.L., Costa Antonio C.L. da, Banin Lindsay F., Britto Costa Patrícia de, Coughlin Sarah I., Domingues Tomas F., Ferreira Leandro V., Giles André, Mencuccini Maurizio, Mercado Lina, Miatto Raquel C., Oliveira Alex, Oliveira Rafael, Meir Patrick, Rowland Lucy.* Small tropical forest trees have a greater capacity to adjust carbon metabolism to long-term drought than large canopy trees // *Plant Cell and Environment*. 2020. 43, 10. 2380–2393.
- Bates Douglas, Machler Martin, Bolker Ben, Walker Steve.* Fitting Linear Mixed-Effects Models Using lme4 // *Journal of Statistical Software*. 2015. 67, 1. 1–48.
- Bauman David, Fortunel Claire, Delhaye Guillaume, Malhi Yadvinder, Cernusak Lucas A., Bentley Lisa Patrick, Rifai Sami W., Aguirre-Gutiérrez Jesús, Menor Imma Oliveras, Phillips Oliver L., McNellis Brandon E., Bradford Matt, Laurance Susan G. W., Hutchinson Michael F., Dempsey Raymond, Santos-Andrade Paul E., Ninantay-Rivera Hugo R., Chambi Paucar Jimmy R., McMahon Sean M.* Tropical tree mortality has increased with rising atmospheric water stress // *Nature*. 8 2022. 608, 7923. 528–533.
- Becker P., Meinzer F. C., Wullschlegel S. D.* Hydraulic limitation of tree height: A critique // *Functional Ecology*. 2000. 14, 1. 4–11.
- Beer C., Reichstein M., Tomelleri E., Ciais P., Jung M., Carvalhais N., Rodenbeck C., Arain M. A., Baldocchi D., Bonan G. B., Bondeau A., Cescatti A., Lasslop G., Lindroth A., Lomas M., Luyssaert S., Margolis H., Oleson K. W., Rouspard O., Veenendaal E., Viovy N., Williams C., Woodward F. I., Papale D.* Terrestrial Gross Carbon Dioxide Uptake: Global Distribution and Covariation with Climate // *Science*. 2010. 329, 5993. 834–838.
- Bennett Amy C., McDowell Nathan G., Allen Craig D., Anderson-Teixeira Kristina J.* Larger trees suffer most during drought in forests worldwide // *Nature Plants*. 2015. 1, 10. 15139.
- Bentley Lisa Patrick, Stegen James C., Savage Van M., Smith Duncan D., Allmen Erica I. von, Sperry John S., Reich Peter B., Enquist Brian J.* An empirical

- assessment of tree branching networks and implications for plant allometric scaling models // *Ecology Letters*. 2013. 16, 8. 1069–1078.
- Berveiller Daniel, Damesin Claire*. Carbon assimilation by tree stems : Potential involvement of phosphoenolpyruvate carboxylase // *Trees*. 2008. May 2014.
- Interspecific variability of stem photosynthesis among tree species. // . 2007. *Evans* 1989. 53–61.
- Binks Oliver, Meir Patrick, Rowland Lucy, Carlos Antonio, Vasconcelos Steel Silva, Antonio Alex, Oliveira Ribeiro De, Ferreira Leandro, Christoffersen Bradley, Nardini Andrea, Mencuccini Maurizio*. Plasticity in leaf-level water relations of tropical rainforest trees in response to experimental drought // *New Phytologist*. 2016.
- Bittencourt Paulo R.L., Oliveira Rafael S., Costa Antonio C.L. da, Giles Andre L., Coughlin Ingrid, Costa Patricia B., Bartholomew David C., Ferreira Leandro V., Vasconcelos Steel S., Barros Fernanda V., Junior Joao A.S., Oliveira Alex A.R., Mencuccini Maurizio, Meir Patrick, Rowland Lucy*. Amazonia trees have limited capacity to acclimate plant hydraulic properties in response to long-term drought // *Global Change Biology*. 2020. 26, 6. 3569–3584.
- Bonal Damien, Bosc Alexandre, Ponton Stéphane, Goret Jean Yves, Burban Benoît T., Gross Patrick, Bonnefond Jean Marc, Elbers Jan, Longdoz Bernard, Epron Daniel, Guehl Jean Marc, Granier André*. Impact of severe dry season on net ecosystem exchange in the Neotropical rainforest of French Guiana // *Global Change Biology*. 8 2008. 14, 8. 1917–1933.
- Brando P. M, Nepstad D. C, Davidson E. A, Trumbore S. E, Ray D., Camargo P.* Drought effects on litterfall, wood production and belowground carbon cycling in an Amazon forest: results of a throughfall reduction experiment // *Philosophical Transactions of the Royal Society B: Biological Sciences*. 2008. 363, 1498. 1839–1848.
- Brando Paulo M., Paolucci Lucas, Ummenhofer Caroline C., Ordway Elsa M., Hartmann Henrik, Cattau Megan E., Rattis Ludmila, Medjibe Vincent, Coe Michael T., Balch Jennifer*. Droughts, Wildfires, and Forest Carbon Cycling: A Pantropical Synthesis // *Annual Review of Earth and Planetary Sciences*. 2019. 47. 555–581.
- Brienen R. J. W., Phillips O. L., Feldpausch T. R., Gloor E., Baker T. R., Lloyd J., Lopez-Gonzalez G., Monteagudo-Mendoza A., Malhi Y., Lewis S. L., Vásquez Martínez R., Alexiades M., Álvarez Dávila E., Alvarez-Loayza P., Andrade A., Aragão L. E. O. C., Araujo-Murakami A., Arets E. J. M. M., Arroyo L., Aymard C. G. A., Bánki O. S., Baraloto C., Barroso J., Bonal D., Boot R. G. A., Camargo J. L. C., Castilho C. V., Chama V., Chao K. J., Chave J., Comiskey J. A., Cornejo Valverde F., Costa L. da, Oliveira E. A. de, Di Fiore A., Erwin T. L., Fauser S., Forsthofer M., Galbraith D. R., Grahame E. S., Groot N., Hérault B., Higuchi N., Honorio Coronado E. N., Keeling H., Killeen T. J., Laurance W. F., Laurance S., Licona J., Magnussen W. E., Marimon B. S., Marimon-Junior B. H., Mendoza C., Neill D. A., Nogueira E. M., Núñez P.,*

- Pallqui Camacho N. C., Parada A., Pardo-Molina G., Peacock J., Peña-Claros M., Pickavance G. C., Pitman N. C. A., Poorter L., Prieto A., Quesada C. A., Ramírez F., Ramírez-Angulo H., Restrepo Z., Roopsind A., Rudas A., Salomão R. P., Schwarz M., Silva N., Silva-Espejo J. E., Silveira M., Stropp J., Talbot J., Steege H. ter, Teran-Aguilar J., Terborgh J., Thomas-Caesar R., Toledo M., Torello-Raventos M., Umetsu R. K., Heijden G. M. F. van der, Hout P. van der, Guimarães Vieira I. C., Vieira S. A., Vilanova E., Vos V. A., Zagt R. J.* Long-term decline of the Amazon carbon sink // *Nature*. 2015. 519, 7543. 344–348.
- Brodribb T. J., Holbrook N. M.* Diurnal depression of leaf hydraulic conductance in a tropical tree species // *Plant, Cell & Environment*. 7 2004. 27, 7. 820–827.
- Brugnera Manfredo Porcia e, Meunier Félicien, Longo Marcos, Krishna Moorthy Sruthi M., De Deurwaerder Hannes, Schnitzer Stefan A., Bonal Damien, Faybishenko Boris, Verbeeck Hans.* Modeling the impact of liana infestation on the demography and carbon cycle of tropical forests // *Global Change Biology*. 11 2019. 25, 11. 3767–3780.
- Brun Philipp, Psomas Achilleas, Ginzler Christian, Thuiller Wilfried, Zappa Mas-similiano, Zimmermann Niklaus E.* Large-scale early-wilting response of Central European forests to the 2018 extreme drought // *Global Change Biology*. 12 2020. 26, 12. 7021–7035.
- Burgess S. S. O., Adams M. A., Turner N. C., Beverly C. R., Ong C. K., Khan A. A. H., Bleby T. M.* An improved heat pulse method to measure low and reverse rates of sap flow in woody plants // *Tree Physiology*. 6 2001. 21, 9. 589–598.
- Burt Andrew, Boni Vicari Matheus, Da Costa Antonio C.L., Coughlin Ingrid, Meir Patrick, Rowland Lucy, Disney Mathias.* New insights into large tropical tree mass and structure from direct harvest and terrestrial lidar // *Royal Society Open Science*. 2 2021. 8, 2.
- Burt Andrew, Calders Kim, Cuni-Sanchez Aida, Gómez-Dans Jose, Lewis Philip, Lewis Simon L., Malhi Yadvinder, Phillips Oliver L., Disney Mathias.* Assessment of Bias in Pan-Tropical Biomass Predictions // *Frontiers in Forests and Global Change*. 2020. 3, February.
- Calders Kim, Adams Jennifer, Armston John, Bartholomeus Harm, Bauwens Sebastien, Bentley Lisa Patrick, Chave Jerome, Danson F. Mark, Demol Miro, Disney Mathias, Gaulton Rachel, Krishna Moorthy Sruthi M., Levick Shaun R., Saarinen Ninni, Schaaf Crystal, Stovall Atticus, Terryn Louise, Wilkes Phil, Verbeeck Hans.* Terrestrial laser scanning in forest ecology: Expanding the horizon // *Remote Sensing of Environment*. 12 2020. 251.
- Calders Kim, Newnham Glenn, Burt Andrew, Murphy Simon, Raumonon Pasi, Herold Martin, Culvenor Darius, Avitabile Valerio, Disney Mathias, Armston John, Kaasalainen Mikko.* Nondestructive estimates of above-ground biomass using terrestrial laser scanning // *Methods in Ecology and Evolution*. 2 2015a. 6, 2. 198–208.
- Calders Kim, Newnham Glenn J, Armston John D, Disney Mathias I, Schaaf Crystal Barker, Paynter Ian.* Terrestrial LIDAR for forest monitoring. 2015b.

- Campioli M., Malhi Y., Vicca S., Luysaert S., Papale D., Peñuelas J., Reichstein M., Migliavacca M., Arain M. A., Janssens I. A.* Evaluating the convergence between eddy-covariance and biometric methods for assessing carbon budgets of forests // *Nature Communications*. 2016. 7, May 2015. 13717.
- Casalini Ana I., Bisigato Alejandro J.* Stress-gradient hypothesis and plant distribution along ecotonal gradients // *Austral Ecology*. 11 2018. 43, 7. 807–816.
- Cavaleri Molly A., Oberbauer Steven F., Ryan Michael G.* Wood CO<sub>2</sub> efflux in a primary tropical rain forest // *Global Change Biology*. 2006. 12, 12. 2442–2458.
- Cernusak Lucas A., Cheesman Alexander W.* The benefits of recycling: How photosynthetic bark can increase drought tolerance // *New Phytologist*. 2015. 208, 4. 995–997.
- Chambers Jeffrey Q., Tribuzy Edgard S., Toledo Ligia C., Crispim Bianca F., Higuchi Niro, Dos Santos Joaquim, Araujo Alessandro C., Kruijt Bart, Nobre Antonio D., Trumbore Susan E.* Respiration from a tropical forest ecosystem: Partitioning of sources and low carbon use efficiency // *Ecological Applications*. 2004. 14.
- Chave Jérôme, Réjou-Méchain Maxime, Búrquez Alberto, Chidumayo Emmanuel, Colgan Matthew S., Delitti Wellington B.C., Duque Alvaro, Eid Tron, Fearnside Philip M., Goodman Rosa C., Henry Matieu, Martínez-Yrizar Angelina, Mugasha Wilson A., Muller-Landau Helene C., Mencuccini Maurizio, Nelson Bruce W., Ngomanda Alfred, Nogueira Euler M., Ortiz-Malavassi Edgar, Péliissier Raphaël, Ploton Pierre, Ryan Casey M., Saldarriaga Juan G., Vieilledent Ghislain.* Improved allometric models to estimate the aboveground biomass of tropical trees // *Global Change Biology*. 2014. 20, 10. 3177–3190.
- Cheng Dong-Liang, Li Tao, Zhong Quan-Lin, Wang Gen-Xuan.* Scaling relationship between tree respiration rates and biomass // *Biology Letters*. 10 2010. 6, 5. 715–717.
- Clark David B., Olivas Paulo C., Oberbauer Steven F., Clark Deborah A., Ryan Michael G.* First direct landscape-scale measurement of tropical rain forest Leaf Area Index, a key driver of global primary productivity // *Ecology Letters*. 2008. 11, 2. 163–172.
- Cleveland Cory C, Taylor P, Chadwick K, E Doughty Cristopher, Malhi Yadvinder, Smith W Kolby, Sullivan Benjamin W, Wieder William R, Townsend Alan R.* Global Biogeochemical Cycles net primary production // *Global Biogeochemical Cycles*. 2015. 29. 1–19.
- Cleveland Cory C, Wieder William R, Reed Sasha C, Townsend Alan R.* Experimental drought in a tropical rain forest increases soil carbon dioxide losses to the atmosphere // *Ecology*. 2010. 91, 8. 2313–2323.
- CloudCompare .* CloudCompare. 2021.

- Condit Richard, Ashton Peter S, Baker Patrick, Bunyavejchewin Sarayudh, Gunatilleke Savithri, Gunatilleke Nimal, Hubbell Stephen P, Foster Robin B, Itoh Akira, Lafrankie James V, Lee Hua Seng, Losos Elizabeth, Manokaran N, Sukumar R.* Spatial Patterns in the Distribution of Tropical Tree Species // *Science*. 2000. 288, May. 1414–1419.
- Coomes David A., Allen Robert B.* Testing the Metabolic Scaling Theory of tree growth // *Journal of Ecology*. 11 2009. 97, 6. 1369–1373.
- Costa Antonio C.L. da, Metcalfe Daniel B., Doughty Chris E., Oliveira Alexandre A.R. de, Neto Guilherme F.C., Costa Mauricio C. da, Silva Junior João de Athaydes, Aragão Luiz E.O.C., Almeida Samuel, Galbraith David R., Rowland Lucy M., Meir Patrick, Malhi Yadvinder.* Ecosystem respiration and net primary productivity after 8-10 years of experimental through-fall reduction in an eastern Amazon forest // *Plant Ecology and Diversity*. 2014. 7, 1-2. 7–24.
- Costa Antonio C.L. da, Rowland Lucy, Oliveira Rafael S., Oliveira Alex A.R., Binks Oliver J., Salmon Yann, Vasconcelos Steel S., Junior João A.S., Ferreira Leandro V., Poyatos Rafael, Mencuccini Maurizio, Meir Patrick.* Stand dynamics modulate water cycling and mortality risk in droughted tropical forest // *Global Change Biology*. 2017. April. 1–10.
- Costa Antonio C.L. da, Rowland Lucy, Oliveira Rafael S., Oliveira Alex A.R., Binks Oliver J., Salmon Yann, Vasconcelos Steel S., Junior João A.S., Ferreira Leandro V., Poyatos Rafael, Mencuccini Maurizio, Meir Patrick.* Stand dynamics modulate water cycling and mortality risk in droughted tropical forest // *Global Change Biology*. 2018. 24, 1. 249–258.
- Costa Antonio Carlos Lola da, Galbraith David, Almeida Samuel, Portela Bruno Takeshi Tanaka, Costa Mauricio da, Athaydes Silva Junior João de, Braga Alan P., Gonçalves Paulo H.L. de, Oliveira Alex Ar de, Fisher Rosie, Phillips Oliver L., Metcalfe Daniel B., Levy Peter, Meir Patrick.* Effect of 7 yr of experimental drought on vegetation dynamics and biomass storage of an eastern Amazonian rainforest // *New Phytologist*. 2010. 187, 3. 579–591.
- Cox P M, Betts R a, Jones C D, Spall S a, Totterdell I J.* Acceleration of global warming due to carbon-cycle feedbacks in a coupled climate model. // *Nature*. 2000. 408, 6809. 184–187.
- Cox Peter M, Pearson David, Booth Ben B, Friedlingstein Pierre, Huntingford Chris, Jones Chris D, Luke Catherine M.* Sensitivity of tropical carbon to climate change constrained by carbon dioxide variability // *Nature*. 2013.
- D’Andrea Ettore, Rezaie Negar, Prislán Peter, Gričar Jozica, Collalti Alessio, Muhr Jan, Matteucci Giorgio.* Frost and drought: Effects of extreme weather events on stem carbon dynamics in a Mediterranean beech forest // *Plant Cell and Environment*. 10 2020. 43, 10. 2365–2379.
- Damesin C, Ceschial E, Goff N Le, Ottorini J-m, Dufrenel E.* Stem and Branch Respiration Estimations of Beech : from tree measurements to estimations at the stand level // *New Phytologist*. 2001. 153, 1. 159–172.

- Davidson Eric A., De Araujo Alessandro C., Artaxo Paulo, Balch Jennifer K., Brown I. Foster, Mercedes Mercedes M., Coe Michael T., Defries Ruth S., Keller Michael, Longo Marcos, Munger J. William, Schroeder Wilfrid, Soares-Filho Britaldo S., Souza Carlos M., Wofsy Steven C.* The Amazon basin in transition // *Nature*. 2012. 481, 7381. 321–328.
- De Roo Linus, Bloemen Jasper, Dupon Yentl, Salomón Roberto Luis, Steppe Kathy.* Axial diffusion of respired CO<sub>2</sub> confounds stem respiration estimates during the dormant season // *Annals of Forest Science*. 2019. 76, 2.
- De Roo Linus, Salomón Roberto Luis, Oleksyn Jacek, Steppe Kathy.* Woody tissue photosynthesis delays drought stress in *Populus tremula* trees and maintains starch reserves in branch xylem tissues // *New Phytologist*. 2020. 228, 1. 70–81.
- Dexter Kyle G., Pennington R. Toby, Oliveira-Filho Ary T., Bueno Marcelo L., Miranda Pedro L. Silva de, Neves Danilo M.* Inserting Tropical Dry Forests Into the Discussion on Biome Transitions in the Tropics // *Frontiers in Ecology and Evolution*. 2018. 6, July. 1–7.
- Díaz Sandra, Kattge Jens, Cornelissen Johannes H.C., Wright Ian J., Lavorel Sandra, Dray Stéphane, Reu Björn, Kleyer Michael, Wirth Christian, Colin Prentice I., Garnier Eric, Bönisch Gerhard, Westoby Mark, Poorter Hendrik, Reich Peter B., Moles Angela T., Dickie John, Gillison Andrew N., Zanne Amy E., Chave Jérôme, Joseph Wright S., Sheremet Ev Serge N., Jactel Hervé, Baraloto Christopher, Cerabolini Bruno, Pierce Simon, Shipley Bill, Kirkup Donald, Casanoves Fernando, Joswig Julia S., Günther Angela, Falczuk Valeria, Rüger Nadja, Mahecha Miguel D., Gorné Lucas D.* The global spectrum of plant form and function // *Nature*. 1 2016. 529, 7585. 167–171.
- Dima Eleni, Manetas Yiannis, Psaras George K.* Chlorophyll distribution pattern in inner stem tissues: Evidence from epifluorescence microscopy and reflectance measurements in 20 woody species // *Trees - Structure and Function*. 2006. 20, 4. 515–521.
- Disney M. I., Boni Vicari M., Calders Kim, Burt Andrew, Lewis Simon L, Raumanen P., Wilkes P.* Weighing trees with lasers: advances, challenges and opportunities // *Royal Society Interface*. 2018.
- Disney Mathias.* Terrestrial LiDAR: a three-dimensional revolution in how we look at trees // *New Phytologist*. 6 2019. 222, 4. 1736–1741.
- Doughty Christopher E., Metcalfe D. B., Girardin C. A.J., Amézquita F. Farfán, Cabrera D. Galiano, Huasco W. Huaraca, Silva-Espejo J. E., Araujo-Murakami A., Da Costa M. C., Rocha W., Feldpausch T. R., Mendoza A. L.M., Da Costa A. C.L., Meir P., Phillips O. L., Malhi Y.* Drought impact on forest carbon dynamics and fluxes in Amazonia // *Nature*. 2015. 519, 7541. 78–82.
- Duffy Philip B., Brando Paulo, Asner Gregory P., Field Christopher B.* Projections of future meteorological drought and wet periods in the Amazon // *Proceedings of the National Academy of Sciences*. 2015. 112, 43. 13172–13177.

- Eller Cleiton, V. Barros Fernanda de, Bittencourt Paulo, Rowland Lucy, Mencuccini Maurizio, Oliveira Rafael.* Xylem hydraulic safety and construction costs determine tropical tree growth // *Plant, Cell & Environment*. 3 2018. 41, 3. 548–562.
- Eller Cleiton B., Rowland Lucy, Mencuccini Maurizio, Rosas Teresa, Williams Karina, Harper Anna, Medlyn Belinda E., Wagner Yael, Klein Tamir, Teodoro Grazielle S., Oliveira Rafael S., Matos Ilaine S., Rosado Bruno H. P., Fuchs Kathrin, Wohlfahrt Georg, Montagnani Leonardo, Meir Patrick, Sitch Stephen, Cox Peter M.* Stomatal optimization based on xylem hydraulics (SOX) improves land surface model simulation of vegetation responses to climate // *New Phytologist*. 6 2020. 226, 6. 1622–1637.
- Enquist Brian J., Kerkhoff Andrew J., Huxman Travis E., Economo Evan P.* Adaptive differences in plant physiology and ecosystem paradoxes: Insights from metabolic scaling theory // *Global Change Biology*. 2007. 13, 3. 591–609.
- Enquist Brian J., West Geoffrey B., Brown James H.* Extensions and evaluations of a general quantitative theory of forest structure and dynamics // *Proceedings of the National Academy of Sciences of the United States of America*. 2009. 106, 17. 7046–7051.
- Fatichi Simone, Pappas Christoforos, Zscheischler Jakob, Leuzinger Sebastian.* Modelling carbon sources and sinks in terrestrial vegetation // *New Phytologist*. 1 2019. 221, 2. 652–668.
- Fauset Sophie, Baker Timothy R., Lewis Simon L, Feldpausch Ted R., Affum-Baffoe Kofi, Foli Ernest G., Hamer Keith C., Swaine Michael D.* Drought-induced shifts in the floristic and functional composition of tropical forests in Ghana // *Ecology Letters*. 2012. 15, 10. 1120–1129.
- Tree height integrated into pantropical forest biomass estimates. // . 2012. 3381–3403.
- Fisher Rosie A., Williams M., Costa A. Lola da, Malhi Y., Costa R. F. da, Almeida S., Meir P.* The response of an Eastern Amazonian rain forest to drought stress: Results and modelling analyses from a throughfall exclusion experiment // *Global Change Biology*. 2007. 13, 11. 2361–2378.
- Fu R., Yin L., Li W., Arias P. A., Dickinson R. E., Huang L., Chakraborty S., Fernandes K., Liebmann B., Fisher R., Myneni R. B.* Increased dry-season length over southern Amazonia in recent decades and its implication for future climate projection // *Proceedings of the National Academy of Sciences*. 2013. 110, 45. 18110–18115.
- Furley Peter.* Savanna formations: ecology and environment // *Progress in Physical Geography: Earth and Environment*. 6 1994. 18, 2. 276–294.
- Galbraith David, Levy Peter E., Sitch Stephen, Huntingford Chris, Cox Peter, Williams Mathew, Meir Patrick.* Multiple mechanisms of Amazonian forest biomass losses in three dynamic global vegetation models under climate change // *New Phytologist*. 2010. 187, 3. 647–665.

- Gansert Dirk, Burgdorf Markus.* Effects of xylem sap flow on carbon dioxide efflux from stems of birch (*Betula pendula* Roth) // *Flora: Morphology, Distribution, Functional Ecology of Plants.* 2005. 200, 5. 444–455.
- Gatti L. V., Basso L. S., Miller J. B., Gloor M., Domingues L. G., Cassol H.L.G., Tejada G., Aragao L. E. O.C, Nobre C.A., Peter W., Marani L., Arai E., Sanches A.H., Correa S.M., Anderson L., Randow C. von, Correia C.S.C., Crispim S.P., Neves R.A.L.* Amazonia as a carbon source linked to deforestation and climate change // *Nature.* 2021. 595, July.
- Giardina Francesco, Konings Alexandra G., Kennedy Daniel, Alemohammad Seyed Hamed, Oliveira Rafael S., Uriarte Maria, Gentine Pierre.* Tall Amazonian forests are less sensitive to precipitation variability // *Nature Geoscience.* 6 2018. 11, 6. 405–409.
- Giles A. L., Rowland L., Bittencourt P. R.L., Bartholomew D. C., Coughlin I., Costa P. B., Domingues T., Miatto R. C., Barros F. V., Ferreira L. V., Groenendijk P., Oliveira A. A.R., Da Costa A. C.L., Meir P., Mencuccini M., Oliveira R. S.* Small understorey trees have greater capacity than canopy trees to adjust hydraulic traits following prolonged experimental drought in a tropical forest // *Tree Physiology.* 2022. 42, 3. 537–556.
- Girardin Cécile A.J., Espejob Javier E.Silva, Doughty Christopher E., Huasco Walter Huaraca, Metcalfe Dan B., Durand-Baca Liliana, Marthews Toby R., Aragao Luiz E.O.C., Farfán-Rios William, García-Cabrera Karina, Halladay Katherine, Fisher Joshua B., Galiano-Cabrera Darcy F., Huaraca-Quispe Lidia P., Alzamora-Taype Ivonne, Equiluz-Mora Luzmila, Revilla Norma Salinas, Silman Miles R., Meir Patrick, Malhi Yadwinder.* Productivity and carbon allocation in a tropical montane cloud forest in the Peruvian Andes // *Plant Ecology and Diversity.* 2014. 7, 1-2. 107–123.
- Good Peter, Jones Chris, Lowe Jason, Betts Richard, Gedney Nicola.* Comparing tropical forest projections from two generations of hadley centre earth system models, HadGEM2-ES and HadCM3LC // *Journal of Climate.* 2013. 26, 2. 495–511.
- Hafner Benjamin D., Hesse Benjamin D., Grams Thorsten E.E.* Friendly neighbours: Hydraulic redistribution accounts for one quarter of water used by neighbouring drought stressed tree saplings // *Plant Cell and Environment.* 2020. April. 1–14.
- Hallé Francis, Oldeman Roelof A. A., Tomlinson Philip B.* *Tropical Trees and Forests.* 1978.
- Harris Nancy L., Gibbs David A., Baccini Alessandro, Birdsey Richard A., Bruin Sytze de, Farina Mary, Fatoyinbo Lola, Hansen Matthew C., Herold Martin, Houghton Richard A., Potapov Peter V., Suarez Daniela Requena, Roman-Cuesta Rosa M., Saatchi Sassan S., Slay Christy M., Turubanova Svetlana A., Tyukavina Alexandra.* Global maps of twenty-first century forest carbon fluxes // *Nature Climate Change.* 3 2021. 11, 3. 234–240.

- He J., Chee C. W., Goh C. J.* ‘Photoinhibition’ of *Heliconia* under natural tropical conditions: the importance of leaf orientation for light interception and leaf temperature // *Plant, Cell & Environment*. 11 1996. 19, 11. 1238–1248.
- Hibberd Julian M., Quick W. Paul.* Characteristics of C4 photosynthesis in stems and petioles of C3 flowering plants // *Nature*. 2002. 415, 6870. 451–454.
- Hilman Boaz, Angert Alon.* Measuring the ratio of CO2 efflux to O2 influx in tree stem respiration // *Tree Physiology*. 2016. May. tpw057.
- Hilman Boaz, Muhr Jan, Trumbore Susan E., Kunert Norbert, Carbone Mariah S., Yuval Päivi, Wright S. Joseph, Moreno Gerardo, Pérez-Priego Oscar, Migliavacca Mirco, Carrara Arnaud, Grünzweig José M., Osem Yagil, Weiner Tal, Angert Alon.* Comparison of CO2 and O2 fluxes demonstrate retention of respired CO2 in tree stems from a range of tree species // *Biogeosciences*. 1 2019. 16, 1. 177–191.
- Hilman Boaz, Weiner Tal, Haran Tom, Masiello Caroline A., Gao Xiaodong, Angert Alon.* The Apparent Respiratory Quotient of Soils and Tree Stems and the Processes That Control It // *Journal of Geophysical Research: Biogeosciences*. 3 2022. 127, 3.
- Hirota Marina, Holmgren Milena, Nes Egbert H. van, Scheffer Marten.* Global Resilience of Tropical Forest // *Science*. 2011. 334, October. 232–235.
- Horn Henry S.* The adaptive geometry of trees. 1971.
- Hubau Wannas, Lewis Simon L., Phillips Oliver L., Affum-Baffoe Kofi, Beekman Hans, Cuní-Sánchez Aida, Daniels Armandu K., Ewango Corneille E.N., Fauset Sophie, Mukinzi Jacques M., Sheil Douglas, Sonké Bonaventure, Sullivan Martin J.P., Sunderland Terry C.H., Taedoumg Hermann, Thomas Sean C., White Lee J.T., Abernethy Katharine A., Adu-Bredu Stephen, Amani Christian A., Baker Timothy R., Banin Lindsay F., Baya Fidèle, Begne Serge K., Bennett Amy C., Benedet Fabrice, Bitariho Robert, Bocko Yannick E., Boeckx Pascal, Boundja Patrick, Brienen Roel J.W., Brncic Terry, Chezeaux Eric, Chuyong George B., Clark Connie J., Collins Murray, Comiskey James A., Coomes David A., Dargie Greta C., Haulleville Thales de, Kamdem Marie Noel Djuikouo, Doucet Jean Louis, Esquivel-Muelbert Adriane, Feldpausch Ted R., Fofanah Alusine, Foli Ernest G., Gilpin Martin, Gloor Emanuel, Gonmadje Christelle, Gourlet-Fleury Sylvie, Hall Jefferson S., Hamilton Alan C., Harris David J., Hart Terese B., Hockemba Mireille B.N., Hladik Annette, Ifo Suspense A., Jeffery Kathryn J., Jucker Tommaso, Yakusu Emmanuel Kasongo, Kearsley Elizabeth, Kenfack David, Koch Alexander, Leal Miguel E., Levesley Aurora, Lindsell Jeremy A., Lisingo Janvier, Lopez-Gonzalez Gabriela, Lovett Jon C., Makana Jean Remy, Malhi Yadvinder, Marshall Andrew R., Martin Jim, Martin Emanuel H., Mbayu Faustin M., Medjibe Vincent P., Mihindou Vianet, Mitchard Edward T.A., Moore Sam, Munishi Pantaleo K.T., Bengone Natacha Nssi, Ojo Lucas, Ondo Fidèle Evouna, Peh Kelvin S.H., Pickavance Georgia C., Poulsen Axel Dalberg, Poulsen John R., Qie Lan, Reitsma Jan, Rovero Francesco, Swaine Michael D., Talbot Joey, Taplin James, Taylor David M., Thomas Duncan W., Toirambe Benjamin, Mukendi John Tshibamba, Tuagben Darlington, Umunay Peter M., Heijden Geertje M.F. van der, Verbeeck Hans, Vleminckx Jason, Willcock*

- Simon, Wöll Hannsjörg, Woods John T., Zemagho Lise.* Asynchronous carbon sink saturation in African and Amazonian tropical forests // *Nature*. 3 2020. 579, 7797. 80–87.
- Huntingford C., Harris P. P., Gedney N., Cox P. M., Betts R. A., Marengo J. A., Gash J. H. C.* Using a GCM analogue model to investigate the potential for Amazonian forest dieback // *Theoretical and Applied Climatology*. 6 2004. 78, 1-3.
- Huntingford Chris, Atkin Owen K, Martinez-De La Torre Alberto, Mercado Lina M, Heskell Mary A, Harper Anna B, Bloomfield Keith J., O’Sullivan Odhran S., Reich Peter B, Wythers Kirk R, Butler Ethan E, Chen Ming, Griffin Kevin L., Meir Patrick, Tjoelker Mark G, Turnbull Matthew H, Sitch Stephen, Wiltshire Andy, Malhi Yadvinder.* Implications of improved representations of plant respiration in a changing climate // *Nature Communications*. 2017. 8, 1. 1–11.
- Huntingford Chris, Fisher Rosie A., Mercado Lina, Booth Ben B.B., Sitch Stephen, Harris Phil P., Cox Peter M., Jones Chris D., Betts Richard A., Malhi Yadvinder, Harris Glen R., Collins Mat, Moorcroft Paul.* Towards quantifying uncertainty in predictions of Amazon 'dieback' // *Philosophical Transactions of the Royal Society B: Biological Sciences*. 2008. 363, 1498. 1857–1864.
- Huntingford Chris, Zelazowski Przemyslaw, Galbraith David, Mercado Lina M, Sitch Stephen, Fisher Rosie, Lomas Mark, Walker Anthony P, Jones Chris D, Booth Ben B B, Malhi Yadvinder, Hemming Debbie, Kay Gillian, Good Peter, Lewis Simon L, Phillips Oliver L, Atkin Owen K, Lloyd Jon, Gloor Emanuel, Zaragoza-castells Joana, Meir Patrick, Betts Richard, Harris Phil P, Nobre Carlos, Marengo Jose, Cox Peter M.* Simulated resilience of tropical rainforests to CO<sub>2</sub>-induced climate change // *Nature Geoscience*. 2013. 6, 4. 268–273.
- Hurlbert Stuart H.* On misinterpretations of pseudoreplication and related matters: a reply to Oksanen // *Oikos*. 3 2004. 104, 3. 591–597.
- Ishii Hiroaki, Asano Shoko.* The role of crown architecture, leaf phenology and photosynthetic activity in promoting complementary use of light among coexisting species in temperate forests // *Ecological Research*. 2010. 25, 4. 715–722.
- Jardine Kolby J., Cobello Leticia O., Teixeira Liliane M., East Malyia Mason S., Levine Sienna, Gimenez Bruno O., Robles Emily, Spanner Gustavo, Koven Charlie, Xu Chongang, Warren Jeffrey M., Higuchi Niro, McDowell Nate, Pastorello Gilberto, Chambers Jeffrey Q.* Stem respiration and growth in a central Amazon rainforest // *Trees - Structure and Function*. 2022. 36, 3. 991–1004.
- Kalácska M., Calvo-Alvarado Julio C., Sánchez-Azofeifa G. A.* Calibration and assessment of seasonal changes in leaf area index of a tropical dry forest in different stages of succession // *Tree Physiology*. 2005. 25, 6. 733–744.
- Kalacska Margaret E.R., Sánchez-Azofeifa G. Arturo, Calvo-Alvarado Julio C., Rivard Benoit, Quesada Mauricio.* Effects of season and successional stage on leaf area index and spectral vegetation indices in three mesoamerican tropical dry forests // *Biotropica*. 12 2005. 37, 4. 486–496.

- Kamakura Mai, Kosugi Yoshiko, Takanashi Satoru, Matsumoto Kazuho, Okumura Motonori, Philip Elizabeth.* Patchy stomatal behavior during midday depression of leaf CO<sub>2</sub> exchange in tropical trees // *Tree Physiology.* 2011. 31, 2. 160–168.
- Katayama Ayumi, Kho Lip Khoon, Makita Naoki, Kume Tomonori, Matsumoto Kazuho, Ohashi Mizue.* Estimating fine root production from ingrowth cores and decomposed roots in a Bornean tropical rainforest // *Forests.* 2019. 10, 1.
- Katayama Ayumi, Kume Tomonori, Komatsu Hikaru, Ohashi Mizue, Matsumoto Kazuho, Ichihashi Ryuji, Kumagai Tomo'omi, Otsuki Kyoichi.* Vertical variations in wood CO<sub>2</sub> efflux for live emergent trees in a Bornean tropical rainforest // *Tree Physiology.* 2014. 34, 5. 503–512.
- Kattge Jens, Bönisch Gerhard, Díaz Sandra, Lavorel Sandra, Prentice Iain Colin, Leadley Paul, Tautenhahn Susanne, Werner Gijbert D.A., Aakala Tuomas, Abedi Mehdi, Acosta Alicia T.R., Adamidis George C., Adamson Kairi, Aiba Masahiro, Albert Cécile H., Alcántara Julio M., Alcázar C Carolina, Aleixo Izabela, Ali Hamada, Amiaud Bernard, Ammer Christian, Amoroso Mariano M., Anand Madhur, Anderson Carolyn, Anten Niels, Antos Joseph, Apgaua Deborah Mattos Guimarães, Ashman Tia Lynn, Asmara Degi Harja, Asner Gregory P., Aspinwall Michael, Atkin Owen, Aubin Isabelle, Baastrup-Spohr Lars, Bahalkeh Khadijeh, Bahn Michael, Baker Timothy, Baker William J., Bakker Jan P., Baldocchi Dennis, Baltzer Jennifer, Banerjee Arindam, Baranger Anne, Barlow Jos, Barneche Diego R., Baruch Zdravko, Bastianelli Denis, Battles John, Bauerle William, Bauters Marijn, Bazzato Erika, Beckmann Michael, Beekman Hans, Beierkuhnlein Carl, Bekker Renee, Belfry Gavin, Belluau Michael, Beloiu Mirela, Benavides Raquel, Benomar Lahcen, Berdugo-Lattke Mary Lee, Berenguer Erika, Bergamin Rodrigo, Bergmann Joana, Bergmann Carlucci Marcos, Berner Logan, Bernhardt-Römermann Markus, Bigler Christof, Bjorkman Anne D., Blackman Chris, Blanco Carolina, Blonder Benjamin, Blumenthal Dana, Bocanegra-González Kelly T., Boeckx Pascal, Bohlman Stephanie, Böhning-Gaese Katrin, Boisvert-Marsh Laura, Bond William, Bond-Lamberty Ben, Boom Arnoud, Boonman Coline C.F., Bordin Kauane, Boughton Elizabeth H., Boukili Vanessa, Bowman David M.J.S., Bravo Sandra, Brendel Marco Richard, Broadley Martin R., Brown Kerry A., Bruelheide Helge, Brumnich Federico, Bruun Hans Henrik, Bruy David, Buchanan Serra W., Bucher Solveig Franziska, Buchmann Nina, Buitenwerf Robert, Bunker Daniel E., Bürger Jana, Burrascano Sabina, Burslem David F.R.P., Butterfield Bradley J., Byun Chaeho, Marques Marcia, Scalón Marina C., Caccianiga Marco, Cadotte Marc, Cailleret Maxime, Camac James, Camarero Jesús Julio, Company Courtney, Campetella Giandiego, Campos Juan Antonio, Cano-Arboleda Laura, Canullo Roberto, Carbognani Michele, Carvalho Fabio, Casanoves Fernando, Castagneyrol Bastien, Catford Jane A., Cavender-Bares Jeannine, Cerabolini Bruno E.L., Cervellini Marco, Chacón-Madrigal Eduardo, Chapin Kenneth, Chapin F. Stuart, Chelli Stefano, Chen Si Chong, Chen Anping, Cherubini Paolo, Chianucci Francesco, Choat Brendan, Chung Kyong Sook, Chytrý Milan, Ciccarelli Daniela, Coll Lluís, Collins Courtney G., Conti Luisa, Coomes David, Cornelissen Johannes H.C., Cornwell William K., Corona Piermaria, Coyea Marie, Craine Joseph, Craven Dylan, Cromsigt Joris P.G.M., Cseceserits Anikó, Cufar Katarina, Cuntz Matthias,*

*Silva Ana Carolina da, Dahlin Kyla M., Dainese Matteo, Dalke Igor, Dalle Fratte Michele, Dang-Le Anh Tuan, Danihelka Jiri, Dannoura Masako, Dawson Samantha, Beer Arend Jacobus de, De Frutos Angel, De Long Jonathan R., Dechant Benjamin, Delagrang Sylvain, Delpierre Nicolas, Derroire Géraldine, Dias Arildo S., Diaz-Toribio Milton Hugo, Dimitrakopoulos Panayiotis G., Dobrowolski Mark, Doktor Daniel, Dřevojan Pavel, Dong Ning, Dransfield John, Dressler Stefan, Duarte Leandro, Ducouret Emilie, Dullinger Stefan, Durka Walter, Dursma Remko, Dymova Olga, E-Vojtkó Anna, Eckstein Rolf Lutz, Ejtehadi Hamid, Elser James, Emilio Thaise, Engemann Kristine, Erfanian Mohammad Bagher, Erfmeier Alexandra, Esquivel-Muelbert Adriane, Esser Gerd, Estiarte Marc, Domingues Tomas F., Fagan William F., Fagúndez Jaime, Falster Daniel S., Fan Ying, Fang Jingyun, Farris Emmanuele, Fazlioglu Fatih, Feng Yanhao, Fernandez-Mendez Fernando, Ferrara Carlotta, Ferreira Joice, Fidelis Alessandra, Finegan Bryan, Firn Jennifer, Flowers Timothy J., Flynn Dan F.B., Fontana Veronika, Forey Estelle, Forgiarini Cristiane, François Louis, Frangipani Marcelo, Frank Dorothea, Frenette-Dussault Cedric, Freschet Grégoire T., Fry Ellen L., Fyllas Nikolaos M., Mazzochini Guilherme G., Gachet Sophie, Gallagher Rachael, Ganade Gislene, Ganga Francesca, García-Palacios Pablo, Gargaglione Verónica, Garnier Eric, Garrido Jose Luis, Gasper André Luis de, Gea-Izquierdo Guillermo, Gibson David, Gillison Andrew N., Giroldo Aelton, Glasenhardt Mary Claire, Gleason Sean, Gliesch Mariana, Goldberg Emma, Gödel Bastian, Gonzalez-Akre Erika, Gonzalez-Andujar Jose L., González-Melo Andrés, González-Robles Ana, Graae Bente Jessen, Granda Elena, Graves Sarah, Green Walton A., Gregor Thomas, Gross Nicolas, Guerin Greg R., Günther Angela, Gutiérrez Alvaro G., Haddock Lillie, Haines Anna, Hall Jefferson, Ham-buckers Alain, Han Wenxuan, Harrison Sandy P., Hattingh Wesley, Hawes Joseph E., He Tianhua, He Pengcheng, Heberling Jacob Mason, Helm Avelina, Hempel Stefan, Hentschel Jörn, Hérault Bruno, Hereş Ana Maria, Herz Katharina, Heuertz Myriam, Hickler Thomas, Hietz Peter, Higuchi Pedro, Hipp Andrew L., Hirons Andrew, Hock Maria, Hogan James Aaron, Holl Karen, Honnay Olivier, Hornstein Daniel, Hou Enqing, Hough-Snee Nate, Hovstad Knut Anders, Ichie Tomoaki, Igić Boris, Illa Estela, Isaac Marney, Ishihara Masae, Ivanov Leonid, Ivanova Larissa, Iversen Colleen M., Izquierdo Jordi, Jackson Robert B., Jackson Benjamin, Jactel Hervé, Jagodzinski Andrzej M., Jandt Ute, Jansen Steven, Jenkins Thomas, Jentsch Anke, Jespersen Jens Rasmus Plantener, Jiang Guo Feng, Johansen Jesper Liengaard, Johnson David, Jokela Eric J., Joly Carlos Alfredo, Jordan Gregory J., Joseph Grant Stuart, Junaedi Decky, Junker Robert R., Justes Eric, Kabzems Richard, Kane Jeffrey, Kaplan Zdenek, Kattenborn Teja, Kavelenova Lyudmila, Kearsley Elizabeth, Kempel Anne, Kenzo Tanaka, Kerkhoff Andrew, Khalil Mohammed I., Kinlock Nicole L., Kissling Wilm Daniel, Kitajima Kaoru, Kitzberger Thomas, Kjøller Rasmus, Klein Tamir, Kleyer Michael, Klimešová Jitka, Klipel Joice, Kloep-pel Brian, Klotz Stefan, Knops Johannes M.H., Kohyama Takashi, Koike Fumito, Kollmann Johannes, Komac Benjamin, Komatsu Kimberly, König Christian, Kraft Nathan J.B., Kramer Koen, Kreft Holger, Kühn Ingolf, Kumarathunge Dushan, Kuppler Jonas, Kurokawa Hiroko, Kurosawa Yoko, Kuyah Shem, Laclau Jean Paul, Lafleur Benoit, Lallai Erik, Lamb Eric, Lamprecht Andrea, Larkin Daniel J., Laughlin Daniel, Le Bagousse-Pinguet Yoann, Maire Gueric le, Roux*

*Peter C. le, Roux Elizabeth le, Lee Tali, Lens Frederic, Lewis Simon L., Lhotsky Barbara, Li Yuanzhi, Li Xine, Lichstein Jeremy W., Liebergesell Mario, Lim Jun Ying, Lin Yan Shih, Linares Juan Carlos, Liu Chunjiang, Liu Daijun, Liu Udayangani, Livingstone Stuart, Llusia Joan, Lohbeck Madelon, López-García Álvaro, Lopez-Gonzalez Gabriela, Lososová Zdeňka, Louault Frédérique, Lukács Balázs A., Lukeš Petr, Luo Yunjian, Lussu Michele, Ma Siyan, Maciel Rabelo Pereira Camilla, Mack Michelle, Maire Vincent, Mäkelä Annikki, Mäkinen Harri, Malhado Ana Claudia Mendes, Mallik Azim, Manning Peter, Manzoni Stefano, Marchetti Zuleica, Marchino Luca, Marcilio-Silva Vinicius, Marcon Eric, Marignani Michela, Markesteijn Lars, Martin Adam, Martínez-Garza Cristina, Martínez-Vilalta Jordi, Mašková Tereza, Mason Kelly, Mason Norman, Massad Tara Joy, Masse Jacynthe, Mayrose Itay, McCarthy James, McCormack M. Luke, McCulloh Katherine, McFadden Ian R., McGill Brian J., McPartland Mara Y., Medeiros Juliana S., Medlyn Belinda, Meerts Pierre, Mehrabi Zia, Meir Patrick, Melo Felipe P.L., Mencuccini Maurizio, Meredieu Céline, Messier Julie, Mészáros Ilona, Metsaranta Juha, Michaletz Sean T., Michelaki Chrysanthi, Migalina Svetlana, Milla Ruben, Miller Jesse E.D., Minden Vanessa, Ming Ray, Mokany Karel, Moles Angela T., Molnár Attila, Molofsky Jane, Molz Martin, Montgomery Rebecca A., Monty Arnaud, Moravcová Lenka, Moreno-Martínez Alvaro, Moretti Marco, Mori Akira S., Mori Shigeta, Morris Dave, Morrison Jane, Mucina Ladislav, Mueller Sandra, Muir Christopher D., Müller Sandra Cristina, Munoz François, Myers-Smith Isla H., Myster Randall W., Nagano Masahiro, Naidu Shawna, Narayanan Ayyappan, Natesan Balachandran, Negoita Luka, Nelson Andrew S., Neuschulz Eike Lena, Ni Jian, Niedrist Georg, Nieto Jhon, Niinemets Ülo, Nolan Rachael, Nottebrock Henning, Nouvellon Yann, Novakovskiy Alexander, Nystuen Kristin Odden, O'Grady Anthony, O'Hara Kevin, O'Reilly-Nugent Andrew, Oakley Simon, Oberhuber Walter, Ohtsuka Toshiyuki, Oliveira Ricardo, Öllerer Kinga, Olson Mark E., Onipchenko Vladimir, Onoda Yusuke, Onstein Renske E., Ordonez Jenny C., Osada Noriyuki, Ostonen Ivika, Ottaviani Gianluigi, Otto Sarah, Overbeck Gerhard E., Ozinga Wim A., Pahl Anna T., Paine C. E. Timothy, Pakeman Robin J., Papageorgiou Aristotelis C., Parfionova Evgeniya, Pärtel Meelis, Patacca Marco, Paula Susana, Paule Juraj, Pauli Harald, Pausas Juli G., Peco Begoña, Penuelas Josep, Perea Antonio, Peri Pablo Luis, Petisco-Souza Ana Carolina, Petraglia Alessandro, Petritan Any Mary, Phillips Oliver L., Pierce Simon, Pillar Valério D., Pisek Jan, Pomogaybin Alexandr, Poorter Hendrik, Portsmouth Angelika, Poschlod Peter, Potvin Catherine, Pounds Devon, Powell A. Shafer, Power Sally A., Prinzing Andreas, Puglielli Giacomo, Pyšek Petr, Raevel Valerie, Rammig Anja, Ransijn Johannes, Ray Courtenay A., Reich Peter B., Reichstein Markus, Reid Douglas E.B., Réjou-Méchain Maxime, Dios Victor Resco de, Ribeiro Sabina, Richardson Sarah, Ribak Kersti, Rillig Matthias C., Riviera Fiamma, Robert Elisabeth M.R., Roberts Scott, Robroek Bjorn, Roddy Adam, Rodrigues Arthur Vinicius, Rogers Alistair, Rollinson Emily, Rolo Victor, Römermann Christine, Ronzhina Dina, Roscher Christiane, Rosell Julieta A., Rosenfield Milena Fermina, Rossi Christian, Roy David B., Royer-Tardif Samuel, Rüger Nadja, Ruiz-Peinado Ricardo, Rumpf Sabine B., Rusch Graciela M., Ryo Masahiro, Sack Lawren, Saldaña Angela, Salgado-Negret Beatriz, Salguero-Gomez Roberto, Santa-Regina Ignacio, Santacruz-García Ana Carolina, Santos Joaquim, Sardans Jordi, Schamp Bran-*

don, Scherer-Lorenzen Michael, Schleuning Matthias, Schmid Bernhard, Schmidt Marco, Schmitt Sylvain, Schneider Julio V., Schowanek Simon D., Schrader Julian, Schrodt Franziska, Schuldt Bernhard, Schurr Frank, Selaya Garvizu Galia, Semchenko Marina, Seymour Colleen, Sfair Julia C., Sharpe Joanne M., Shepard Christine S., Sheremetiev Serge, Shiodera Satomi, Shipley Bill, Shovon Tanvir Ahmed, Siebenkäs Alrun, Sierra Carlos, Silva Vasco, Silva Mateus, Sitzia Tommaso, Sjöman Henrik, Slot Martijn, Smith Nicholas G., Sodhi Darwin, Soltis Pamela, Soltis Douglas, Somers Ben, Sonnier Grégory, Sørensen Mia Vedel, Sosinski Enio Egon, Soudzilovskaia Nadejda A., Souza Alexandre F., Spasojevic Marko, Sperandii Marta Gaia, Stan Amanda B., Stegen James, Steinbauer Klaus, Stephan Jörg G., Sterck Frank, Stojanovic Dejan B., Strydom Tanya, Suarez Maria Laura, Svenning Jens Christian, Svitková Ivana, Svitok Marek, Svoboda Miroslav, Swaine Emily, Swenson Nathan, Tabarelli Marcelo, Takagi Kentaro, Tappeiner Ulrike, Tarifa Rubén, Tauougourdeau Simon, Tausanoglu Cagatay, Beest Mariska te, Tedersoo Leho, Thiffault Nelson, Thom Dominik, Thomas Evert, Thompson Ken, Thornton Peter E., Thuiller Wilfried, Tichý Lubomír, Tissue David, Tjoelker Mark G., Tng David Yue Phin, Tobias Joseph, Török Péter, Tarin Tonantzin, Torres-Ruiz José M., Tóthmérész Béla, Treurnicht Martina, Trivellone Valeria, Trolliet Franck, Trotsiuk Volodymyr, Tsakalos James L., Tsiripidis Ioannis, Tysklind Niklas, Umehara Toru, Usoltsev Vladimir, Vadeboncoeur Matthew, Vaezi Jamil, Valladares Fernando, Vamosi Jana, Bodegom Peter M. van, Breugel Michiel van, Van Cleemput Elisa, Weg Martine van de, Merwe Stephni van der, Plas Fons van der, Sande Masha T. van der, Kleunen Mark van, Van Meerbeek Koenraad, Vanderwel Mark, Vanselow Kim André, Vårhammar Angelica, Varone Laura, Vasquez Valderrama Maribel Yesenia, Vassilev Kiril, Velend Mark, Veneklaas Erik J., Verbeeck Hans, Verheyen Kris, Vibrans Alexander, Vieira Ima, Villacís Jaime, Violle Cyrille, Vivek Pandi, Wagner Katrin, Waldram Matthew, Waldron Anthony, Walker Anthony P., Waller Martyn, Walther Gabriel, Wang Han, Wang Feng, Wang Weiqi, Watkins Harry, Watkins James, Weber Ulrich, Weedon James T., Wei Liping, Weigelt Patrick, Weiher Evan, Wells Aidan W., Wellstein Camilla, Wenk Elizabeth, Westoby Mark, Westwood Alana, White Philip John, Whitten Mark, Williams Mathew, Winkler Daniel E., Winter Klaus, Womack Chevonne, Wright Ian J., Wright S. Joseph, Wright Justin, Pinho Bruno X., Ximenes Fabiano, Yamada Toshihiro, Yamaji Keiko, Yanai Ruth, Yankov Nikolay, Yguel Benjamin, Zanini Kátia Janaina, Zanne Amy E., Zelený David, Zhao Yun Peng, Zheng Jingming, Zheng Ji, Ziemińska Kasia, Zirbel Chad R., Zizka Georg, Zo-Bi Irié Casimir, Zotz Gerhard, Wirth Christian. TRY plant trait database – enhanced coverage and open access // *Global Change Biology*. 2020. 26, 1. 119–188.

Kattge Jens, Ogle Kiona, Bönisch Gerhard, Díaz Sandra, Lavorel Sandra, Madin Joshua, Nadrowski Karin, Nöllert Stephanie, Sartor Karla, Wirth Christian. A generic structure for plant trait databases // *Methods in Ecology and Evolution*. 4 2011. 2, 2. 202–213.

Kawamura Koji. A conceptual framework for the study of modular responses to local environmental heterogeneity within the plant crown and a review of related concepts // *Ecological Research*. 2010. 25, 4. 733–744.

- Kleiber Max.* Body size and metabolism // *Hilgardia*. 1 1932. 6, 11. 315–353.
- Koçillari Loren, Olson Mark E., Suweis Samir, Rocha Rodrigo P., Lovison Alberto, Cardin Franco, Dawson Todd E., Echeverría Alberto, Fajardo Alex, Lechthaler Silvia, Martínez-Pérez Cecilia, Marcati Carmen Regina, Chung Kuo-Fang, Rosell Julieta A., Segovia-Rivas Alí, Williams Cameron B., Petrone-Mendoza Emilio, Rinaldo Andrea, Anfodillo Tommaso, Banavar Jayanth R., Maritan Amos.* The Widened Pipe Model of plant hydraulic evolution // *Proceedings of the National Academy of Sciences*. 2021. 118, 22. e2100314118.
- Kunz Matthias, Fichtner Andreas, Härdtle Werner, Raumonon Pasi, Bruelheide Helge, Oheimb Goddert von.* Neighbour species richness and local structural variability modulate aboveground allocation patterns and crown morphology of individual trees // *Ecology Letters*. 2019. 22, 12. 2130–2140.
- Lan Guoyu, Zhu Hua, Cao Min, Hu Yuehua, Wang Hong, Deng Xiaobao, Zhou Shishun, Cui Jingyun, Huang Jianguo, He Youcai, Liu Linyun, Xu Hailong, Song Junping.* Spatial dispersion patterns of trees in a tropical rainforest in Xishuangbanna, southwest China // *Ecological Research*. 9 2009. 24, 5. 1117–1124.
- Lau Alvaro, Calders Kim, Bartholomeus Harm, Martius Christopher, Raumonon Pasi, Herold Martin, Vicari Matheus, Sukhdeo Hansrajie, Singh Jeremy, Goodman Rosa.* Tree Biomass Equations from Terrestrial LiDAR: A Case Study in Guyana // *Forests*. 6 2019a. 10, 6. 527.
- Lau Alvaro, Martius Christopher, Bartholomeus Harm, Shenkin Alexander, Jackson Tobias, Malhi Yadvinder, Herold Martin, Bentley Lisa Patrick.* Estimating architecture-based metabolic scaling exponents of tropical trees using terrestrial LiDAR and 3D modelling // *Forest Ecology and Management*. 5 2019b. 439. 132–145.
- Lauriks Fran, Salomón Roberto L., De Roo Linus, Sobrino-Plata Juan, Rodríguez-García Aida, Steppe Kathy.* Limited mitigating effects of elevated CO<sub>2</sub> in young aspen trees to face drought stress // *Environmental and Experimental Botany*. 9 2022. 201. 104942.
- Law Richard, Illian Janine, Burslem David F. R. P., Gratzner Georg, Gunatilleke C. V. S., Gunatilleke I. A. U. N.* Ecological information from spatial patterns of plants: insights from point process theory // *Journal of Ecology*. 7 2009. 97, 4. 616–628.
- Ledo Alicia, Schnitzer Stefan A.* Disturbance and clonal reproduction determine liana distribution and maintain liana diversity in a tropical forest // *Ecology*. 8 2014. 95, 8. 2169–2178.
- Leitold Veronika, Morton Douglas C., Longo Marcos, Santos Maiza Nara dos, Keller Michael, Scaranello Marcos.* El Niño drought increased canopy turnover in Amazon forests // *New Phytologist*. 2018. 219, 3. 959–971.
- Levy P E, Meir P, Allen S J, Jarvis P G.* The effect of aqueous transport of CO<sub>2</sub> in xylem sap on gas exchange in woody plants // *Tree Physiology*. 1999. 19, 1. 53–58.

- Li Ximeng, Blackman Chris J., Choat Brendan, Duursma Remko A., Rymer Paul D., Medlyn Belinda E., Tissue David T.* Tree hydraulic traits are coordinated and strongly linked to climate-of-origin across a rainfall gradient // *Plant, Cell & Environment*. 3 2018. 41, 3. 646–660.
- Likens Gene E., Bormann F. Herbert, Johnson Noye M., Fisher D. W., Pierce Robert S.* Effects of Forest Cutting and Herbicide Treatment on Nutrient Budgets in the Hubbard Brook Watershed-Ecosystem // *Ecological Monographs*. 12 1970. 40, 1. 23–47.
- Liu Hui, Gleason Sean M., Hao Guangyou, Hua Lei, He Pengcheng, Goldstein Guillermo, Ye Qing.* Hydraulic traits are coordinated with maximum plant height at the global scale // *Science Advances*. 2 2019. 5, 2.
- Liu Junjie, Wunch Debra, Menemenlis Dimitris, Frankenberg Christian, Sun Ying, Bloom A. Anthony, Lee Meemong, Bowman Kevin W., Schimel David S., Crisp David, Gurney Kevin R., Eldering Annmarie, Jiang Zhe, O'Dell Christopher W., Gierach Michelle, Parazoo Nicolas C.* Contrasting carbon cycle responses of the tropical continents to the 2015–2016 El Niño // *Science*. 2017. 358, 6360. eaam5690.
- Lloret Francisco, Siscart Daniel, Dalmases Carles.* Canopy recovery after drought dieback in holm-oak Mediterranean forests of Catalonia (NE Spain) // *Global Change Biology*. 12 2004. 10, 12. 2092–2099.
- Longo Marcos, Keller Michael, dos-Santos Maiza N., Leitold Veronika, Pinagé Ekena R., Baccini Alessandro, Saatchi Sassan, Nogueira Euler M., Batistella Mateus, Morton Douglas C.* Aboveground biomass variability across intact and degraded forests in the Brazilian Amazon // *Global Biogeochemical Cycles*. 11 2016. 30, 11. 1639–1660.
- Lovelock Catherine E., Ball Marilyn C., Choat Brendan, Engelbrecht Bettina M. J., Holbrook N. Michelle, Feller Ilka C.* Linking physiological processes with mangrove forest structure: phosphorus deficiency limits canopy development, hydraulic conductivity and photosynthetic carbon gain in dwarf *Rhizophora* mangle // *Plant, Cell and Environment*. 5 2006. 29, 5. 793–802.
- Malhi Yadvinder.* New perspectives on the ecology of tree structure and tree communities through terrestrial laser scanning // *Interface Focus*. 2018.
- Malhi Yadvinder, Aragao L. E. O. C., Galbraith David, Huntingford Chris, Fisher Rosie, Zelazowski Przemyslaw, Sitch Stephen, McSweeney Carol, Meir Patrick.* Exploring the likelihood and mechanism of a climate-change-induced dieback of the Amazon rainforest // *Proceedings of the National Academy of Sciences*. 2009a. 106, 49. 20610–20615.
- Malhi Yadvinder, Aragão Luiz Eduardo O.C., Metcalfe Daniel B., Paiva Romilda, Quesada Carlos A., Almeida Samuel, Anderson Liana, Brando Paulo, Chambers Jeffrey Q., Costa Antonio C.L. da, Hutyrá Lucy R., Oliveira Paulo, Patiño Sandra, Pyle Elizabeth H., Robertson Amanda L., Teixeira Lilliane M.* Comprehensive assessment of carbon productivity, allocation and storage in three Amazonian forests // *Global Change Biology*. 2009b. 15, 5. 1255–1274.

- Marengo Jose A., Souza Carlos M., Thonicke Kirsten, Burton Chantelle, Halladay Kate, Betts Richard A., Alves Lincoln M., Soares Wagner R.* Changes in Climate and Land Use Over the Amazon Region: Current and Future Variability and Trends // *Frontiers in Earth Science*. 12 2018. 6.
- Mayle Francis E., Beerling David J., Gosling William D., Bush Mark B.* Responses of Amazonian ecosystems to climatic and atmospheric carbon dioxide changes since the last glacial maximum // *Philosophical Transactions of the Royal Society B: Biological Sciences*. 2004. 359, 1443. 499–514.
- McDowell Nate, Pockman William T., Allen Craig D., Breshears David D., Cobb Neil, Kolb Thomas, Plaut Jennifer, Sperry John, West Adam, Williams David G., Yezzer Enrico A.* Mechanisms of plant survival and mortality during drought: Why do some plants survive while others succumb to drought? // *New Phytologist*. 2008. 178, 4. 719–739.
- McGuire M. A., Marshall J. D., Teskey R. O.* Assimilation of xylem-transported  $^{13}\text{C}$ -labelled  $\text{CO}_2$  in leaves and branches of sycamore (*Platanus occidentalis* L.) // *Journal of Experimental Botany*. 2009. 60, 13. 3809–3817.
- McGuire M. A., Teskey R. O.* Microelectrode technique for in situ measurement of carbon dioxide concentrations in xylem sap of trees // *Tree Physiology*. 2002. 22, 11. 807–811.
- Meakem Victoria, Tepley Alan J., Gonzalez-Akre Erika B., Herrmann Valentine, Muller-Landau Helene C., Wright S. Joseph, Hubbell Stephen P., Condit Richard, Anderson-Teixeira Kristina J.* Role of tree size in moist tropical forest carbon cycling and water deficit responses // *New Phytologist*. 2017. June.
- Medina E., Sobrado M., Herrera R.* Significance of leaf orientation for leaf temperature in an amazonian sclerophyll vegetation // *Radiation and Environmental Biophysics* 1978 15:2. 6 1978. 15, 2. 131–140.
- Meir P, Brando P M, Nepstad D, Vasconcelos S, Costa A C L, Davidson E, Almeida S, Fisher R A, Sotta E D, Zarin D, Cardinot G.* The Effects of Drought on Amazonian Rain Forests // *Amazonia and Global Change*. 2009. 186. 429–449.
- Meir P., Grace J., Miranda A. C.* Leaf respiration in two tropical rainforests: Constraints on physiology by phosphorus, nitrogen and temperature // *Functional Ecology*. 2001. 15, 3. 378–387.
- Meir P., Metcalfe D. B., Costa A. C.L., Fisher R. A.* The fate of assimilated carbon during drought: Impacts on respiration in Amazon rainforests // *Philosophical Transactions of the Royal Society B: Biological Sciences*. 2008. 363, 1498. 1849–1855.
- Meir Patrick, Grace J.* Scaling relationships for woody tissue respiration in two tropical rain forests // *Plant, Cell and Environment*. 2002. 25, 8. 963–973.
- Meir Patrick, Rowland Lucy, Binks Oliver, Costa Antonio Lola da, Mencuccini Maurizio, Ferreira Leandro.* Short-term effects of drought on tropical forest do not fully predict impacts of repeated or long-term drought: photosynthetic capacity

- vs growth // *Philosophical Transactions of the Royal Society A: Mathematical, Physical and Engineering Sciences*. 2018. 1–22.
- Meir Patrick, Shenkin Alexander, Disney Mathias, Rowland Lucy, Malhi Yadvinder, Herold Martin, Costa Antonio C L da*. Plant Structure-Function Relationships and Woody Tissue Respiration: Upscaling to Forests from Laser-Derived Measurements // *Plant Respiration: Metabolic Fluxes and Carbon Balance*. 2017. 89–105.
- Meir Patrick, Wood Tana E., Galbraith David R., Brando Paulo M., Da Costa Antonio C. L., Rowland Lucy, Ferreira Leandro V*. Threshold Responses to Soil Moisture Deficit by Trees and Soil in Tropical Rain Forests: Insights from Field Experiments // *BioScience*. 9 2015. 65, 9. 882–892.
- Mencuccini Maurizio, Hölttä Teemu, Petit Gaii, Magnani Federico*. Sanio’s laws revisited. Size-dependent changes in the xylem architecture of trees // *Ecology Letters*. 2007. 10, 11. 1084–1093.
- Mencuccini Maurizio, Salmon Yann, Mitchell Patrick, Hölttä Teemu, Choat Brendan, Meir Patrick, O’Grady Anthony, Tissue David, Zweifel Roman, Sevanto Sanna, Pfautsch Sebastian*. An empirical method that separates irreversible stem radial growth from bark water content changes in trees: theory and case studies // *Plant Cell and Environment*. 2017. 40, 2. 290–303.
- Metcalfe D. B., Meir P., Aragao L. E O C, Vale R. Lobo-do, Galbraith D., Fisher R. A., Chaves M. M., Maroco J. P., Costa A. C L da, Almeida S. S. de, Braga A. P., Goncalves P. H L, Athaydes J. de, Costa M. da, Portela T. T B, Oliveira A. A R de, Malhi Y., Williams M*. Shifts in plant respiration and carbon use efficiency at a large-scale drought experiment in the eastern Amazon // *New Phytologist*. 2010a. 187, 3. 608–621.
- Metcalfe Daniel B, Lobo-Do-Vale Raquel, Chaves Manuela M, Maroco Joao P, Araújo Luiz E O C, Malhi Yadvinder, Da Costa Antonio L, Braga Alan P, Gonçalves Paulo L, De Athaydes Joao, Da Costa Mauricio, Almeida Samuel S, Campbell Catherine, Hurry Vaughan, Williams Mathew, Meir Patrick*. Impacts of experimentally imposed drought on leaf respiration and morphology in an Amazon rain forest // *Ecology*. 2010b. 24, 3. 524–533.
- Moeur Melinda*. Characterizing Spatial Patterns of Trees Using Stem-Mapped Data // *Forest Science*. 1993. 39, 4. 756–775.
- Momo Stéphane Takoudjou, Ploton Pierre, Martin-Ducup Olivier, Lehnebach Romain, Fortunel Claire, Sagang Le Bienfaiteur Takougoum, Boyemba Faustin, Couteron Pierre, Fayolle Adeline, Libalah Moses, Loumeto Joel, Medjibe Vincent, Ngomanda Alfred, Obiang Diosdado, Péliissier Raphaël, Rossi Vivien, Yongo Olga, Bocko Yannick, Fonton Noël, Kamdem Narcisse, Katembo John, Kondoule Henriette Josiane, Maïdou Hervé Martial, Mankou Géraud, Mbasi Michel, Mengui Thomas, Mofack Gislain I.I., Moundounga Cynel, Moundounga Quentin, Nguimbous Lydie, Ncham Norberto Nsue, Asue Francisco Ondo Meye, Senguela Yvon Patrick, Viard Lionel, Zapfack Louis, Sonké Bonaventure, Barbier Nicolas*. Leveraging Signatures of Plant Functional Strategies in Wood Density Profiles

of African Trees to Correct Mass Estimations From Terrestrial Laser Data // Scientific Reports. 2020. 10, 1. 1–11.

*Mori S., Yamaji K., Ishida A., Prokushkin S. G., Masyagina O. V., Hagihara A., Hoque A. T. M. R., Suwa R., Osawa A., Nishizono T., Ueda T., Kinjo M., Miyagi T., Kajimoto T., Koike T., Matsuura Y., Toma T., Zyryanova O. A., Abaimov A. P., Awaya Y., Araki M. G., Kawasaki T., Chiba Y., Umari M.* Mixed-power scaling of whole-plant respiration from seedlings to giant trees // Proceedings of the National Academy of Sciences. 2010. 107, 4. 1447–1451.

*Moser Gerald, Schuldt Bernhard, Hertel Dietrich, Horna Viviana, Coners Heinz, Barus Henry, Leuschner Christoph.* Replicated throughfall exclusion experiment in an Indonesian perhumid rainforest: wood production, litter fall and fine root growth under simulated drought // Global Change Biology. 5 2014. 20, 5. 1481–1497.

*Mueller-Dombois Dieter.* Canopy Dieback and Successional Processes in Pacific Forests // Pacific Science. 1983. 37 (4), 4. 317–325.

*Muller-Landau Helene C., Condit Richard S., Harms Kyle E., Marks Christian O., Thomas Sean C., Bunyavejchewin Sarayudh, Chuyong George, Co Leonardo, Davies Stuart, Foster Robin, Gunatilleke Savitri, Gunatilleke Nimal, Hart Terese, Hubbell Stephen P., Itoh Akira, Kassim Abd Rahman, Kenfack David, LaFrankie James V., Lagunzad Daniel, Lee Hua Seng, Losos Elizabeth, Makana Jean Remy, Ohkubo Tatsuhiko, Samper Cristian, Sukumar Raman, Sun I. Fang, Nur Supardi M. N., Tan Sylvester, Thomas Duncan, Thompson Jill, Valencia Renato, Vallejo Martha Isabel, Muñoz Gorky Villa, Yamakura Takuo, Zimmerman Jess K., Dattaraja Handanakere Shavaramaiah, Esufali Shameema, Hall Pamela, He Fangliang, Hernandez Consuelo, Kiratiprayoon Somboon, Suresh Hebbalalu S., Wills Christopher, Ashton Peter.* Comparing tropical forest tree size distributions with the predictions of metabolic ecology and equilibrium models // Ecology Letters. 2006. 9, 5. 589–602.

*Muller-Landau Helene C., Cushman K. C., Arroyo Eva E., Martinez Cano Isabel, Anderson-Teixeira Kristina J., Backiel Bogumila.* Patterns and mechanisms of spatial variation in tropical forest productivity, woody residence time, and biomass // New Phytologist. 2020.

*Murphy Brett P., Bowman David M.J.S.* What controls the distribution of tropical forest and savanna? // Ecology Letters. 2012. 15, 7. 748–758.

*Negisi Kenitiroo.* Diurnal Fluctuation of CO<sub>2</sub> Release from the Stem Bark of Standing Young *Pinus densiflora* Trees // Journal of Japanese Forestry Society. 1975. 57, 11. 375–383.

*Nepstad Daniel C, Tohver Ingrid Marisa, Ray David, Moutinho Paulo, Ecology Source, Sep No, Nepstad C.* Mortality of Large Trees and Lianas following Experimental Drought in an Amazon Forest // Ecology. 2015. 88, 9. 2259–2269.

*Niinemets Ülo.* Responses of forest trees to single and multiple environmental stresses from seedlings to mature plants: Past stress history, stress interactions,

- tolerance and acclimation // *Forest Ecology and Management*. 2010. 260, 10. 1623–1639.
- Niklas Karl J., Enquist Brian J.* Invariant scaling relationships for interspecific plant biomass production rates and body size // *Proceedings of the National Academy of Sciences of the United States of America*. 2001. 98, 5. 2922–2927.
- Nobre Carlos A., Sampaio Gilvan, Borma Laura S., Castilla-Rubio Juan Carlos, Silva José S., Cardoso Manoel.* Land-use and climate change risks in the Amazon and the need of a novel sustainable development paradigm // *Proceedings of the National Academy of Sciences*. 9 2016. 113, 39. 10759–10768.
- Nolan Rachael H., Gauthey Alice, Losso Adriano, Medlyn Belinda E., Smith Rhannon, Chhajed Shubham S., Fuller Kathryn, Song Magnolia, Li Xine, Beaumont Linda J., Boer Matthias M., Wright Ian J., Choat Brendan.* Hydraulic failure and tree size linked with canopy die-back in eucalypt forest during extreme drought // *New Phytologist*. 5 2021. 230, 4. 1354–1365.
- Olivas Paulo C., Oberbauer Steven F., Clark David B., Clark Deborah A., Ryan Michael G., O'Brien Joseph J., Ordoñez Harlyn.* Comparison of direct and indirect methods for assessing leaf area index across a tropical rain forest landscape // *Agricultural and Forest Meteorology*. 2013. 177. 110–116.
- Oliveira Rafael S., Dawson Todd E., Burgess Stephen S. O., Nepstad Daniel C.* Hydraulic redistribution in three Amazonian trees // *Oecologia*. 9 2005. 145, 3. 354–363.
- Olson Mark E., Anfodillo Tommaso, Gleason Sean M., McCulloh Katherine A.* Tip-to-base xylem conduit widening as an adaptation: causes, consequences, and empirical priorities // *New Phytologist*. 2021. 229, 4. 1877–1893.
- Olson Mark E, Rosell Julieta A.* Vessel diameter-stem diameter scaling across woody angiosperms and the ecological causes of xylem vessel diameter variation // *New Phytologist*. 2013. 197, 4. 1204–1213.
- Olson Mark E., Soriano Diana, Rosell Julieta A., Anfodillo Tommaso, Donoghue Michael J., Edwards Erika J., León-Gómez Calixto, Dawson Todd, Julio Camarero Martínez J., Castorena Matiss, Echeverría Alberto, Espinosa Carlos I., Fajardo Alex, Gazol Antonio, Isnard Sandrine, Lima Rivete S., Marcati Carmen R., Méndez-Alonzo Rodrigo.* Plant height and hydraulic vulnerability to drought and cold // *Proceedings of the National Academy of Sciences of the United States of America*. 2018. 115, 29. 7551–7556.
- O'Brien Michael J., Leuzinger Sebastian, Philipson Christopher D., Tay John, Hector Andy.* Drought survival of tropical tree seedlings enhanced by non-structural carbohydrate levels // *Nature Climate Change*. 8 2014. 4, 8. 710–714.
- Pan Yude, Birdsey Richard A, Fang Jingyun, Houghton Richard, Kauppi Pekka E, Kurz Werner A, Phillips Oliver L, Shvidenko Anatoly, Lewis Simon L, Canadell Josep G, Ciais Philippe, Jackson Robert B, Pacala Stephen W, McGuire A David, Piao Shilong, Rautiainen Aapo, Sitch Stephen, Hayes Daniel.* A large and persistent carbon sink in the world's forests. // *Science*. 2011. 333, 6045. 988–93.

*Patiño S., Lloyd J., Paiva R., Quesada C. A., Baker T. R., Santos A. J. B., Mercado L. M., Malhi Y., Phillips O. L., Aguilar A., Alvarez E., Arroyo L., Bonal D., Costa A. C. L., Czimczik C. I., Gallo J., Herrera R., Higuchi N., Horna V., Hoyos E. J., Jimenez E. M., Killeen T., Leal E., Luizão F., Meir P., Monteagudo A., Neill D., Núñez-Vargas P., Palomino W., Peacock J., Peña-Cruz A., Peñuela M. C., Pitman N., Priante Filho N., Prieto A., Panfil S. N., Rudas A., Salomão R., Silva N., Silveira M., Almeida S. Soares de, Torres-Lezama A., Turriago J. D., Vásquez-Martínez R., Schwarz M., Sota A., Schmerler J., Vieira I., Villanueva B., Vitzthum P.* Branch xylem density variations across Amazonia // *Biogeosciences Discussions*. 2008. 5, 3. 2003–2047.

*Pessenda L. C.R., Gomes B. M., Aravena R., Ribeiro A. S., Boulet R., Gouveia S. E.M.* The carbon isotope record in soils along a forest-cerrado ecosystem transect: Implications for vegetation changes in the Rondonia state, southwestern Brazilian Amazon region // *Holocene*. 1998. 8, 5. 599–603.

*Pfanz H., Aschan G., Langenfeld-Heyser R., Wittmann C., Loose M.* Ecology and ecophysiology of tree stems: Corticular and wood photosynthesis // *Naturwissenschaften*. 2002. 89, 4. 147–162.

*Phillips Oliver L, Aragão Luiz E O C, Lewis Simon L, Fisher Joshua B, Lloyd Jon, López-González Gabriela, Malhi Yadvinder, Monteagudo Abel, Peacock Julie, Quesada Carlos a, Heijden Geertje van der, Almeida Samuel, Amaral Iêda, Arroyo Luzmila, Aymard Gerardo, Baker Tim R, Bánki Olaf, Blanc Lilian, Bonal Damien, Brando Paulo, Chave Jerome, Oliveira Atila Cristina Alves de, Cardozo Nallaret Dávila, Czimczik Claudia I, Feldpausch Ted R, Freitas Maria Aparecida, Gloor Emanuel, Higuchi Niro, Jiménez Eliana, Lloyd Gareth, Meir Patrick, Mendoza Casimiro, Morel Alexandra, Neill David a, Nepstad Daniel, Patiño Sandra, Peñuela Maria Cristina, Prieto Adriana, Ramírez Fredy, Schwarz Michael, Silva Javier, Silveira Marcos, Thomas Anne Sota, Steege Hans Ter, Stropp Juliana, Vásquez Rodolfo, Zelazowski Przemyslaw, Alvarez Dávila Esteban, Andelman Sandy, Andrade Ana, Chao Kuo-jung, Erwin Terry, Di Fiore Anthony, Honorio C Eurídice, Keeling Helen, Killeen Tim J, Laurance William F, Peña Cruz Antonio, Pitman Nigel C a, Núñez Vargas Percy, Ramírez-Angulo Hirma, Rudas Agustín, Salamão Rafael, Silva Natalino, Terborgh John, Torres-Lezama Armando, Heijden Geertje Van Der, Cristina Átila, Oliveira Alves De, Dávila Esteban Alvarez, Fiore Anthony Di, C Eurídice Honorio, Cruz Antonio Peña, Vargas Percy Núñez.* Drought sensitivity of the Amazon Rainforest // *Science*. 2009. 323, 5919. 1344–1347.

*Phillips Oliver L, Heijden Geertje Van Der, Lewis Simon L, Lo Gabriela, Lloyd Jon, Malhi Yadvinder, Monteagudo Abel, Almeida Samuel, Da Esteban Alvarez, Andelman Sandy, Andrade Ana, Arroyo Luzmila, Aymard Gerardo, Baker Tim R, Costa Lola, Feldpausch Ted R, Fisher Joshua B, Fyllas Nikolaos M, Freitas Maria Aparecida, Jime Eliana, Keeling Helen, Tim J, Gloor Emanuel, Higuchi Niro, Lovett Jon C, Meir Patrick, Mendoza Casimiro, Morel Alexandra, Nu Percy, Prieto Adriana, Quesada Carlos A, Peh Kelvin S-h, Pen Antonio, Schwarz Michael, Silva Javier, Silveira Marcos, Slik J. W.Ferry, Sonké B., Sota Thomas Anne, Stropp Juliana, Taplin James RD, Vasquez Rodolfo, Vilanova Emilio.*

- Drought–mortality relationships for tropical forests // *New Phytologist*. 2010. 187. 631–646.
- Pillet Michiel, Joetzjer Emilie, Belmin Camille, Chave Jérôme, Ciais Philippe, Dourdain Aurélie, Evans Margaret, Hérault Bruno, Luyssaert Sebastiaan, Poulter Benjamin.* Disentangling competitive vs. climatic drivers of tropical forest mortality // *Journal of Ecology*. 5 2018. 106, 3. 1165–1179.
- Pivovarovff Alexandria L., McDowell Nate G., Rodrigues Tayana Barrozo, Brodribb Tim, Cernusak Lucas A., Choat Brendan, Grossiord Charlotte, Ishida Yoko, Jardine Kolby J., Laurance Susan, Leff Riley, Li Weibin, Liddell Michael, Mackay D. Scott, Pacheco Heather, Peters Jennifer, J. Sampaio Filho Israel, Souza Daisy C., Wang Wenzhi, Zhang Peipei, Chambers Jeff.* Stability of tropical forest tree carbon-water relations in a rainfall exclusion treatment through shifts in effective water uptake depth // *Global Change Biology*. 12 2021. 27, 24. 6454–6466.
- Pons Thijs L, Welschen Rob a M.* Midday depression of net photosynthesis in the tropical rainforest tree *Eperua grandiflora*: contributions of stomatal and internal conductances, respiration and Rubisco functioning. // *Tree physiology*. 2003. 23. 937–947.
- Pretzsch Hans.* Tree growth as affected by stem and crown structure // *Trees*. 6 2021. 35, 3. 947–960.
- Price Charles A., Ogle Kiona, White Ethan P., Weitz Joshua S.* Evaluating scaling models in biology using hierarchical Bayesian approaches // *Ecology Letters*. 7 2009. 12, 7. 641–651.
- R Core Team .* R: A Language and environment for statistical computing. Vienna, Austria, 2021.
- Raumonon P., Casella E., Calders K., Murphy S., Åkerbloma M., Kaasalainen M.* Massive-Scale Tree Modelling From Tls Data // *ISPRS Annals of Photogrammetry, Remote Sensing and Spatial Information Sciences*. 2015. II-3/W4, March. 189–196.
- Raumonon Pasi, Kaasalainen Mikko, Åkerblom Markku, Kaasalainen Sanna, Kaartinen Harri, Vastaranta Mikko, Holopainen Markus, Disney Mathias, Lewis Philip.* Fast Automatic Precision Tree Models from Terrestrial Laser Scanner Data // *Remote Sensing*. 2013. 5, 2. 491–520.
- Rayment M. B., Loustau D., Jarvis P. G.* Photosynthesis and respiration of black spruce at three organizational scales: Shoot, branch and canopy // *Tree Physiology*. 2002. 22, 4. 219–229.
- Reich Peter B., Stefanski Artur, Rich Roy L., Sendall Kerrie M., Wei Xiaorong, Zhao Changming, Hou Jihua, Montgomery Rebecca A., Bermudez Raimundo.* Assessing the relevant time frame for temperature acclimation of leaf dark respiration: A test with 10 boreal and temperate species // *Global Change Biology*. 6 2021. 27, 12. 2945–2958.

- Reich Peter B., Tjoelker Mark G., Machado Jose Luis, Oleksyn Jacek. Universal scaling of respiratory metabolism, size and nitrogen in plants // *Nature*. 2006. 439, 7075. 457–461.
- Rifai Sami W., Girardin Cécile A.J., Berenguer Erika, Del Aguila-Pasquel Jhon, Dahlsjö Cecilia A.L., Doughty Christopher E., Jeffery Kathryn J., Moore Sam, Oliveras Imma, Riutta Terhi, Rowland Lucy M., Murakami Alejandro Araujo, Addo-Danso Shalom D., Brando Paulo, Burton Chad, Ondo Fidèle Evouna, Duah-Gyamfi Akwasi, Amézquita Filio Farfán, Freitag Renata, Pacha Fernando Hancco, Huasco Walter Huaraca, Ibrahim Forzia, Mbou Armel T., Mihindou Vianet Mihindou, Peixoto Karine S., Rocha Wanderley, Rossi Liana C., Seixas Marina, Silva-Espejo Javier E., Abernethy Katharine A., Adu-Bredu Stephen, Barlow Jos, Da Costa Antonio C.L., Marimon Beatriz S., Marimon-Junior Ben H., Meir Patrick, Metcalfe Daniel B., Phillips Oliver L., White Lee J.T., Malhi Yadvinder. ENSO Drives interannual variation of forest woody growth across the tropics // *Philosophical Transactions of the Royal Society B: Biological Sciences*. 2018. 373, 1760.
- Rodríguez-Calcerrada Jesús, Martin-StPaul Nicolas K., Lempereur Morine, Ourcival Jean Marc, Rey María del Carmen del, Joffre Richard, Rambal Serge. Stem CO<sub>2</sub> efflux and its contribution to ecosystem CO<sub>2</sub> efflux decrease with drought in a Mediterranean forest stand // *Agricultural and Forest Meteorology*. 9 2014. 195–196. 61–72.
- Rodríguez-Calcerrada Jesús, Rodrigues Ana M., António Carla, Perdiguero Pedro, Pita Pilar, Collada Carmen, Li Meng, Gil Luis. Stem metabolism under drought stress – a paradox of increasing respiratory substrates and decreasing respiratory rates // *Physiologia Plantarum*. 6 2021. 172, 2. 391–404.
- Rood Stewart B., Patino Sandra, Coombs Krista, Tyree Melvin T. Branch sacrifice: cavitation-associated drought adaptation of riparian cottonwoods // *Trees*. 2000. 14. 248–257.
- Rowland L., Da Costa A. C.L., Galbraith D. R., Oliveira R. S., Binks O. J., Oliveira A. A.R., Pullen A. M., Doughty C. E., Metcalfe D. B., Vasconcelos S. S., Ferreira L. V., Malhi Y., Grace J., Mencuccini M., Meir P. Death from drought in tropical forests is triggered by hydraulics not carbon starvation // *Nature*. 2015. 528, 7580. 119–122.
- Rowland L., Stahl C., Bonal D., Siebicke L., Williams M., Meir P. The Response of Tropical Rainforest Dead Wood Respiration to Seasonal Drought // *Ecosystems*. 11 2013. 16, 7. 1294–1309.
- Rowland Lucy, Costa Antonio C. L. da, Oliveira Alex A. R., Oliveira Rafael S., Bittencourt Paulo L., Costa Patricia B., Giles Andre L., Sosa Azul I., Coughlin Ingrid, Godlee John L., Vasconcelos Steel S., Junior João A. S., Ferreira Leandro V., Mencuccini Maurizio, Meir Patrick. Drought stress and tree size determine stem CO<sub>2</sub> efflux in a tropical forest // *New Phytologist*. 2018.
- Rowland Lucy, Costa Antonio C.L. da, Oliveira Rafael S., Bittencourt Paulo R.L., Giles André L., Coughlin Ingrid, Britto Costa Patricia de, Bartholomew David,

- Domingues Tomas F., Miatto Raquel C., Ferreira Leandro V., Vasconcelos Steel S., Junior Joao A.S., Oliveira Alex A.R., Mencuccini Maurizio, Meir Patrick.* The response of carbon assimilation and storage to long-term drought in tropical trees is dependent on light availability // *Functional Ecology*. 2021a. 35, 1. 43–53.
- Rowland Lucy, Oliveira Rafael S., Bittencourt Paulo R.L., Giles Andre L., Coughlin Ingrid, Costa Patricia de Britto, Domingues Tomas, Ferreira Leandro V., Vasconcelos Steel S., Junior João A.S., Oliveira Alex A.R., Costa Antonio C.L. da, Meir Patrick, Mencuccini Maurizio.* Plant traits controlling growth change in response to a drier climate // *New Phytologist*. 2021b. 229, 3. 1363–1374.
- Ruivo M.L.P, Cunha E.S.* Mineral and organic components in archaeological black earth and yellow latosol in Caxiuana, Amazon, Brazil // *Transactions on Ecology and the Environment*. 2003. 64.
- Ryan Michael G.* Growth and maintenance respiration in stems of *Pinus contorta* and *Picea engelmannii* // *Canadian Journal of Forest Research*. 1990. 20, 1. 48–57.
- Ryan Michael G., Hubbard Robert M., Clark Deborah A., Sanford Robert L.* Woody-tissue respiration for *Simarouba amara* and *Minquartia guianensis*, two tropical wet forest trees with different growth habits // *Oecologia*. 1994. 100, 3. 213–220.
- Saatchi S., Asefi-Najafabady S., Malhi Y., Aragao L. E. O. C., Anderson L. O., Myneni R. B., Nemani R.* Persistent effects of a severe drought on Amazonian forest canopy // *Proceedings of the National Academy of Sciences*. 2013. 110, 2. 565–570.
- Salas Christian, LeMay Valerie, Núñez Patricio, Pacheco Patricio, Espinosa Alejandro.* Spatial patterns in an old-growth *Nothofagus obliqua* forest in south-central Chile // *Forest Ecology and Management*. 8 2006. 231, 1-3. 38–46.
- Salomón Roberto L., De Roo Linus, Oleksyn Jacek, De Pauw Dirk J.W., Steppe Kathy.* TReSpire – a biophysical TRee Stem respiration model // *New Phytologist*. 2020. 225, 5. 2214–2230.
- Salomón Roberto L., De Schepper Veerle, Valbuena-Carabaña María, Gil Luis, Steppe Kathy.* Daytime depression in temperature-normalised stem CO<sub>2</sub> efflux in young poplar trees is dominated by low turgor pressure rather than by internal transport of respired CO<sub>2</sub> // *New Phytologist*. 2018. 217, 2. 586–598.
- Salomón Roberto L., Valbuena-Carabaña María, Gil Luis, McGuire Mary Anne, Teskey Robert O., Aubrey Doug P., González-Doncel Inés, Rodríguez-Calcerrada Jesús.* Temporal and spatial patterns of internal and external stem CO<sub>2</sub> fluxes in a sub-Mediterranean oak // *Tree Physiology*. 2016.
- Sampaio Gilvan, Nobre Carlos, Costa Marcos Heil, Satyamurty Prakki, Soares-Filho Britaldo Silveira, Cardoso Manoel.* Regional climate change over eastern Amazonia caused by pasture and soybean cropland expansion // *Geophysical Research Letters*. 9 2007. 34, 17. L17709.

- Saveyn An, Steppe Kathy, Lemeur Raoul.* Daytime depression in tree stem CO<sub>2</sub> efflux rates: Is it caused by low stem turgor pressure? // *Annals of Botany.* 2007. 99, 3. 477–485.
- Schymanski Stanislaus J., Or Dani.* Wind increases leaf water use efficiency // *Plant Cell and Environment.* 2016. 39, 7. 1448–1459.
- Shen Jing Xian, Zhang Yong Jiang, Maenpuen Phisamai, Zhang Shu Bin, Zhang Lan, Yang Lin, Tao Lian Bin, Yan Peng Yun, Zhang Zhi Ming, Li Shu Qiong, Yuan Xia, Kongjarat Wanwalee, Kaewkamol Sasiwimol, Tinprabat Pimnara, Chen Ya Jun.* Response of four evergreen savanna shrubs to an incidence of extreme drought: High embolism resistance, branch shedding and maintenance of nonstructural carbohydrates // *Tree Physiology.* 4 2022. 42, 4. 740–753.
- Shenkin Alexander, Bentley Lisa Patrick, Oliveras Imma, Salinas Norma, Adu-Bredu Stephen, Marimon-Junior Ben Hur, Marimon Beatriz S., Peprah Theresa, Choque Efrain Lopez, Trujillo Rodriguez Lucio, Clemente Arenas Edith Rosario, Adonteng Christian, Seidu John, Passos Fabio Barbosa, Reis Simone Matias, Blonder Benjamin, Silman Miles, Enquist Brian J., Asner Gregory P., Malhi Yadvinder.* The Influence of Ecosystem and Phylogeny on Tropical Tree Crown Size and Shape // *Frontiers in Forests and Global Change.* 10 2020. 3.
- Silva Carlos, Crookston Nicholas, Hudak Andrew, Vierling Lee, Klauberg Carine, Cardil Adrian.* rLiDAR: LiDAR Data Processing and Visualization. 2017.
- Slik J. W. F., Aiba Shin-Ichiro, Brearley Francis Q., Cannon Chuck H., Forshed Olle, Kitayama Kanehiro, Nagamasu Hidetoshi, Nilus Reuben, Payne John, Paoli Gary, Poulsen Axel D., Raes Niels, Sheil Douglas, Sidiyasa Kade, Suzuki Eizi, Valkenburg Johan L. C. H. van.* Environmental correlates of tree biomass, basal area, wood specific gravity and stem density gradients in Borneo's tropical forests // *Global Ecology and Biogeography.* 1 2010. 19, 1. 50–60.
- Slik J. W. Ferry, Paoli Gary, Mcguire Krista, Amaral Ieda, Barroso Jorcely, Bastian Meredith, Blanc Lilian, Bongers Frans, Boundja Patrick, Clark Connie, Collins Murray, Dauby Gilles, Ding Yi, Doucet Jean Louis, Eler Eduardo, Ferreira Leandro, Forshed Olle, Fredriksson Gabriella, Gillet Jean Francois, Harris David, Leal Miguel, Laumonier Yves, Malhi Yadvinder, Mansor Asyraf, Martin Emanuel, Miyamoto Kazuki, Araujo-Murakami Alejandro, Nagamasu Hidetoshi, Nilus Reuben, Nurtjahya Eddy, Oliveira Átila, Onrizal Onrizal, Parada-Gutierrez Alexander, Permana Andrea, Poorter Lourens, Poulsen John, Ramirez-Angulo Hirma, Reitsma Jan, Rovero Francesco, Rozak Andes, Sheil Douglas, Silva-Espejo Javier, Silveira Marcos, Spironelo Wilson, Steege Hans ter, Stevart Tariq, Navarro-Aguilar Gilberto Enrique, Sunderland Terry, Suzuki Eizi, Tang Jianwei, Theilade Ida, Heijden Geertje van der, Valkenburg Johan van, Van Do Tran, Vilanova Emilio, Vos Vincent, Wich Serge, Wöll Hannsjoerg, Yoneda Tsuyoshi, Zang Runguo, Zhang Ming Gang, Zweifel Nicole.* Large trees drive forest above-ground biomass variation in moist lowland forests across the tropics // *Global Ecology and Biogeography.* 2013. 22, 12. 1261–1271.

- Slot Martijn, Kitajima Kaoru.* General patterns of acclimation of leaf respiration to elevated temperatures across biomes and plant types // *Oecologia*. 3 2015. 177, 3. 885–900.
- Smith Duncan D., Sperry John S.* Coordination between water transport capacity, biomass growth, metabolic scaling and species stature in co-occurring shrub and tree species // *Plant, Cell & Environment*. 12 2014. 37, 12. 2679–2690.
- Smith Marielle N., Stark Scott C., Taylor Tyeen C., Ferreira Mauricio, Oliveira Eronaldo de, Restrepo-Coupe Natalia, Chen Shuli, Woodcock Tara K., Santos Darlisson Bentes dos, Alves Luciana F., Figueira Michela, Camargo Plinio B. de, Oliveira Raimundo C. de, Aragão Luiz E. O. C., Falk Donald A., McMahon Sean M., Huxman Travis E., Saleska Scott R.* Monthly ground-based lidar reveals seasonal and drought related changes in leaf area profiles with dependencies on height and light environment in an Amazon forest. 2019. 1–22.
- Sotta Eleneide Doff, Veldkamp Edzo, Schwendenmann Luitgard, Guimaraes Brenda Rocha, Paixao Rosiene Keila, Ruivo Maria de Lourdes P., Costa Antonio Carlos Lola da, Meir Patrick.* Effects of an induced drought on soil carbon dioxide (CO<sub>2</sub>) efflux and soil CO<sub>2</sub> production in an Eastern Amazonian rainforest, Brazil // *Global Change Biology*. 10 2007. 13, 10. 2218–2229.
- Sperry John S., Smith Duncan D., Savage Van M., Enquist Brian J., McCulloh Katherine A., Reich Peter B., Bentley Lisa P., Allmen Erica I. von.* A species-level model for metabolic scaling in trees I. Exploring boundaries to scaling space within and across species // *Functional Ecology*. 10 2012. 26, 5. 1054–1065.
- Spicer R., Holbrook N. M.* Parenchyma cell respiration and survival in secondary xylem: does metabolic activity decline with cell age? // *Plant, Cell & Environment*. 8 2007. 30, 8. 934–943.
- Spiess Andrej-Nikolai.* Package 'propagate'. 2018.
- Sprugel Douglas G.* Components of woody-tissue respiration in young *Abies amabilis* (Dougl.) Forbes trees // *Trees*. 1990. 4, 2. 88–98.
- Staver A. Carla, Archibald Sally, Levin Simon A.* The Global Extent and Determinants of Savanna and Forest as Alternative Biome States // *Science*. 10 2011. 334, 6053. 230–232.
- Steppe Kathy, Sterck Frank, Deslauriers Annie.* Diel growth dynamics in tree stems: Linking anatomy and ecophysiology // *Trends in Plant Science*. 2015. 20, 6. 335–343.
- Szmyt Janusz.* Spatial statistics in ecological analysis: from indices to functions // *Silva Fennica*. 2014. 48, 1. 1–31.
- Tanago Jose Gonzalez de, Lau Alvaro, Bartholomeus Harm, Herold Martin, Avitabile Valerio, Raumonon Pasi, Martius Christopher, Goodman Rosa C., Disney Mathias, Manuri Solichin, Burt Andrew, Calders Kim.* Estimation of above-ground biomass of large tropical trees with terrestrial LiDAR // *Methods in Ecology and Evolution*. 2 2018. 9, 2. 223–234.

- Terryn Louise, Calders Kim, Disney Mathias, Origo Niall, Malhi Yadvinder, Newnham Glenn, Raumonon Pasi, Å kerblom Markku, Verbeeck Hans.* Tree species classification using structural features derived from terrestrial laser scanning // ISPRS Journal of Photogrammetry and Remote Sensing. 2020. 168, February. 170–181.
- Teskey R. O., McGuire M. A.* Carbon dioxide transport in xylem causes errors in estimation of rates of respiration in stems and branches of trees // Plant, Cell & Environment. 11 2002. 25, 11. 1571–1577.
- Teskey Robert O, McGuire Mary Anne, Bloemen Jasper, Aubrey Doug P, Steppe Kathy.* Respiration and CO<sub>2</sub> Fluxes in Trees // Plant Respiration: Metabolic Fluxes and Carbon Balance. Cham: Springer International Publishing, 2017. 181–207.
- Teskey Robert O., Saveyn An, Steppe Kathy, McGuire Mary Anne.* Origin, fate and significance of CO<sub>2</sub> in tree stems // New Phytologist. 2008. 177, 1. 17–32.
- Tng David Y. P., Apgaua Deborah M. G., Ishida Yoko F., Mencuccini Maurizio, Lloyd Jon, Laurance William F., Laurance Susan G.W.* Rainforest trees respond to drought by modifying their hydraulic architecture // Ecology and Evolution. 12 2018. 8, 24. 12479–12491.
- Valladares Fernando, Gianoli Ernesto, Gómez José M.* Ecological limits to plant phenotypic plasticity // New Phytologist. 2007. 176, 4. 749–763.
- Vanderwel Mark C., Slot Martijn, Lichstein Jeremy W., Reich Peter B., Kattge Jens, Atkin Owen K., Bloomfield Keith J., Tjoelker Mark G., Kitajima Kaoru.* Global convergence in leaf respiration from estimates of thermal acclimation across time and space // New Phytologist. 9 2015. 207, 4. 1026–1037.
- Verbeeck Hans, Bauters Marijn, Jackson Tobias, Shenkin Alexander, Disney Mathias, Calders Kim.* Time for a Plant Structural Economics Spectrum // Frontiers in Forests and Global Change. 2019. 2, August. 1–5.
- Vicari Matheus B., Disney Mathias, Wilkes Phil, Burt Andrew, Calders Kim, Woodgate William.* Leaf and wood classification framework for terrestrial LiDAR point clouds // Methods in Ecology and Evolution. 2019. 10, 5. 680–694.
- TLSeparation/source: TLSeparation-1.2.1.5. // . 1 2018.
- Wang Xuhui, Piao Shilong, Ciais Philippe, Friedlingstein Pierre, Myneni Ranga B, Cox Peter, Heimann Martin, Miller John, Peng Shushi, Wang Tao, Yang Hui, Chen Anping.* A two-fold increase of carbon cycle sensitivity to tropical temperature variations // Nature. 2014. 506, 7487. 212–215.
- West Brown J. H. & Enquist B. J. G. B.* General Model for the Origin of Allometric Scaling Laws in Biology. // Science. 1997. 276, 1997. 122–126.
- West Geoffrey B., Brown James H., Enquist Brian J.* A general model for the structure and allometry of plant vascular systems // Nature. 1999. 400, 6745. 664–667.

- Wilkes Phil, Shenkin Alexander, Disney Mathias, Malhi Yadvinder, Bentley Lisa Patrick, Vicari Matheus Boni.* Terrestrial laser scanning to reconstruct branch architecture from harvested branches // *Methods in Ecology and Evolution.* 12 2021. 12, 12. 2487–2500.
- Wright Ian J, Reich Peter B, Westoby Mark, Ackerly David D, Baruch Zdravko, Bongers Frans, Cavender-Bares Jeannine, Chapin Terry, Cornelissen Johannes H C, Diemer Matthias, Flexas Jaume, Garnier Eric, Groom Philip K, Gulias Javier, Hikosaka Kouki, Lamont Byron B, Lee Tali, Lee William, Lusk Christopher, Midgley Jeremy J, Navas Marie-Laure, Lo Niinemets U , Oleksyn Jacek, Osada Noriyuki, Poorter Hendrik, Poot Pieter, Prior Lynda, Pyankov Vladimir I, Roumet Catherine, Thomas Sean C, Tjoelker Mark G, Veneklaas Erik J, Villar Rafael.* The worldwide leaf economics spectrum // *Nature.* 2004.
- Xu Chi, Staal Arie, Hantson Stijn, Holmgren Milena, Nes Egbert H. van, Scheffer Marten.* Remotely sensed canopy height reveals three pantropical ecosystem states // *Ecology.* 1 2016. 97, 9. 2518–2521.
- Yang Jinyan, He Yujie, Aubrey Doug P., Zhuang Qianlai, Teskey Robert O.* Global patterns and predictors of stem CO<sub>2</sub> efflux in forest ecosystems // *Global Change Biology.* 2016. 22, 4. 1433–1444.
- Yoda Koji.* Community respiration in a lowland rain forest in Pasoh, Peninsular Malaysia // *Japanese Journal of Ecology.* 1983. 33, 2. 183–197.
- Zang Lipeng, Xu Han, Li Yide, Zang Runguo.* Conspecific negative density dependence of trees varies with plant functional traits and environmental conditions across scales in a 60-ha tropical rainforest dynamics plot // *Biotropica.* 3 2021. 53, 2. 693–702.
- Zemp Delphine Clara, Schleussner Carl-Friedrich, Barbosa Henrique M. J., Hirota Marina, Montade Vincent, Sampaio Gilvan, Staal Arie, Wang-Erlandsson Lan, Rammig Anja.* Self-amplified Amazon forest loss due to vegetation-atmosphere feedbacks // *Nature Communications.* 4 2017. 8, 1. 14681.
- Zhang Shuzi, Huang Yunfeng, Zang Runguo.* The assembly and interactions of tree species in tropical forests based on spatial analysis // *Ecosphere.* 7 2017. 8, 7. e01903.
- Zhou Liguo, Liu Yuntong, Zhang Yiping, Sha Liqing, Song Qinghai, Zhou Wenjun, Balasubramanian D., Palingamoorthy Gnanamoorthy, Gao Jinbo, Lin Youxing, Li Jing, Zhou Ruiwu, Zar Myo Sai Tay, Tang Xianhui, Zhang Jin, Zhang Peng, Wang Shusen, Grace John.* Soil respiration after six years of continuous drought stress in the tropical rainforest in Southwest China // *Soil Biology and Biochemistry.* 11 2019. 138.
- Ziemińska Kasia, Westoby Mark, Wright Ian J.* Broad Anatomical Variation within a Narrow Wood Density Range—A Study of Twig Wood across 69 Australian Angiosperms // *PLOS ONE.* 4 2015. 10, 4. e0124892.

*Zscheischler Jakob, Mahecha Miguel D., Avitabile Valerio, Calle Leonardo, Carvalhais Nuno, Ciais Philippe, Gans Fabian, Gruber Nicolas, Hartmann Jens, Herold Martin, Ichii Kazuhito, Jung Martin, Landschützer Peter, Laruelle Goulsen G., Lauerwald Ronny, Papale Dario, Peylin Philippe, Poulter Benjamin, Ray Deepak, Regnier Pierre, Rödenbeck Christian, Roman-Cuesta Rosa M., Schwalm Christopher, Tramontana Gianluca, Tyukavina Alexandra, Valentini Riccardo, Van Der Werf Guido, West Tristram O., Wolf Julie E., Reichstein Markus.* Reviews and syntheses: An empirical spatiotemporal description of the global surface-atmosphere carbon fluxes: Opportunities and data limitations // *Biogeosciences*. 8 2017. 14, 15. 3685–3703.

*Zuur Alain F., Ieno Elena, Walker Neil, Saveliev Anatoly, Smith Graham.* Mixed Effect Models and Extensions in Ecology with R. 2009.